AD-A111 187 OHIO UNIV ATHENS DEPT OF ELECTRICAL ENGINEERING F/G 17/7
LOW-FREQUENCY BEACON SIGNAL STRENGTH DETERMINATION,(U)
JAN 80 J L BASH, R J LUEBBERS DOT-FA79WA-4278
UNCLASSIFIED EER-41-2 FAA-R-8050.2 NL

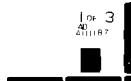

Report No. FAA-R-6050.2

LOW-FREQUENCY BEACON SIGNAL STRENGTH DETERMINATION

AD A111187

JERRY L. BASH
RAYMOND J. LUEBBERS

Avionics Engineering Center
Department of Electrical Engineering
Ohio University
Athens, Ohio 45701

JANUARY 1980

FINAL REPORT

Document is available to the public through the
National Technical Information Service,
Springfield, Virginia 22161.

DTIC
ELECTE
FEB 2 2 1982
S
A

Prepared for

FEDERAL AVIATION ADMINISTRATION
Airway Facilities Service
Washington, D. C.
Contract DOT-FA79WA-4278

DTIC FILE COPY

NOTICE

This document is disseminated under the sponsorship of the Department of Transportation *in the interest* of information exchange. The United States Government assumes no liability for the contents or use thereof.

TECHNICAL REPORT STANDARD TITLE PAGE

1. Report No.	2. Government Accession No.	3. Recipient's Catalog No.
FAA-R-6050.2	AD-A111 187	

4. Title and Subtitle	5. Report Date
LOW-FREQUENCY BEACON SIGNAL STRENGTH DETERMINATION	January 1980
	6. Performing Organization Code

7. Author(s)	8. Performing Organization Report No.
Jerry L. Bash Raymond J. Luebbers	EER 41-2

9. Performing Organization Name and Address	10. Work Unit No.
Avionics Engineering Center, Department of Electrical Engr. Ohio University Athens, Ohio 45701	11. Contract or Grant No. DOT-FA79WA-4278

12. Sponsoring Agency Name and Address	13. Type of Report and Period Covered
Federal Aviation Administration Airway Facilities Service Washington, D. C. 20591	FINAL REPORT Jan. 19, 1970 - Feb. 19, 1980
	14. Sponsoring Agency Code

15. Supplementary Notes

16. Abstract

Mathematical models and computer programs have been developed which allow the prediction of signal strength magnitudes produced by low-frequency, non-directional beacons commonly used for aircraft navigation aids. In addition, a calibrator has been designed, built and tested which allows quantitative signal strength data to be collected using ground vehicles or airplanes. Good correlation between predications and measurements has been observed. Predications for signal-in-space values can be based either on theory or ground observations. Accuracies typically can be expected to be within 5 dB.

17. Key Words	18. Distribution Statement
Radio Wave Propagation, Non-Directional Beacon, Coverage Radius, Interference Radius, Terrain Effects, Ionospheric Effects, Electric Field Strength, Correlation	This document is available to the U.S. public through the National Technical Information Service, Springfield, Virginia 22161.

19. Security Classif. (of this report)	20. Security Classif. (of this page)	21. No. of Pages	22. Price
Unclassified	Unclassified	185	

Form DOT F 1700.7 (8-69)

METRIC CONVERSION FACTORS

Approximate Conversions to Metric Measures

Symbol	When You Know	Multiply by	To Find	Symbol
	LENGTH			
in	inches	*2.5	centimeters	cm
ft	feet	30	centimeters	cm
yd	yards	0.9	meters	m
mi	miles	1.6	kilometers	km
	AREA			
in^2	square inches	6.5	square centimeters	cm^2
ft^2	square feet	0.09	square meters	m^2
yd^2	square yards	0.8	square meters	m^2
mi^2	square miles	2.6	square kilometers	km^2
	acres	0.4	hectares	ha
	MASS (weight)			
oz	ounces	28	grams	g
lb	pounds	0.45	kilograms	kg
	short tons (2000 lb)	0.9	tonnes	t
	VOLUME			
tsp	teaspoons	5	milliliters	ml
Tbsp	tablespoons	15	milliliters	ml
fl oz	fluid ounces	30	milliliters	ml
c	cups	0.24	liters	l
pt	pints	0.47	liters	l
qt	quarts	0.95	liters	l
gal	gallons	3.8	liters	l
ft^3	cubic feet	0.03	cubic meters	m^3
yd^3	cubic yards	0.76	cubic meters	m^3
	TEMPERATURE (exact)			
°F	Fahrenheit temperature	5/9 (after subtracting 32)	Celsius temperature	°C

*1 in = 2.54 (exactly). For other exact conversions and more detailed tables, see NBS Misc. Pub. 286, Units of Weights and Measures, Price $2.25, SD Catalog No. C13.10:286.

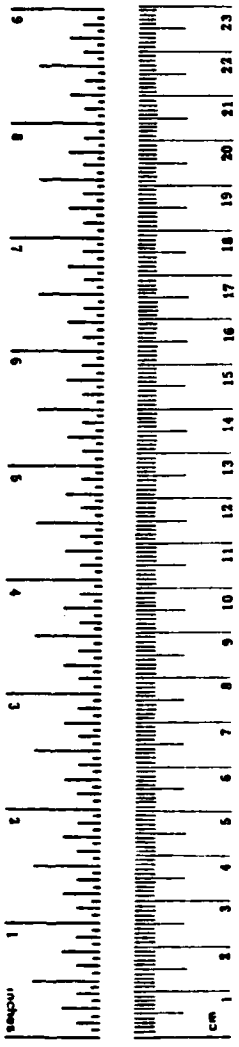

Approximate Conversions from Metric Measures

Symbol	When You Know	Multiply by	To Find	Symbol
	LENGTH			
mm	millimeters	0.04	inches	in
cm	centimeters	0.4	inches	in
m	meters	3.3	feet	ft
m	meters	1.1	yards	yd
km	kilometers	0.6	miles	mi
	AREA			
cm^2	square centimeters	0.16	square inches	in^2
m^2	square meters	1.2	square yards	yd^2
km^2	square kilometers	0.4	square miles	mi^2
ha	hectares (10,000 m^2)	2.5	acres	
	MASS (weight)			
g	grams	0.035	ounces	oz
kg	kilograms	2.2	pounds	lb
t	tonnes (1000 kg)	1.1	short tons	
	VOLUME			
ml	milliliters	0.03	fluid ounces	fl oz
l	liters	2.1	pints	pt
l	liters	1.06	quarts	qt
l	liters	0.26	gallons	gal
m^3	cubic meters	35	cubic feet	ft^3
m^2	cubic meters	1.3	cubic yards	yd^3
	TEMPERATURE (exact)			
°C	Celsius temperature	9/5 (then add 32)	Fahrenheit temperature	°F

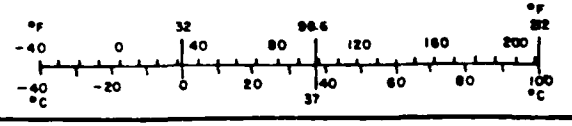

TABLE OF CONTENTS

LIST OF FIGURES

LIST OF TABLES

I. INTRODUCTION, SUMMARY, AND BACKGROUND

A technical work effort has been completed which successfully addressed the requirements to determine a method for measurement of absolute field strength of low-frequency signals using aircraft receivers and to develop a capability to predict theoretically low-frequency propagation and signal strength as a function of distance, elevation, frequency, time of day and season, terrain and atmospheric conditions. Further, measurements have been accomplished which provide data for correlating ground derived data with that from airborne measurements and that predicted using the mathematical model.

One fundamental motive for conduct of this work was to provide a theoretical capability to predict signal strengths which would be produced by low-frequency, non-directional beacons and to provide a simple means of obtaining field strength data both on the ground and in the air which would be consistent with the predictions. Once consistent measurements are available on the ground and in the air the FAA then has a justifiable means for reducing flight check operations involving the non-directional beacon navigation aids.

The objectives have been successfully met. A mathematical model now exists which will provide the desired predictions. Considerable data has been obtained using a truck and an aircraft and consistency in the data is apparent.

Remaining to be accomplished, perhaps, is the more extensive data collection and correlation using FAA equipment and implementations of the equipment designed on this project.

Although a special calibrator was designed and built by Ohio University, it now is one-of-a-kind which needs to be produced in small quantities for more extensive applications in the various regions of the United States. The measurement techniques using this small, low-cost box are simple and straightforward and should permit an implementation of this technique which should ultimately save significant amounts of flight check time and fuel.

Significant to the success of this work was the availability of the theoretical background work previously accomplished by the National Bureau of Standards. Using this work as a base, the investigation required by this project proceeded smoothly to produce the desired prediction capabilities. Available now as a result of all work are,

1. The capability to calculate the signal strength expected from a low frequency beacon given altitude, range, terrain, and season.

2. The capability to measure simply the strength of the beacon signal using either a ground vehicle or an aircraft.

Variations between measured and predicted can be expected to be typically 5 dB and between repeated measurements only 1 dB. Variations in signal strength at a point in the airspace between that predicted based on a ground measurement and that actually measured in the aircraft can be expected to be near 3 dB. As the knowledgeable engineer will know, this represents a significant improvement over present capabilities.

Three different propagation models have been used, with each one making different assumptions in its calculation of field strength. A model assuming a smooth, homogeneous, finitely conducting earth and a homogeneous atmosphere is discussed in Section II. The result of these assumptions about the propagation medium is that the sky wave contribution, which is the wave that is reflected off the upper atmosphere, is neglected in the calculation and the ground wave is computed for an idealized case. However, measured data is also presented in Section II which shows that these assumptions can provide accurate results under many circumstances, particularly at the relatively short distances (100 nm or less) of interest for NDB's. Also, these assumptions allow a more economical solution. In Section III, the same model is again utilized to examine parametrically effects of frequency, ground constants, receiver altitude and effective earth radius on ground wave propagation. Section IV discusses a model which allows an inhomogeneous atmosphere; therefore including the sky wave terms in the solution. Additional factors such as time of day and season thus can affect propagation of the wave. These are input to the model, from which reflection coefficients of the ionosphere are chosen and the sky wave component is added to the ground wave to obtain the total field. Section V introduces yet another model in which the atmosphere is again assumed homogeneous, but an irregular and inhomogeneous terrain is allowed. Therefore, the sky wave is ignored, but the earth's surface need not be considered smooth and homogeneous as before. This model is used in Section V to make field strength computations over terrain profiles in Montana,and measured data is then compared to the predicted values. Field strength is also computed for terrain profiles of an Ohio location using this model, showing that terrain irregularities of the magnitude found in that area have little effect on field strength at frequencies from 200-500 KHz. Finally, Section VI summarizes the results of this study.

In the Appendix are details of the design, fabrication, and testing of the signal strength measurement unit. Data is present in this report which will allow the reader to draw his own impressions of the credibility which can be ascribed to the models and measurement methods.

The theoretical prediction of electric field strength in the frequency range of 200-500 KHz presents special problems not encountered at frequencies above and below this range. At higher frequencies, the wavelengths are much shorter than the dimensions involved in the propagation medium, such as the distance between the earth's surface and the ionosphere, as well as the radius of the earth itself. For these short wavelengths, the boundaries of the propagating medium are at much greater distances (in terms of wavelengths) and, therefore, the conventional geometrical optical theory may be applied. However, as frequency is decreased, the wavelength is no longer small compared to the

critical dimensions of the propagation medium and, therefore, the geometrical optics treatment is no longer valid.

The requirement for a more rigorous mathematical treatment of wave propagation at lower frequencies can be met by applying Maxwell's equations to the problem, specifying appropriate boundary conditions and describing electrically the propagation medium. At frequencies below 200 KHz, this procedure yields a type of propagation referred to as "waveguide mode propagation", since the wave propagates essentially in a waveguide formed by the surface of the earth and the ionosphere. This solution is, of course, also valid for higher frequencies, but since the wavelength becomes small in comparison to the waveguide as frequency is increased, the number of modes which must be considered is large. Therefore, the analysis using this approach is quite involved and complex.

In the frequency range of interest for the work with non-directional aircraft navigational beacons (200-500 KHz) a rigorous mathematical solution is desired, but is difficult to achieve. The approximations which can be made at higher frequencies are no longer valid, and the rigorous mathematical development which allows a solution at lower frequencies is applicable but not practical to use in the same form. Thus, in order to obtain accurate theoretical prediction of radio wave propagation in this frequency range, certain approximations and transformations become necessary before a practical solution can be realized. It should also be noted that, even in this frequency range, different approximations may be valid under different conditions. In other words, one particular solution which will be of practical value in all cases in this frequency range does not exist.

Only in recent years have high speed digital computers been available to allow a numerical solution to the radio wave propagation problem in the frequency range of interest. Previously, the theoretical prediction necessarily consisted basically of graphical techniques based on the propagation formulas.

For purposes of comparison with predicted values, very little experimental data on field strength in this frequency range has previously been taken. Very few ground based measurements are available, and apparently little of this type of data has been taken from the air. Therefore, nearly all experimental data contained in this report has been obtained using the techniques discussed in the Appendix.

The capability to predict accurately electric field strength allows all related engineering decisions to be made with confidence. The ability to model mathematically the propagation mechanism of radio waves is important in many areas of communications and navigation. In this frequency range in particular, the coverage range of all non-directional beacons (NDB's) is determined based on this theoretical prediction. Therefore, accurate propagation prediction capabilities are necessary to determine the geographical separation of these beacons required to avoid interference problems from co-channel and adjacent-channel facilities.

II. GROUND WAVE PROPAGATION

A. Wave Propagation in General. As was discussed in Section I, the propagation mechanism for radio waves in the frequency range of 200-500 KHz is quite complex. By necessity, therefore, the mathematical modeling of this propagation mechanism is also very complex. This section will deal with the theoretical solution of equations describing ground wave propagation. This solution has recently been modeled [1] to allow prediction capabilities with a digital computer. Using this existing model, which has been adapted for use on the Ohio University Computer system, a comparison of this predicted field strength and measured values is then made.

Keeping in mind the assumption of a homogeneous atmosphere, the propagation of waves under these conditions consists entirely of the ground wave. Ground wave propagation can be separated into two different types of propagation, referred to as the surface wave and the space wave. Surface waves propagate along the boundary of two different media, those media here being the earth and the atmosphere. The space wave can be further divided into a direct wave and a ground-reflected wave. Both these propagation mechanisms require that the receiver and transmitter are within line-of-sight. As the terms suggest, the direct wave travels from the transmitter to the receiver directly. The ground reflected wave is reflected off the ground before reaching the receiver. Figure 2-1 illustrates these different types of ground wave propagation.

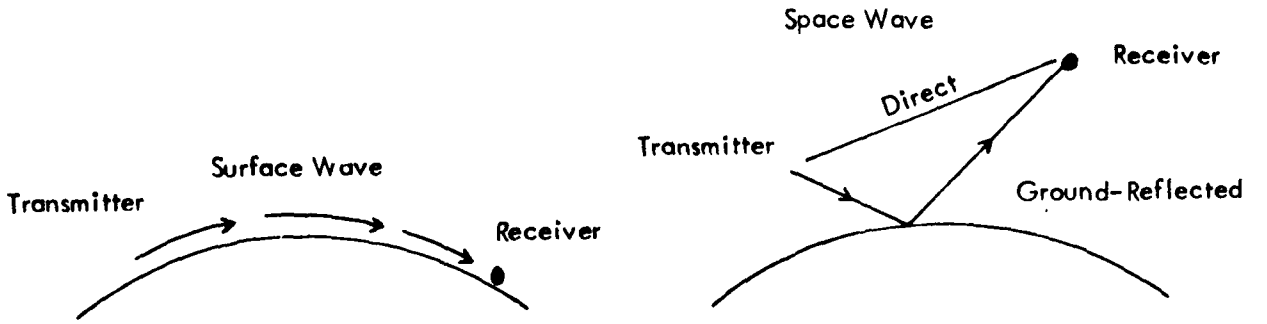

Figure 2-1. Modes of Ground Wave Propagation [2].

B. Ground Wave Propagation in the Frequency Range of 200-500 KHz. Because of the properties of the ionosphere and their variation with time of day and season (which will be discussed in Section IV), it can generally be stated that at these frequencies the contribution of the sky wave at short distances is insignificant compared to the total field. As a rule, in daytime, at distances less than 300 Km the sky wave contribution need not be considered. At night, due to changes in the

ionosphere resulting in less attenuation of the sky wave, it may be significant at distances as near as 100 Km. However, in this section only the ground wave solution is considered.

As has been stated, the ground wave consists of a space wave and a surface wave. For transmission of a radio wave from point-to-point on or in the vicinity of the earth's surface, therefore, the receiver and transmitter will be within line-of-sight only at short distances. For this reason, it is clear that the space wave is only important at relatively short distances, since propagation by this method requires line-of-sight conditions. When the receiving antenna is beyond the radio horizon when viewed from the transmitting antenna, the wave must propagate as a surface wave.

In the particular case of propagation from NDB's, the major area of interest for this report, the fact that the antenna must be within line-of-sight is clearly restrictive, since the transmitter is situated directly on the earth's surface. Thus, the surface wave is responsible for the propagation even at relatively short distances. It should be pointed out here that it is quite possible, under certain conditions, for both the surface wave and the space wave to make significant contributions. Of course, the field due to one of these propagation mechanisms cannot, in general, be experimentally distinguished from the other. These circumstances also usually necessitate the use of analytical techniques developed specifically for these conditions.

C. Mathematical Modeling of Ground Wave Propagation. For a complete theoretical description of ground wave propagation, all these propagation mechanisms must be modeled. These again include the direct and ground reflected wave of the space wave as well as the surface wave. These types of propagation generally will require different methods of solution depending on the exact conditions specified in the problem. The use of different methods of solution is necessary to maintain accuracy in the predicted field strength and also allows a final solution to be obtained with greater speed and less effort and, therefore, more economically.

The choice of which method will be used to make the calculation in a given instance is based on the distance separating the transmitting and receiving antenna, the altitude of the receiving antenna, the radio frequency, ground constants along the propagation path, and the value of earth radius factor. Knowing these parameters, decisions can be made concerning the validity of a particular model in a particular case. Program GWSNR (Ground Wave Signal-to-Noise Ratio), a propagation model obtained from ITS [1], uses four different methods to compute field strength. The program transfers control internally to certain points based on a comparison of the parameters mentioned above, assuring that the field strength calculation will be made using the appropriate model. The program incorporates the flat earth model, the method of geometrical optics, numerical integration techniques, and a residue series solution as possible methods of field strength computation.

1. Flat Earth Model. The radio wave will propagate as a surface wave if both the transmitting and receiving antenna are near the surface of the earth. The actual distance from the earth's surface beyond which the flat earth model will not be valid is somewhat arbitrary. As was mentioned earlier, the transition point from

one model to another is not always a clearly defined point, and the valid areas of application of the various models may in some instances overlap. Nevertheless, the criterion that the transmitting and receiving antenna be near the earth's surface can be meaningful only if those heights are measured in wavelengths. Now, assuming that both antenna are within a few wavelengths of the earth's surface, and that they are separated by a short distance (such that the curvature of the earth is negligible), the flat earth model can be used. The advantage of using the flat earth model, where it is applicable, is that simpler formulas can be used in making a field strength calculation and, therefore, less computer time is required.

The use of the flat earth model essentially entails a calculation of field strength over an infinitely conducting earth, and then modifying this result by multiplication by a factor which accounts for attenuation of the wave due to the fact that the earth is finitely conducting. This factor is known as the flat earth attenuation function [3]. Figure 2-2 illustrates a vertical electric monopole of length l and carrying current I located on the surface of a finitely conducting earth.

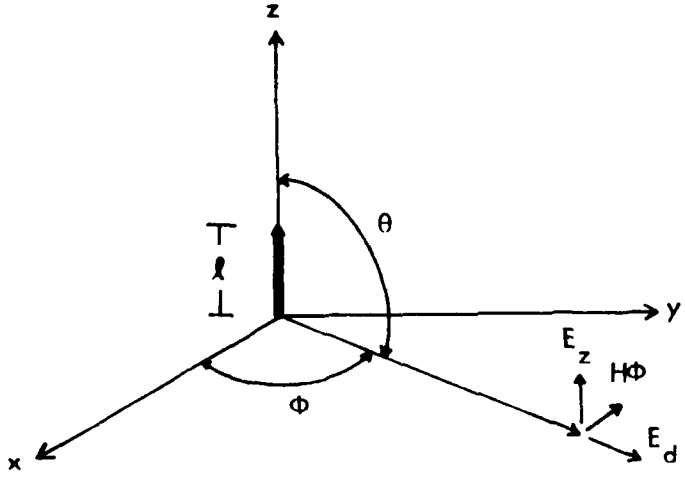

Figure 2-2. Geometry of Flat Earth Model.

The fields in this situation are well known and have been calculated by many authorities for the case where the monopole is located in free space. Harrington [4], for example, has used the concept of vector potentials to obtain a solution for this case. The final solution for the far fields from a current element in free space is

$$E_\theta = \eta \frac{j I \ell}{2 \lambda d} e^{-jkd} \sin \theta^* \qquad (2.1)$$

Since we are not concerned at this point with the time harmonic properties of the wave, we can neglect all phase information and be satisfied with describing the magnitude of electric field. Also, since we are interested only in the field strength due to the surface wave, the sin θ variation can be neglected. So we have,

* See Glossary for definition of terms.

$$E_\theta = \frac{\eta I \ell}{2\lambda d} \tag{2.2}$$

Since, in our case, the current element $I\ell$ is situated on the surface of the earth, which is for the time being assumed infinitely conducting, due to image theory the far field terms will be exactly doubled. Therefore,

$$E_\theta = \frac{\eta I \ell}{\lambda d} \tag{2.3}$$

Now to determine the power radiated by this current element, it is necessary to integrate the Poynting vector ($\bar{E} \times \bar{H}^*$) over the surface of a sphere enclosing the current element and of a radius large compared to one wavelength.

We have

$$E_\theta = \frac{\eta j I \ell}{\lambda d} e^{-jkd} \sin\theta \text{ and } H_\Phi = \frac{j I \ell}{\lambda d} e^{-jkd} \sin\theta \tag{2.4}$$

Therefore,

$$P_f = \iint \bar{E} \times \bar{H}^* = \int_0^{2\pi} d\Phi \int_0^{\pi/2} r^2 \sin\theta E_\theta H_\Phi^* d\theta = \eta \frac{4\pi}{3} \left|\frac{I\ell}{\lambda}\right|^2 \left(1 - \frac{j}{(kd)^3}\right) \tag{2.5}$$

when P_f is the complex power radiated. Now the actual average power radiated by the current element is the real part of P_f, or

$$P_r = R_e \left|P_f\right| = \eta \frac{4}{3}\pi \left|\frac{I\ell}{\lambda}\right|^2 \tag{2.6}$$

Generally in a practical situation the radiated power of a system is more readily available and easier to determine than the effective height of the antenna and the current of the antenna as a function of its height. Therefore, to define the field strength in the far field in terms of effective radiated power (ERP), a simple substitution of Equation (2.6) into Equation (2.3) is required. From Equation (2.6),

$$I = \lambda \sqrt{\frac{3P_r}{4\eta\pi}} \tag{2.7}$$

Now substituting Equation (2.7) into Equation (2.3),

$$E_\theta = \sqrt{\frac{\eta 3}{\pi 4}} \frac{\sqrt{P_r}}{d} = 9.487 \frac{\sqrt{P_r}}{d} \tag{2.8}$$

Equation (2.8) is the correct expression for the field produced by a vertical current element radiating over an infinitely conducting flat earth. The attenuation function accounting for the wave propagation over a finitely conducting earth must now be considered to obtain an accurate description for the field strength. The flat earth attenuation function has been developed by Wait [3] by assuming a current element

located over an impedance plane with a given surface impedance δ. Since the assumption of an infinitely conducting earth has now been eliminated, the boundary conditions at the interface of free space and the earth's surface are now,

$$E_d = -\delta H_\Phi. \tag{2.9}$$

The total electric field can now be thought of as consisting of three components. Equation (2.8) contains only two of these components: the direct wave and the image, or reflected wave. The third component must be included as a correction term since the propagation medium is no longer assumed infinitely conducting. Wait's development essentially shows that this correction can be represented as,

$$E(d) = \frac{9.487}{d} \sqrt{P_r}\,(1 - R_o\,\delta\, e^{z^2}\,\mathrm{erfc}\,(z)) \tag{2.10}$$

where

$$\delta = \frac{\sqrt{\eta - 1}}{\eta} \tag{2.11}$$

and

$$\eta = \epsilon_r - i\,\frac{1.8 \times 10^7 \sigma}{f} \tag{2.12}$$

for vertical polarization

with ϵ_r and σ the relative permittivity and conductivity in mhos/m of the earth, respectively, f the radio frequency in kilohertz,

$$R_o = e^{i\frac{\pi}{4}}\sqrt{\pi k D/2} \tag{2.13}$$

and

$$D = \sqrt{d^2 + (h_1 - h_2)^2} \tag{2.14}$$

with $k = 2\pi/\lambda$, λ being the free space wavelength. erfc is the complementary error function as defined by Abramowitz and Stegun [5] and

$$z = e^{i\frac{\pi}{4}}\sqrt{\frac{kD}{2}}\,\delta\,(1 + \frac{h_1 + h_2}{\delta D}) \tag{2.15}$$

where h_1 and h_2 are the heights of the antennas and d is the separation of these antenna along the earth's surface. This development is subject to the condition that $|\delta| << \eta_o$ where η_o is the intrinsic impedance of free space. This condition is not, however, restrictive in any real physical situation involving wave propagation over the earth and, therefore, is of no consequence in the results here. It is necessary only in the method by which the attenuation function term is evaluated, which makes use of a modified saddle point method [6].

Thus it can be seen that the computation involved in the flat earth model is not extensive, and considerable time can be saved by applying it to situations where it is valid.

2. The Method of Geometrical Optics. For cases where one antenna is well above the radio horizon when viewed from the other and both antennas are removed from the earth's surface, the method of geometrical optics can be applied to the problem to determine electric field strength. This method can also be utilized when the distance between the two antennas are great enough that the curvature of the earth must be considered. The geometry involved in this case is illustrated in Figure 2-3.

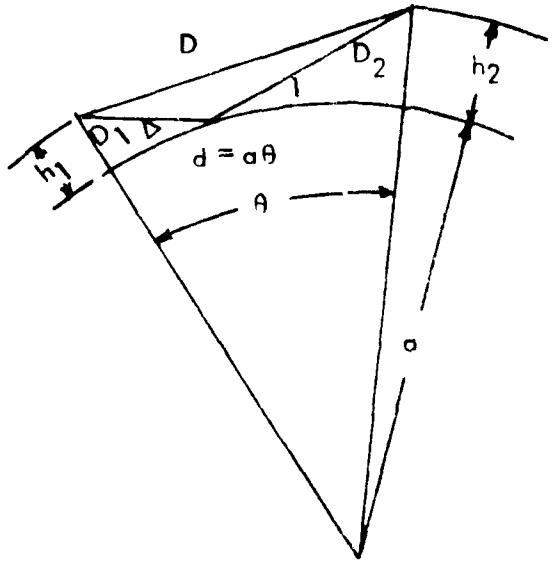

Figure 2-3. Geometry Applying to Geometrical Optics Method of Solution.

Since the transmitting antenna is now no longer situated on the surface of the earth, the field strength due to the current element in free space can now be used to describe the direct wave. This field strength will be exactly 1/2 that determined earlier for the current element on the surface of an infinitely conducting plane (Equation (2.10)). However, since under these conditions two different propagation mechanisms are involved (the direct wave and the ground-reflected wave), the total field at the receiving antenna will be the sum of the field due to each of these mechanisms. One is still concerned only with the magnitude of the total electric field, but in order to add the field strength of the direct and ground-reflected waves, the phase of each must be considered. Once the complex fields at the receiving antenna are added, taking into account the phase information, the magnitude can then be determined.

To insure that the waves are added with the proper phases, one can arbitrarily choose as a reference the distance d between the transmitting and receiving antennas over the earth's surface. Therefore, the electric field at the receiving antenna can be written as:

$$E = 9.487 \frac{\sqrt{P_r}}{2D} e^{-jk(D-d)} \left(1 + R_g e^{-jk(D_1+D_2-D)}\right) \qquad (2.16)$$

Here P_r is the effective radiated power of the transmitting antenna and R_g is the ground reflection coefficient. This ground reflection coefficient is a function of the angle of incidence of the wave, radio frequency, and the ground constants along the propagation path. It is, in general, a complex value. The equations for reflection coefficients derived for reflection from perfect dielectrics are valid for a finitely conducting earth provided that the complex dielectric constant is used in place of the real dielectric constant used for the case of perfect dielectrics [7]. So,

$$\hat{\epsilon} = \left(\epsilon + \frac{\sigma}{j\omega}\right) \qquad (2.17)$$

Making these substitutions, the reflection coefficient for vertically polarized waves is:

$$R_g = \frac{\sin\Delta - \frac{\sqrt{(\epsilon_r - jx) - \cos^2\Delta}}{\epsilon_r - jx}}{\sin\Delta + \frac{\sqrt{(\epsilon_r - jx) + \cos^2\Delta}}{(\epsilon_r - jx)}} \qquad (2.18)$$

where

$$x = \frac{\sigma}{\omega\epsilon_o} = \frac{18\times10^9\sigma}{f} \qquad (2.19)$$

The geometry involved in the problem allows computation of the distance between the antenna, D, through a rather lengthy, but straightforward formula. The distances D_1 and D_2 cannot be determined by a closed form solution, but iterative techniques can be easily applied [1].

3. Numerical Integration. Special problems in computation are encountered when the receiving antenna is near the radio horizon when viewed from the transmitting antenna. At this point, the direct ray is still present but the effects of diffraction of the wave around the earth's surface are also significant. In this region a transformation solution of the physical problem with an assumed smooth, homogeneous, spherical earth yields the following expression, which must be numerically integrated to obtain a solution,

$$E = 9.487\sqrt{P}\sqrt{\frac{v}{12\sin\theta}}\,\frac{e^{-i3\pi/4}}{9}\int_r e^{-ixt} F_1(q,t)\,dt \qquad (2.20)$$

where $v = (ka/2)^{1/3}$, $x = v\theta$, and $q = iv\delta$. (2.21)

$$F_1(q,t) = \frac{H_1(h_1)\,H_2(h_2)}{\frac{w'(t)}{w_1(t)} - q} \qquad (2.22)$$

The transformation involved here allows the contour integral to be used as an alternative to an infinite summation of Legendre functions.

As can be seen, the function $F_1(q,z)$ is totally dependent upon the Airy functions and related to the geometry and physical conditions encountered, since the height-gain functions are expressed in terms of the Airy functions [3].

$$H_1(h) = \frac{w_1(t-y)}{w_1(t)} \tag{2.23}$$

and

$$H_2(h) = -.5i(w_2(t-y)\,[w_1'(t) - qw_1(t)] - w_1(t-y)\,[w_2'(t) - qw_2(t)] \tag{2.24}$$

Airy functions can be related to Hankel functions and are useful in solutions to many problems involving spherical coordinates. They are functions which satisfy the equation

$$w_n''(t) = tw_n(t) \tag{2.25}$$

and have been tabulated [5,6].

4. Residue Series Solution. When the receiving antenna is beyond the radio horizon when viewed from the transmitting antenna, the direct ray cannot contribute to the field and, therefore, the field strength is made up of only the surface wave, still assuming a homogeneous atmosphere. The approximations that can be made under these circumstances allow a solution usually referred to as a residue series, since the transformation leading to this solution makes use of the theory of residues to evaluate the contour integral. This particular transformation is based on the work of Watson and has been referred to as the Watson transformation. A brief outline of the steps used in this solution will be presented here, but the complete solution procedure is available from many sources [3, 9, 10]. The steps of the solution prior to the use of the Watson transformation lead to a solution of the form of Equation (2.20), and the Watson transformation actually allows a solution of this integral equation using the residue series rather than numerical integration. This is made possible because the geometry of the problem forces conditions when the two antennas are not within line-of-sight (so that the direct field is not present) that are not valid assumptions when the antennas are within the radio horizon.

The model is again assumed to be a smooth, spherical, homogeneous earth and the geometry is shown in Figure 2-4. The earth's radius is a and the source dipole is located at a height h, where a cylindrical coordinate system (r,θ,Φ) has been chosen.

A potential function U is chosen which satisfies the wave equation for $r > a$.

$$(\nabla^2 + k^2)\,U = 0 \tag{2.26}$$

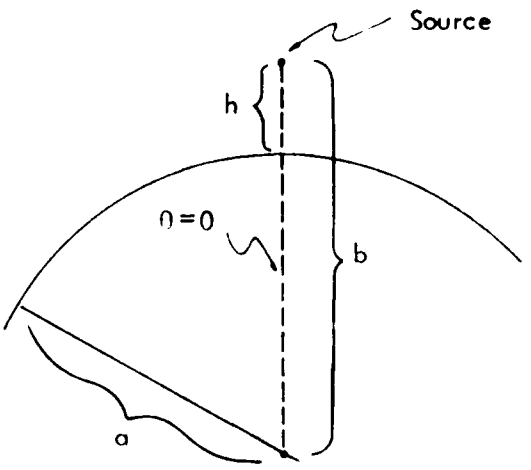

Figure 2-4. Geometry Applying to Residue Series Solution.

Then the various components of the field are:

$$E_r = (k^2 + \frac{\partial}{\partial r^2})\ rU \tag{2.27}$$

$$E_\theta = \frac{1}{r}\ \frac{\partial^2}{\partial r \partial \theta}\ (rU) \tag{2.28}$$

$$H_\Phi = -ie\,\omega\ \frac{\partial U}{\partial \theta} \tag{2.29}$$

$$E_\theta = H_r = H_\Phi = 0 \tag{2.30}$$

The solution of these equations in spherical coordinates allows the potential function U to be expressed in terms of an infinite summation of spherical Hankel functions of the first and second kind ($h_n^{(1)}(kr)$ and $h_n^{(2)}(kr)$) and Legendre polynomials ($P_n(\cos\theta)$). Next the boundary conditions are applied. This again is

$$E_\theta = -\delta H_\Phi \text{ at } r = a \tag{2.31}$$

which is equivalent to Equation (2.9) but expressed now in the spherical coordinate system defined in Figure 2-4. Of course this expression assumes that the influence of the earth is completely described by its surface impedance δ, which is equal to the ratio of tangential electrical and magnetic fields for a vertically polarized wave incident upon the earth's surface at a grazing angle. The total field in terms of the potential function U is then expressed in the form of the infinite summation

$$U = \sum_{n=0}^{\infty} (2n+1)\, f(n)\, P_n(\cos\theta) \tag{2.32}$$

where f(n) is a known function of Hankel functions of the first and second kinds. However, for very low radio frequencies, this expression requires a calculation of too many terms to be useful. Therefore, using the Watson transformation, the summation can be expressed as a contour integral (Equation (2.23)) for which the contour can be chosen to allow the potential function to be computed by summing the residues of the poles of the integrand.

$$U = i \int_C \frac{n\, dn}{\cos n}\, f(n-\tfrac{1}{2})\, P_{(n-\frac{1}{2})}[\cos\pi - \theta] \tag{2.33}$$

The computation procedure has now been transformed to one of location of the poles of the integrand, which involves the function $f(n-\frac{1}{2})$ of Hankel functions. Since Airy functions are closely related to Hankel functions and are found to permit the computer implementation with less difficulty, the potential function U has been expressed using these Airy functions.

$$U = U_o\, e^{-i\pi/4}\, 2(\pi x)^{\frac{1}{2}} \sum_s \frac{e^{-ixt_s}}{1 - \frac{t_s}{q^2}} \quad \frac{w(t_s - y_1)}{w_1(t_s)} \quad \frac{w_1(t_s - y_2)}{w_1(t_s)} \tag{2.34}$$

where

$$y = \left(\frac{2}{ka}\right)^{1/3} k\, h_i \tag{2.35}$$

$$x = \left(\frac{ka}{2}\right)^{1/3} \theta \tag{2.36}$$

and

$$q = -i \left(\frac{ka}{2}\right)^{1/3} \left(\frac{V_o}{V_1}\left(1 - \frac{V_o^2}{V_1^2}\right)^{\frac{1}{2}}\right) \tag{2.37}$$

where $V_o = ik$, V_1 is the propagation constant of the earth, and $w_1(t)$ is an Airy integral. The roots t_s are solutions to the equation

$$w_1'(t) - q w_1(t) = 0\,. \tag{2.38}$$

Program GWSNR uses the concepts introduced here in its computation of field strength for great distances. As can be seen in Equation (2.34), the Airy Function is used in both the root determining equation and the height-gain function. The reduction of calculations involved using this procedure has made possible the computation of field strength which otherwise would have been prohibitive. Again, further details of the transformation solution can be found in the references previously sited.

D. Analysis of Measured Data. In this section the accuracy and reliability with which the electric field strength can be predicted will be investigated by comparing the values predicted by model GWSNR with measured field strength values. The measured field strength values have been obtained by using a Fairchild EMC-25 selective voltmeter and loop antenna for ground based measurements, a King KR-86, or a Bendix DFA-70 receiver with a CNA-70A control panel for airborne data collection. The receiver systems used for airborne measurements were calibrated using a procedure outlined in reports of the National Bureau of Standards [11]. The measurement technique is described in Appendix A. The procedure essentially entails calibration of the aircraft receiver system by utilizing certain facts concerning the near-zone coupling of loop antennas. Although only a system using a loop antenna can be calibrated directly using this procedure, receiving systems using other types of antennas can be calibrated indirectly. However, all measurements reported here were made using a loop antenna.

The program GWSNR computes field strength assuming a smooth, homogeneous earth and a homogeneous atmosphere, so all terrain irregularities, as well as any inhomogeneity along the propagation path and sky wave effects, are neglected in the theoretical computation.

1. Theoretical - Measured Correlation. All ground comparisons presented here are taken from NDB facilities in southern Ohio. Most of the flight data as well has been collected in southern Ohio, but a few measurements were available from beacons in Pennsylvania, Massachusetts, Connecticut, and New Hampshire. All figures here show the theoretical curve as the solid line with the measured values plotted using a symbol to indicate the date the measurements were taken. The generation of the theoretical curves required the radio frequency of the beacon, its effective radiated power, the earth radius factor to be used, and the ground constants along the propagation path as inputs to the computer model. With exception of the ERP, all these parameters can be determined with little difficulty. The effective earth radius is a factor which accounts for refraction caused by the lower atmosphere. It will be considered more fully in Section III, where its variation within reasonable limits is found to cause insignificant changes in computed field strength at distances of interest for NDB's. The ground constants have been determined from charts prepared by Arcove and Delany [12]. The effective radiated power of each beacon has been determined experimentally essentially using a procedure suggested in the FAA Handbook 6050.10 [13]. This method assumes the normal inverse distance attenuation of field strength, which can be seen to be valid, under the assumptions made in the theoretical calculations, to distances of at least 3 or 4 nautical miles from the antenna. Manipulation of the basic equations enables the use of the following formula for ERP determination:

$$ERP = 10^{\left(2 \log_{10} \frac{\text{measured signal (mV/m)}}{162 \text{ mV/m}} - 2 \log_{10} \frac{1}{\text{measuring distance}}\right)} \times 1 \text{ kw} \qquad (2.39)$$

The 162 mV/m is the signal strength which would be measured at a distance of 1 nautical mile from a facility radiating 1 kw ERP, which is used as the reference in this calculation.

This formula has been used to compute the ERP of all facilities for which ground measurements were available within 4 nm. Where more than 1 measurement point was taken within 4nm, an average of all points was taken. For beacons outside the State of Ohio, the ground measurements were not available. This required that the ERP value be determined from published data. The transmitter power for these facilities is listed in FAA Master Radio Frequency List, RIS AF-6050-12 [14]. Using this value and assuming performance for these facilities as indicated in FAA Handbook 6050.10, ERP values of 0.536 watt and 1.072 watts for facilities with transmitter powers of 25 and 50 watts, respectively, have been obtained. The experimentally determined ERP was found to vary considerably among the beacons checked, as its value is dependent upon many factors (such as antenna type, transmitter power, ground conductivity in the immediate vicinity, and frequency). This variation is shown in Table 2-1, where the "published" values used for reference have been determined using the FAA references previously mentioned. (An exception is the Columbus, Ohio facility which has increased transmitter power since the FAA Master Radio Frequency list of April 1979.) The table shows values of ERP measured and determined from published data and their difference (in dB) for each facility for which ERP measurements have been taken. As can be seen from this data, the published values are not a reliable indication of the actual ERP, as variations from -14.739 to +7.628 dB are found. No definite trend can be noted here, such as variation with frequency or other parameter, but the inaccuracy of the ERP determined from the published data can be established. When available, the measured ERP is used as input to the computer model in this study.

Once all input parameters had been determined, the theoretical curves could be computed and plotted. This then allowed the comparison between theoretical and measured values to be made. To make these comparisons, the measured values have been plotted on the appropriate graphs corresponding to a particular beacon and altitude of measurement. The results are shown in Figures 2-5 through 2-28. Figures 2-5 through 2-22 show results for beacons located in southern Ohio, while beacons outside Ohio are shown in Figures 2-23 through 2-28. Since effective radiated power measurements were not made on beacons outside Ohio, the ERP values indicated on these figures were obtained assuming performance as given in FAA Handbook 6050.10 for facilities of appropriate transmitter power, determined from FAA Master Radio Frequency List 6050-12, April 1979.

Considering first the southern Ohio beacon facilities, note that the plotted results are arranged in order of increasing frequency and altitude. Figures 2-5 and 2-6 illustrate predicted and measured data for the NDB facility located at Cambridge, Ohio operating at 233.51 KHz. Its call sign is CDI and the ERP measured for this facility is 0.598 watt. Figure 2-5, showing the ground based data, illustrates agreement within 3 dB of all points measured for this facility, with one exception, which is located at a distance of 16 nm and is 7 dB below the predicted value of field strength. The flight data for this facility, as shown in Figure 2-6, consists of only one point, which agrees very well with the predicted value. Although in general the agreement shown here is good, the data for this facility is insufficient to yield conclusive results. The variation in measured field strength illustrated here could be due to one or a combination of many factors. A beacon operating at a frequency very close to the Cambridge

Location	Call Sign	Frequency (KHz)	Measured ERP (Watts)	Determined ERP from Published Data (Watts)	Difference (dB)
Cambridge, Ohio	CDI	223.51	0.598	0.536	+0.475
Chillicothe, Ohio	RZT	236.51	1.024	0.536	+2.811
Albany, Ohio	UNI	250.00	0.700	0.536	+1.159
Zanesville, Ohio	ZZV	332.00	0.296	0.536	-2.579
Circleville, Ohio	CYO	366.51	0.018	0.536	-14.739
Columbus, Ohio	CMH	391.00	9.683	1.672	+7.628

Table 2-1. Comparisons of Measured and Determined ERP for NDB's in Southern Ohio.

facility is located at Chillicothe, Ohio which transmits at 236.51 KHz with a measured ERP of 1.024 watts. The call sign of this beacon is RZT and results of comparisons of measurements with the predicted values for this facility are shown in Figures 2-7 through 2-9. The agreement here is seen to be usually within about 5 dB, with a worst case of 8 dB. While the variation in field strength may be caused by terrain irregularities, this is unlikely at a frequency as low as this. Observing all three figures for the Chillicothe beacon, it is immediately obvious that nearly all measured values fall below that predicted by the theoretical curve. It is, therefore, quite possible that the ERP experimentally determined for this beacon is slightly higher than the actual value, at least at the time that the remainder of the measurements were made. This could happen for a number of reasons, such as a slightly higher ground conductivity in the vicinity of the antenna or possibly an inaccurate reading caused by noise interference. Also it should be kept in mind that the tolerance of the Fairchild EMC-25 selective voltmeter is $\pm$ 2 dB, and this could contribute to the error in the measurements. Therefore, although it is possible that the terrain irregularities could cause slight variations in electric field strength, at these low frequencies, this factor is not expected to have significant effects on field strength. Effects of irregular terrain are considered in more detail in Section V.

One further point concerning the presentation of data for this and the remaining sets of plots illustrating correlation between theoretical and measured field strength should be made. The data is plotted in these figures corresponding to the altitude closest to which the data actually was taken. In some cases it has not been taken exactly at the height for which the predicted curve has been generated. However, it will be shown later (Section II, D.2) that the altitude at which the measurement is taken has very little influence on the value of field strength determined within a range of roughly $\pm$ 1000 feet. This is to be expected, given the long wavelength of the waves at the frequencies in question. It is also shown in Section III that the model predicts that the receiver altitude is, in general, not significant to field strength at a given distance. In summarizing the data presented for these two facilities, then, it can be noted that the data is regular and, for the Chillicothe beacon, consistently below the predicted values. The most probable explanation for this is that the ERP determined experimentally for the facility and used in the generation of the theoretical curves is slightly higher than the actual value.

Figures 2-10 through 2-14 have been prepared using data obtained from the NDB facility located at Albany, Ohio (UNI) operating at 250 KHz with a measured ERP of 0.700 watt. All data gathered for this facility shows very good agreement with the corresponding theoretical curves. The maximum deviation from the predicted curves is around 7 dB in all these curves and nearly all points are within 3 or 4 dB. The data also illustrates repeatability of measurements, since ground measurements are shown for six different times and flight data has been taken at five different times, including one set of points taken under nighttime conditions. As can be seen, and as expected, the sky wave effects even at night have not affected the field strength noticeably for the distances of interest for navigational beacons of this type. Also, the flight data for the Albany beacon illustrates field strength measurements taken with different aircraft. The largest discrepancy between measured and predicted field strength in Figure 2-11

occurs with data taken with the DC-3 on 6/19/79, which runs 5 to 7 dB above the predicted values, but this data is only 3-4 dB above data taken with a smaller aircraft such as a Cherokee. Also, data taken at higher altitudes with the DC-3 indicates much better agreement with predicted values, with differences of only 2-3 dB, and data taken 6/1/79 with the DC-3 does not vary from the predicted value by more than 2 dB with exception of one point on Figure 2-12 at 26 nm, where the field strength is small and noise interference can be a major factor. Aircraft fuselage effects will be further discussed later in this section, but indications here are that the aircraft does not significantly alter the field strength value measured.

Figures 2-15 and 2-16 illustrate the comparison of theoretical and measured values of field strength for the beacon located at Zanesville, Ohio. With a call sign of ZZV, its operating frequency is 332 KHz and the measured effective radiated power was 0.296 watt. The ground-based data, shown in Figure 2-15, shows excellent agreement in predicted and measured values. With the exception of one point, at 4.5 nm for which the measured value is 4 dB above the predicted value, all points agree within 2 dB. Figure 2-16, illustrating data taken at an altitude of 6000 feet, also shows good agreement. All data points, again with the exception of one point, fall within 5 dB of the predicted value. The exception, however, shows nearly a 10 dB difference at 8 nm.

Figures 2-17 through 2-19 show results of data taken on the Circleville, Ohio beacon facility (CDI), which operates at 366.51 KHz with a measured effective radiated power of 0.018 watt. The measured data plotted on these figures shows a worst case disagreement of 8 dB. With the exception of two points, however, all data on the ground-based measurements and the 3000-foot receiver altitude curve (Figure 2-17 and 2-18) agrees with the predicted value within 4 dB. All data points on the 6000-foot receiver altitude curve are within 3 dB of the predicted value. A possible explanation for these observations is that, as the frequency has been increased slightly, the same terrain irregularities are more significant to the propagation wave of smaller wavelength. Therefore, closer to the earth's surface, the measured data is more scattered and unpredictable. At increased altitudes, the wave is a sufficient distance from the surface of the earth that its irregularities do not cause significant effects on the electric field strength. It can also be noted for this particular case that the noise levels can be quite significant, since the effective radiated power of this facility is very low. Therefore, the signal becomes low at relatively short distances, and the noise interference can cause significant deviation in the measured values.

Figures 2-20 through 2-22 illustrate the correlation between theoretical and experimental values determined from the Columbus, Ohio beacon (CMH), operating at 391 KHz with a measured ERP of 9.683 watts. Again, the ground data, shown in Figure 2-20, exhibits a slightly more scattered distribution than the previous facility measurements, although it is still fairly well grouped for distances of less than 40 nm, with the maximum deviation from the predicted value being 6 dB for this range of distances. The worst case agreement occurs at 56 nm, where the measured signal is 13 dB below that predicted. At great distances, however, the signal level is low so that noise could be a factor in causing this variation. The majority of measured values in this set of figures fall below the predicted level, again indicating a possible

false ERP level determination. This is indeed a possibility in the case of this beacon, as well as the Cambridge, Ohio beacon since situations dictated that the measurement to determine ERP be made three months later than the other measurements. All measured points for the flight data for the Columbus beacon fall below the predicted value, but agreement is still within 6 dB for all except two points on the curve for a receiver altitude of 6000 feet. Since this frequency is also high in the range considered, the terrain irregularities along the propagation path could possibly cause some slight attenuation. Figure 2-21 also illustrates two data points taken with the DC-3 aircraft. This data again follows general trends established in data taken with the smaller aircraft, such as Cherokee or Piper, indicating that the aircraft, even at this frequency, has little effect on measurements.

The following six figures (Figures 2-23 to 2-28) demonstrate the comparison of theoretical and experimental data for beacons outside Ohio. They are also arranged in order of increasing frequency, and the altitude is indicated on each graph. In general, the results reinforce all comments previously made. This data does allow the capability of the model to predict field strength under conditions of different ground constants to be demonstrated, but it must be recalled that the ERP of these facilities has not been directly measured and, therefore, values corresponding to transmitter powers given in FAA Master Radio Frequency List, RIS AF-6050-12, April 1979 are assumed. A change in ERP results in simply shifting the predicted curve up or down on the graph since the model is linear.

Comparisons in Figure 2-23 for the Fitchburg, Massachusetts beacon indeed suggest that this facility is not operating at 0.536 watt (ERP), but rather at a level 5 or 6 dB below this. Nevertheless, the measured data is regular and the comparisons illustrate the model's capability to predict field strengths on ground of low conductivity. Of course, operating at the low power and over this poorly conducting earth, the signal levels become very low at relatively short distances making measurement at greater distances impossible due to interference from atmospheric noise. The measured data presented in Figure 2-23 also illustrates that the measurements can be repeated with good agreement. Two separate passes flying toward the beacon along the same path are indicated, and all points on both passes fall very close to the same line (which agrees well with the theoretical curve shifted downward 5 dB). Also indicated on the figure is a point taken flying away from the beacon which also agrees well with the previous two passes. The agreement here suggests that the presence of the aircraft does not significantly affect measured results, since the measured field strength is not noticeably different for different aircraft orientation with respect to the beacon. This can also be considered somewhat of a worst case, since the aircraft used in these measurements is a DC-3 and is considerably larger than aircraft used in making other measurements. This fact has been verified in other measurements taken on the Columbus, Ohio beacon on 6/1/79 also using the DC-3. This set of data, presented in Table 2-2, was taken at the same point 18.5 nm from the beacon at an altitude of 3000 feet. The variable here is the aircraft heading which is given in degrees east or north. Under these conditions, the largest variation seen in all points is 1.4 dB, a difference which is well within the receiver tolerance and one which could easily be caused by noise interference.

Aircraft Heading (° E of N)	Measured Field Strength (dB Relative to 1 μV/m)
60	48.23
90	48.03
180	48.37
180 (repeated)	48.23
270	49.43

Table 2-2. Effect of Aircraft Orientation on Measured Field Strength (6/1/79). Altitude - 3000 feet; Aircraft - DC-3; Receiver - Bendix ADF; 18.5 nm from Columbus, Ohio (CMH) Beacon (391 KHz).

Data from an NDB facility also operating at a very low frequency (209.51 KHz) but located in Stoystown, Pennsylvania is presented in Figure 2-24. Because of improved ground conductivity in this case, the wave propagates with less attenuation. The measured data is very regular for distances less than 25 nm, but again the ERP of the facility appears not to be the 0.536 watt determined by using the transmitter power shown in the Master Radio Frequency List, but rather about 10 dB above this value. The drastic attenuation exhibited in measured data beyond 25 nm could be caused by noise interference or terrain irregularities in the vicinity, though effects of terrain are unlikely to cause such a change in measured field strength, particularly at these low frequencies.

Figures 2-25 and 2-26 also illustrate regularity of measured data, but in both cases the beacon apparently is operating above 0.536 watt ERP. The Amherst, New Hampshire beacon (Figure 2-25) appears to be around 9 dB above 0.536 watt, and the Brainard, Connecticut beacon (Figure 2-26) is over 15 dB above this value. Figures 2-27 and 2-28, however, give no reason to suggest that the ERP of these facilities varies significantly from the expected value. The measured data in these cases is slightly more scattered than the previous data, but in most cases is within 5 dB of the predicted value. The scattering may be a result of the higher frequency of these facilities, which means that the wave propagation will be more vulnerable to all factors affecting wave propagation, such as ground conductivity, irregular terrain, and large metal structures along the propagation path.

To summarize the results of the previous comparisons, it can be seen that using the methods suggested here the field strength can, in general, be predicted within 5 dB for 95% of the measurements taken. This statement is made on the basis of data taken from facilities operating in the frequency range of 233 to 391 KHz on terrain conditions of southern Ohio, Pennsylvania, Massachusetts, Connecticut, and New Hampshire. Possible sources of error in the measurement techniques are noise interference, terrain irregularities which significantly affect wave propagation, and receiver tolerance. The prediction accuracy is directly dependent upon the accuracy of the ERP value input to the computer model.

The presence of more irregularities in measurements of higher frequencies also suggests that these waves, as would be expected, are more affected by terrain irregularities and, in general, to all obstacles of propagation than are the lower frequencies. Signals of all frequencies at the low level used for NDB's are subject to noise interference which can significantly alter the signal strength measurement.

It has also been seen that the effective radiated power levels as determined by using the transmitter power values given in the Master Radio Frequency List are unreliable and, therefore, cannot be used in comparisons of absolute field strength. As was seen for all beacons for which ERP measurements were not made, the trend in the data was in agreement but the predicted value appeared to be shifted, sometimes up to 15 dB. The measurements of ERP presented in Table 2-1 indicate that a variation of this amount is certainly possible. Finally, data in Table 2-2 has shown that the presence of the aircraft does not significantly affect the measured values. Also, the agreement with the predicted values confirms the insignificance of the aircraft in introducing measurement error at these frequencies.

2. Air-Ground Correlation and the Effect of Receiver Altitude on Measured Field Strength. The previous discussion and its accompanying figures have illustrated that electric field strength in general can be reliably predicted. The comparisons of the theoretical curves with the measured data have been made without regard for the propagation path of the radio wave, and the agreement of the data in most cases strongly suggests that terrain irregularities of the magnitude found in the southern Ohio area do not have significant effects on radio wave propagation in the frequency range of 200-500 KHz. It does appear that the higher frequencies in this range exhibit more irregular data, showing that these shorter wavelength waves are more susceptible to not only terrain irregularities but to all obstacles along the propagation path, as can be expected.

In this section the feasibility of air-ground field strength correlation will be investigated and data is presented in Figures 2-29 through 2-31 that demonstrates this correlation. These figures show results of data taken on the NDB facilities located at Chillicothe, Ohio (236.51 KHz), Circleville, Ohio (366.51 KHz), and Columbus, Ohio (391.00 KHz), respectively. The plotted data represents data taken at exactly the same ground point but at various receiver altitudes, which are indicated by the appropriate symbol on the figure. Looking first to Figure 2-29, the data illustrated here suggests that there is a good correlation in air and ground measurements. For example, when the ground-based measurement is noticeably below the expected value at 12 nm, the flight data taken at 3500 feet and 7500 feet is also reduced. When the ground data increased again at 13 nm, flight data at 2500 and 7500 feet also reflects this change. This change in the ground data could be due to obstacles along the propagation path, whether by terrain irregularities or some type of metal structure large enough to affect the wave propagation. But whatever the cause of the variation, it is seen to be noticeable in the flight data as well. There is a trend throughout the entire range of data taken for this facility, from 2.4 to 18.5 nm, for the ground based data to demonstrate more irregularities than the airborne data. In other words, as altitude is increased, the data seems to be more regular and predictable indicating that as the receiver is elevated above the earth's surface the factors causing the variations in the data become less important. This can again be expected, since as the receiver moves away from an obstacle the effect of that obstacle should be less noticeable.

Comparisons made in Figure 2-30 for the Circleville, Ohio beacon lead to the same conclusions made for the Chillicothe beacon. The frequency here is higher (366.51 KHz) and it appears that all data exhibits more irregularity because of this. However, the air-ground measurement correlation is still evident when comparing measured field strength at distances of 7.8 and 9.5 nm. The data at 7.8, 11.3 and 13.0 nm also indicates repeatability of ground measurements. As indicated, two separate ground measurements have been made at each of these points, with agreement between the two always within 4.1 dB. The ground data for these points has been tabulated in Table 2-3.

Date \ Distance	Field Strength (dB Relative to 1 μV/m)		
	7.8 nm	11.3 nm	13.1 nm
8/3/79	36.0	42.7	32.0
8/13/79	38.1	39.1	36.1

Table 2-3. Repeatability of Ground-Based Measurements Chillicothe, Ohio Beacon.

Figure 2-31 has been prepared using data for the Columbus, Ohio beacon and again demonstrates that airborne and ground-based data can be correlated. The more apparent example of this is evident at 20.5 nm where all data, air and ground, is above the norm for that distance. Again in this figure, though the air-ground correlation is evident, it is also seen that the higher altitude measurements (7500 feet) are far more regular and apparently are less affected by propagation obstacles than are the ground-based measurements. This has already been explained concerning Figure 2-29, but the irregularities here of ground-based measurements are more noticeable, possibly due to the higher operating frequency of this facility.

The good agreement between all airborne measurements regardless of altitude in Figures 2-29 through 2-31 is also illustrated in Tables 2-4 through 2-8. The data presented in these tables has been taken over the same point at various altitudes. These tables are also arranged in order of increasing frequency for the beacons for which data of this type was available.

Table 2-4 shows data taken on the Cambridge, Ohio NDB at distances of 14.0 and 16.7 nm for altitudes ranging from 2000 to 7000 feet. All points vary by not more than 3.7 dB at the 14.0 nm distance and not more than 1.5 dB at a distance of 16.7 nm from the beacon. This agreement is good, but actually is found to be among the worst found for all the beacons considered. For instance, Table 2-5 for the Albany, Ohio facility demonstrates a variation of 0.2 dB for a distance of 3.5 nm and altitudes of 2500 to 5500 feet for measurements taken 7/3/79. Also included with some measurements in this table is data regarding repeatability of measured field strength. For four distances data taken 7/3/79 was repeated as a check on 8/3/79 and for another distance on 8/8/79. These points show good agreement between the measured data for all dates, the maximum deviation being 2.3 dB, within tolerance of the receiver. As for effects of altitude on measurements from this beacon, agreement is within 2.4 dB for all measurements at any distance taken at the same time. Thus these tables show that the effects of altitude on field strength from NDB's is negligible, and the slight variation illustrated in the data could be caused by noise interference, as nearly all agreement is within the tolerance of the standard used to calibrate the receiver, the Fairchild EMC-25 selective voltmeter.

Altitude (Feet)	Field Strength 14.0 nm from Beacon (dB Relative to 1 μV/m)	Field Strength 16.6 nm from Beacon (dB Relative to 1 μV/m)
2000		41.4
2500	41.9	
3000		41.9
4000	40.9	42.5
5000		40.9
5500	43.3	
6000		40.9
7000	44.6	41.1
	Variation = 3.7 dB	Variation = 1.6 dB

Table 2-4. Effect of Receiver Altitude Cambridge, Ohio Beacon (223.51 KHz). Measurements taken 9/15/79 with Cherokee equipped with King ADF receiver (distances are ground track).

Altitude (Feet)	Field Strength (dB Relative to 1 μV/m)								
	Ground Track from Beacon (nm)								
	3.5	4.5		4.7	5.3		5.4	6.1	20.7
0					58.3				
500					57.86				
1000					57.9				
1500						57.3			
2000	62.7*			59.2*	58.1	56.9		55.1	
2500	60.8	60.4	60.8	56.9	56.6	57.3	57.9	55.1*	
3000	60.8	59.9		56.		56.4		56.6	
3500	60.6	60.4	61.0	57.3		56.9	57.3	55.1	
4000	60.8	59.2		57.9		55.4		55.1	44.3
4500	60.8	59.0	60.6	56.4		55.7		55.7	
5000						55.7	57.3		
5500		59.5				56.1	57.9	55.7	
6000						55.7	58.4		43.9
6500						55.1	57.9		
7000						55.1	57.6		
7500						54.9	56.6		44.1
Date of Measurement	7/3/79 *8/3/79	7/3/79	8/3/79	7/3/79 *8/3/79	7/3/79	8/8/79	9/15/79	7/3/79 *8/3/79 repeated	9/15/79

Table 2-5. Effect of Receiver Altitude Albany, Ohio Beacon (250 KHz). Data taken with Cherokee equipped with King ADF receiver.

Table 2-6 presents data from the Zanesville, Ohio beacon at distances of 23.0 nm and 28.1 nm and differences of 2.5 dB are shown in each for altitudes ranging from 2500 to 7500 feet. Table 2-7 shows results of measurements from the Gallipolis, Ohio beacon showing variation of field strength with altitude and allows a check on repeatability of measurements as well. At 5.7 nm from this facility the measured field strength variation from 1500 to 7500 feet is 2.9 dB, with measurements showing repeatability within 1.2 dB. Checking measurements at 8.0 nm, the largest difference in the data taken at different times occurs at 7000 feet and is 1.3 dB. Viewing the two sets of data separately, the 8/8/79 data has an agreement of 1.5 dB for altitudes from 2000 to 8500 feet, and the 9/15/79 data agrees within 2.7 dB from 2000 to 8000 feet. Finally, Table 2-8 shows data taken 18.15 nm from the NDB located at Columbus, Ohio on 7/3/79, which agrees within 2.4 dB for an altitude range from 2500 to 7600 feet. Note that in Tables 2-6 through 2-8, the agreement of the data with altitudes varying is very good, even though data from these higher frequency beacons has displayed more scattering than the beacons operating at lower frequencies. Therefore, as suggested by Figures 2-29 through 2-31, the factors causing variation in field strength affect measurements at all altitudes.

The tabular data presented in this section has illustrated that receiver altitude is not a major factor in electric field strength measurements for NDB's. In fact, the measurements are well within the receiver tolerance for nearly all cases. The data has also shown that a correlation does exist between air and ground-based data. When the measured ground-based field strength measurement is lower than the norm for any given distance, the flight data reflects this fact also. All data taken also demonstrates that the field strength measurements made in this report are repeatable, which results in confidence in the measurement technique as well as the conclusions arising from these measurements. Finally, it is shown by the good agreement (usually within 5 dB) between airborne measurements and predictions that the presence of the aircraft does not significantly alter the electric field at these frequencies.

Altitude	Field Strength (dB Relative to 1 μV/m)at	
	2.3 nm	28.1 nm
2500		35.4
3000	57.3	
3500		34.2
4500	58.0	34.5
5500		37.1
6000	55.5	
6500		36.0
7500	57.3	37.3

Table 2-6. Effect of Receiver Altitude Zanesville, Ohio Beacon (332.00 KHz). Measurements taken 9/15/79 with Cherokee equipped with King ADF receiver (distances are ground track).

Altitude	Field Strength (dB Relative to 1 μV/m) at			
	5.7 nm		8.0 nm	
1500	44.7	44.5		
2000	44.1	42.9	42.7	42.7
2500		43.1	42.6	
3000		43.1		42.1
3500		42.9		42.3
4000				42.2
4500				41.8
5000			42.9	42.0
5500		45.6	42.6	41.8
6000			42.2	42.1
6500		45.6	42.0	41.8
7000			42.0	40.7
7500		45.8	41.6	41.2
8000				40.0
Date	8/8/79	9/15/79	8/8/79	9/15/79

Table 2-7. Effect of Receiver Altitude Gallipolis, Ohio Beacon (362.51 KHz). Measurements taken with Cherokee equipped with King ADF receiver (distances are ground track).

Altitude	Field Strength (dB Relative to 1 μV/m) at 18.15 nm
2500	49.9
3000	49.1
3500	48.9
4500	49.1
5500	48.9
6500	47.8
7500	50.2
7600	49.5

Table 2-8. Effect of Receiver Altitude Columbus, Ohio Beacon (391 KHz). Measurements taken 7/3/79 with Cherokee equipped with King ADF receiver (distances are ground track).

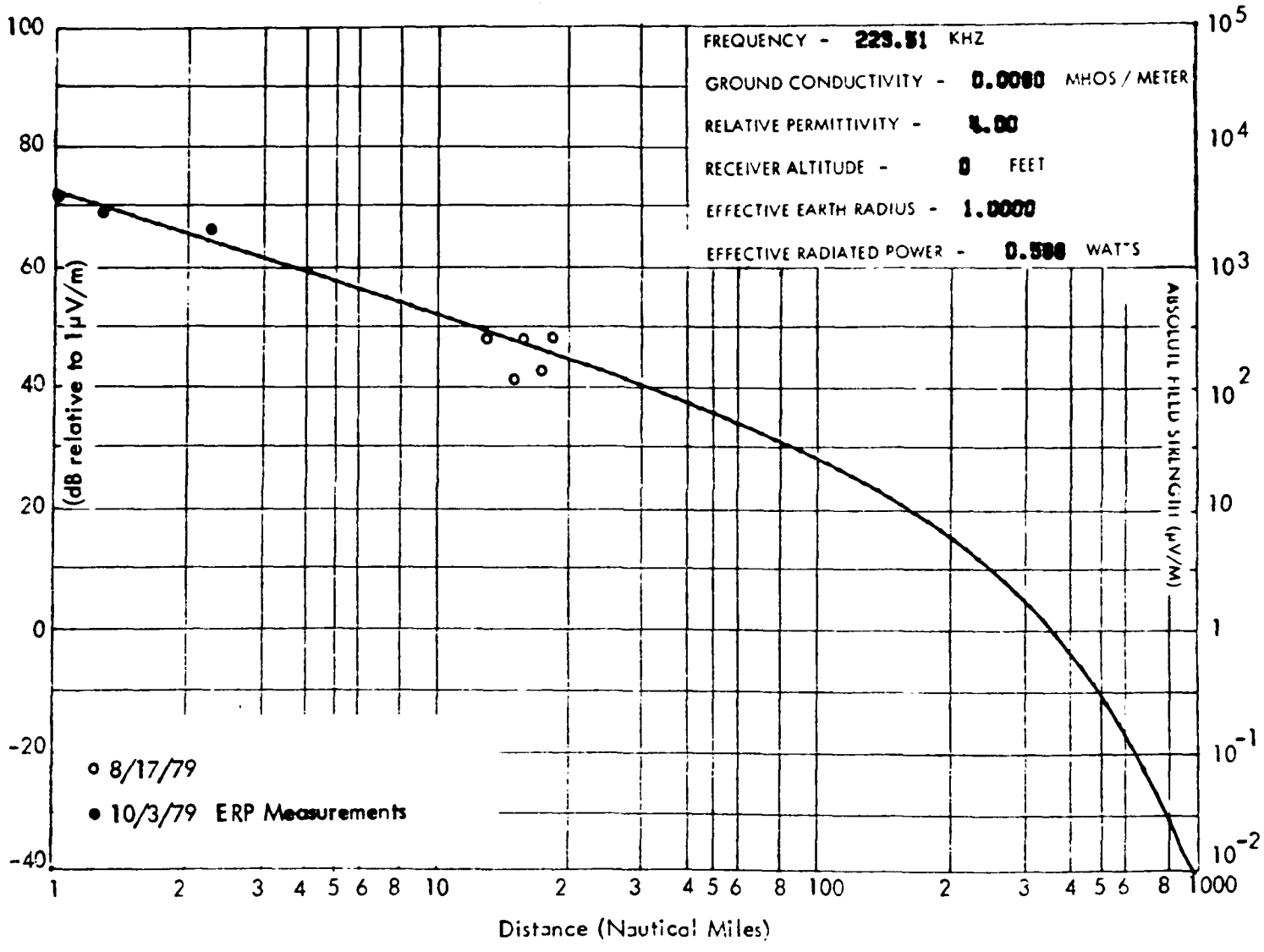

Figure 2-5. Ground Level Measurements on Cambridge, Ohio Beacon. Coordinates: 39°57'50"N, 81°35'18"W; Call Sign: CDI; Transmitter Power: 25 watts.

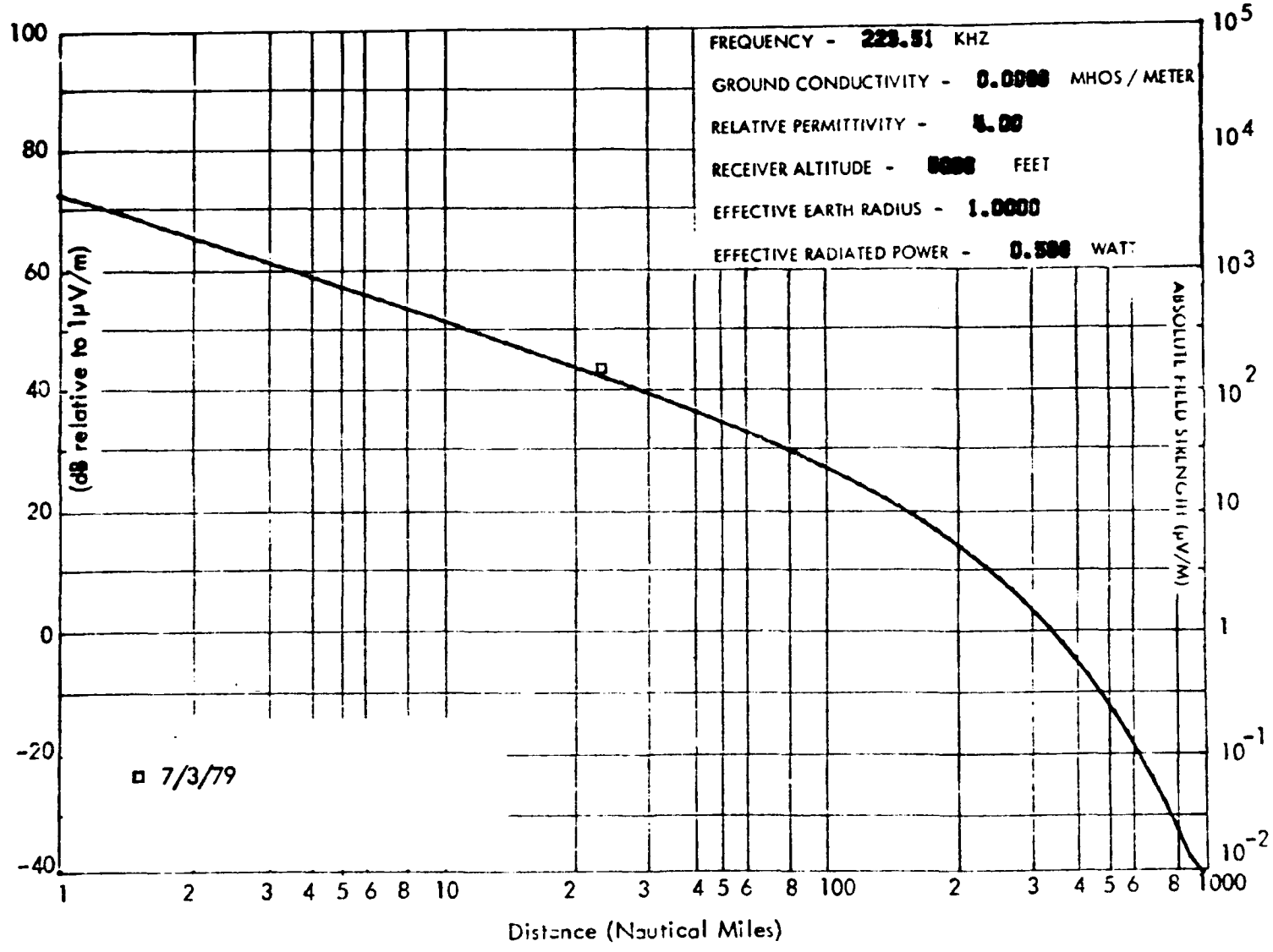

Figure 2-6. Flight Data on Cambridge, Ohio Beacon. Coordinates: 39°57'50"N, 81°35'18"W; Call Sign: CDI; Transmitter Power: 25 watts.

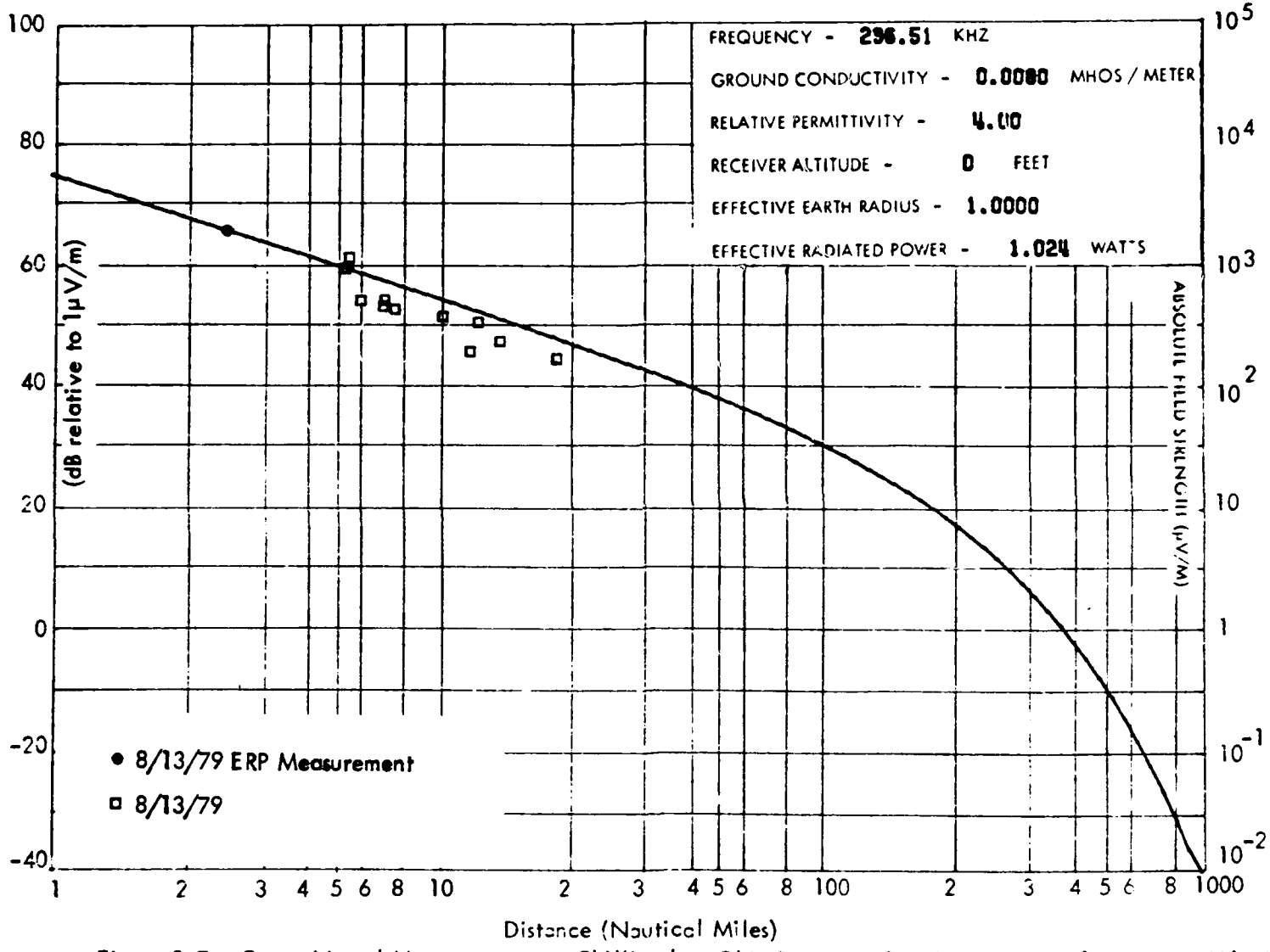

Figure 2-7. Ground Level Measurements on Chillicothe, Ohio Beacon. Coordinates: 39°26'22"N, 83°01'39"W; Call Sign: RZT: Transmitter Power: 25 watts.

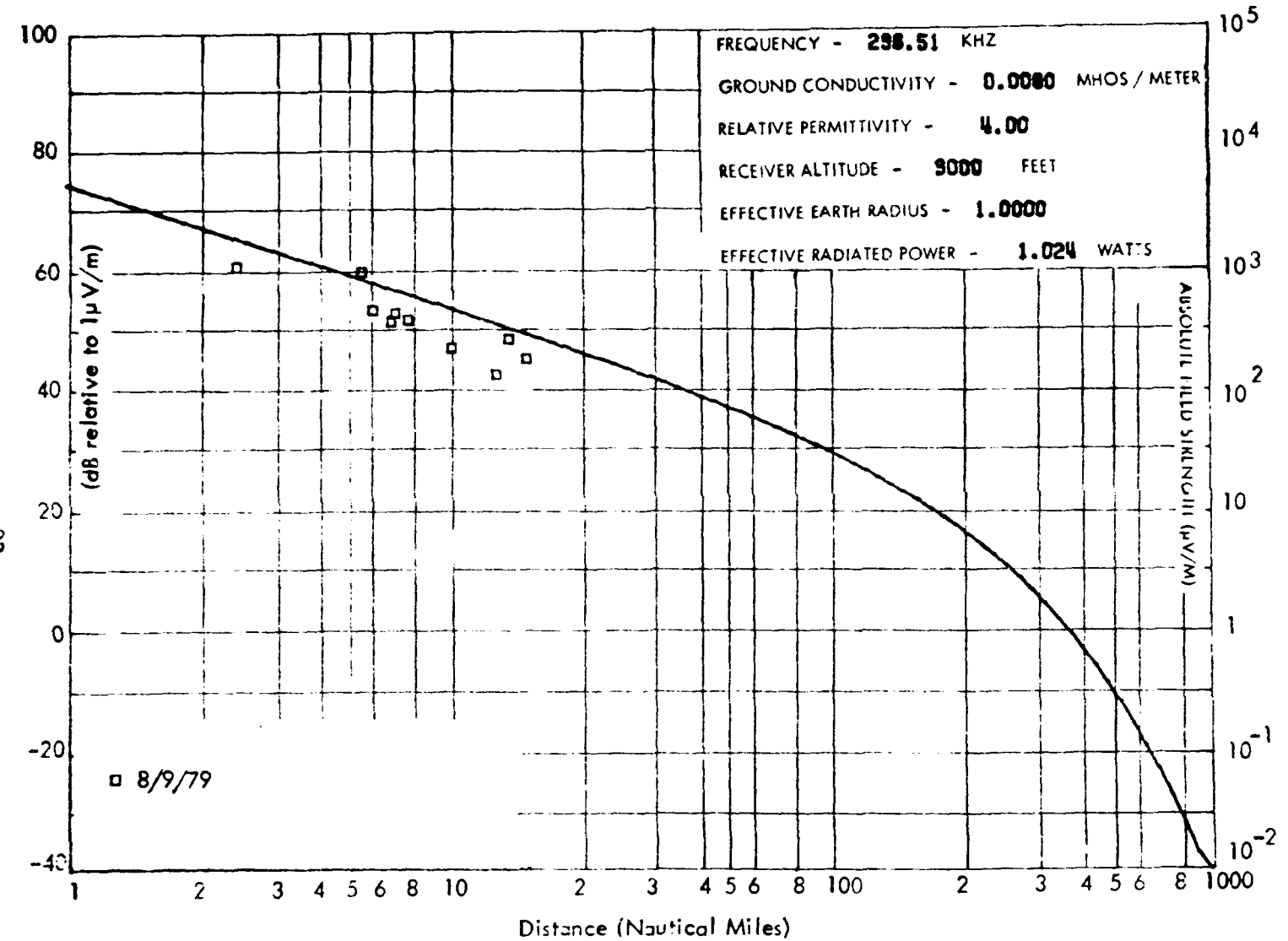

Figure 2-8. Flight Data on Chillicothe, Ohio Beacon. Coordinates: 39°26'22"N,83°01'39"W; Call Sign: RTZ; Transmitter Power: 25 watts.

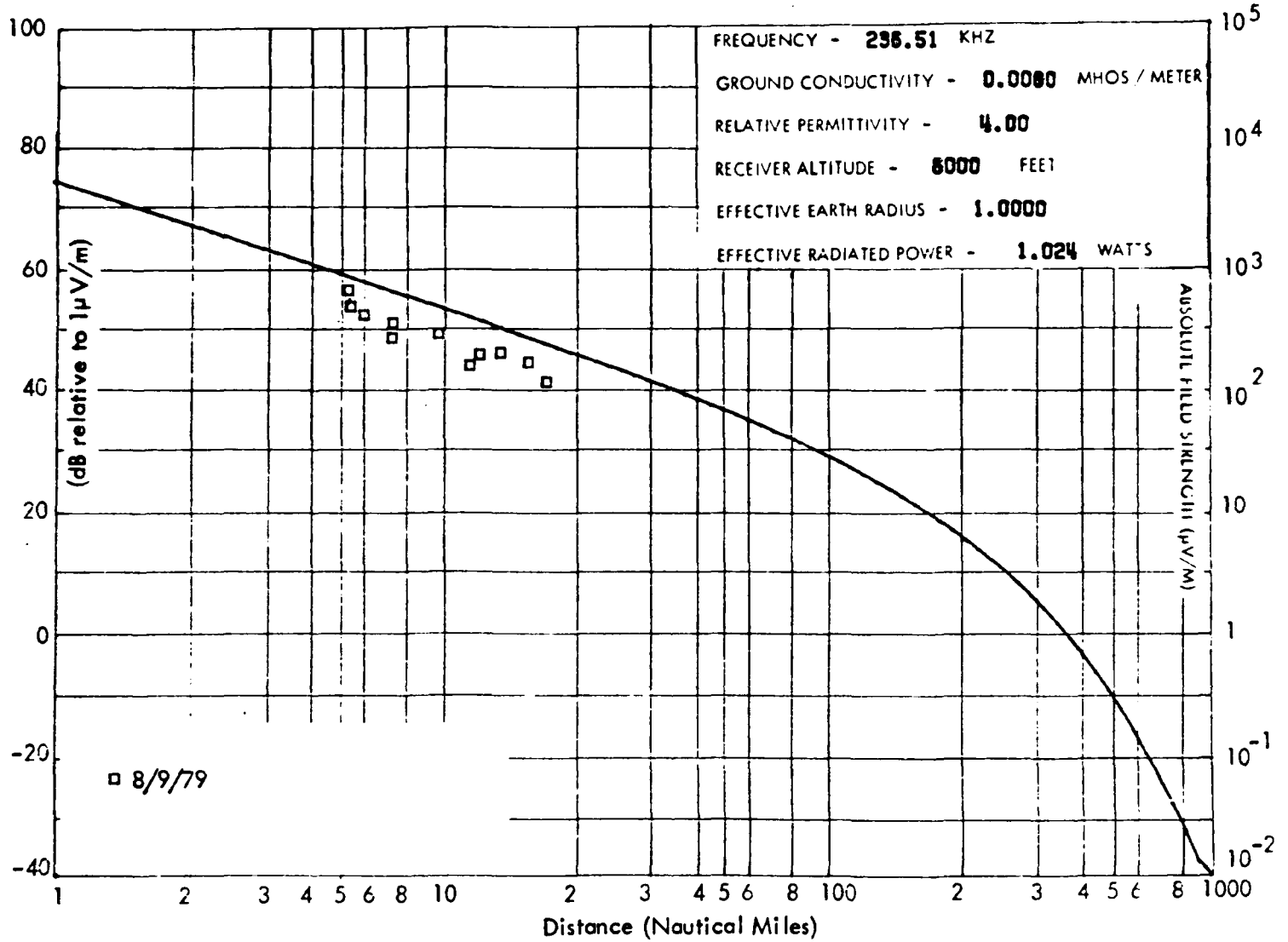

Figure 2-9. Flight Data on Chillicothe, Ohio Beacon. Coordinates: 39°26'22"N,83°01'39"W; Call Sign: RTZ; Transmitter Power: 25 watts.

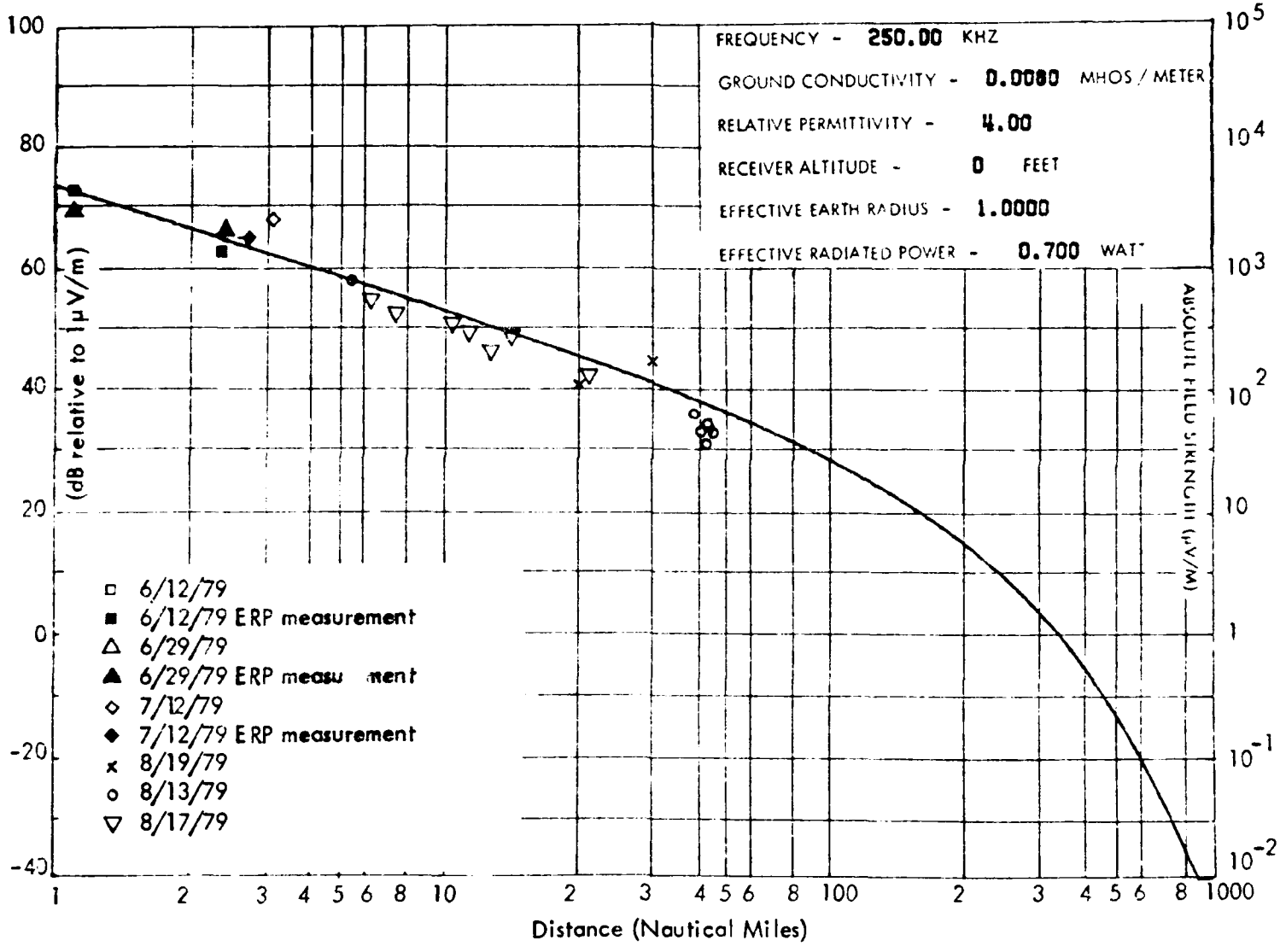

Figure 2-10. Ground Level Data on Albany, Ohio Beacon. Coordinates: 39°16'03"N, 82°07'44"W; Call Sign: UNI; Transmitter Power: 25 watts.

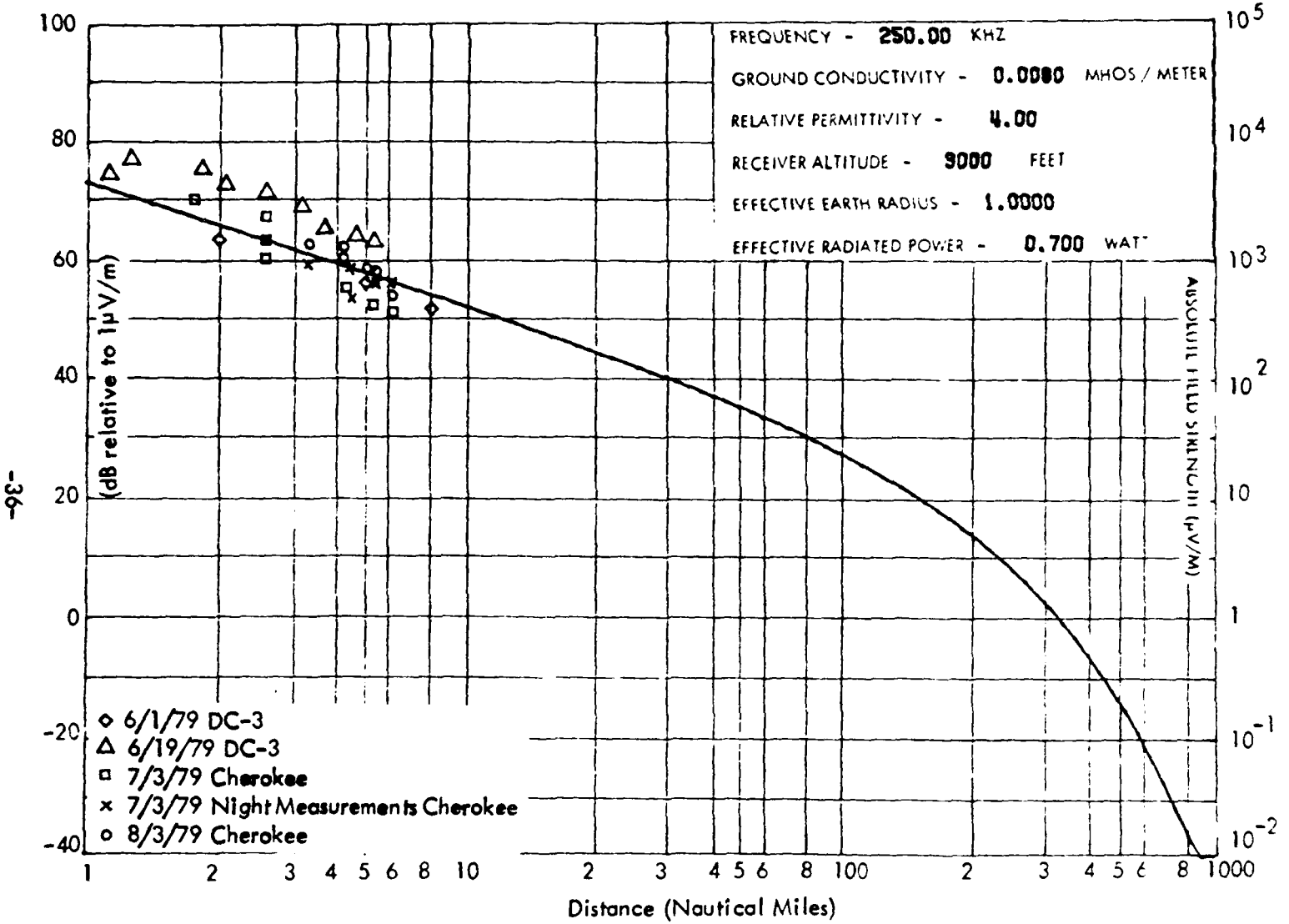

Figure 2-11. Flight Data on Albany, Ohio Beacon. Coordinates: 39°16'03"N,82°07'44"W; Call Sign: UNI; Transmitter Power: 25 watts.

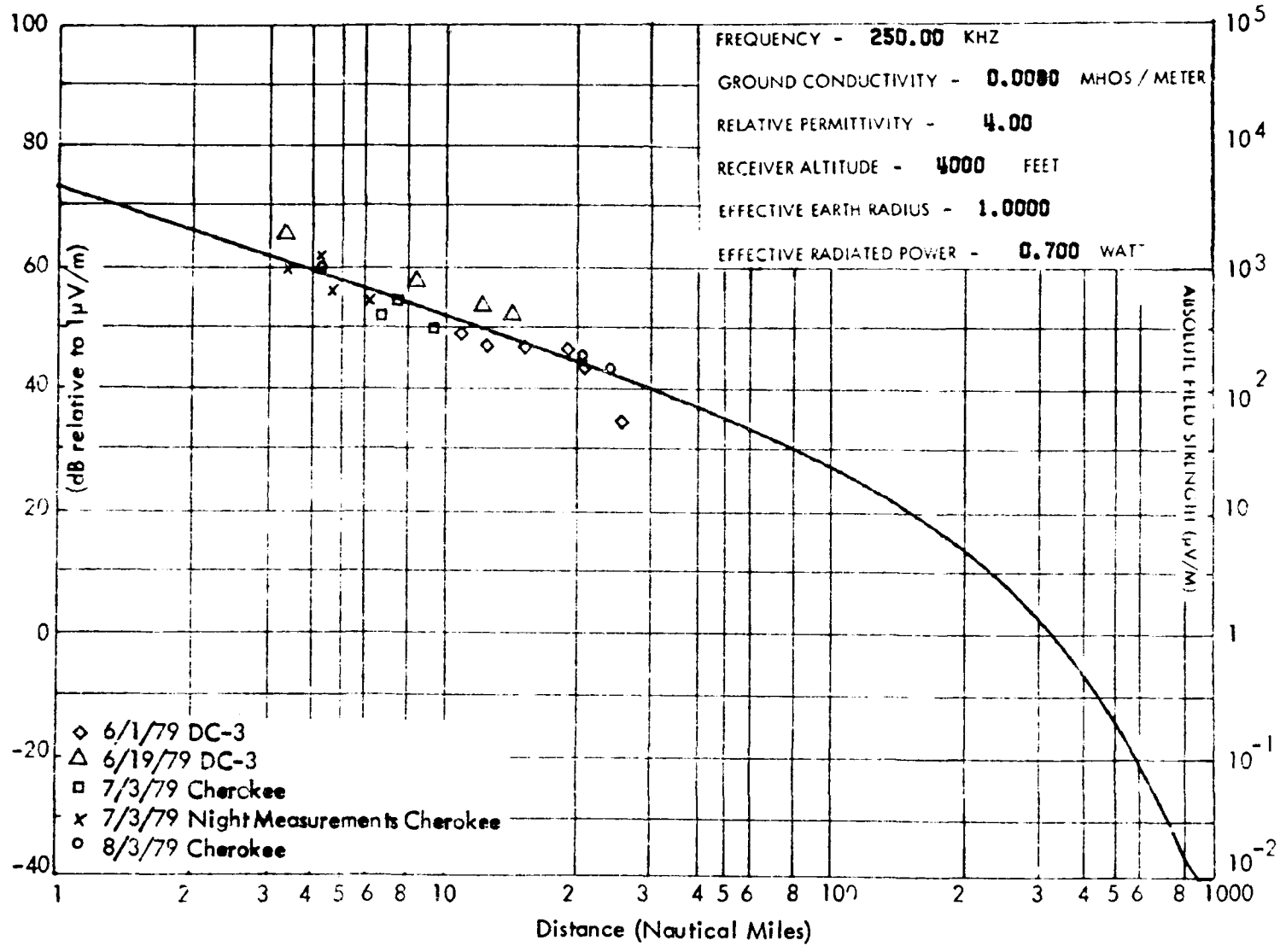

Figure 2-12. Flight Data on Albany, Ohio Beacon. Coordinates: 39°16'03"N,82°07'44"W; Call Sign: UNI; Transmitter Power: 25 watts.

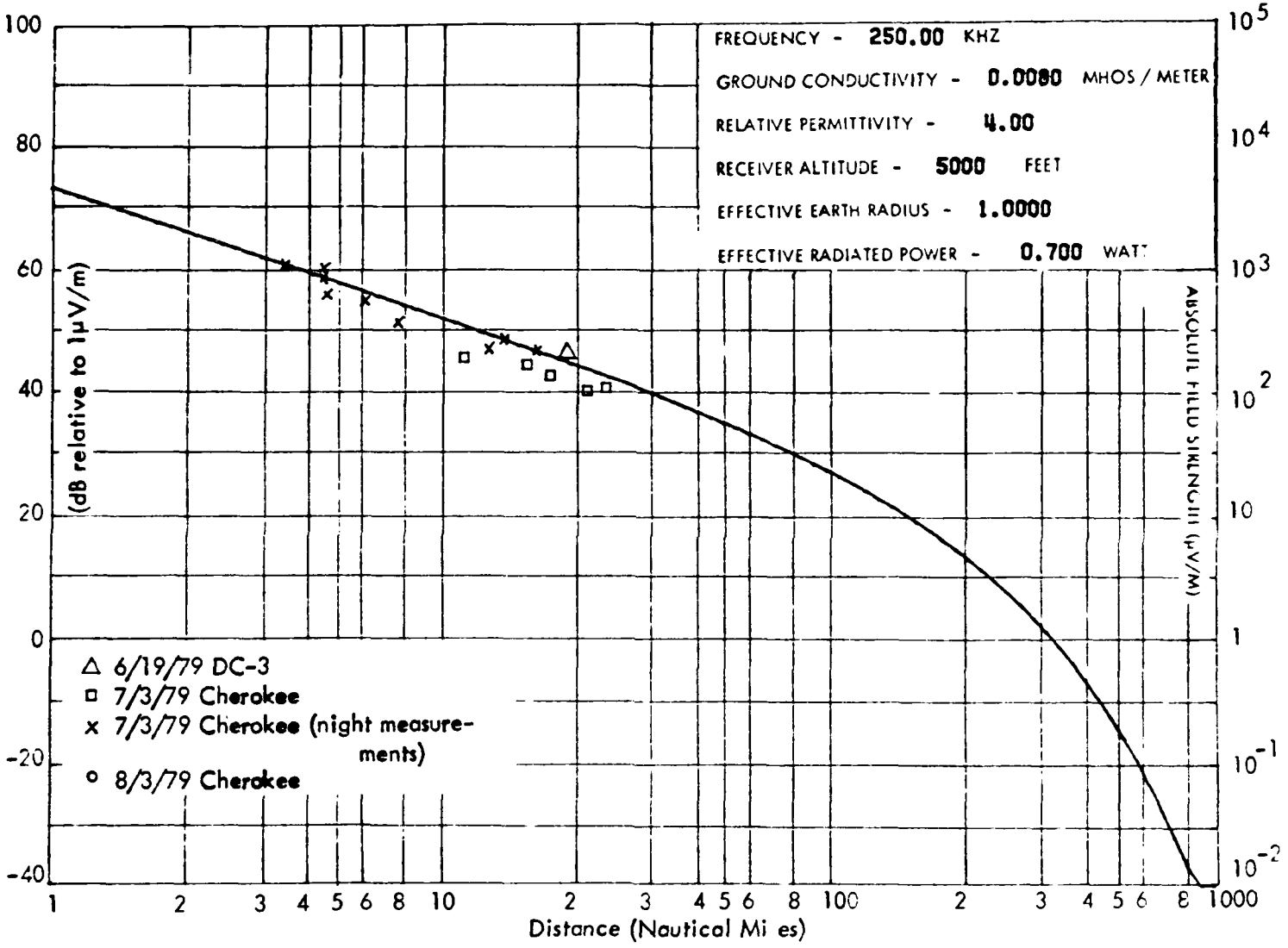

Figure 2-13. Flight Data on Albany, Ohio Beacon. Coordinates: 39°16'03"N,82°07'44"W; Call Sign: UNI; Transmitter Power: 25 watts.

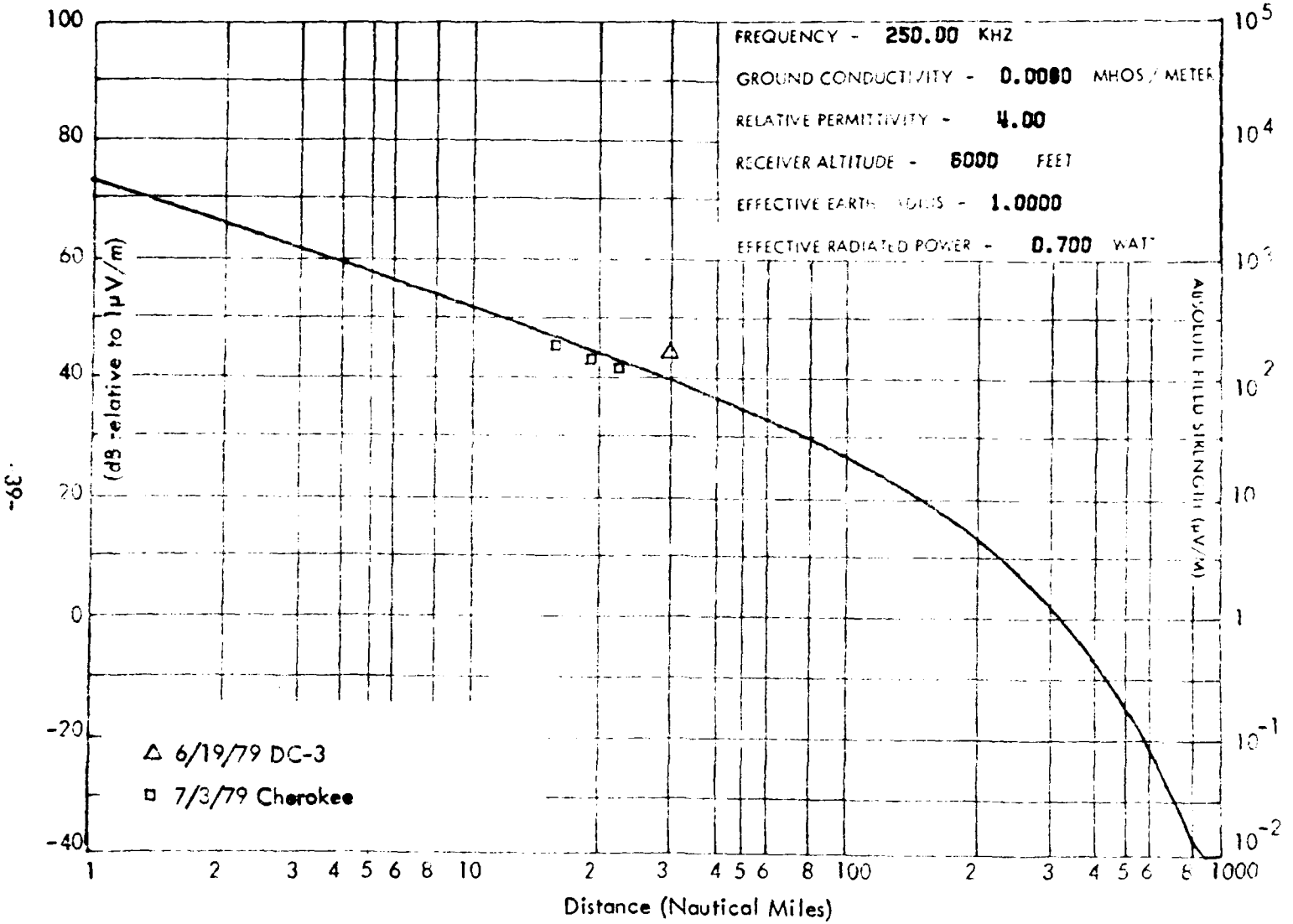

Figure 2-14. Flight Data on Albany, Ohio Beacon. Coordinates: 39°16'03"N, 82°07'44"W; Call Sign: UNI; Transmitter Power: 25 watts.

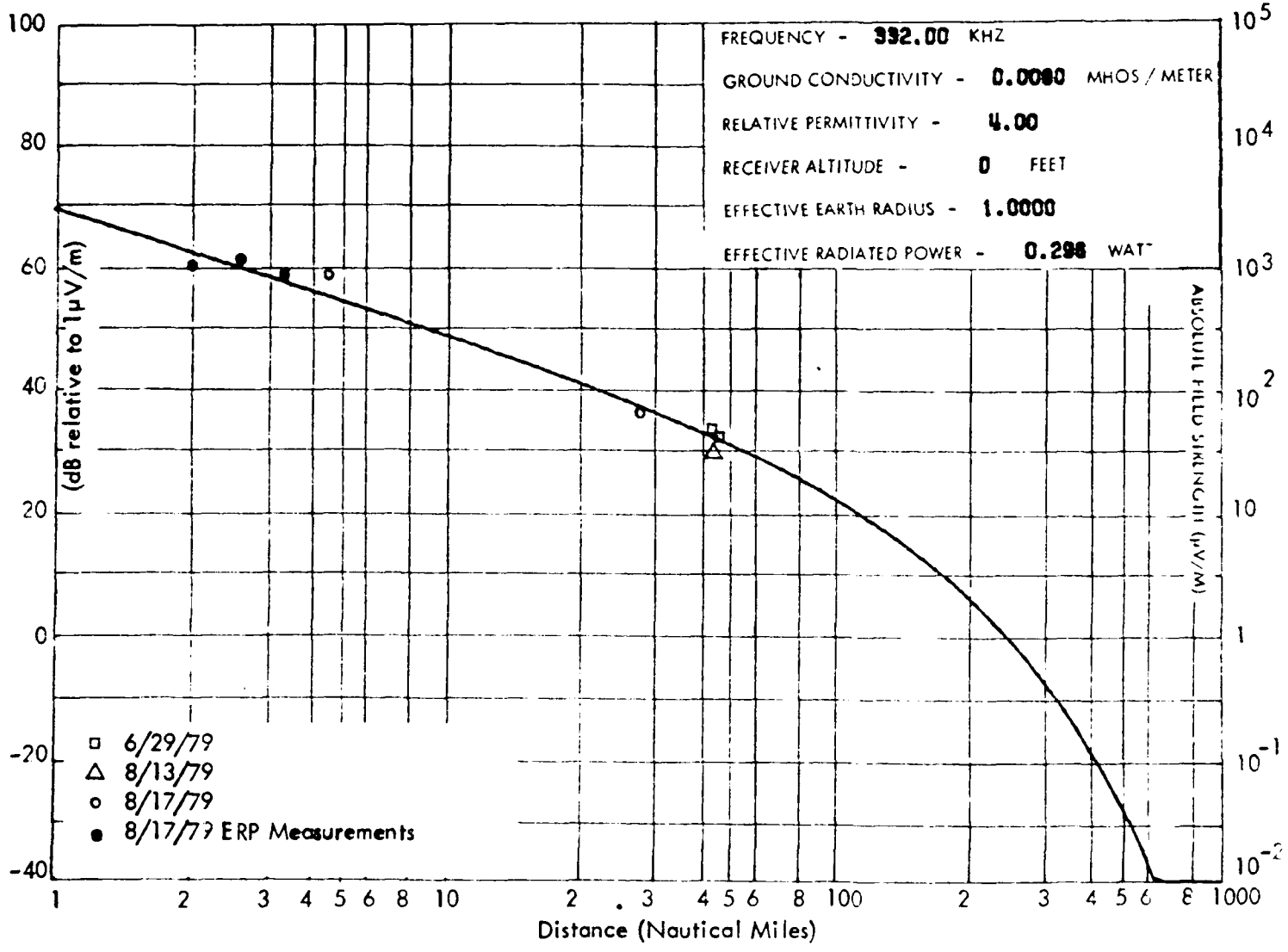

Figure 2-15. Ground Level Data on Zanesville, Ohio Beacon. Coordinates: 39°54'29"N,81°55'10"W; Call Sign: ZZV; Transmitter Power: 25 watts.

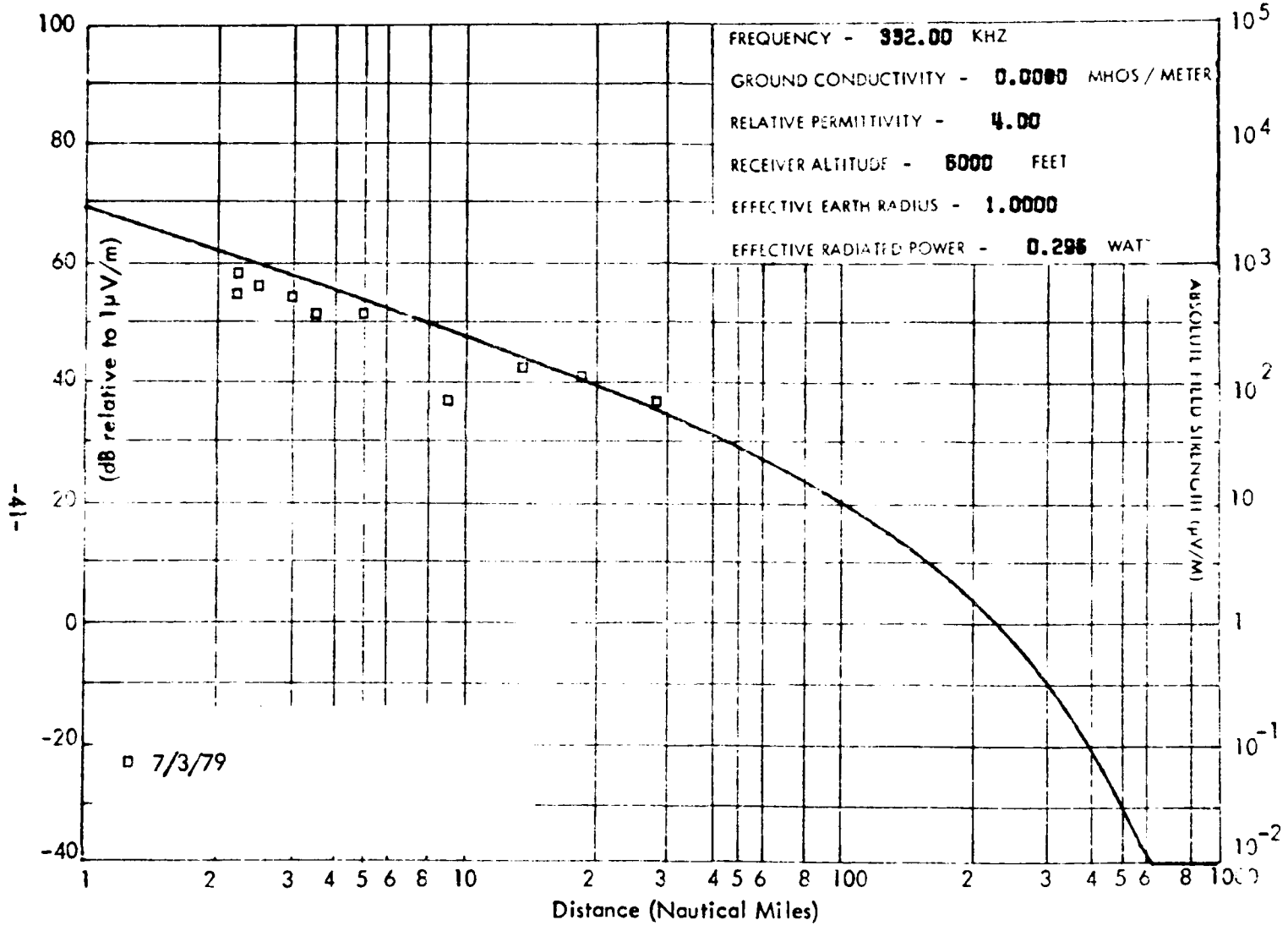

Figure 2-16. Flight Data on Zanesville, Ohio Beacon. Coordinates: 39°54'29"N,81°55'10"W; Call Sign: ZZV: Transmitter Power: 25 watts.

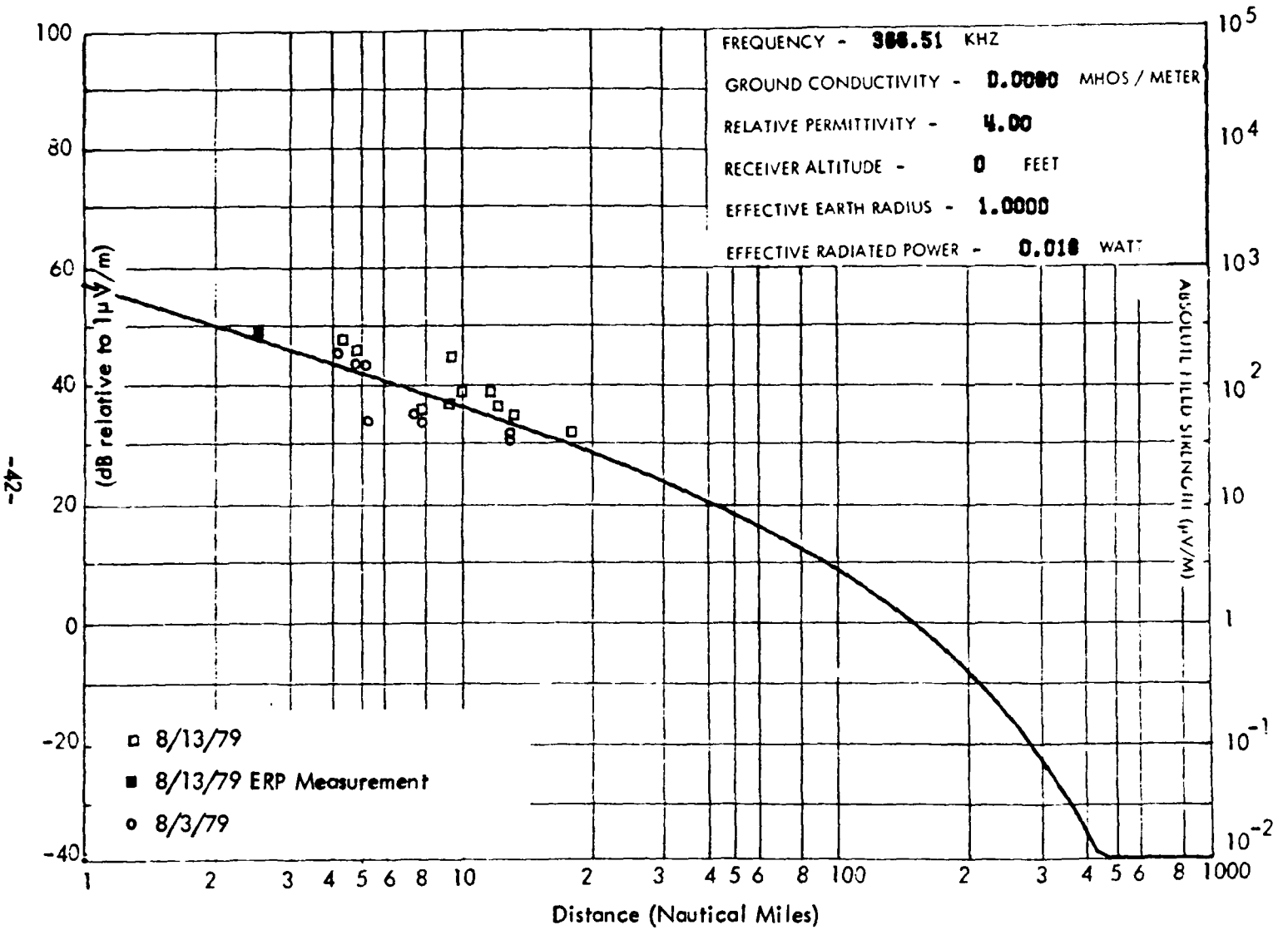

Figure 2-17. Ground Level Data on Circleville, Ohio Beacon. Coordinates: 39°31'11"N, 82°58'47"W; Call Sign: CYO; Transmitter Power: 25 watts.

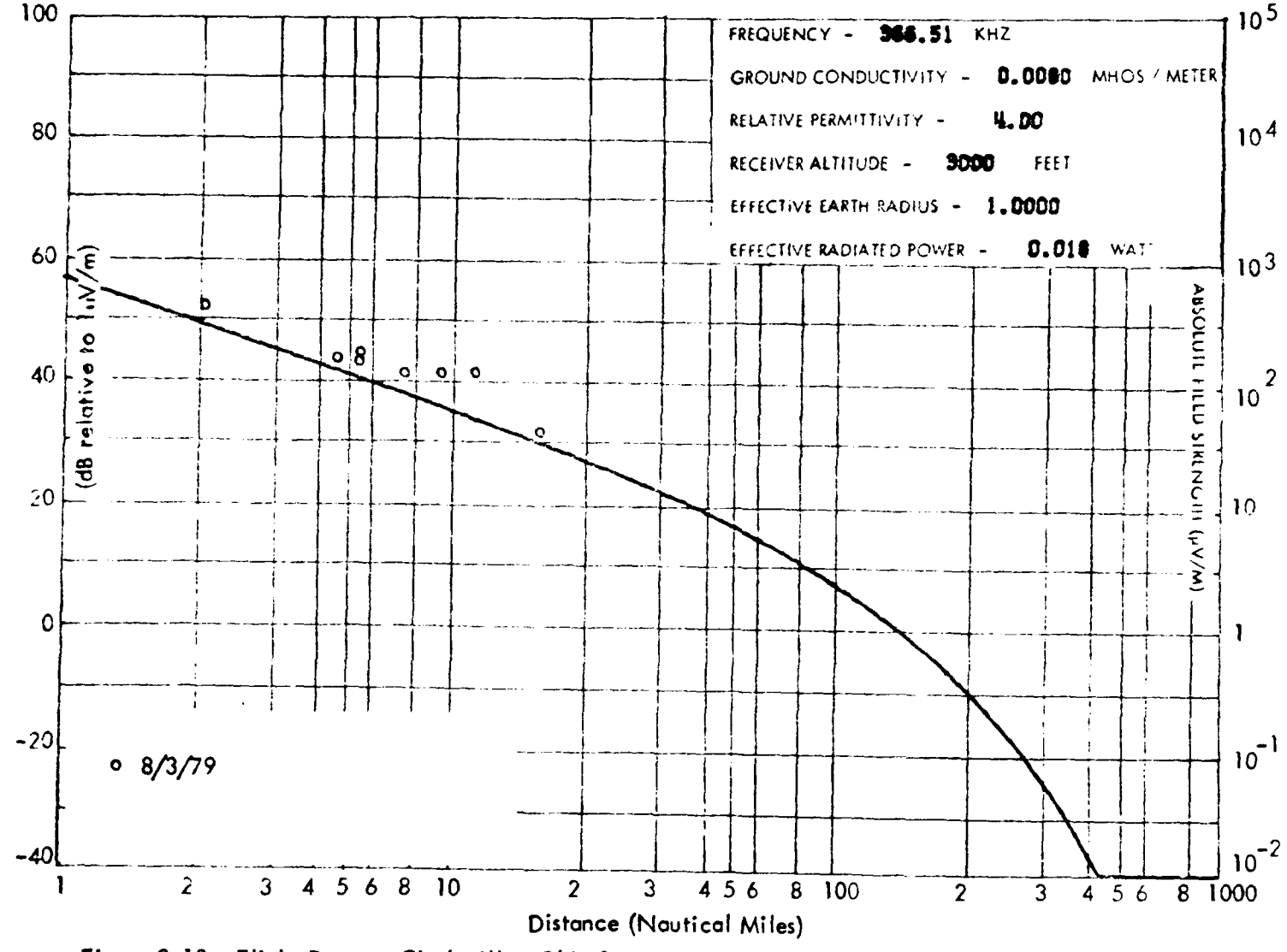

Figure 2-18. Flight Data on Circleville, Ohio Beacon. Coordinates: 39°31'11"N,82°58'47"W; Call Sign: CYO; Transmitter Power: 25 watts.

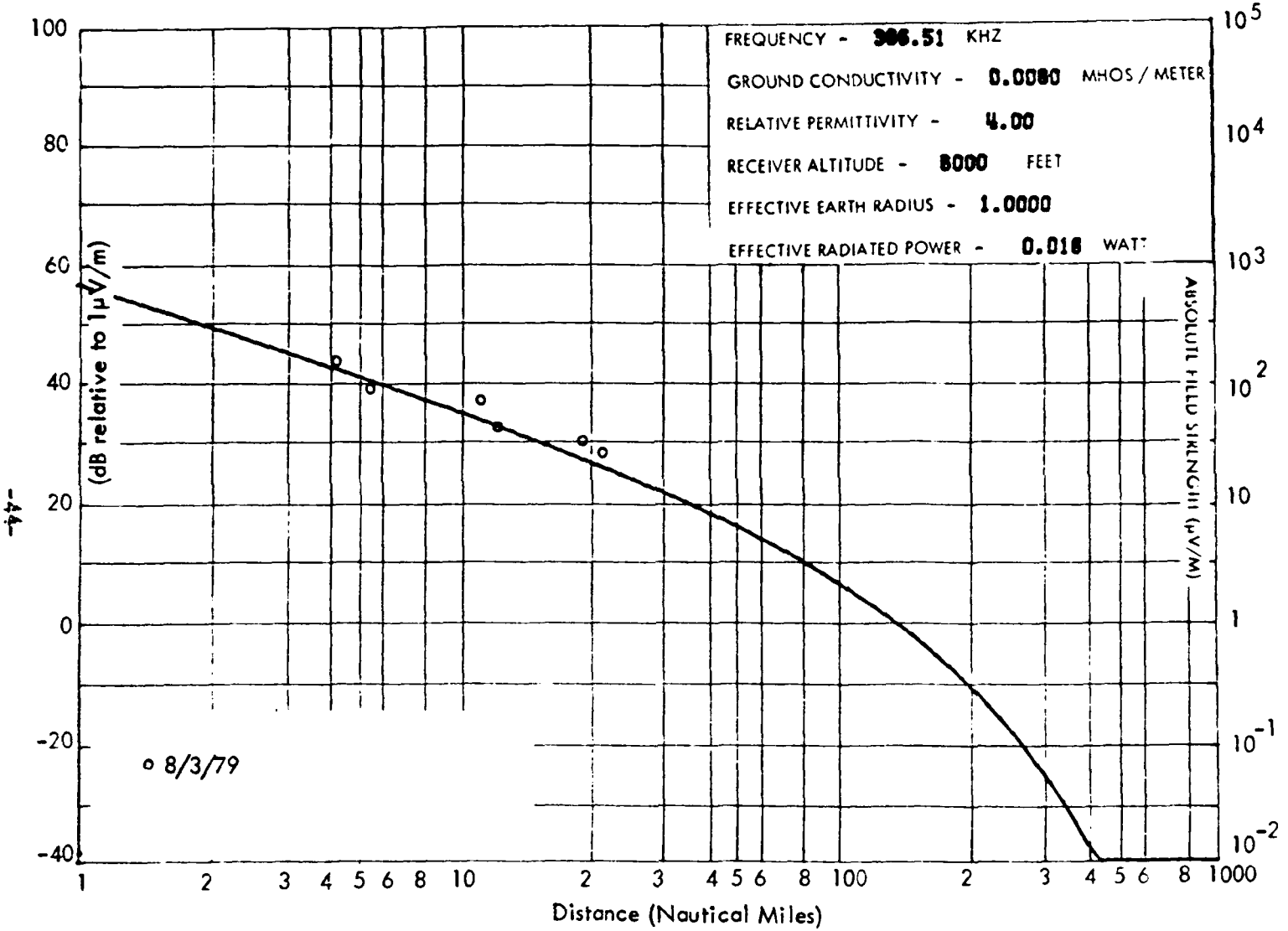

Figure 2-19. Flight Data on Circleville, Ohio Beacon. Coordinates: 39°31'11"N,82°58'47"W; Call Sign: CYO; Transmitter Power: 25 watts.

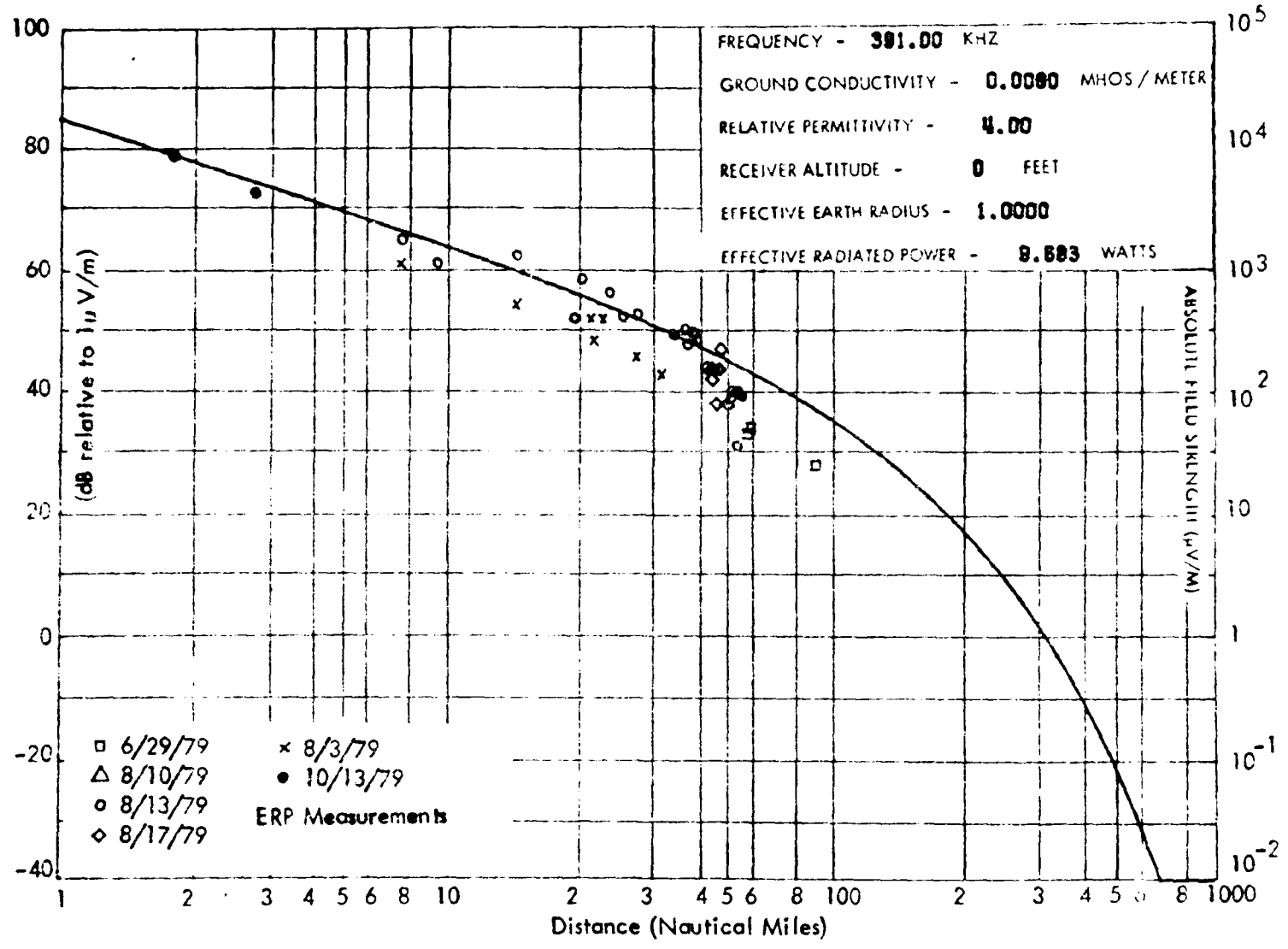

Figure 2-20. Ground Level Data on Columbus, Ohio Beacon. Coordinates: 39°51'19"N, 82°55'17.7W; Call Sign: CMH; Transmitter Power: 78 watts.

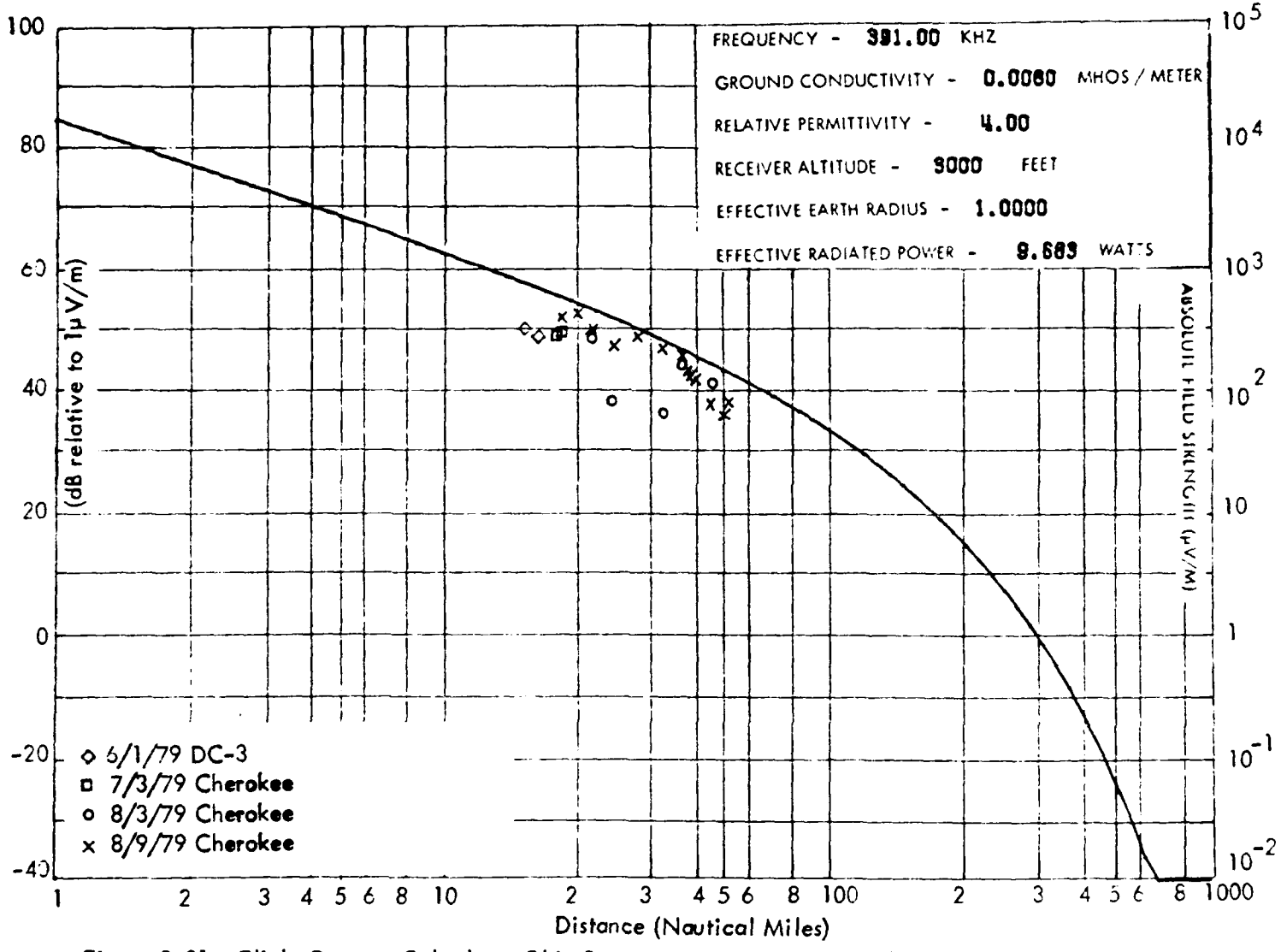

Figure 2-21. Flight Data on Columbus, Ohio Beacon. Coordinates: 39°59'19"N,82°55'17.7W: Call Sign: CMH; Transmitter Power: 78 watts.

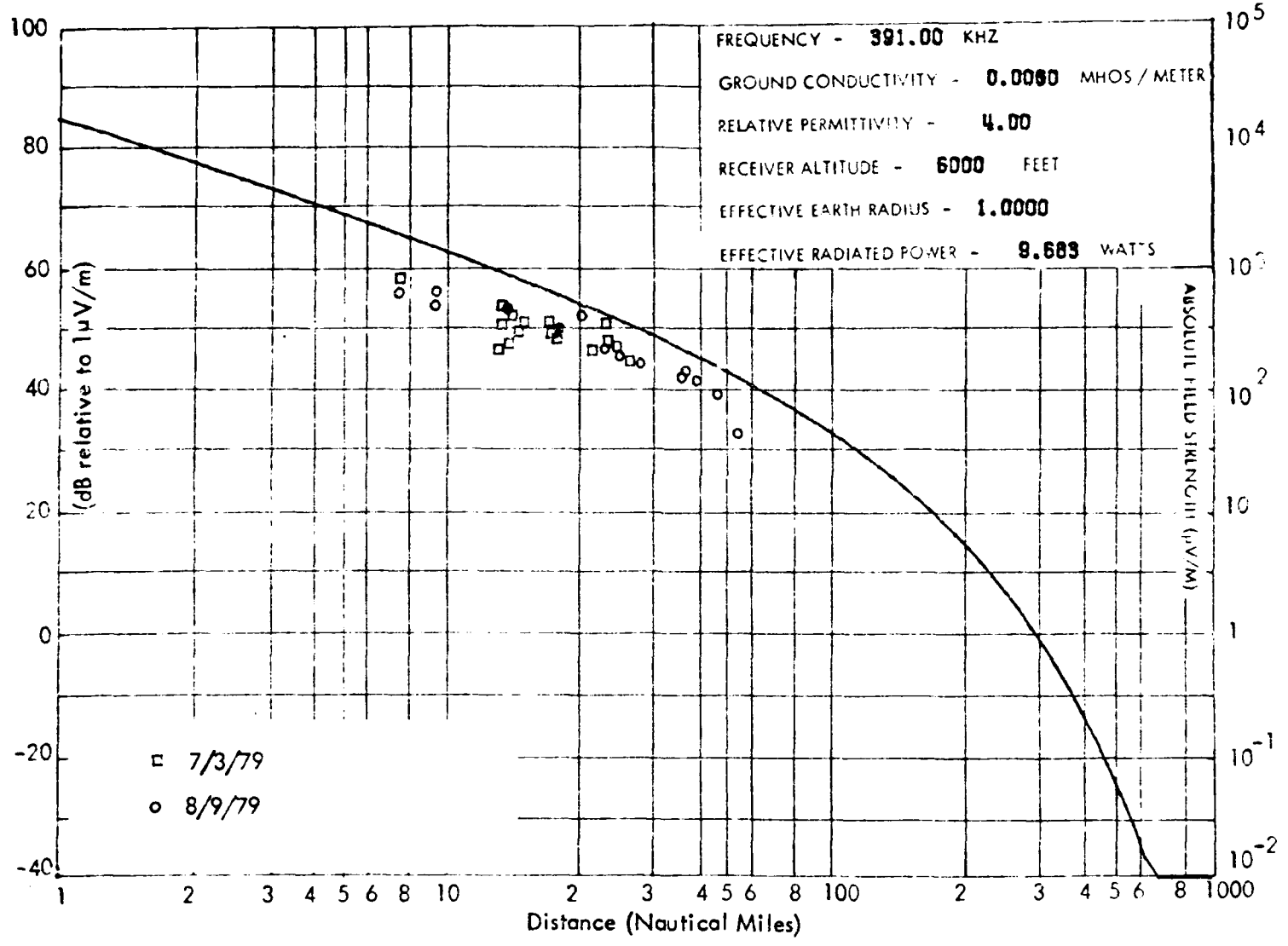

Figure 2-22. Flight Data for Columbus, Ohio Beacon. Coordinates: 39°59'19"N, 82°55'17.7"W; Call Sign: CMH; Transmitter Power: 78 watts.

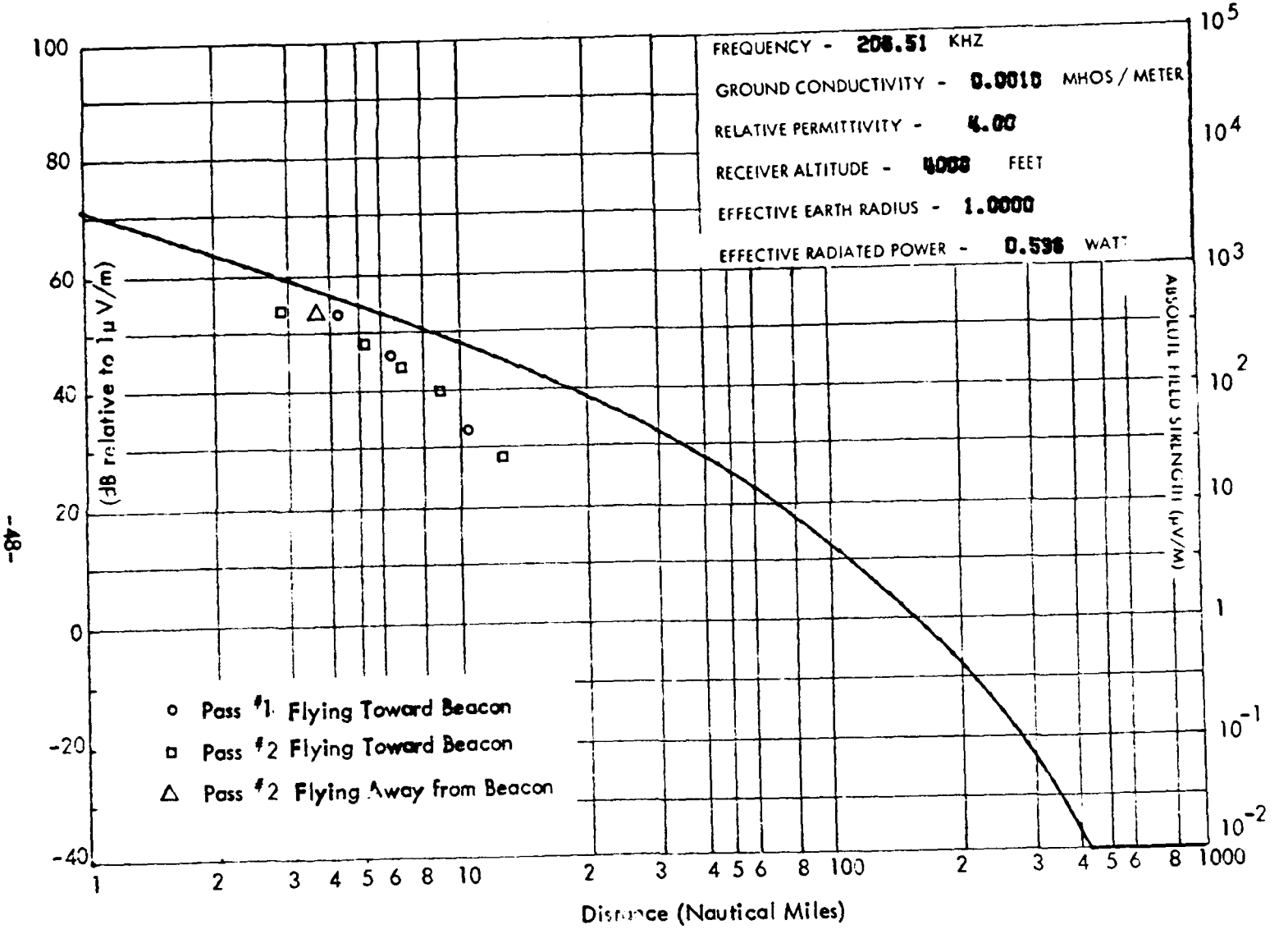

Figure 2-23. Flight Data for Fitchburg, Massachusetts Beacon; 6/19/79; DC-3. Coordinates: 42°33'20"N, 71°45'20"W; Call Sign: FIT; Transmitter Power: 25 watts.

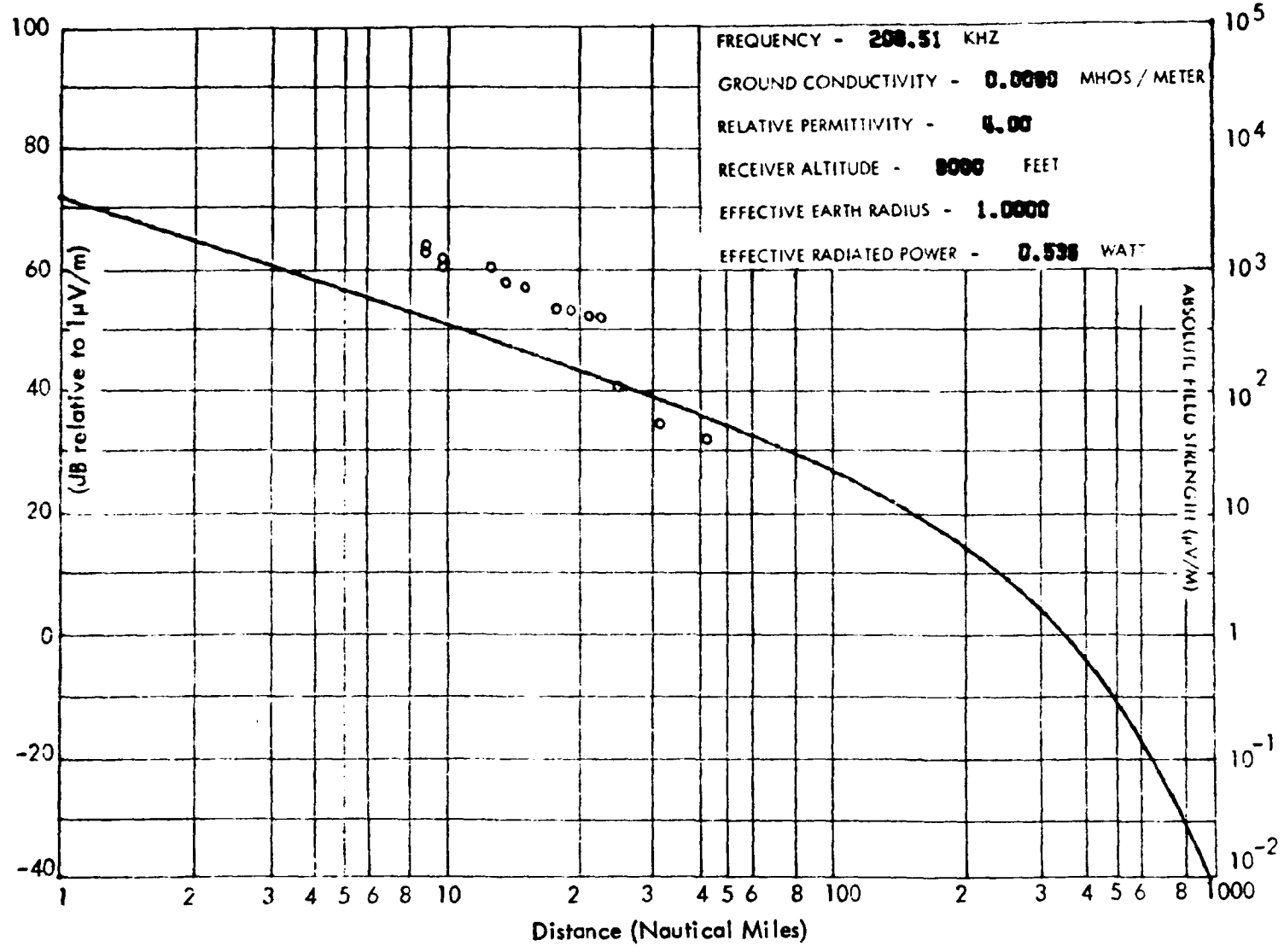

Figure 2-24. Flight Data on Stoystown, Pennsylvania Beacon; 6/19/79; DC-3. Coordinates: 40°05'09"N, 78°55'00"W; Call Sign: SYS; Transmitter Power: 25 watts.

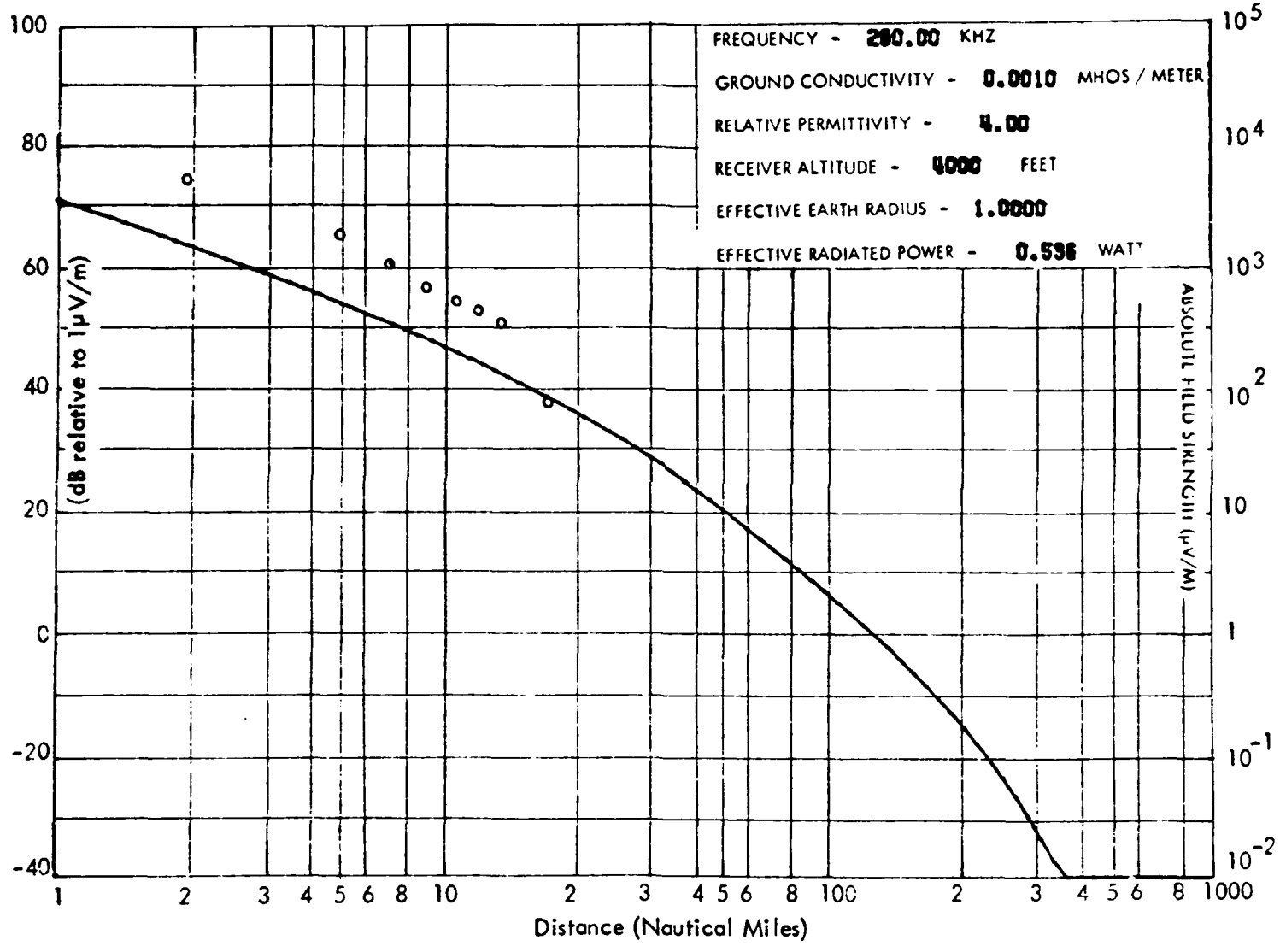

Figure 2-25. Flight Data on Amherst, New Hampshire Beacon; 6/19/79; DC-3. Coordinates: 42°49'05"N, 71°35'35"W; Call Sign: AMH; Transmitter Power: 25 watts.

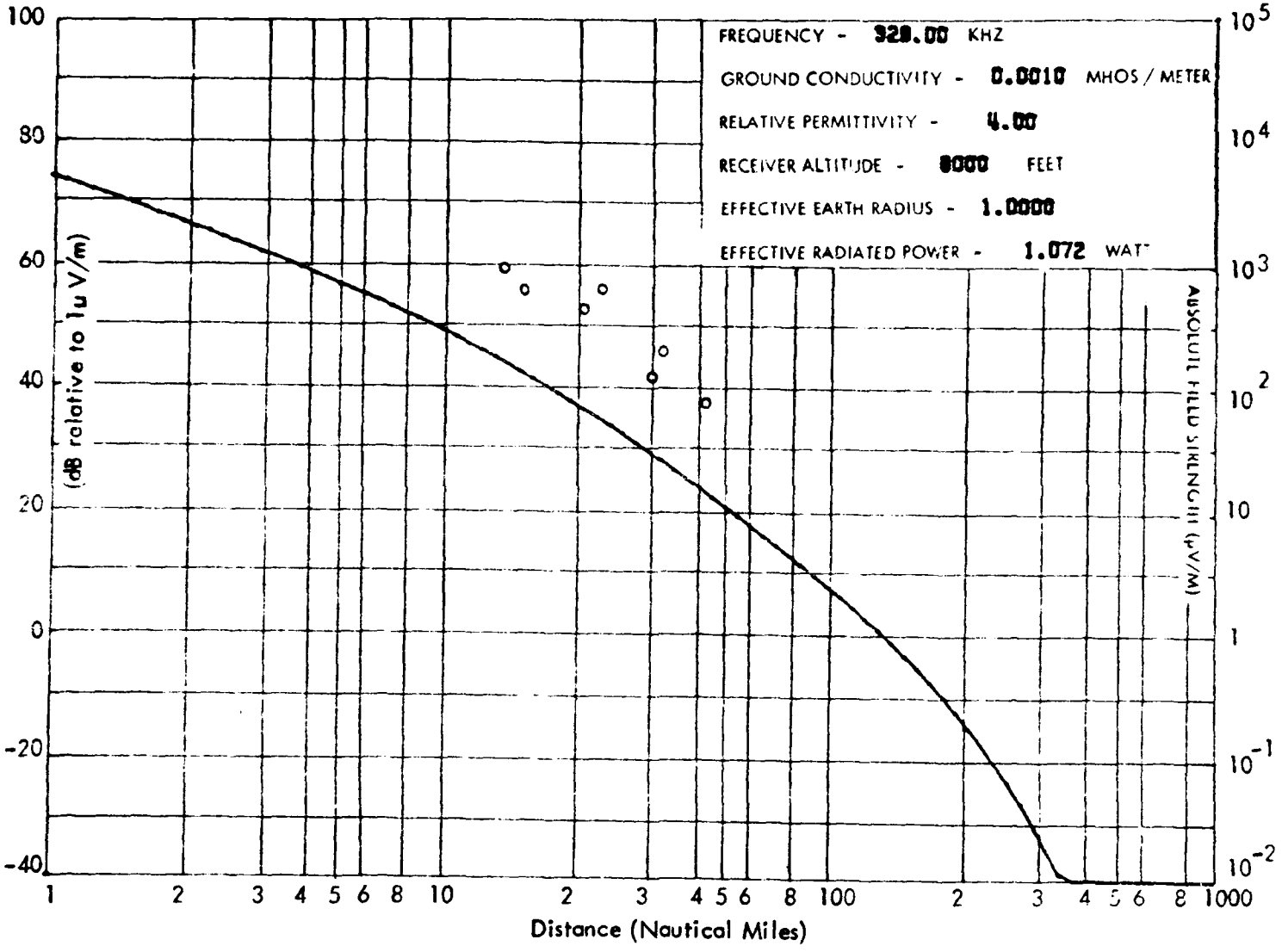

Figure 2-26. Flight Data on Brainard, Connecticut Beacon; 6/19/79; DC-3. Coordinates: 41°42'51"N, 72°36'48"W; Call Sign: AQD; Transmitter Power: 50 watts.

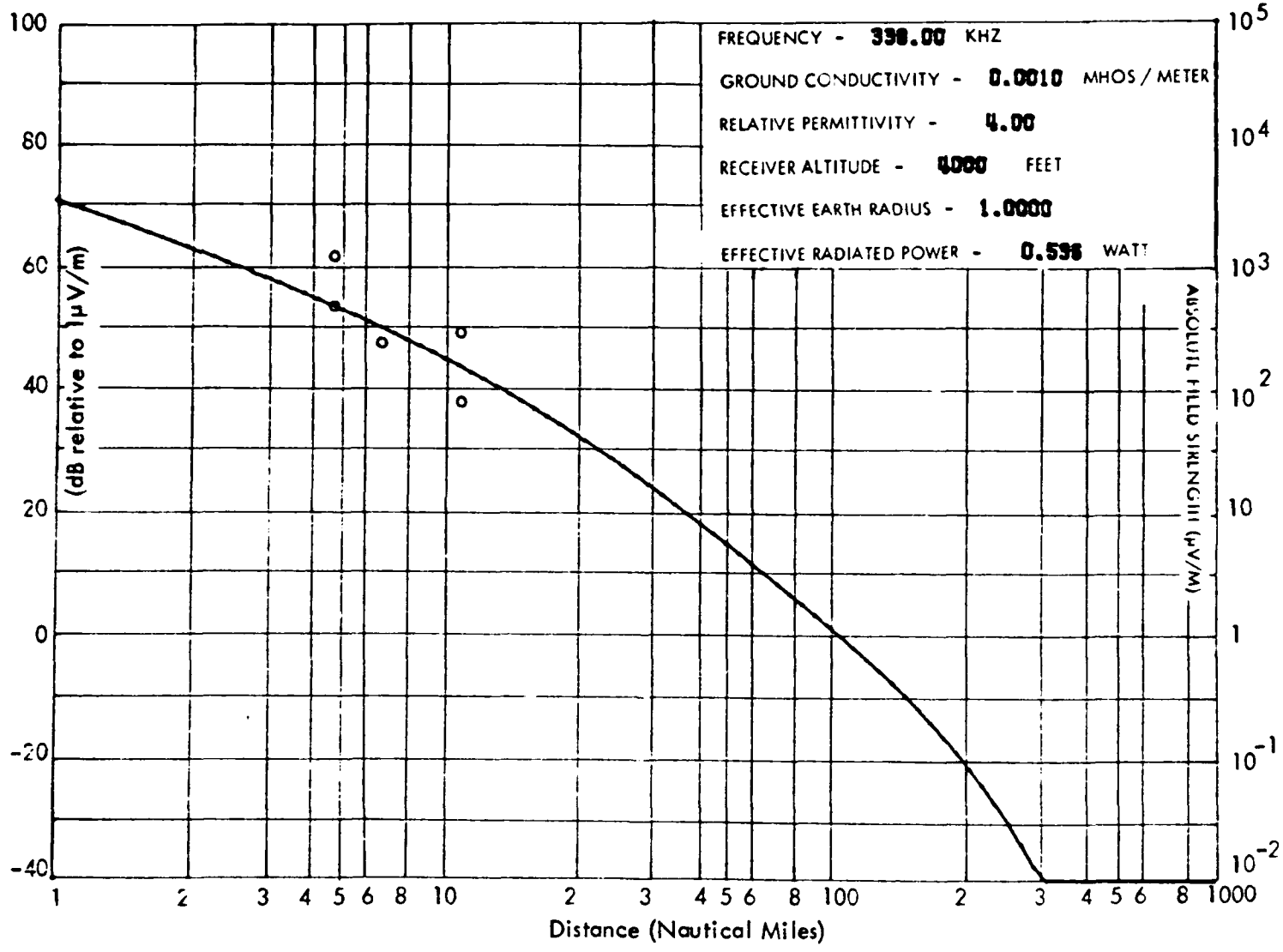

Figure 2-27. Flight Data on Derry, New Hampshire Beacon; 6/19/79; DC-3. Coordinates: 42°52'12"N, 71°23'51"W; Call Sign: DRY; Transmitter Power: 25 watts.

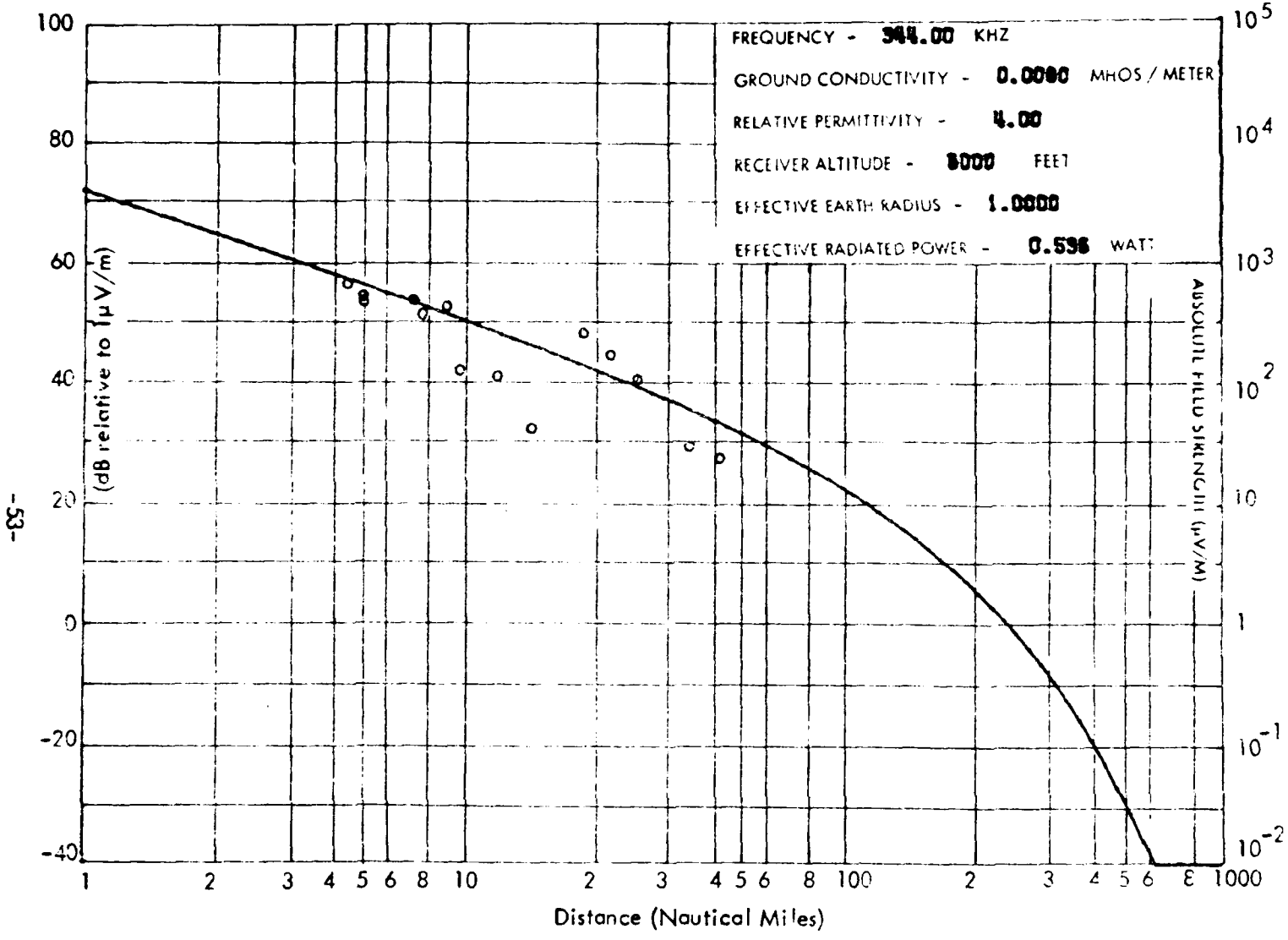

Figure 2-28. Flight Data on Picture Rocks, Pennsylvania Beacon; 6/19/79; DC-3. Coordinates: 41°16'38"N, 76°42'24"W; Call Sign: PIX; Transmitter Power: 25 watts.

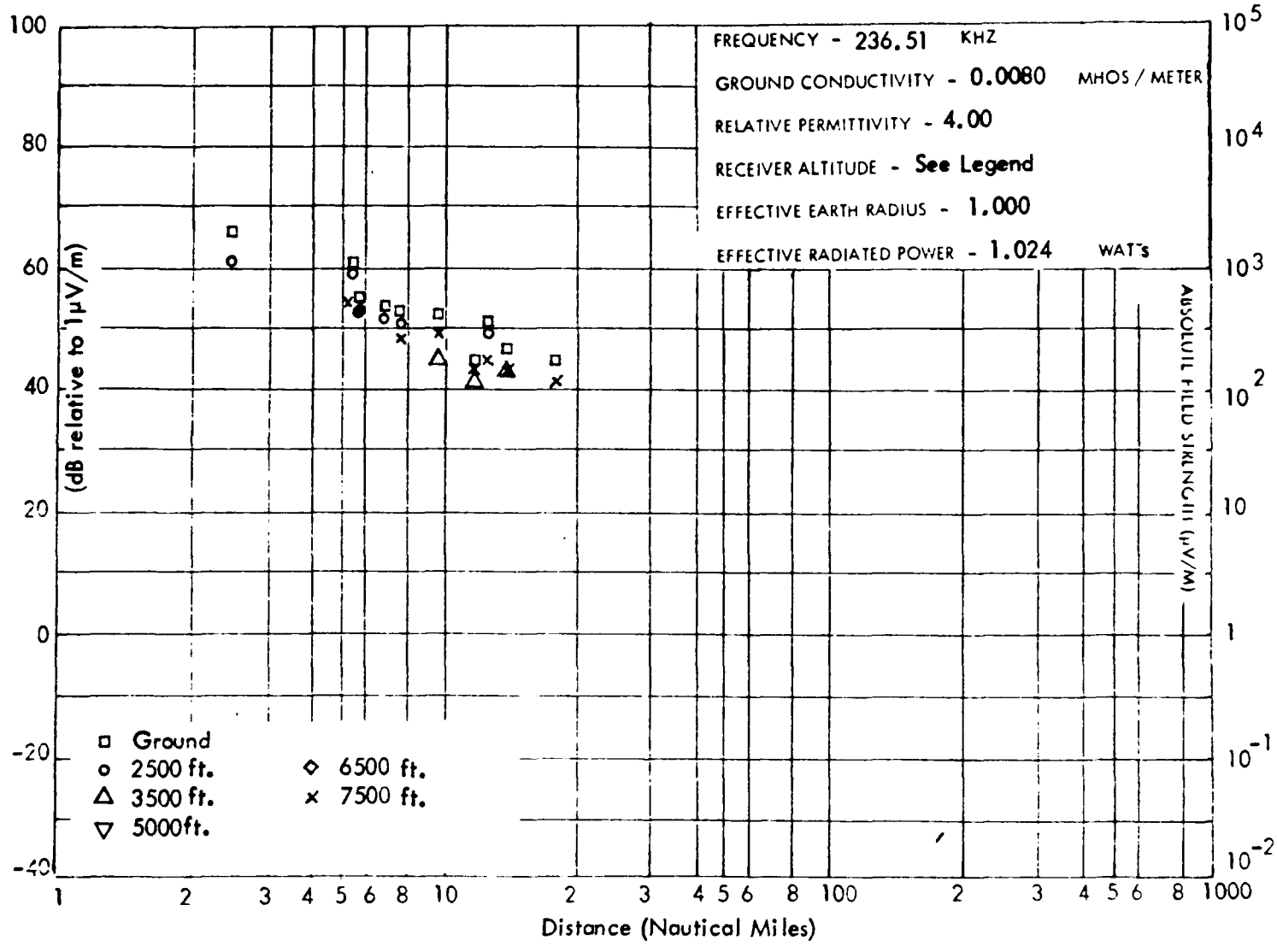

Figure 2-29. Effect of Receiver Altitude on Measured Field Strength, Chillicothe, Ohio Beacon. Coordinates: 39°26'22"N, 83°01'39"W; Call Sign: RZT: Transmitter Power: 25 watts.

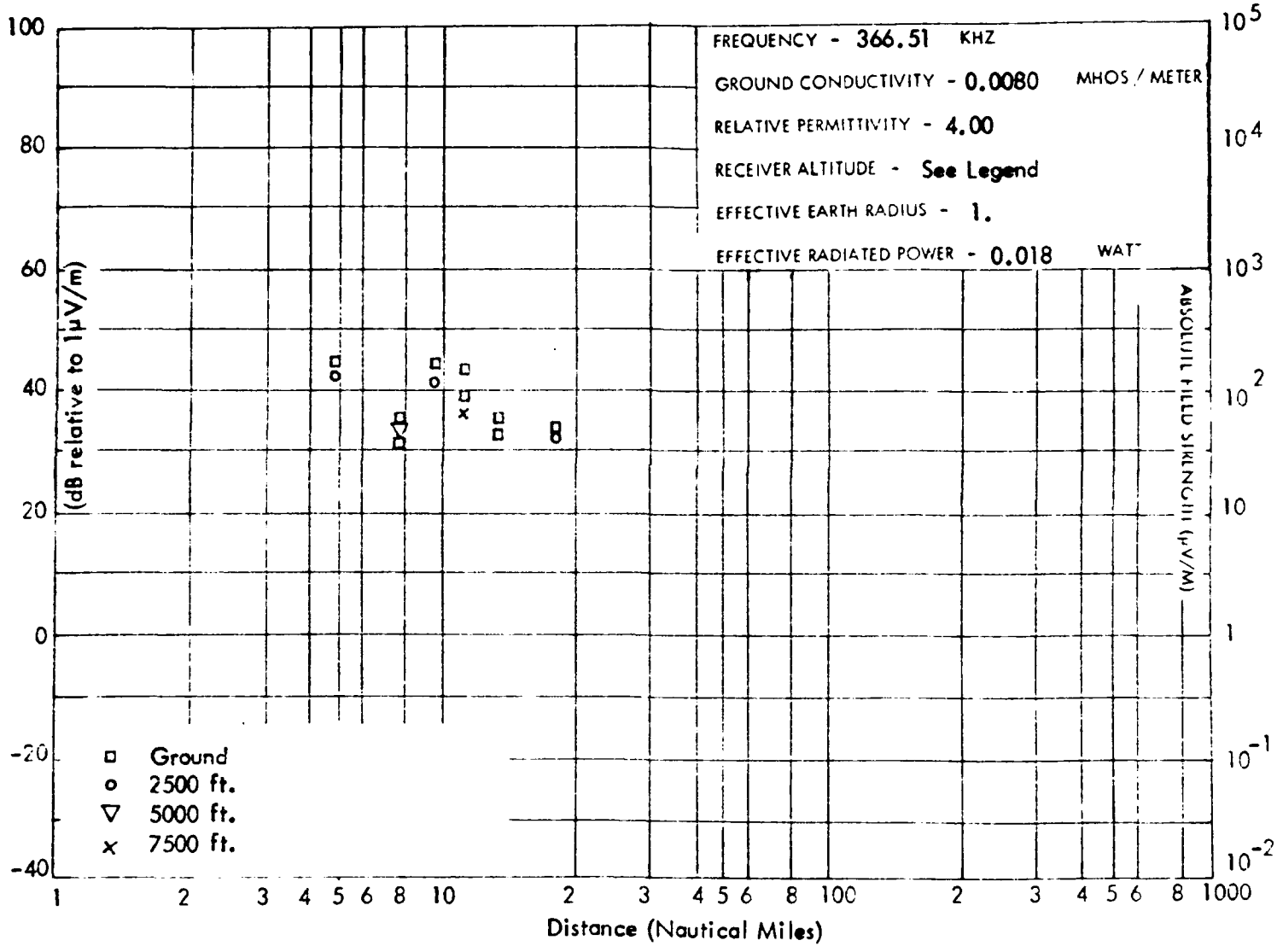

Figure 2-30. Effect of Receiver Altitude on Measured Field Strength, Circleville, Ohio Beacon. Coordinates: 39°31'11"N, 82°58'47"W; Call Sign: CYO; Transmitter Power: 25 watts.

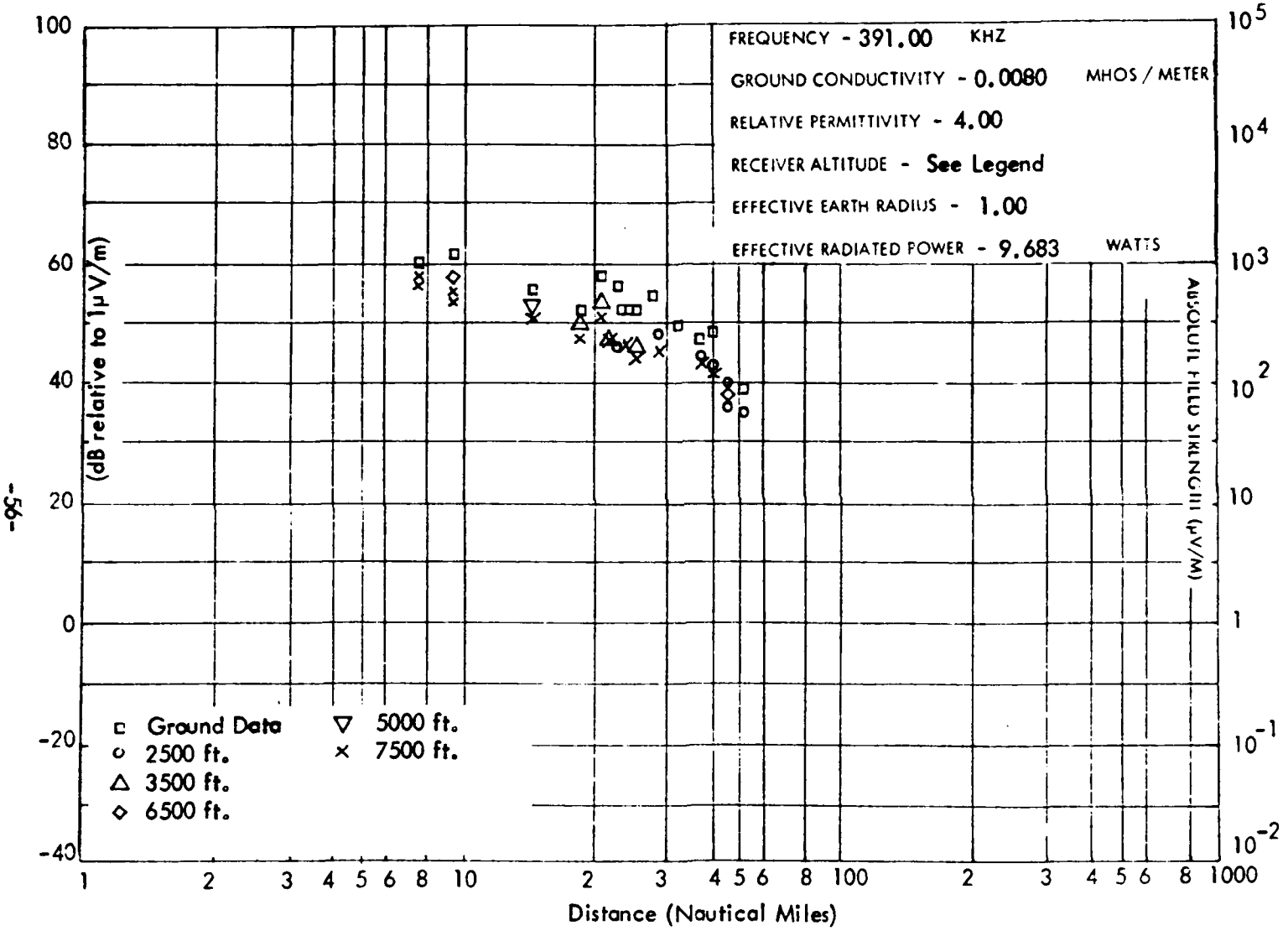

Figure 2-31. Effect of Receiver Altitude on Measured Field Strength, Columbus, Ohio Beacon. Coordinates: 39°59'19"N,84°55'17.7"W; Call Sign: CMH; Transmitter Power: 78 watts.

III. PARAMETRIC STUDY

The basic theory used to make ground wave field strength calculations under various conditions, but neglecting the sky wave, has been detailed in the previous section, as well as in several of the references mentioned there. The purpose of this section is to examine the effects of various parameters, such as ground conductivity, receiver altitude, and earth radius factor used in these calculations. All curves generated here assume an effective radiated power to 1000 watts to agree with curves given in the CCIR Report [15]. The field strength computed is a linear function of effective radiated power (i.e., a 10 dB decrease in ERP yields a 10 dB decrease in calculated field strength at any given distance). Conductivity of soil at VLF in various geographical locations in the United States is available [12] and methods for measuring this conductivity have also been discussed [16]. Relative permittivity of soil is readily available from many standard tables [4], and receiver altitude is available from the aircraft altimeter. The final parameter under investigation, effective earth radius, will be discussed in greater detail later in this section. However, here the concern is only with the effect of these parameters on the radio wave as they affect reliable and accurate field strength prediction, and not with the determination of these ground constants in various geographical locations or measurement of the other parameters involved.

To this end, Figures 3-1 through 3-4 demonstrate the effect of ground conductivity on the radio wave propagation. These curves essentially reproduce the curves published by the CCIR [15,17]and are those used as a basis for FAA coverage range prediction of NDB's [13]. These four figures assume the receiver and transmitter are located on the earth's surface, a relative permittivity of 4.0, and an effective earth radius of 1.0. The effects of these parameters will be investigated in the following paragraphs. Figure 3-1 shows computed field strength for an earth conductivity of 0.001 mhos/meter. This set of ground constants is normally chosen to model desert. As is evident by comparing these four figures, this low-ground conductivity is quite detrimental to ground-wave propagation and has a similar effect on all frequencies considered here. As is illustrated by all curves in this section, a lower frequency wave propagates better than a higher frequency wave under the same conditions. This, of course, is to be expected since all models considered here place the receiver and transmitter in the vicinity of the earth and the earth itself presents a smaller obstacle, in terms of wavelengths, to a lower frequency wave than a wave of higher frequency. Figures 3-2, 3-3 and 3-4 demonstrate that propagation improves as ground conductivity increases. Figure 3-4 ($\sigma = 0.03$ mhos/meter) is often used as a model of ground of "good" conductivity, while Figure 3-3 ($\sigma = 0.01$ mhos/meter) is usually considered "medium" ground. Figure 3-5 is presented as a demonstration of radio wave propagation over sea water. Note that the permittivity here has been changed to 80.0, that of normal sea water, so no comparison with the previous four curves is intended. It is presented for completeness and will be used in later comparisons.

Since Figure 3-3 ($\sigma = .01$ mhos/meter, $\epsilon_r = 4.0$) represents medium or average ground conductivity, it has been arbitrarily chosen as a reference against which effects

of all other parameters can be compared. Thus, Figures 3-6 through 3-12 show the effect of the relative permittivity of the ground along the propagation path on the radio waves propagation. By comparing Figures 3-6 through 3-8 with Figure 3-3, we can see that the relative permittivity of the ground is of little importance in field strength calculations for medium soil conductivities at these frequencies. Figures 3-6 and 3-7, with a relative permittivity of 1.0 and 10.0 respectively, are virtually indistinguishable from our reference, Figure 3-3, with a relative permittivity of 4.0. Figure 3-8 ($\epsilon_r = 100.$) shows slightly more attenuation than Figure 3-3, especially at the higher frequencies, but the difference is certainly not significant since the curves are all within 1 dB at all frequencies and distances shown. Figures 3-9 and 3-10, compared to Figure 3-1, show effects of relative permittivity on ground wave propagation over ground of poor conductivity ($\sigma = 0.001$ mhos/meter), illustrating field strengths for relative permittivities of 1 and 100, respectively. Again, no major effects are demonstrated for the lower frequency curves, although the effect here is greater for higher frequencies than that for medium ground conductivity. Figure 3-9, with a relative permittivity of 1.0, shows field strengths which are indistinguishable from those of Figure 3-1 (ϵ_r of 4.0). However, Figure 3-10, with a relative permittivity of 100, shows variations in field strength of up to 2 dB for 200 KHz waves out to a distance of 300 nm. At 500 KHz, the variation is as large as 8 dB at 100 nm. However, a relative permittivity of 100 is obviously not a practical value and, therefore, the differences here are of little importance in that respect. The value of 100 is used here as an example of an extreme case and will never be encountered in practice. Figures 3-11 and 3-12 also show virtually no variation with relative permittivity when a propagation path of ground conductivity of that of sea water is considered. Curves for ϵ_r of 1, 80 and 100 (Figures 3-11, 3-5, 3-12, respectively) are essentially identical and, therefore, one can conclude that relative permittivity under these conditions of ground conductivity is not an important parameter. In general, conclusions that can be drawn from these comparisons are that relative permittivity has more significant effect on wave propagation at higher frequencies and for propagation paths of lower ground conductivity. However, variation over practical values of relative permittivity does not significantly alter field strength and, therefore, the average values of relative permittivity of soil and sea water of 4.0 and 80. are considered to be adequate for use in this study. This is particularly true for NDB's, since their coverage range is usually limited to 100 nm or less.

Figures 3-13 and 3-14 show the computed electric field strength when the transmitter is on the earth's surface and the receiver is elevated 10,000 and 20,000 feet, respectively. It can be seen here that the effect of raising the receiver may initially seem surprising, since the field strength shown in Figure 3-13 for the receiver at 10,000 feet is actually slightly lower than that computed with the receiver placed on the ground. Also contrary to intuition is the fact that the difference in the lower frequency curves are slightly more noticeable than that of the 500 KHz curve. Since at 10,000 feet the receiver of 500 KHz is a greater number of wavelengths away from the earth's surface, it would seem that the higher frequencies should be affected more by the change in altitude. Though this difference is less than 2 dB over the entire frequency range and distance ranges covered, the reason for this difference is explainable. This phenomena is considered by Wait [18] where the theoretical height-gain

functions are given in terms of Airy functions, since the geometry of the problem is spherical and can be computed numerically in this form or expanded into a power series. The results of Wait's calculations show that the field strength should indeed increase as the receiver altitude increases for ground of infinite conductivity. However, when finitely conducting earth is considered, the height-gain function of the receiving antenna decreases slightly for relatively low (a few wavelengths) heights, and it appears that this effect is greater at lower frequencies.

As the receiver altitude is increased further, however, the earth becomes less of an obstacle and the height-gain function increases (up to a height of 40-45 km, according to Wait's computations). As the height is increased, intuitively again the higher frequencies should be affected more than the lower frequencies. This time, this intuitive supposition is borne out, both by Wait's calculations and by comparison of Figure 3-14 with Figure 3-3. In making this comparison, it is noted that the field strength computed for the curve of 200 KHz is not noticeably different in these two figures. However, as higher frequencies are considered, the differences in these figures become more apparent. At 400 KHz, differences of 2 dB can be seen. Even more difference (5 dB) can be noted in the 500 KHz curves. Further increases in altitude, up to around 40 km, should yield further increases in electric field strength. Higher altitude curves are not shown here, as it was felt that 20,000 feet was more than sufficient as a practical limit of NDB usage.

The final parameter under investigation in this section is the effective earth radius (also referred to as the earth radius factor or equivalent earth radius). The equivalent earth radius concept has been used by many authors [18,19,20] to account for effects of the troposphere on the radio wave. These effects differ from those of the ionosphere in that the troposphere causes a refraction of the wave due to the unequal density of the air in the lower atmosphere at different heights, whereas the wave is reflected from the ionosphere, due to the free electrons, or ionization, present in the upper atmosphere. This concept has been justified by Bremmer [19] using the theory of geometrical optics and has also been verified by Wait [18] and Fock [20] in a more rigorous development.

If the equivalent earth radius is defined as $a_e = \alpha a$ where a is the actual earth radius and α is the effective earth radius factor, then α can be expressed in terms of the water vapor pressure e in millibars, the water vapor pressure gradient with respect to height h above the earth's surface, and the temperature gradient with respect to h. Bremmer has expressed the effective earth radius as:

$$a_e = \frac{a}{0.766 - (0.068a + 0.00237\, e)\frac{dT}{dh} + 0.306\frac{de}{dh}} \qquad (3.1)$$

where the unit of h in each case is 100 m and T is expressed in degree celsius.

To obtain this usable form several approximations about the lower atmosphere were necessary. However, these approximations will very likely not cause any error

greater than the uncertainty with which the values on the right hand side of Equation (3.1) are known due to inaccuracies in measurement as well as variation of the values along the propagation path. A value often used for the effective earth radius factor is 4/3, as this value of a is computed from Equation (3.1) at average atmospheric values. Though a is usually greater than 1, it is clear from Equation (3.1) that this is not always the case. Therefore, we see that a can vary with atmospheric conditions much the same as the ionization levels in the upper atmosphere can vary. However, it should be pointed out that the variation of a is usually considered to be not nearly as great in effect as the variation in ionospheric conditions.

The effect of a value of a of 4/3 would, of course, improve ground wave propagation of the radio wave since this effectually reduces the curvature of the earth. This specifically can have the effect of moving points which are actually in the shadow region closer to the radio horizon. Also, the wave suffers less attenuation when traversing a surface of less curvature, thus increasing field strength when values of a greater than 1 are present. These effects are illustrated for desert, medium ground, and sea water in Figures 3-5, 3-16, 3-17, respectively. As is evident when comparing these figures with Figures 3-1, 3-3, and 3-5, the effective earth radius of 4/3 significantly improves radio wave propagation over all types of earth. The improvement does vary with the soil conductivity, as shown by this comparison.

For soil of poor conductivity (Figures 3-1 and 3-15) the differences in the two figures become significant at distances greater than 100 nautical miles (nm). At ranges closer than this, the computed field strength at each of the frequencies are nearly identical. The higher frequencies are apparently more affected by the increase in a than are the lower frequencies. This again is to be expected since the change in the earth's curvature is comparatively greater to waves of smaller wavelength. Thus at 200 nm the 200 KHz wave with an a of 4/3 is approximately 1 dB above that using an a of 1 in the calculation, and for 500 KHz the field strength amplitude has increased between 3 and 4 dB. The differences in all curves increase as distance is increased. The same trends are also true for different types of ground as shown by comparison of the remaining figures. However, the differences are less noticeable for ground of medium conductivity, as in comparing Figures 3-3 and 3-16 it can be seen that at 200 nm there is only roughly a 1 dB difference in the curves of all frequencies. Again, as distance is increased the effective earth radius has more effect on the propagation.

Therefore, to summarize the effects of all parameters studied in this section, the conclusion is that ground conductivity has by far the most effect on ground wave propagation in the frequency range of 200-500 KHz. For instance, comparison of Figures 3-1 and 3-4 shows that a change in ground conductivity from 0.0010 mhos/meter to 0.0300 mhos/meter results in a 14 dB increase in field strength at 100 nm for a frequency of 200 KHz. At 500 KHz for the same ground constants and distance, a change of 22 dB in field strength is seen, illustrating also that higher frequencies are affected more by ground conductivity. Radio wave propagation is not affected significantly by changes in relative permittivity and, therefore, typical, average values can be used to make field strength calculations without fear of any meaningful error in the results. The effect of the receiver altitude, within the range considered here, is more

significant than changes in relative permittivity. At 500 KHz this difference is as much as 3 dB at 100 nm and 5 dB at 200 nm when comparing the receiver on the ground and at 20,000 feet. It should be remembered, however, that the model used to make these calculations assumes a perfectly smooth earth. Effects of irregular terrain are not included in the solution and these effects may be more significant as the receiver is brought nearer the earth's surface. Varying the effective earth radius from 1 to 4/3 also produces significant differences in field strength computation at all frequencies and over all types of propagation paths, especially at great distances. Comparisons at 300 nm and 200 KHz show a difference in field strength of 3 dB for propagation over desert conditions and 2 dB over medium earth and sea water. For 500 KHz differences of 7 dB for desert conditions, 7 dB for medium earth, and 2 dB for sea water conditions at 300 nm can result. However, comparison of the curves presented here shows that effects of the receiver altitude and effective earth radius become less significant at shorter distances. Therefore, the implication of these findings to non-directional beacons, whose coverage range is usually limited to 100 nm or less, is that the effective earth radius and receiver altitude are not important parameters unless one is considering potential interference from distant transmitters.

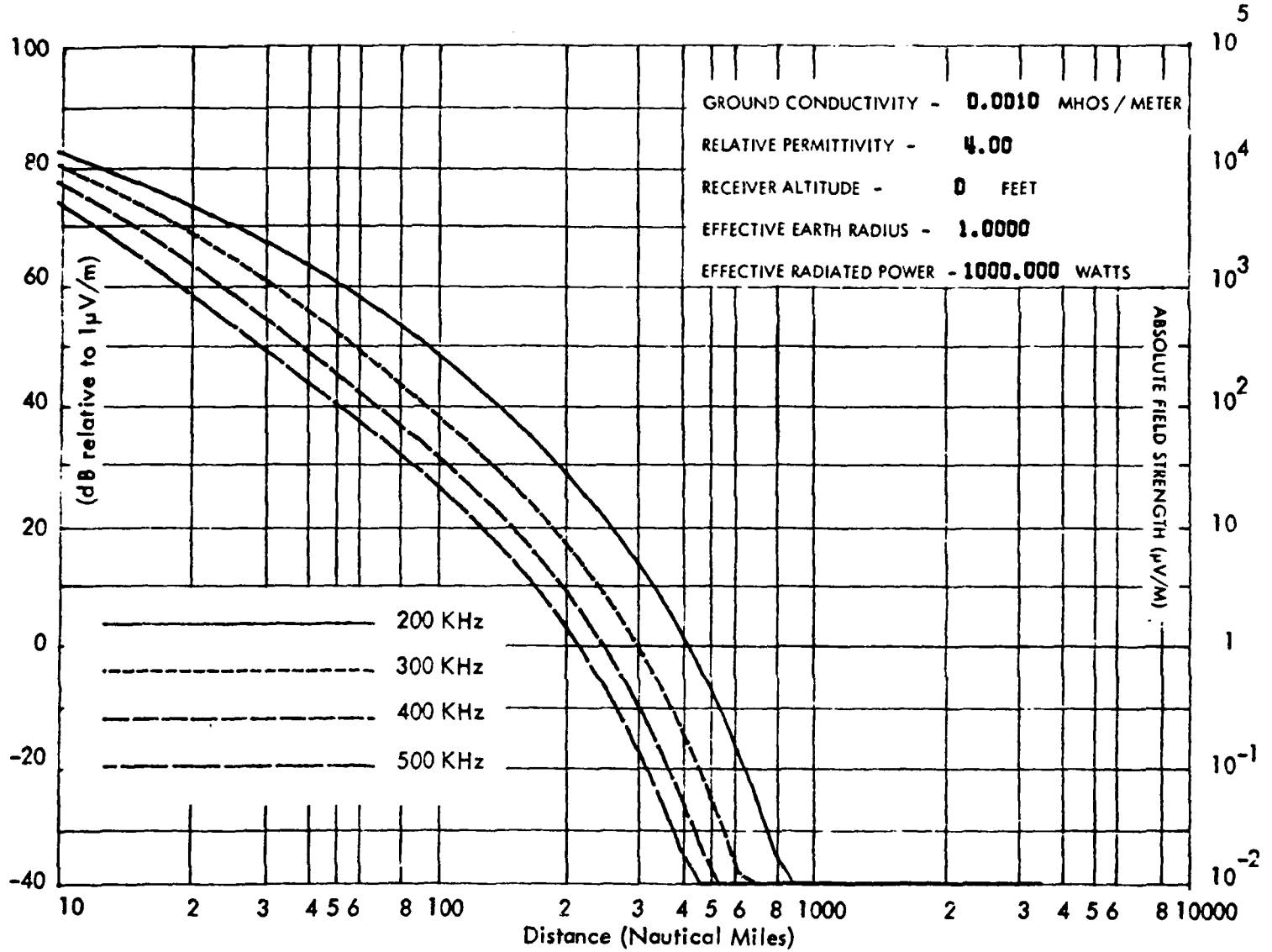

Figure 3-1. Ground Wave Propagation over Desert Conditions.

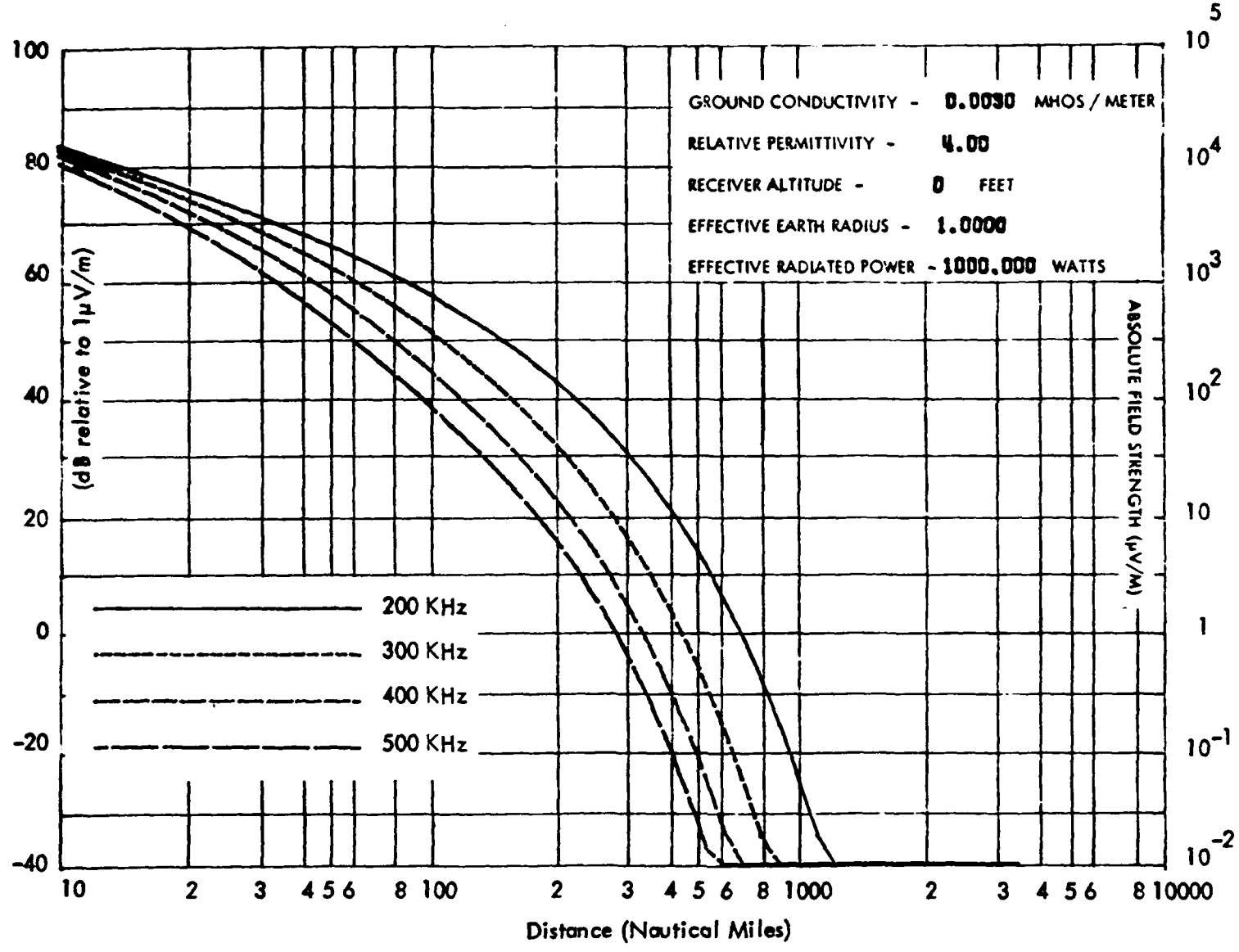

Figure 3-2. Ground Wave Propagation. Below Normal Ground Conductivity.

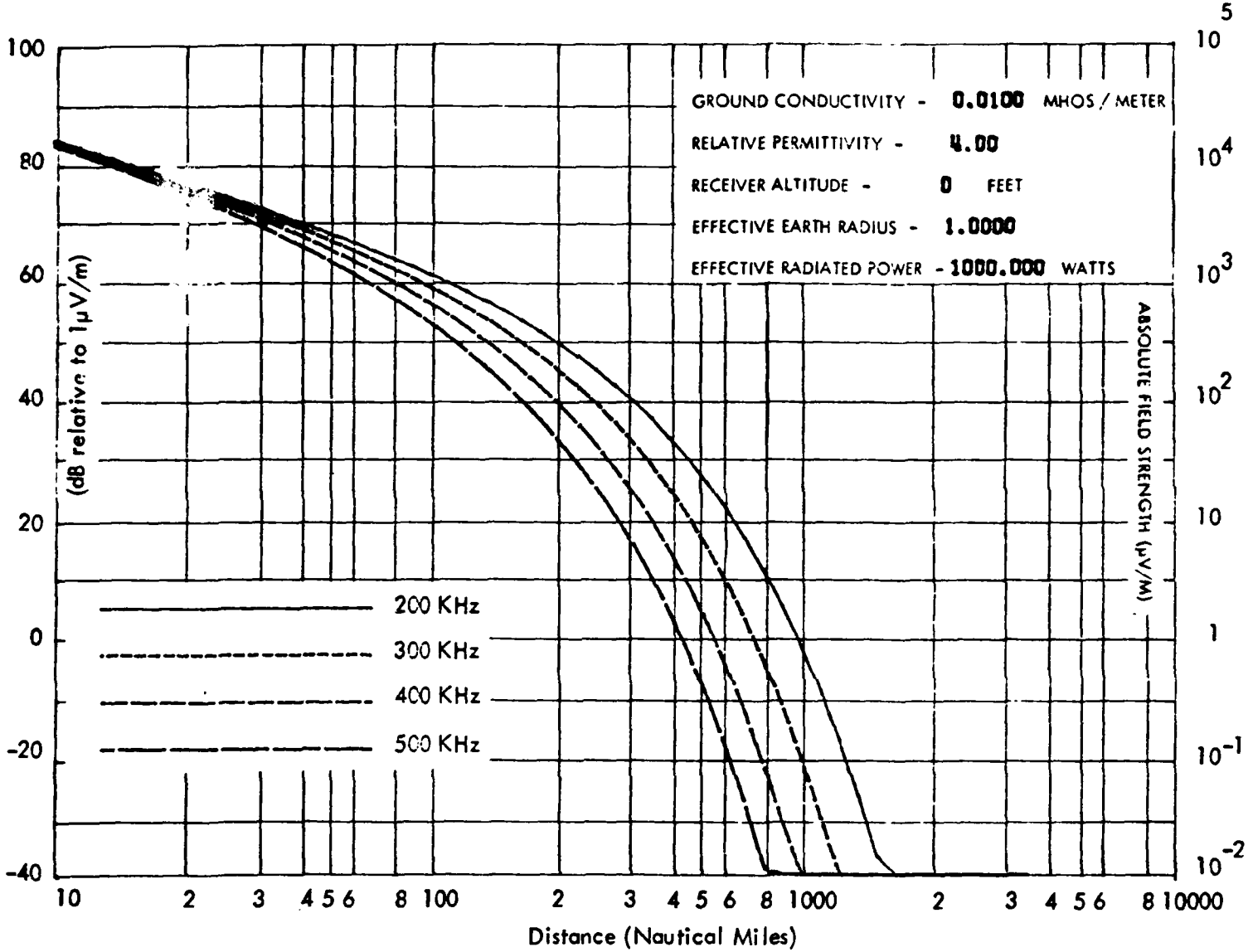

Figure 3-3. Ground Wave Propagation over Earth of "Medium" Conductivity.

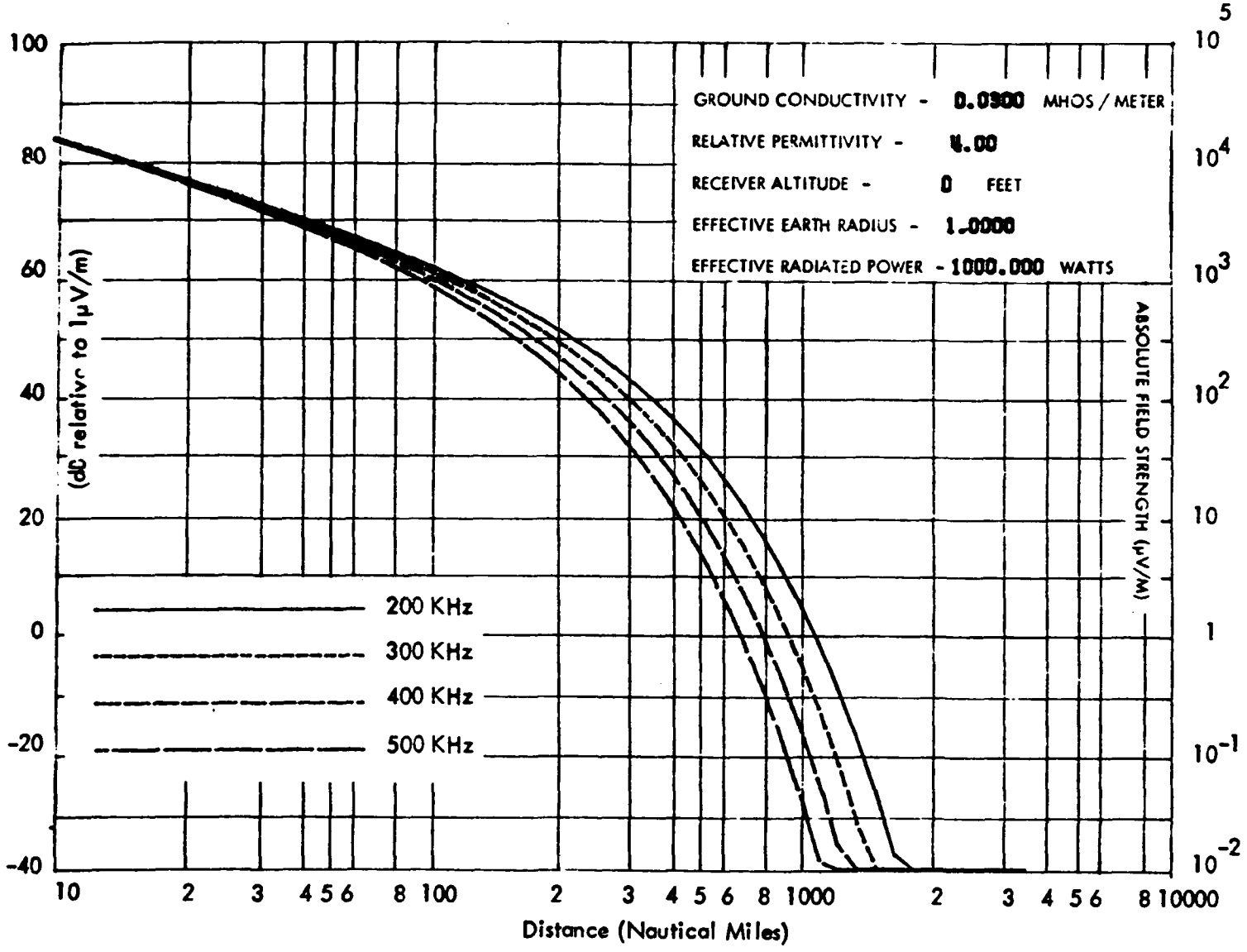

Figure 3-4. Ground Wave Propagation over Earth of "Good" Conductivity.

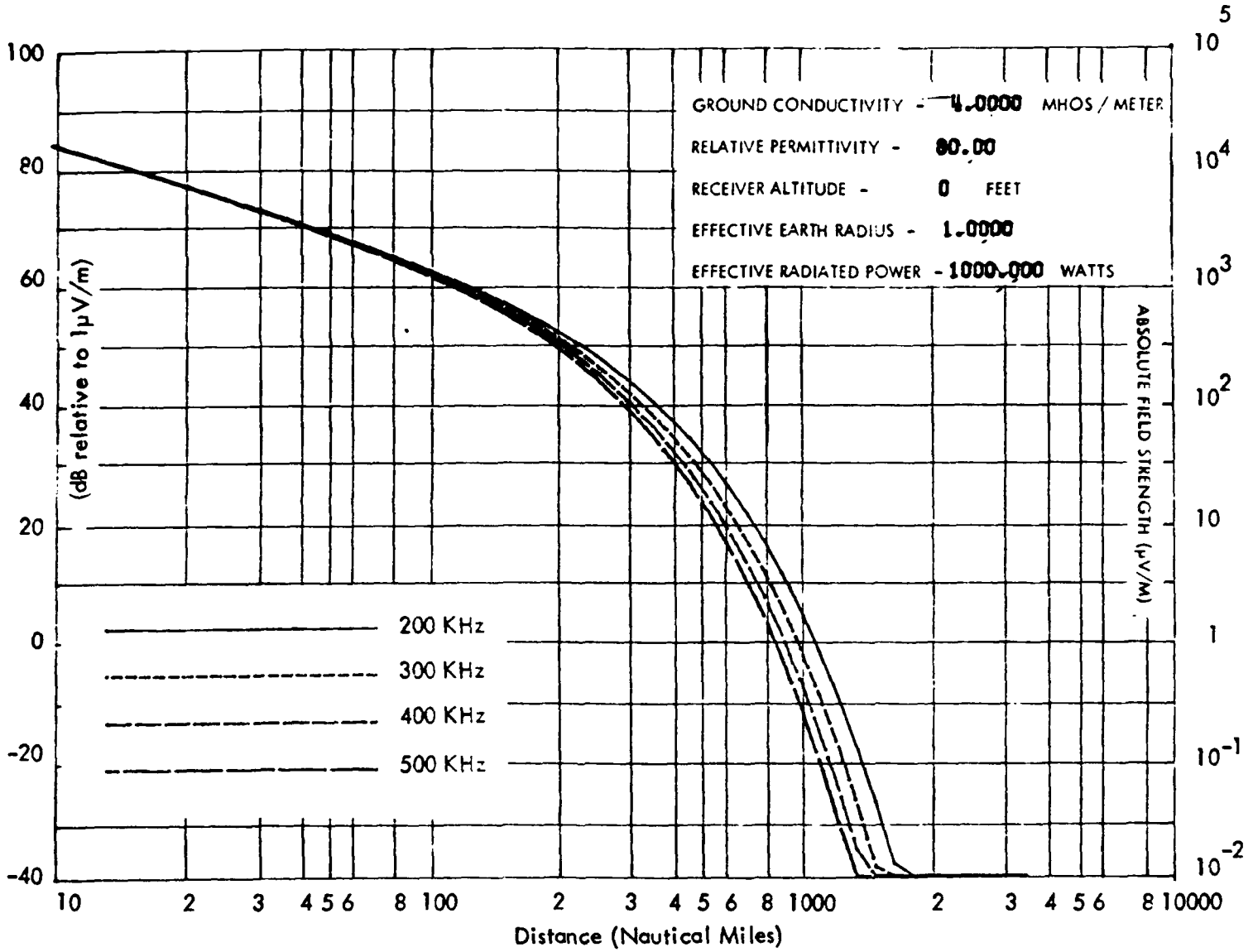

Figure 3-5. Ground Wave Propagation over Sea Water.

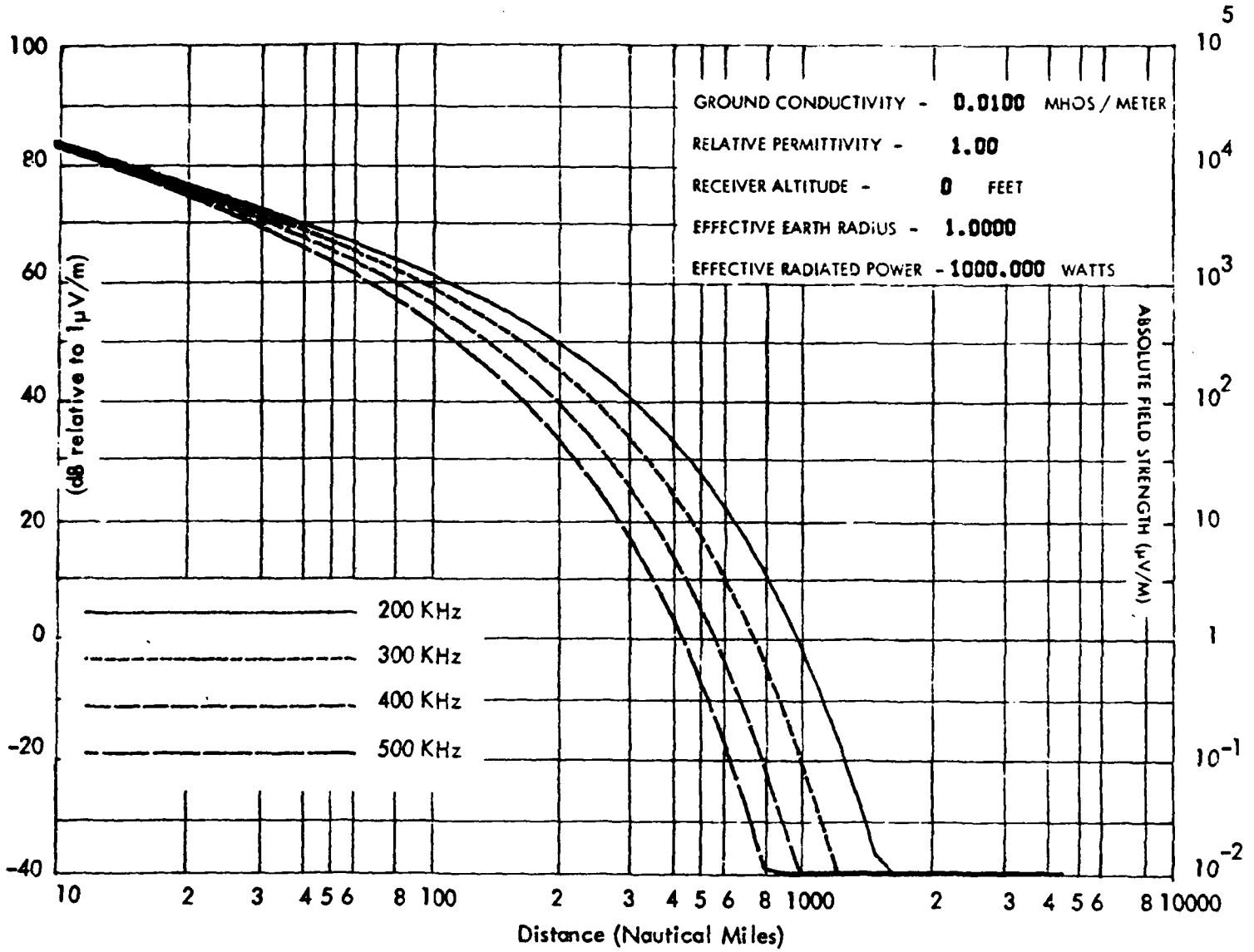

Figure 3-6. Demonstration of the Effects of Relative Permittivity; Ground of Medium Conductivity; Compare to Figures 3-7 and 3-8.

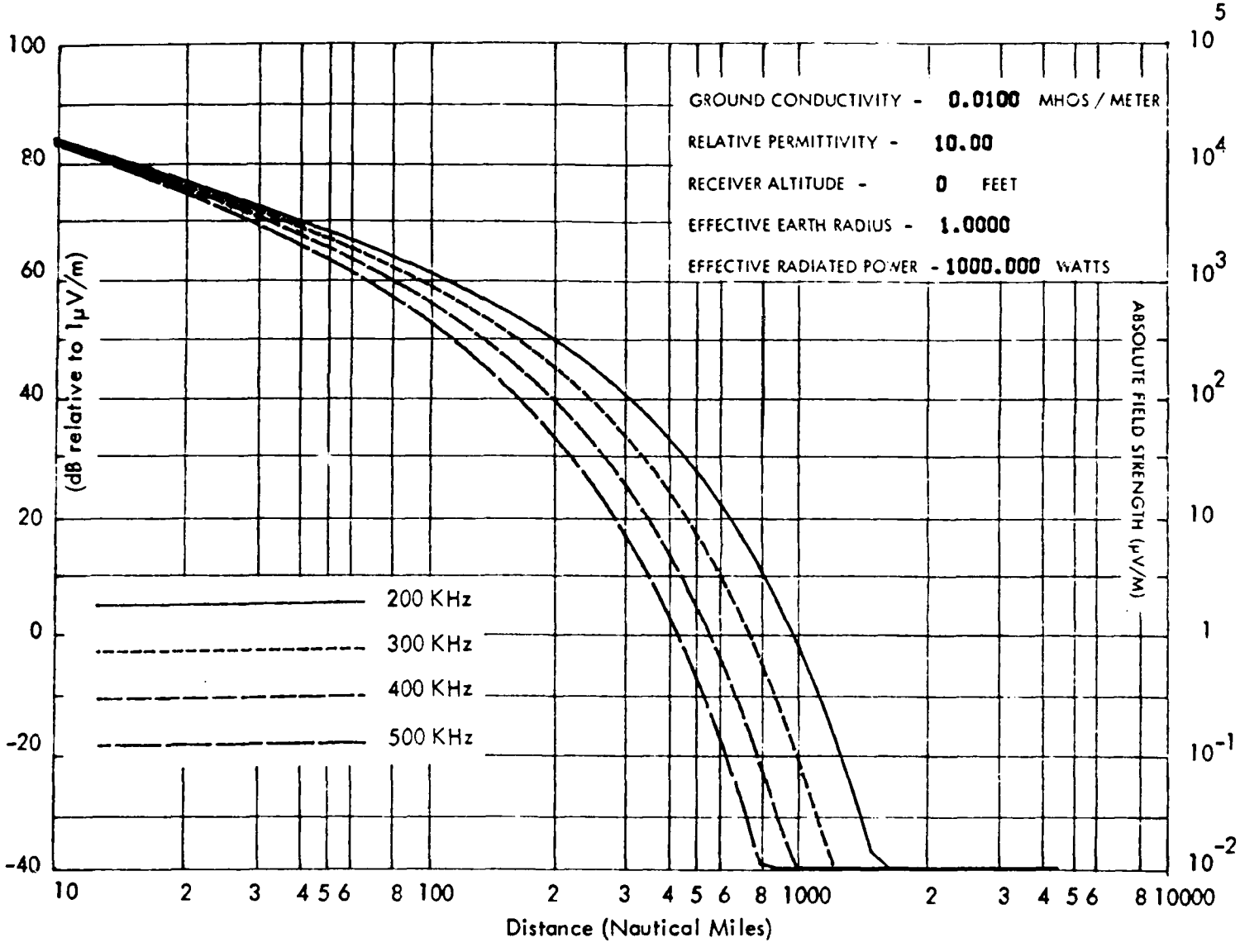

Figure 3-7. Demonstration of the Effects of Relative Permittivity; Ground of Medium Conductivity:

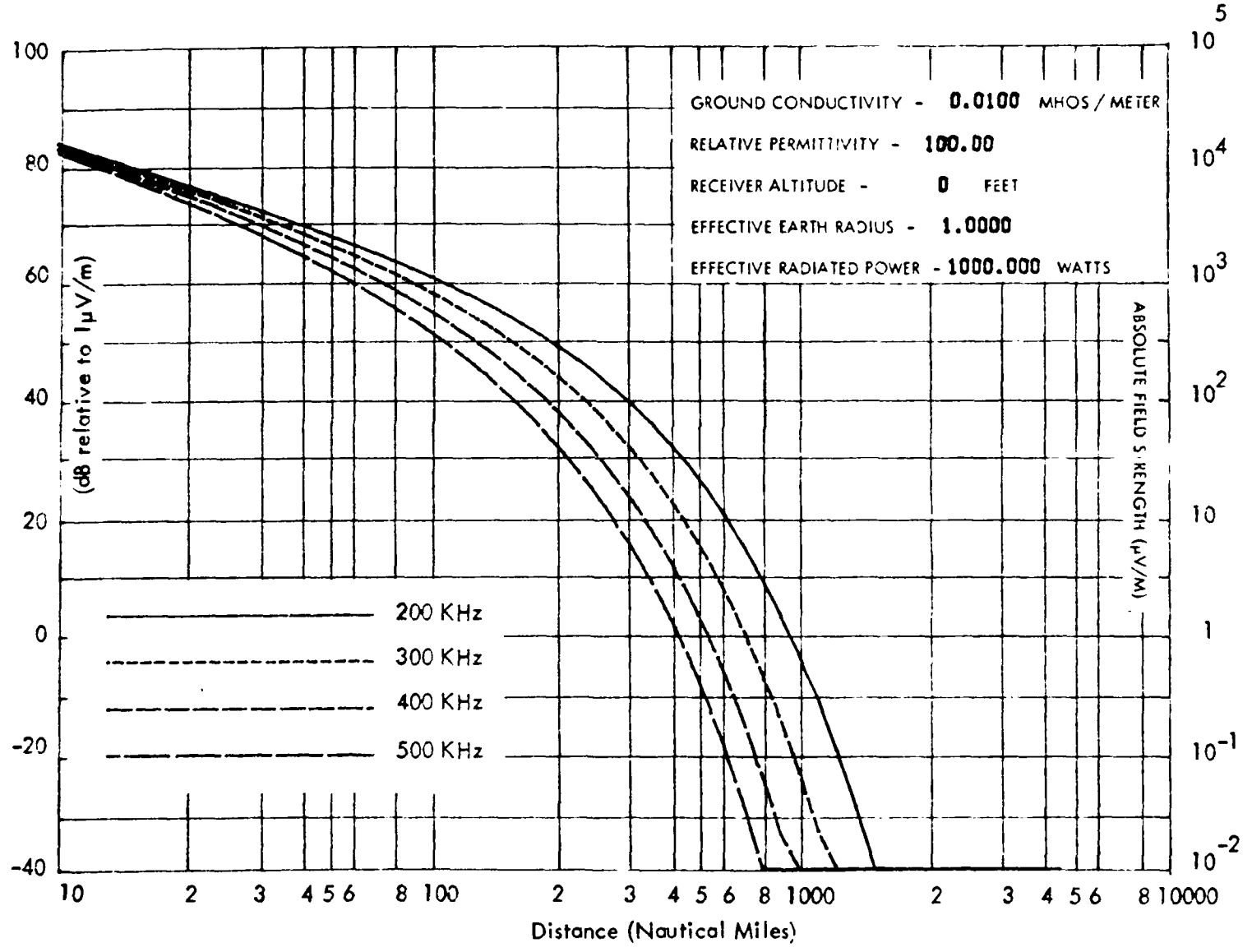

Figure 3-8. Demonstration of the Effects of Relative Permittivity; Ground of Medium Conductivity; Compare to Figures 3-6 and 3-7.

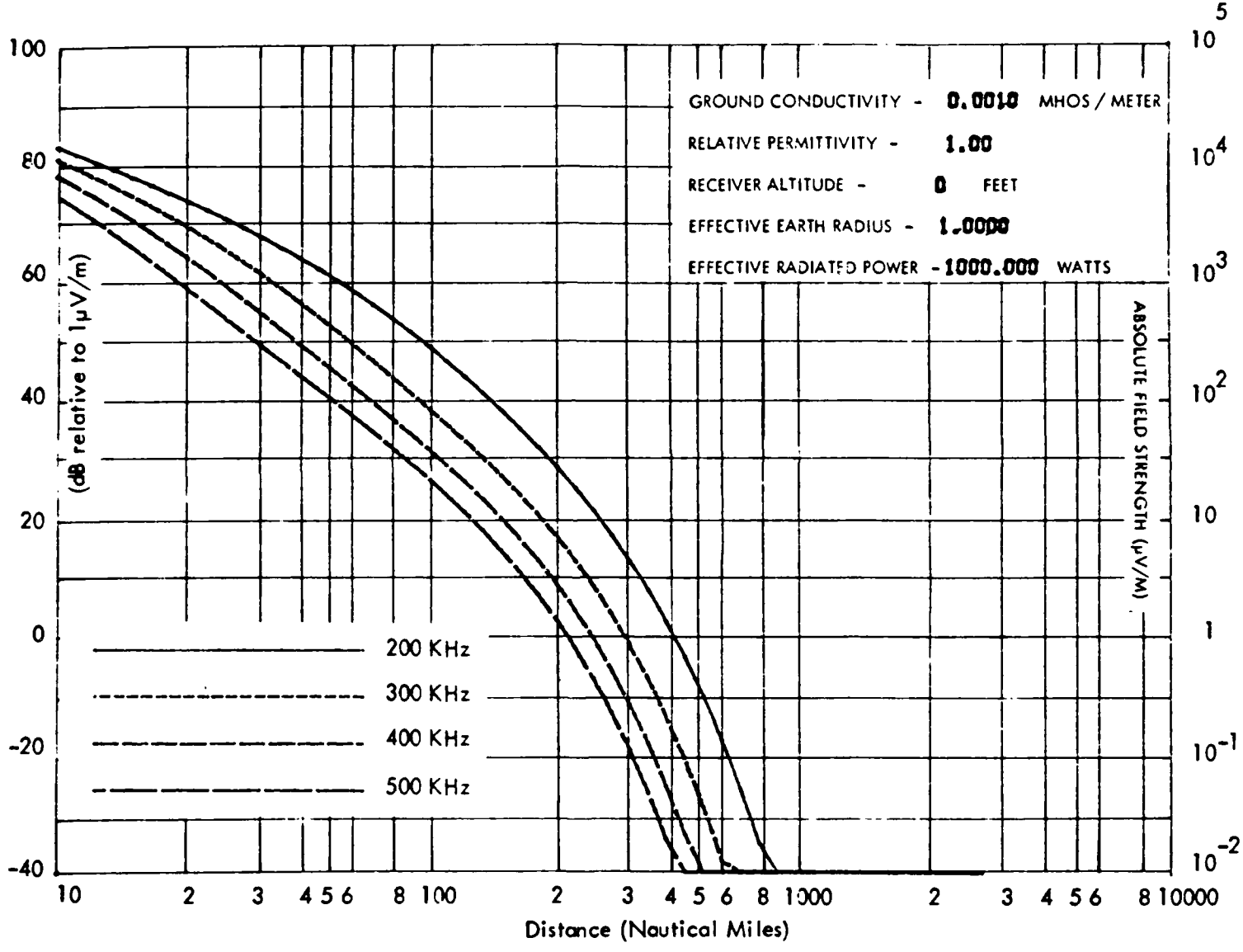

Figure 3-9. Demonstration of Effects of Relative Permittivity; Ground of Poor Conductivity; Compare to Figures 3-1 and 3-10.

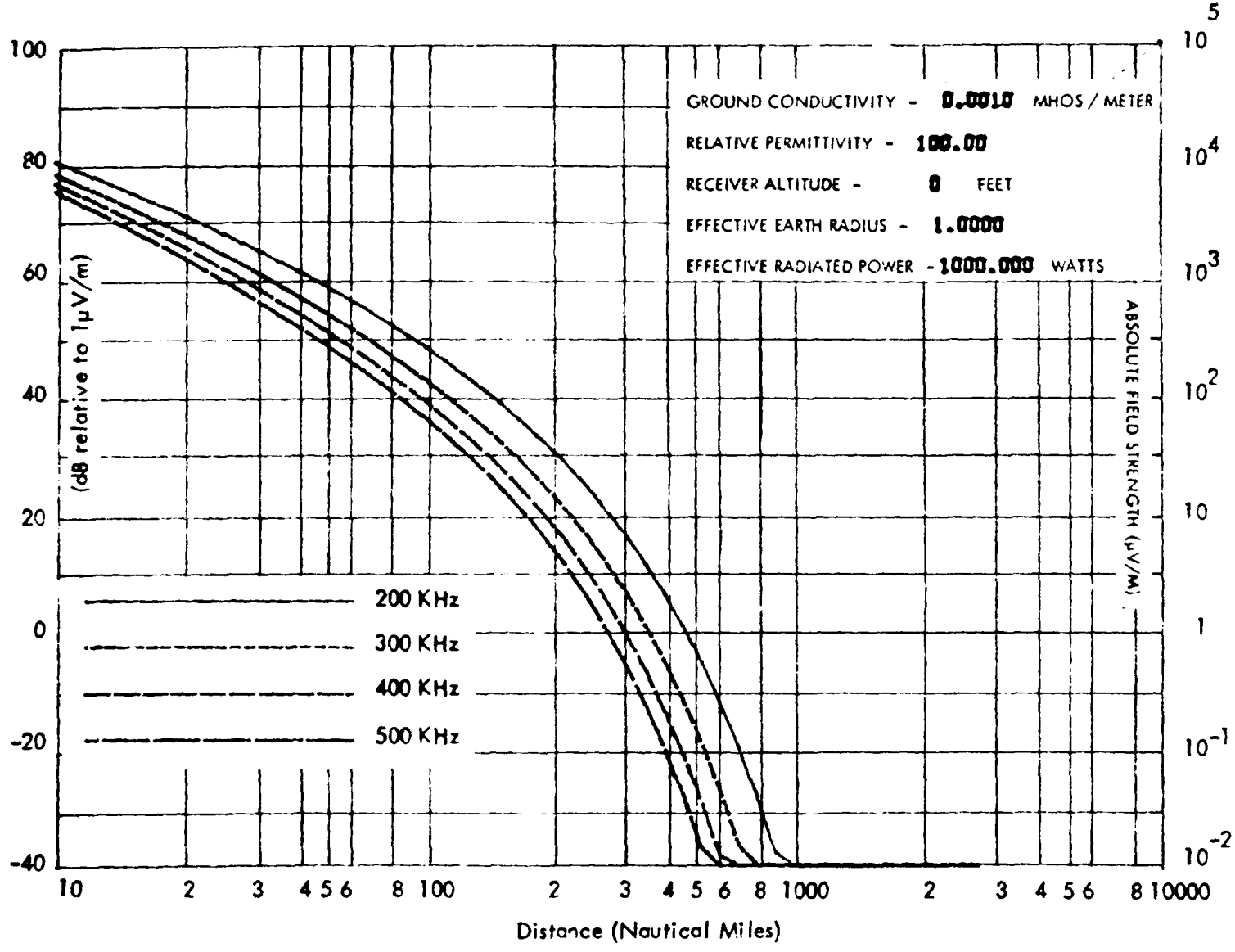

Figure 3-10. Demonstration of Effects of Relative Permittivity; Ground of Poor Conductivity; Compare to Figures 3-1 and 3-9.

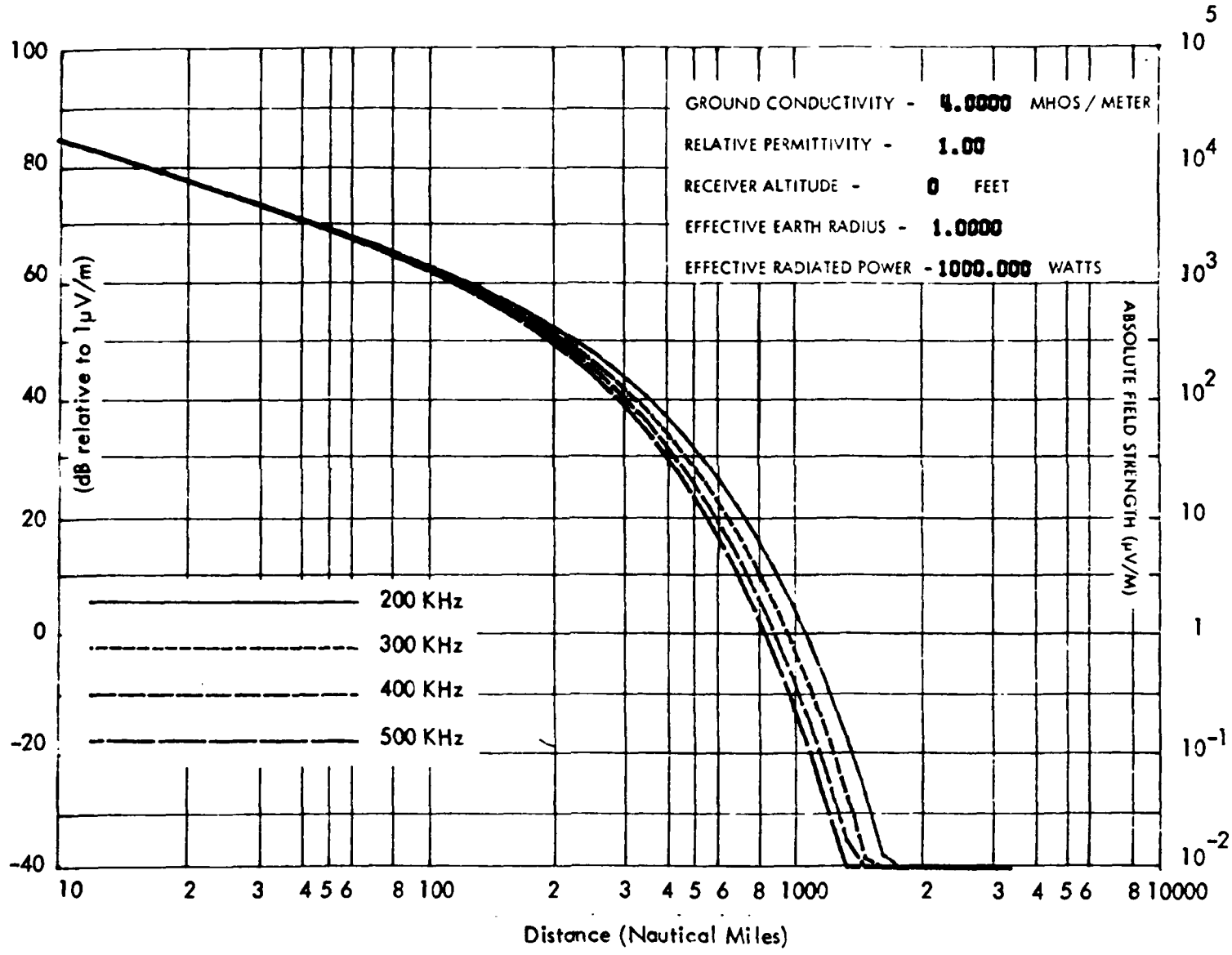

Figure 3-11. Demonstration of Effects of Relative Permittivity; Sea Water; Compare to Figures 3-5 and 3-12.

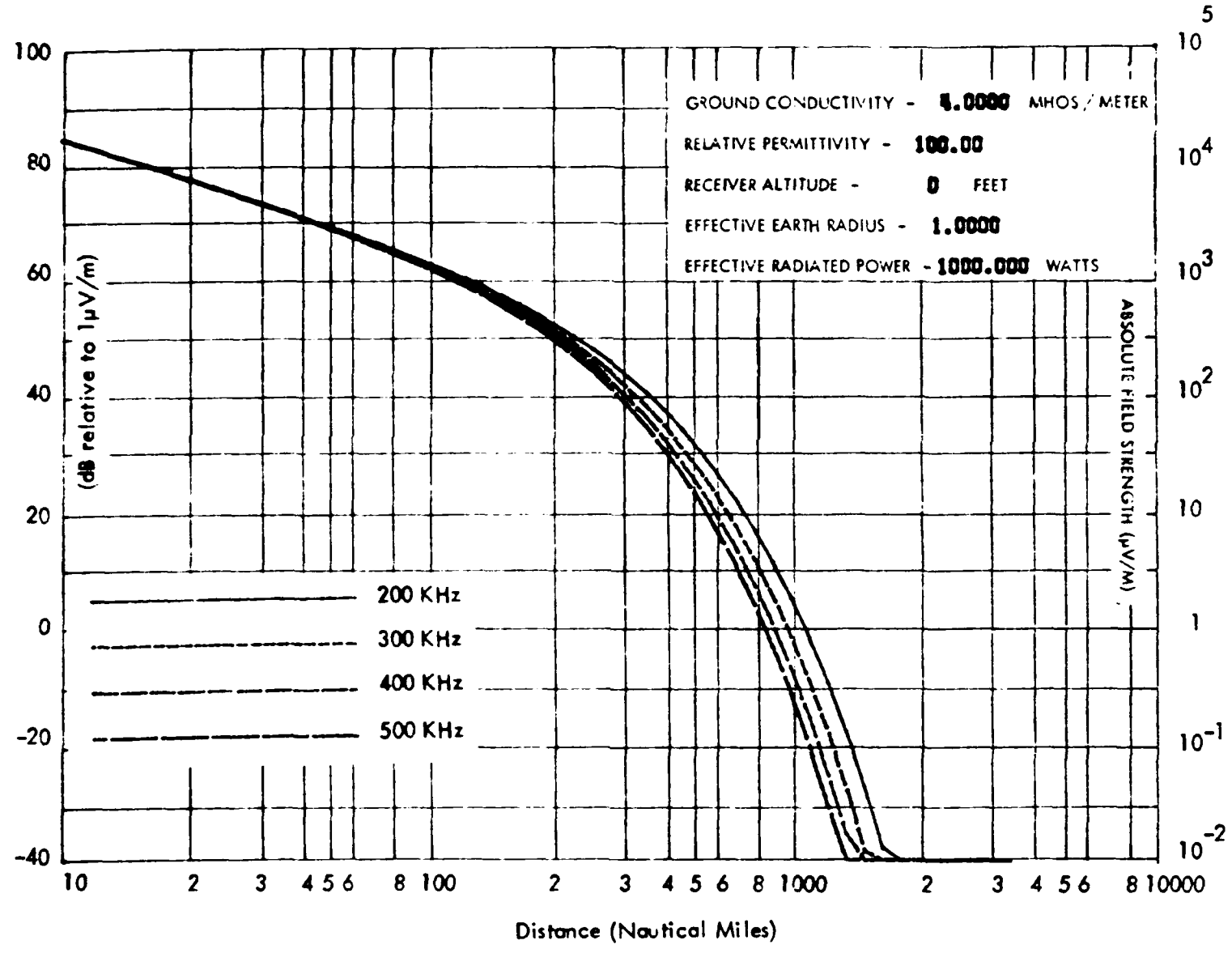

Figure 3-12. Demonstration of Effects of Relative Permittivity; Sea Water; Compare to Figures 3-5 and 3-11.

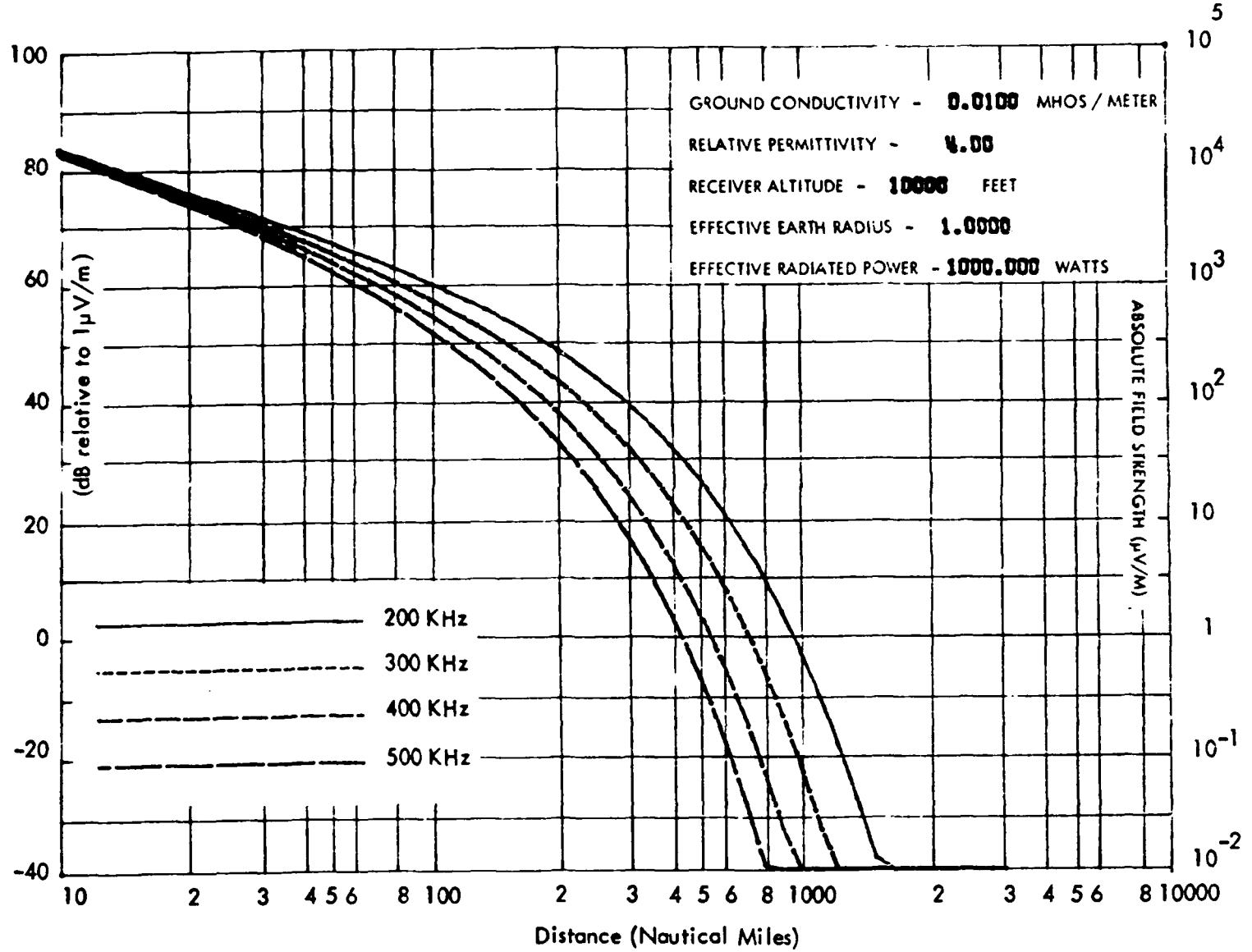

Figure 3-13. Demonstration of Effects of an Elevated Receiver; Compare to Figures 3-3 and 3-14.

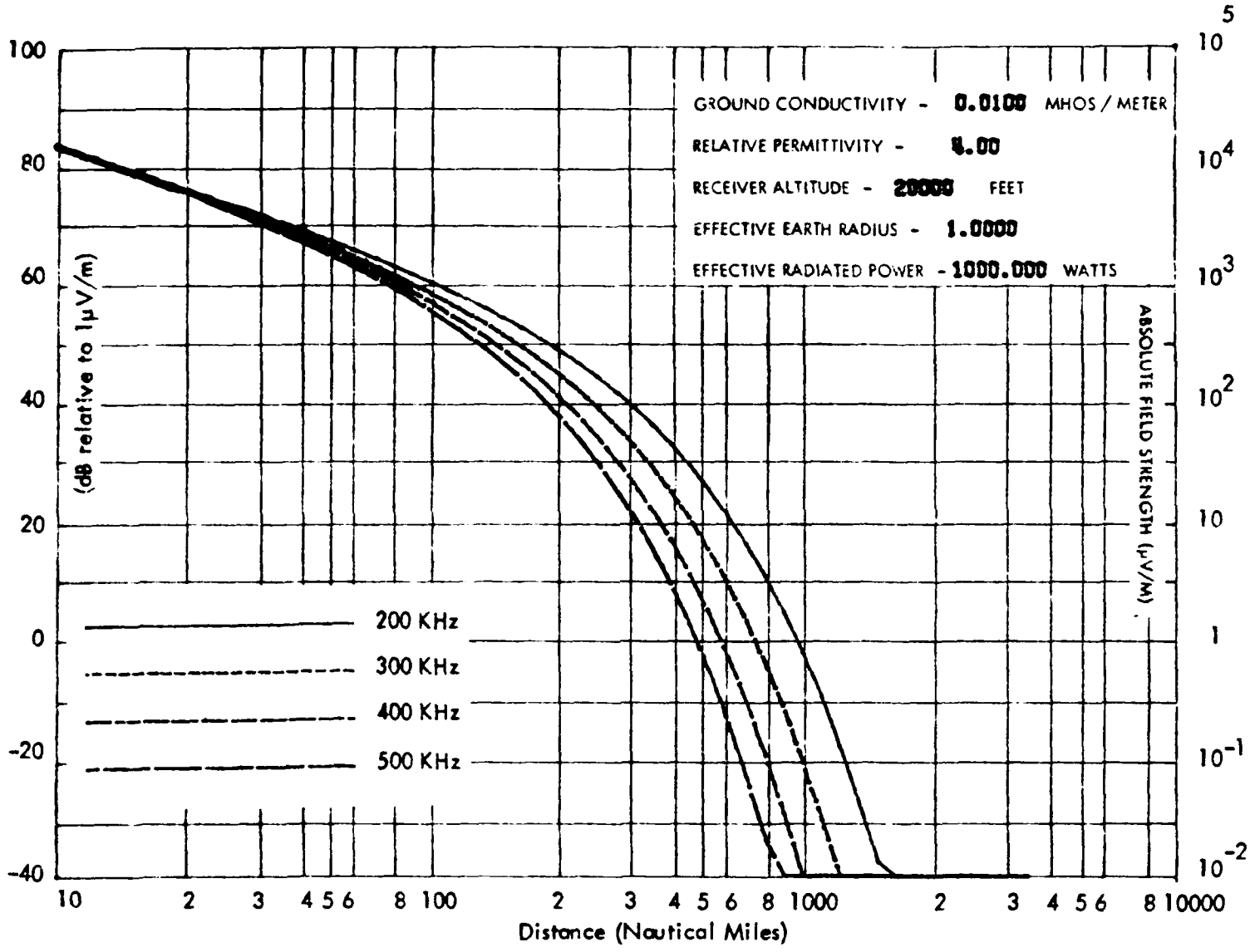

Figure 3-14. Demonstration of Effects of an Elevated Receiver; Compare to Figures 3-3 and 3-13.

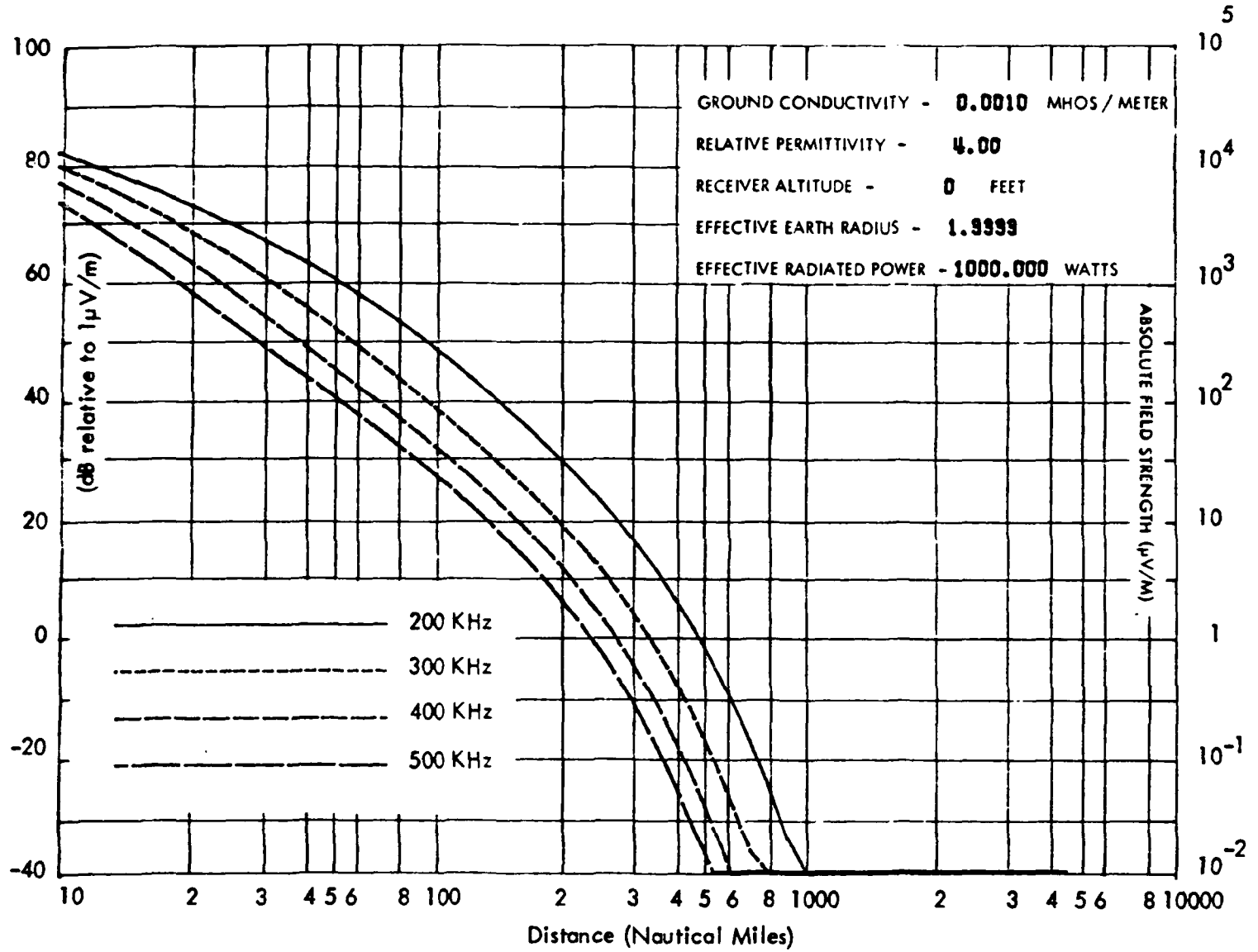

Figure 3-15. Demonstration of Effects of Earth Radius Factor over Ground of Poor Conductivity; Compare to Figure 3-1.

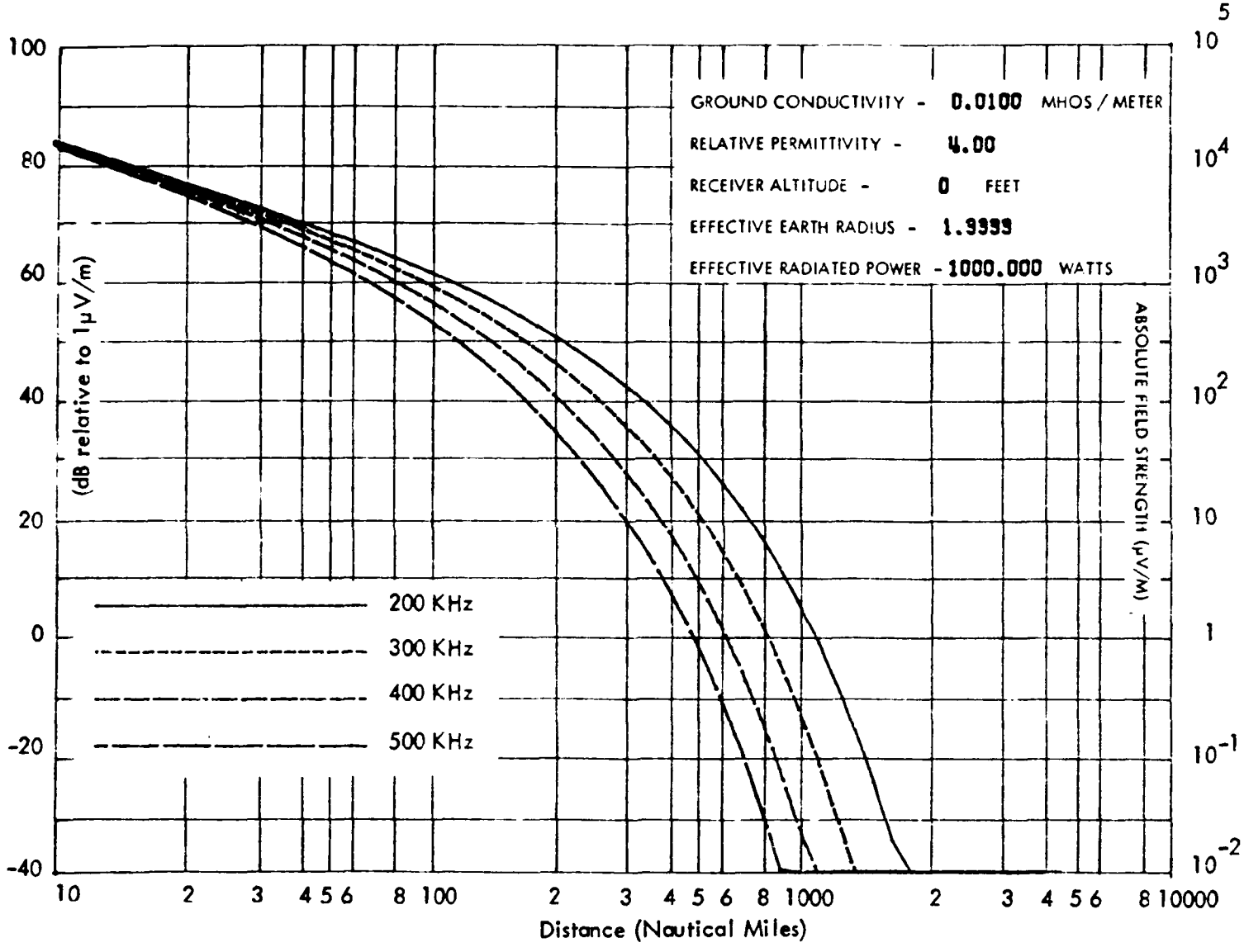

Figure 3-16. Demonstration of Effects of Earth Radius Factor over Ground of Medium Conductivity; Compare to Figure 3-3.

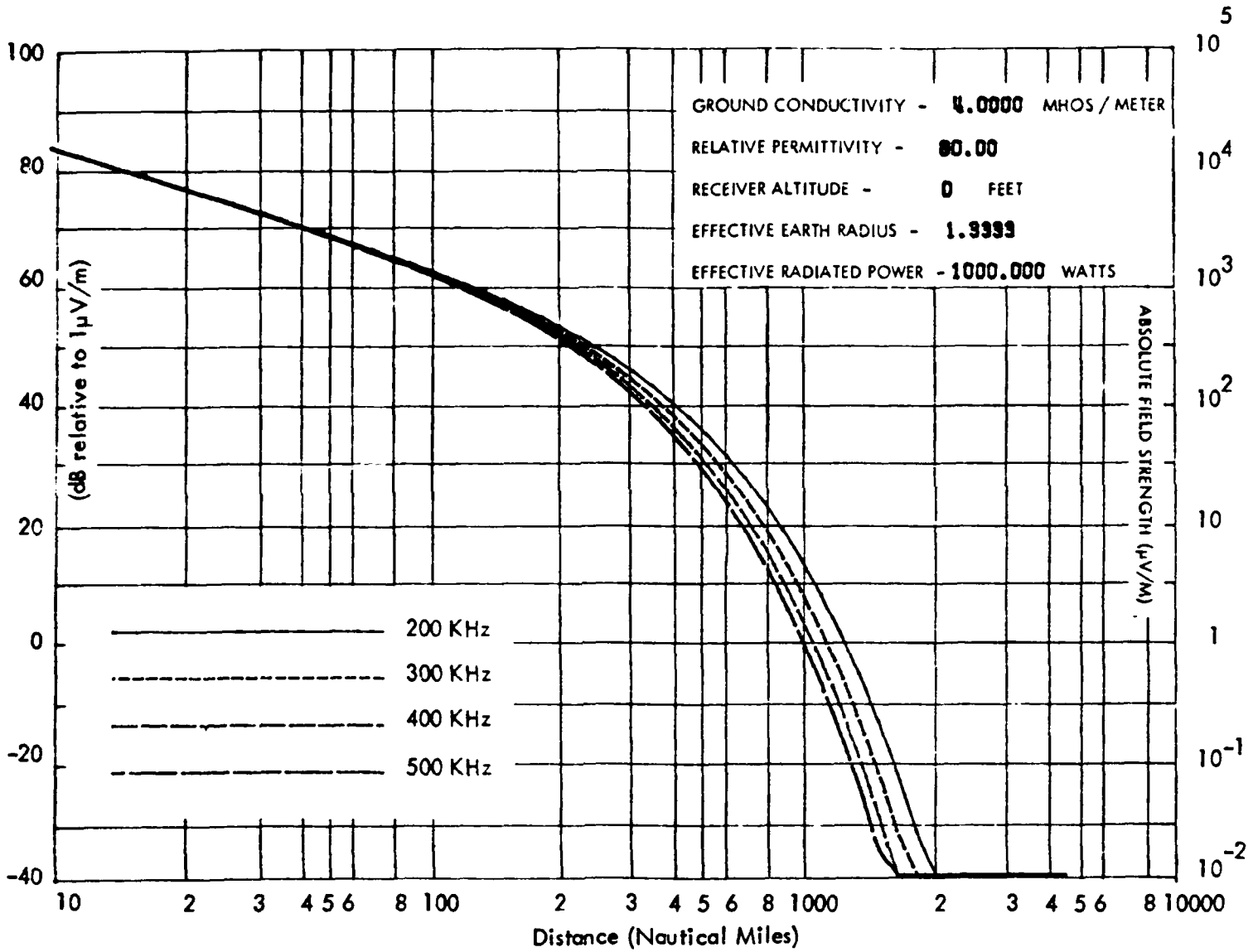

Figure 3-17. Demonstration of Effects of Earth Radius Factor over Sea Water; Compare to Figure 3-5.

IV. SKY WAVE PROPAGATION

The previous two sections have dealt with the propagation of radio waves assuming a smooth, homogeneous, finitely conducting earth and a homogeneous atmosphere. The theoretical computation of wave propagation made under these restraints is usually adequate to describe the propagation mechanism at short distances (less than 300 Km in daytime and 100 Km at night) provided that the propagation path does not deviate considerably from the other assumptions made. Obviously, in reality none of the above assumptions are totally correct in any practical situation, but are made to simplify the propagation model in the interest of time and economy of computation. Data generated under these assumptions is in many cases quite useful as has been seen. However, as distance increases the assumptions become increasingly erroneous. In this section the implication of assuming a homogeneous atmosphere will be reviewed, and a method of computation to allow effects of an inhomogeneous atmosphere to be investigated will be discussed. The next section will deal with the assumption of a smooth, homogeneous earth and the necessary adjustments or modifications required to compute field strength over an irregular, inhomogeneous propagation path.

A. Modeling Sky Wave Effects. By assuming a homogeneous atmosphere as in the previous two sections, the models allowed the waves well above the radio horizon to travel indefinitely in their original direction, thereby having no effect whatsoever on the field strength in the vicinity of the earth's surface. In actuality, the atmosphere is not a homogeneous medium but rather the ionization of the molecules which make up the atmosphere varies. This variation is a complex function of many variables making exact prediction of the ionization levels of the atmosphere impossible. However, variation of this atmospheric makeup can be related to some of the major variables involved such as height, time of day, and season and modeled with sufficient accuracy to generally determine effects of an inhomogeneous atmosphere on radio wave propagation for the frequencies at which we are interested.

The effect that this inhomogeneous atmosphere has on the propagated wave can be modeled as a reflection from a concentric sphere around the earth of radius a + h, with a being the radius of the earth. The geometry of the wave hop propagation model is shown in Figure 4-1.

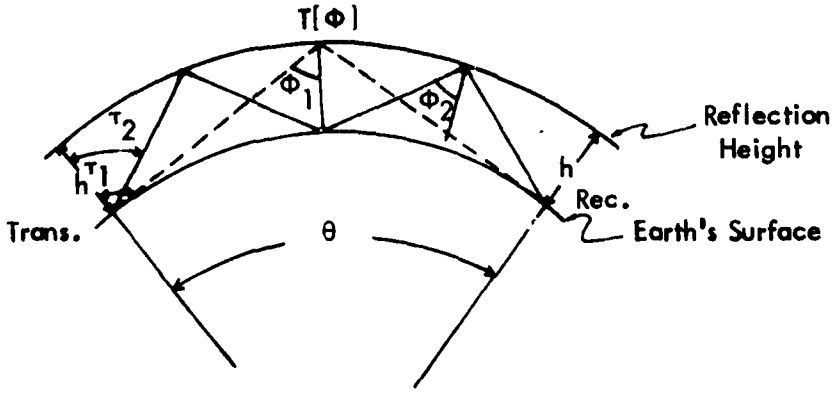

Figure 4-1. Sky Wave Propagation Model.

Since the effect on wave propagation is primarily due to the inhomogeneity in the upper atmosphere, or ionosphere, this type of radio wave propagation is referred to as ionospheric wave propagation. In actuality, of course, the atmosphere cannot be labeled as distinctly as may be suggested by Figure 4-1. The variation in ionization, in general, does not abruptly change at a certain height h above the earth's surface. For instance, Wait [21] has presented methods for calculating these ionospheric reflection coefficients for an exponentially varying isotropic ionosphere. However, the effects of the ionosphere can be reduced to the effects of a concentric sphere of radius a + h and possessing a reflection coefficient matrix T [Φ]. This reflection coefficient matrix is defined as:

$$\begin{bmatrix} E_{re} \\ E_{rm} \end{bmatrix} = \begin{bmatrix} T_{ee} & T_{me} \\ T_{em} & T_{mm} \end{bmatrix} \begin{bmatrix} E_{ie} \\ E_{im} \end{bmatrix} \qquad (4.1)$$

where subscripts r and i indicate reflected or incident electric field, respectively, and subscripts e and m denote vertical or horizontal polarization of the electric field, respectively. As indicated, the values of the reflection coefficients are functions of the angle of incidence of the wave on the ionospheric reflection height.

At the low frequencies that are of interest, this model can be successfully used. However, it can be intuitively seen that the model may become less applicable to higher frequencies. At the low frequencies with long wavelengths, the atmospheric ionization may change considerably over a height differential of one wavelength. Therefore, the ionosphere may closely resemble the sharply bounded concentric sphere that has been assumed. As the frequency is increased, this change in ionization will not be as noticeable over a one wavelength height differential. So again, as in the case of ground wave propagation in Section II, a change in models for the sky wave may be necessary for reliable propagation prediction at different radio frequencies. However, the model suggested in Figure 4-1 has been found to yield acceptable results over the frequency range of our interest (200-500 KHz), although the actual method of computation of field strength may vary depending upon the angle of incidence of the wave on the effective reflection height h.

L. A. Berry has developed a computer model to predict electric field strength due to both the ground wave and sky wave components [1]. Some of the assumptions used in this model are discussed briefly here. More complete documentation of the formulas used in this model has been presented by Berry and Herman [22]. In LFSNR, empirical ionospheric reflection coefficients from CCIR Report 265 [23] have been incorporated into the data base. Being empirical data, these reflection coefficients represent average values, but by incorporating them in the program the need for inputting ionospheric data, such as ionization levels or electron density profiles, is eliminated. Also, in LFSNR, the elements of the T [Φ] matrix T_{em} and T_{me} have been set equal to zero. These cross-polarization coefficients are not available from the CCIR Report 265 as empirical data, and the electric field computation is simplified somewhat by assuming they are zero. Physically this assumption is equivalent to ignoring

the effects of the magnetic field of the earth, so propagation will not be a function of azimuth direction of propagation from the source. Wait [24] has presented the effects of the earth's magnetic field at VLF (very low frequencies). For radio waves in the VLF range, radio wave propagation is enhanced for propagation from east to west and attenuated for propagation from west to east due to effects of the earth's magnetic field. However, the effect is only significant for magnetic latitudes less than 20 degrees [1]. Maps of magnetic latitude indicate that all of the continental United States is above a magnetic latitude [25] of 50°N and, therefore, the earth's magnetic field will have negligible effects on the propagating wave.

Since the sky wave becomes significant only at relatively large distances, LFSNR has provision for calculating the ground wave with only the residue series (see Section II). The electric field components of the significant sky wave hops are then added in phase to the ground wave component to obtain the total field. LFSNR uses geometrical optics to compute the sky wave at short distances, numerical integration techniques along the ray path at medium distances, and a residue series at long distances. As previously mentioned, all formulas used, as well as notes on computer implementation of these procedures, are documented in Berry and Herman [22].

B. Sky Wave Interference Study. The curves generated in this section show the effects the sky wave component has on the total electric field as a function of distance, time of day, month of the year, and for various ground constants. Since our major interest in this report deals with navigational NDB's, some typical values of these facilities have been chosen to determine possible adjacent-channel or co-channel interference due to the sky wave. All curves assume an earth radius factor of 1. As mentioned earlier, most of the more recent literature suggests using an earth radius factor of 4/3, but the effect of the sky wave can be demonstrated here regardless. The choice of an earth radius factor of 1 is made to allow comparison with existing FAA (6050.10) and CCIR (1959 and 1970) curves presently in use.

As mentioned, the purpose of this study is to determine whether or not sky waves will affect the total electric field at any time to create significant interference with adjacent-channel or co-channel beacons. Interference due to sky wave is possible since geographical separation of NDB's is usually determined according to the ground wave field strength. The specifications of the coverage range of an NDB is that area over which the field strength of that particular beacon is 70 μV/m or greater. Similarly, the interference range of a beacon is defined as the area inside which the field strength of that beacon is 12.5 μV/m or greater. Therefore, any beacon site must be located at a point such that its interference range does not overlap with the range of any other NDB, and its coverage range is not co-existent at any point with the interference range of any other NDB. Thus the signal from any co-channel NDB within the coverage range of a given NDB under normal conditions is to be 15 dB or more below that of the original NDB. However, since the monitor alarm on most NDB facilities is not activated until the power output of the facility is at one-half its normal value, a difference in the signals from the desired beacon and an interfering beacon of 12 dB is all that is insured. In addition to geographical separation as a means of insuring that NDB interference is not encountered, FAA specifications allow receiver

selectivity, or rejection of adjacent channel signals to be considered in NDB siting. The rejection provided by the receiver is given in FAA Handbook 6050.10 and is reproduced here in Table 4-1. Thus protection of a given beacon from an adjacent channel beacon can be provided by receiver rejection as well as geographical separation. The combination of these two means of eliminating adjacent channel interference must result in a signal of 15 dB or more higher for the beacon everywhere in its coverage range than the signals from surrounding beacons.

As a means of examining the effects of the sky wave to determine a possibility of interference, program LFSNR has been utilized to generate data under various conditions which may be encountered by non-directional beacons. This data has been plotted and is presented in this section. As indicated, in each curve an effective radiated power of 10 watts has been assumed. Although this value is greater than the ERP of all NDB facilities in this report, its assumption is not restrictive, since the model is completely linear in its calculation of field strength and, therefore, a simple shift of the curve is all that is necessary to apply the curves presented here to a facility of any particular ERP. Each curve also indicates the ground wave component of the total electric field with a dashed line so that effects of the sky wave will be readily ascertained. All data generated here is for the extremes in our frequency range under consideration (200 and 500 KHz) as the sky wave effects of intermediate frequencies are of a similar nature as effects present for these frequencies. All other information used by the model, such as ground constants, time of day, and sun spot activity, is given with each figure.

Figures 4-2 through 4-6 indicate the effects of the sky wave on a beacon operating at 200 KHz. The ground constants used correspond to what is usually considered ground of medium conductivity and each figure shows the amplitude of electric field strength as a function of distance for various times of day and season. Clearly the effects at night are the most severe of all conditions. It should be noted here that this computer model uses the same ionospheric reflection coefficients for all nighttime calculations regardless of the season. The reason for this is that the seasonal variation of ionospheric makeup is much less at nighttime than it is in the day. This fact has been reported by Kenneth Davies in Ionospheric Radio Propagation [26]. In measuring electron density profiles for three different geographical locations, the variation of the profiles at midnight for all three locations is considerably less than the variation at noon.

The caption for these figures also indicates that this data was generated by program LFSNR for conditions of maximum sun spot activity. LFSNR has provision to choose different sets of ionospheric reflection coefficients for maximum and minimum sun spot activity. These coefficients are, of course, empirical and are obtained from the same reference sited earlier (CCIR Report 265 [23]). The solar cycle has demonstrated periodicity with a cycle time of lasting approximately 11 years [27]. As we will see later, the solar cycle has noticeable, but not major, effects on radio wave propagation in the frequency range of 200-500 KHz. Generally a more important consequence of the solar cycle at these frequencies is its effect on atmospheric noise and, therefore, on the signal-to-noise ratio for NDB signals.

AD-A111 187 OHIO UNIV ATHENS DEPT OF ELECTRICAL ENGINEERING F/G 17/7
LOW-FREQUENCY BEACON SIGNAL STRENGTH DETERMINATION.(U)
JAN 80 J L BASH, R J LUEBBERS DOT-FA79WA-4278
UNCLASSIFIED EER-81-2 FAA-R-6050.2 NL

2 OF 3
AD
A111187

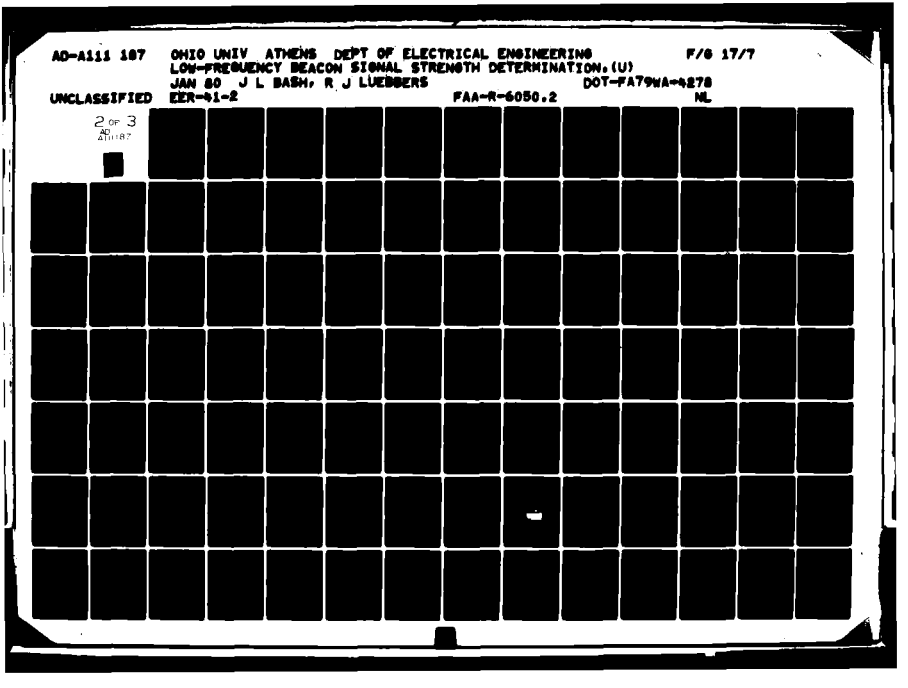

Frequency Off-Set From Desired Signal	Receiver Rejection
1 KHz	0 dB
2 KHz	1 dB
3 KHz	12 dB
4 KHz	28 dB
5 KHz	40 dB
6 KHz	50 dB

Table 4-1. Adjacent Channel Receiver Rejection [19].

As can be seen by observing Figures 4-2 through 4-6, the effects of the ionospheric wave on the 200 KHz signal are most prominent at night. At this time the conditions in the ionosphere are such that the maximum reflection of the electromagnetic wave occurs. Therefore, more hops of the sky wave become significant at any given distance and the constructive and destructive interference of these hop contributions lead to irregular field strength as illustrated in Figures 4-2 and 4-6. It should be pointed out here that if experimental measurements of field strength were made at distances great enough for the sky wave effects to become significant, the graphs shown here do not intend to suggest that this exact variation of field strength would occur. In other words, the calculations used by the model assume statistically average values in determining ionospheric reflection coefficients for the particular season and time of day under consideration. The figures in this section merely indicate field strength variation for these average conditions. Perhaps a more useful or meaningful computation would be one that could set upper and lower limits on the field strength at a given distance such that the actual measured field strength under the circumstances specified would be within those limits a certain percentage of the time. However, since this is an introduction to ionospheric effects, such a study has not been made. It is felt that the accompanying curves sufficiently illustrate ionospheric effects for the purposes of this report. Keeping these effects in mind, it is evident that next to nighttime the interference to the ground wave component is most severe on winter days (Figure 4-3). Here the effects of the ionosphere are not as significant at larger distances as they are at night, but certainly are more noticeable than at summer or equinox conditions (Figures 4-4 and 4-5, respectively). As a rough method for comparison of the effects of various seasons and times of day, the distances on each of the curves where the ionospheric wave causes the field strength to vary from the ground wave component by 3 dB can be noted. Figure 4-2 shows that this distance could be 110 nm for nighttime conditions. In the daytime, in winter, the first 3 dB variation occurs around 240 nm, in summer at 800 nm, and at equinox this distance would be around 530 nm.

Figures 4-7 through 4-11 illustrate the effects of the ionosphere on the wave propagation of 500 KHz under the same conditions as Figures 4-2 through 4-6 for 200 KHz. The general conclusions that can be drawn are very much the same as for the 200 KHz curves. However, the differences between the ground wave component and the total field appears to be slightly greater for the 500 KHz wave, since the ground wave in this case is attenuated at a faster rate for the higher frequencies. Nevertheless, the nighttime effects are clearly the most significant, followed by winter, equinox, and summer days as is the case with the 200 KHz curves. Again, Figures 4-7 and 4-11 show identical curves since the model assumes all nighttime coefficients are equal without regard for season. In terms of the 3 dB variation of the total field from the ground wave, the approximate distances at 500 KHz are as follows: nighttime - 110 nm; winter day - 200 nm; summer day - 440 nm; and equinox day - 320 nm. Thus it can be seen by comparing these distances with those from the 200 KHz curves that since the 500 KHz ground wave component is at a much lower level at larger distances than that of 200 KHz, the sky wave becomes more significant at 500 KHz.

The next set of Figures (4-12 through 4-15) have been generated for the same conditions as Figures 4-2 through 4-6 with the exception that Figures 4-12 through 4-15 assume a minimum in the sun spot cycle in the sky wave calculations. Note that the figure for conditions of summer night has been omitted here since all nighttime calculations assume identical ionospheric reflection coefficients and, therefore, all nighttime propagation curves for a given set of ground constants and time periods will be identical. A comparison of Figures 4-2 and 4-12 shows that during the minimum of the sun spot cycle, the ionospheric wave is slightly less prevalent at nighttime conditions. Figure 4-12 shows that the wave propagation is definitely affected more at night than under any other conditions for the minimum sun spot cycle as well, but this effect is not quite as evident as for the maximum sun spot cycle. The 3 dB variation for nighttime at a minimum in the sun spot cycle is around 150 nm as compared to the 110 nm found for a maximum sun spot cycle. Comparing Figure 4-13 with Figure 4-3, we see that here also the propagated wave is less affected by the ionosphere during the period of minimum sun spot cycle for winter day also. The 3 dB variation in Figure 4-13 is at 300 nm. This compared with 240 nm in Figure 4-3. For summer days, Figure 4-14 shows the field strength computed for minimum sun spot cycles, as compared to the maximum sun spot cycles shown in Figure 4-4. As is evident, the 3 dB point is still around 800 nm but beyond that point the curve for minimum sun spot cycles is affected slightly more by the sky wave. This is apparently due to the relative phasing of the components of the ground wave and the various hops as they are added in the calculation. The equinox curves (Figures 4-5 and 4-15) illustrate that wave propagation at minimum sun spot cycles is also affected slightly more by the ionosphere than under conditions of maximum sun spot cycles at this time. The computed curves of total electric field are similar with the exception of a sharp relative minima at 530 nm in Figure 4-15, but even at shorter distances, more sky wave interference is noticeable. This is verified by the fact that the first 3 dB variation occurs at 400 nm for the minimum sun spot cycle, as compared to 530 nm for the maximum cycle. Summarizing the results of the comparison of these four figures, it can be said that the sky wave component under the worst cases (nighttime and winter day) causes slightly less interference with the ground wave component at the minimum sun spot cycle than at maximum sun spot cycles. At summer and equinox day times, sky wave effects appear to be slightly more evident for minimum sun spot cycles. The major difference is noticeable in the equinox curves, when conditions are the most unstable, due to relatively large variations in the weather at these periods of time. Therefore, the significant changes in the field strength calculations for these curves cannot be directly attributed to the changes in the sun spot cycle, but rather to inherent variations in the ionospheric makeup during the equinox period. These variations could easily have accounted for the slightly different ionospheric reflection coefficients measured at this time and used in program LFSNR's calculation.

Figures 4-16 through 4-19 are included to show effects of the sun spot cycle on 500 KHz wave propagation. To determine these effects, they can be compared with Figures 4-7 through 4-10. The conclusions that may be drawn from this comparison are almost the same as those drawn when comparing the 200 KHz curves. Again, the nighttime curve demonstrates slightly less sky wave effect under conditions of minimum sun spot cycle. The same is true for the winter day (Figure 4-17), and in the case also for

summer day (Figure 4-18). Comparison of the 500 KHz equinox curves also gives us the same information as the 200 KHz curves. Here Figure 4-19, the minimum sun spot cycle, has a sharp minimum at 380 nm; but aside from this, the sky wave effects are no more prevalent for minimum than for the maximum sun spot cycles. Evaluation of these figures to obtain the 3 dB variation reveals that for nighttime the first 3 dB variation occurs at 110 nm, for winter day at 200 nm, summer day at 550 nm, and equinox day at 340 nm.

Now that the effects of an inhomogeneous ionosphere on radio wave propagation have been demonstrated for 200 and 500 KHz on average ground conditions, it may be well to consider briefly the physical significance of the variations in electric field strength shown in the figures in this section. Of course, it is clear that these variations are caused by the various hops contributing to the total field by adding as phasors to the ground wave component, sometimes providing constructive interference and sometimes destructive interference. Perhaps by examining some of the curves in more detail a physical explanation for the phenomena illustrated will be possible. Since the output of program LFSNR includes the separate contribution of each hop, the distances at which any given hop makes a significant contribution can be determined.

Since the major effect of the sky wave is apparent at night and on winter days, an examination of Figures 4-2, 4-3, 4-7 and 4-8 will be made here. Beginning with Figure 4-2, the output of LFSNR from which this plot was generated indicates that the first hop of the sky wave component is equal in magnitude to the ground wave component at around 290 nm. Also at shorter distances the major fluctuations in field strength are due to the first hop wave, since all other hops are at least 10 dB below the first hop in amplitude. This first hop adding to the ground wave causes variations of 6 to 8 dB in field strength between 290 and 500 nm. At this distance, however, the ground wave is becoming insignificant in the total electric field and the first sky wave hop is the major contributor to the total field. The irregularities between 500 and 1300 nm are caused by the interaction of the first and second hops of the sky wave. At roughly 1300 nm the amplitude of these two components is equal and, therefore, the very irregular curve at this distance results. At the limit of the model, at 1800 or 1900 nm, the second hop becomes the major factor in the total field strength, surpassing the first hop in amplitude. Beyond this point, the variations in total field strength are caused by interactions of the second hop with both the first hop and the third hop. The first hop is attenuated rapidly and is about 10 dB below the second hop at around 2200 nm. This attenuation can be expected upon consideration in Figure 4-2, since the calculation point at large distances is moving into the shadow region for the first hop wave. Toward the end of the computation, the third hop is becoming significant and is causing further interference with the second hop.

Much the same comments can be made concerning Figure 4-3. However, since the sky wave is slightly less significant, the distances at which the various hops become significant are greater. For instance, the distance at which the amplitude of the first hop sky wave term exceeds the ground wave component is nearly 400 nm. From this point on some phasor additions of the first and second hops result in the variation of the electric field out to 1800 nm, where the second hop sky wave term exceeds the

first. From 1800 nm to the end of the calculation the second hop is the significant contributor to total electric field.

Figures 4-7 and 4-8 reinforce the statements previously made in this regard for the 200 KHz curves. However, since the higher frequency ground wave component has more attenuation, the sky wave components in general make up more of the total field at a given distance. In Figure 4-7 the first hop of the sky wave is equal to the ground wave term at 200 nm where it makes the major contribution to the electric field out to around 1300 nm, at which point the second hop is equal in magnitude to the first hop term. At 1300 nm, the interference between these two components is evident in the figure as their phases are changing with respect to one another. Beyond this point the first hop component is quickly attenuated when moving into its shadow region and the second hop takes over. Figure 4-8 is similar to Figure 4-7, but again in daytime the sky wave has a little less effect so the distances at which the first hop equals the ground wave component is greater. This distance is, in fact, 300 nm and the second hop effects are evident at the very end of the calculation at around 1300 nm where its interference with the first hop is just beginning.

Some general comments concerning the physical significance illustrated by these curves can now be made. Again referring to Figure 4-8, and keeping in mind the model used in Figure 4-1, the somewhat drastic variations in field strength at distances less than 400 nm can be expected as the first hop phase changes very slowly (compared with the ground wave) for a movement of a given distance along the earth's surface. Then as one moves away from the transmitter the angle at which the first hop strikes the earth's surface approaches grazing. Therefore, the phase of the sky wave changes at about the same rate as the ground wave, since a change in distance along the earth's surface is basically a movement parallel to the direction of propagation. This accounts for the relatively smooth curve in Figure 4-8 between 500 and 1200 nm. This smooth portion of the curve is evident to varying degrees in all these curves, depending upon the distances at which the multiple hops begin interfering with the first hop. As distance from the transmitter is further increased, the calculation point moves into the shadow area and the first hop becomes insignificant compared to the total field. For the second hop the process repeats in a similar manner, except that as distances increase additional hops can become significant, so it is possible to have any number of hops contributing to the field at any given time. This is the case at large distances in Figure 4-2, where the second and third hops both are strong enough to provide noticeable contributions to the total field. This, of course, results in the large fluctuations at distances around 2000 nm.

The final four curves in this section are included to illustrate the effects of the sky wave over different propagation media. Since all previous figures illustrated that conditions of nighttime and a maximum sun spot cycle resulted in the most significant effect of the sky wave, those conditions have been used here. Figure 4-20 shows the total electric field as well as the ground wave component for propagation over ground with a conductivity of 0.001 mhos/meter and a relative permittivity of 4.0, the ground constants normally used to model desert. The basic differences in these two conditions, of course, are that of the more serious attenuation of the ground wave over this ground of low conductivity and the change in the reflection off the

ground of the multiple hop components. Thus it can be seen that since the ground wave provides less signal strength, the sky wave is more significant under these conditions. While the field strength levels are lower for all distances, differences between the total field and the ground wave component are greater. The first hop equals the ground wave in amplitude at a distance of 150 nm. The second hop effects are noticeable at around 800 nm, and the second hop amplitude is equal to the first at 1300 nm.

Figure 4-21 shows sky wave propagation at 200 KHz over sea water. These conditions allow the ground wave to achieve greater distances and, therefore, the total field strength is high. The irregular field strength curve also is indicative of the multiple hop ionospheric waves reflecting well not only off the ionosphere, since nighttime conditions are present, but off the surface of the sea water as well since its conductivity is greater than soil. This effect is apparent from the interference that the first hop receives from the second at distances between 400 and 1200 nm, as well as at distances beyond 1300 nm where the third and fourth hops are providing interference to the second hop.

Figures 4-22 and 4-23 illustrate the same effects as Figures 4-20 and 4-21, respectively, for a frequency of 500 KHz. Figure 4-21 shows that the sky wave effects for desert are similar to the effects on medium earth, but the sky wave is much more significant because of the attenuation of the ground wave over the poorly conducting earth. Again in Figure 4-23 the sea water propagation path is conducive to wave propagation of multiple hops since the surface of the sea water provides better reflection than that of the earth.

In an attempt to make this sky wave interference study more quantitative, the figures illustrated and referred to in this section will be utilized to determine the possibility of interference from the sky wave of co-channel beacons geographically separated by a distance conforming to the specifications given in FAA Handbook 6050.10 when only the ground wave is considered. The linearity of the model will be used to determine the possibility of interference for beacons of different power outputs. Although it is evident that the most significant interference will occur at night, the other times of day and season will also be considered in order to quantitatively compare these sky wave effects.

The procedure followed in determining the possibility of co-channel interference is briefly outlined here. First, the coverage radius and interference radius of the beacons in question will be determined from the ground wave component in each of the figures. The beacons will then be assumed to be geographically separated from the minimum distance required so that their respective coverage areas and interference areas do not overlap when the ground wave only is considered. These minimum distances, along with the corresponding coverage and interference radii, for the various ground constants at 200 KHz are given in Table 4-2 and at 500 KHz in Table 4-3. Next, the sky wave components will be considered and the interference created by the sky wave will be determined from the figures. This involves connecting the relative minima in the vicinity of the coverage radius given in Tables 4-2 and 4-3 with a straight-line. The assumed field strength at the coverage radius will then be the point where this line crosses the exact coverage radius. This procedure essentially is equivalent to a

Propagation Path	Coverage Radii, Interference Radii, and Minimum Separation Distance								
	1 Watt ERP			10 Watts ERP			100 Watts ERP		
	Coverage Radius(nm)	Interf. Radius(nm)	Separation Dist.(nm)	Coverage Radius(nm)	Interf. Radius(nm)	Separation Dist.(nm)	Coverage Radius(nm)	Interf. Radius(nm)	Separation Dist.(nm)
Earth of Medium Con-ductivity	70	190	260	140	280	420	240	400	640
Desert	33	85	118	70	140	210	120	190	310
Sea Water	70	200	270	170	330	500	270	550	770

Table 4-2. Minimum Separation Distances Determined from Ground Wave for Equal-Powered Facilities Operating at 200 KHz.

Propagation Path	Coverage Radii, Interference Radii, and Minimum Separation Distance								
	1 Watt ERP			10 Watts ERP			100 Watts ERP		
	Coverage Radius(nm)	Interf. Radius(nm)	Separation Dist. (nm)	Coverage Radius(nm)	Interf. Radius(nm)	Separation Dist. (nm)	Coverage Radius(nm)	Interf. Radius(nm)	Separation Dist. (nm)
Earth of Medium Conductivity	40	110	150	85	160	245	130	210	340
Desert	16	29	47	23	49	72	35	80	115
Sea Water	70	190	260	140	280	420	230	380	610

Table 4-3. Minimum Separation Distances Determined from Ground Wave for Equal-Powered Facilities Operating at 500 KHz.

weighted average of the relative minima in the vicinity of the coverage radius. A similar technique is used in computing the field strength when considering sky wave effects at the interference radius, with the exception that the relative maxima are used. This procedure, of course, assumes minimum signal strength or destructive interference with the ground wave at the coverage radius and maximum field strength, or constructive interference at the interference radius. This is clearly the worst case, but this is obviously the one that must be considered when examining possible co-channel interference caused by sky wave effects. The method has been applied using those curves generated for a maximum sun spot cycle. However, the differences for a minimum sun spot cycle have already been found to be insignificant.

Tables 4-4 through 4-7 show the results of this comparison. These figures are determined assuming two beacons of the same ERP and, therefore, having identical coverage radii. These tables show the minimum field strength at the coverage radius distance (the point where the ground wave field strength is 70 μV/m, or 37 dB relative to 1 μV/m from which the maximum field strength at the interference radius (the point at which the ground wave field strength is 12.5 μV/m, or 22 dB relative to 1 μV/m) is subtracted to find the difference of the two signals. The desired difference between these signals is 15 dB, as noted in the FAA Handbook. The tables show that the effects at night are obviously the most severe of all. Also, since the sky wave becomes more significant at greater distances, the high power beacons are clearly more prone to cause interference, as their operation is intended for greater distances.

As the comparison was constructed, there can be no problem with interference of even the beacon of 100 watts ERP over normal earth in summer or equinox days. However, at night the interfering signal can actually be stronger than the desired signal from the primary beacon, as indicated in Table 4-4 for the high power facility. Also as expected sea water and desert conditions present interference problems at night (Tables 4-6 and 4-7) since the sea water allows the sky wave to reflect off its surface well, and the ground wave does not propagate well in desert conditions.

As is apparent from the tables, the field strength of the beacon at its coverage radius is always very nearly the desired 37 dB amplitude. Only in the case of the 100 watt ERP facility propagating over sea water does this value vary by more than 3 dB. But clearly, under all nighttime conditions for beacons of over 1 w ERP, the interfering signal is significantly above the 22 dB relative to 1 μV/m required to obtain a difference of 15 dB. This is also illustrated if the nighttime curves over medium ground are considered once again. In Figure 4-2 we see that the interference radius determined by the ground wave component is only 280 nm for a 10 W ERP facility operating at 200 KHz. However, the sky wave causes interference which enables the total electric field to maintain an amplitude of 12.5 μV/m out to distances of 800 nm. For beacons operating at 100 W ERP, these figures are 400 nm when considering the ground wave only and 1200 nm when the total field is considered. These distances for nighttime conditions for various types of earth are given in Table 4-8 for 200 KHz and in Table 4-9 for 500 KHz facilities.

Conditions	Minimum Field Strength at Coverage Radius (dB relative to 1 μV/m)	- Maximum Field Strength at Interference Radius (dB relative to 1 μV/m)	= Difference (dB)
	1 Watt ERP	10 Watts ERP	100 Watts ERP
Nighttime	37 - 25 = 12	35 - 28 = 7	31 - 36 = -5
Winter Day	37 - 23 = 14	37 - 26 = 11	35 - 32 = 3
Summer Day	37 - 22 = 15	37 - 22 = 15	37 - 22 = 15
Equinox Day	37 - 22 = 15	37 - 23 = 15	37 - 23 = 14

Table 4-4. NDB Sky Wave Interference of Equal-Powered Facilities at 200 KHz Operating on Soil of Medium Conductivity. Separation Distances as Given in Table 4-2.

Conditions	Minimum Field Strength at Coverage Radius (dB relative to 1 μV/m)	- Maximum Field Strength at Interference Radius (dB relative to 1 μV/m)	= Difference (dB)
	1 Watt ERP	10 Watts ERP	100 Watts ERP
Nighttime	37 - 24 = 13	36 - 27 = 9	35 - 32 = 3
Winter Day	37 - 22 = 15	37 - 22 = 15	37 - 24 = 13
Summer Day	37 - 22 = 15	37 - 22 = 15	37 - 22 = 15
Equinox Day	37 - 22 = 15	37 - 22 = 15	37 - 22 = 15

Table 4-5. NDB Sky Wave Interference of Equal-Powered Facilities at 500 KHz Operating on Soil of Medium Conductivity Separation Distances as Given in Table 4-3.

Propagation Path	Minimum Field Strength at Coverage Radius (dB relative to 1 μV/m)	− Maximum Field Strength at Interference Radius (dB relative to 1 μV/m)	= Difference (dB)
	1 Watt ERP	10 Watts ERP	100 Watts ERP
Earth of Medium Conductivity	37 - 25 = 12	35 - 28 = 7	31 - 36 = -5
Desert	37 - 24 = 13	37 - 28 = 8	34 - 35 = -1
Sea Water	37 - 27 = 11	34 - 30 = 4	27 - 36 = -9

Table 4-6. NDB Sky Wave Interference Under Nighttime Conditions for Equal-Powered Facilities Operating at 200 KHz Separation Distances as Given in Table 4-2.

Propataion Path	Minimum Field Strength at Coverage Radius (dB relative to 1μV/m)	-	Maximum Field Strength at Interference Radius (dB relative to 1μV/m)	=	Difference (dB)
	1 Watt ERP		10 Watts ERP		100 Watts ERP
Earth of Medium Conductivity	37 - 24 = 13		36 - 27 = 9		35 - 32 = 3
Desert	37 - 22 = 15		37 - 24 = 13		37 - 29 = 8
Sea Water	37 - 24 = 13		37 - 27 = 10		25 - 34 = -9

Table 4-7. NDB Sky Wave Interference Under Nighttime Conditions for Equal-Powered Facilities Operating at 500 KHz Separation Distances as Given in Table 4-3.

Propagation Path	Maximum Distance at Which Field Strength is 12.5 μV/m (nm)					
	Considering Only Ground Wave Component			Considering Total Field		
	1 Watt ERP	10 Watts ERP	100 Watts ERP	1 Watt ERP	10 Watts ERP	100 Watts ERP
Earth of Medium Conductivity	190	280	400	230	800	1200
Desert	85	140	190	95	300	800
Sea Water	200	330	500	290	1200	1600

Table 4-8. Effect of Considering Sky Wave on NDB Interference Radius at 200 KHz Under Nighttime Conditions.

Propagation Path	Maximum Distance at Which Field Strength is 12.5 μV/m (nm)					
	Considering Only Ground Wave Component			Considering Total Field		
	1 Watt ERP	10 Watts ERP	100 Watts ERP	1 Watt ERP	10 Watts ERP	100 Watts ERP
Earth of Medium Conductivity	110	160	210	120	220	850
Desert	29	49	80	29	57	380
Sea Water	190	280	380	200	950	1300

Table 4-9. Effect of Considering Sky Wave on NDB Interference Radius at 500 KHz under Nighttime Conditions.

Another calculation which can be made to provide some means of showing sky wave effects present is to determine what percentage of the original coverage area of a co-channel beacon separated the minimum distance allowed considering ground wave only is subject to interference when sky wave effects are included. For the facilities considered in this section, this computation has been made assuming sky wave effects under nighttime conditions. Figure 4-24 illustrates the geometry of the problem, where the beacons are seen to be separated by a distance corresponding to the sum of the coverage radius, r_c, and the interference radius, r_{ig}, given in Tables 4-2 and 4-3. Then the interference radii of the beacons are assumed to be increased to the amount shown in Tables 4-8 and 4-9, r_{it}. Using this extended interference radius, the amount of the original coverage area subject to interference from the other beacon has been computed, and the results are shown in Table 4-10 for 200 KHz and Table 4-11 for 500 KHz. As an example, consider the case of earth of medium conductivity, 1 watt ERP, and operating at 200 KHz given in Table 4-10. The coverage radius, r_c, the interference radius considering only the ground wave, r_{ig}, and the separation distance for this case are given in Table 4-2 and are found to be 70 nm, 190 nm, and 260 nm, respectively. Table 4-8 then shows that the interference radius when the total field is considered for nighttime conditions, or r_{it}, is 230 nm. Using this interference radius, extended from 190 to 230 nm, it can be found that 21% of the original coverage area could be subject to interference from another equal-powered facility. Cases for the various propagation paths and effective radiated powers have been computed in a similar manner and tabulated in Tables 4-10 and 4-11.

As the data in these tables illustrates, the 100 watt ERP beacon can cause interference over the total coverage area of an adjacent 100 watt ERP facility under all ground conditions considered. This is also true of the 10 watt ERP beacons operating at 200 KHz. Even the beacon radiating 1 watt of effective power can cause interference in a significant portion of the coverage area of an adjacent beacon. The effect is less severe for lower powered beacons operating at a frequency of 500 KHz, since the coverage and interference ranges defined by the ground wave are at shorter distances and, therefore, sky wave interference is less of a problem.

In conclusion, then, it would certainly appear that co-channel and adjacent channel interference of NDB facilities is possible if the minimum geographical separation is determined by considering the ground wave component only, especially for higher powered facilities. Although this study is not intended to be exhaustive and the accompanying figures represent typical interference under the given conditions, the results suggest that the sky wave propagation must be considered in geographical separation determinations if co-channel interference from this source is to be properly predicted.

Propagation Path	Portion of Coverage Area Subject to Interference Due to Sky Wave		
	1 Watt ERP	10 Watts ERP	100 Watts ERP
Earth of Medium Conductivity	21%	100%	100%
Desert	9%	100%	100%
Sea Water	63%	100%	100%

Table 4-10. Portion of Coverage Area of Equal-Powered Facilities Subject to Interference under Nighttime Conditions when Sky Wave is Considered. Operating Frequency -200 KHz. Separation Distance as Given in Table 4-2.

Propagation Path	Portion of Coverage Area Subject to Interference Due to Sky Wave		
	1 Watt ERP	10 Watts ERP	100 Watts ERP
Earth of Medium Conductivity	6%	28%	100%
Desert	0.0%	12%	100%
Sea Water	3%	100%	100%

Table 4-11. Portion of Coverage Area of Equal-Powered Facilities Subject to Interference under Nighttime Conditions when Sky Wave is Considered. Operating Frequency -500 KHz. Separation Distances as Given in Table 4-3.

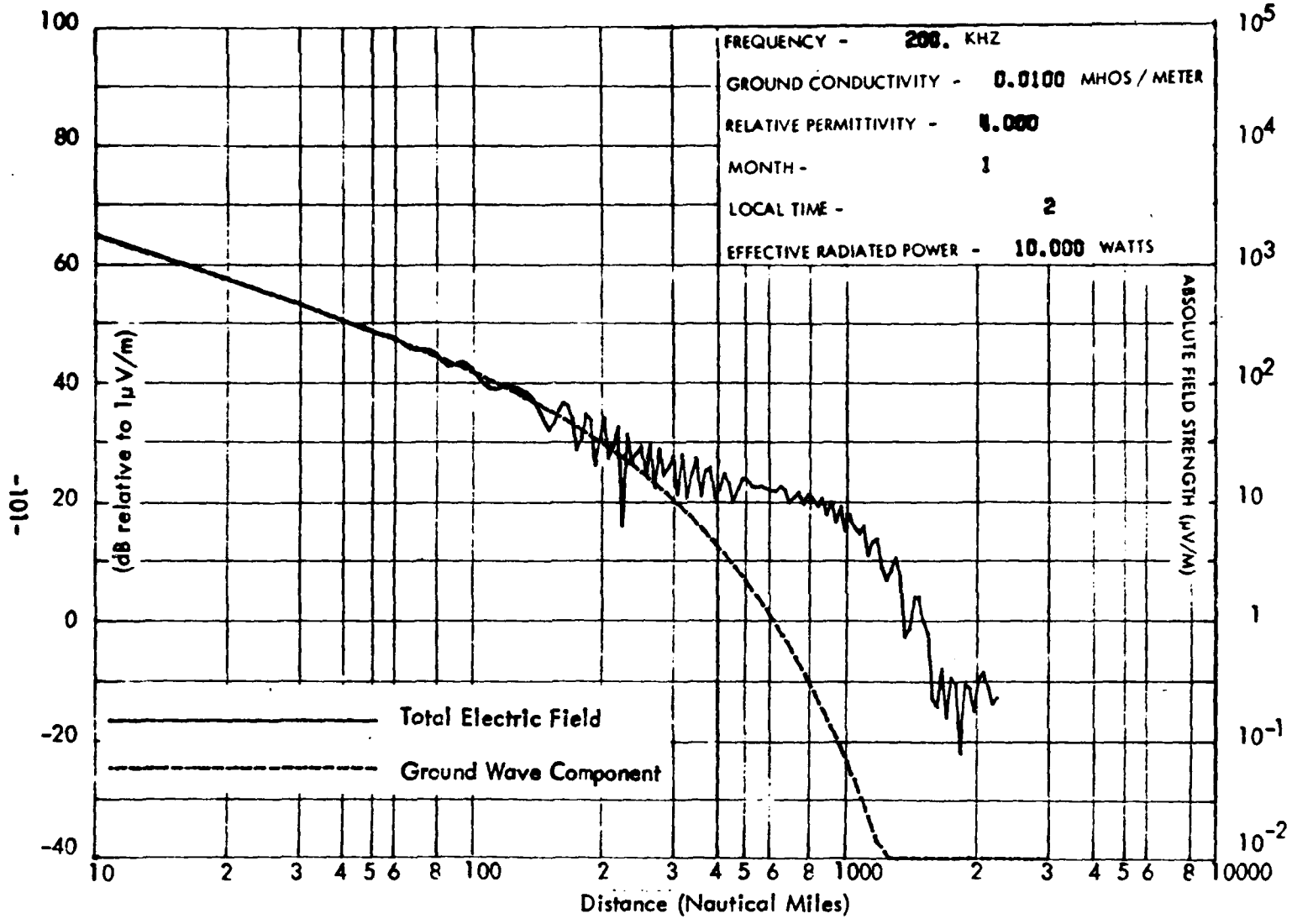

Figure 4-2. Medium Earth Conductivity - Maximum Sun Spot Cycle.

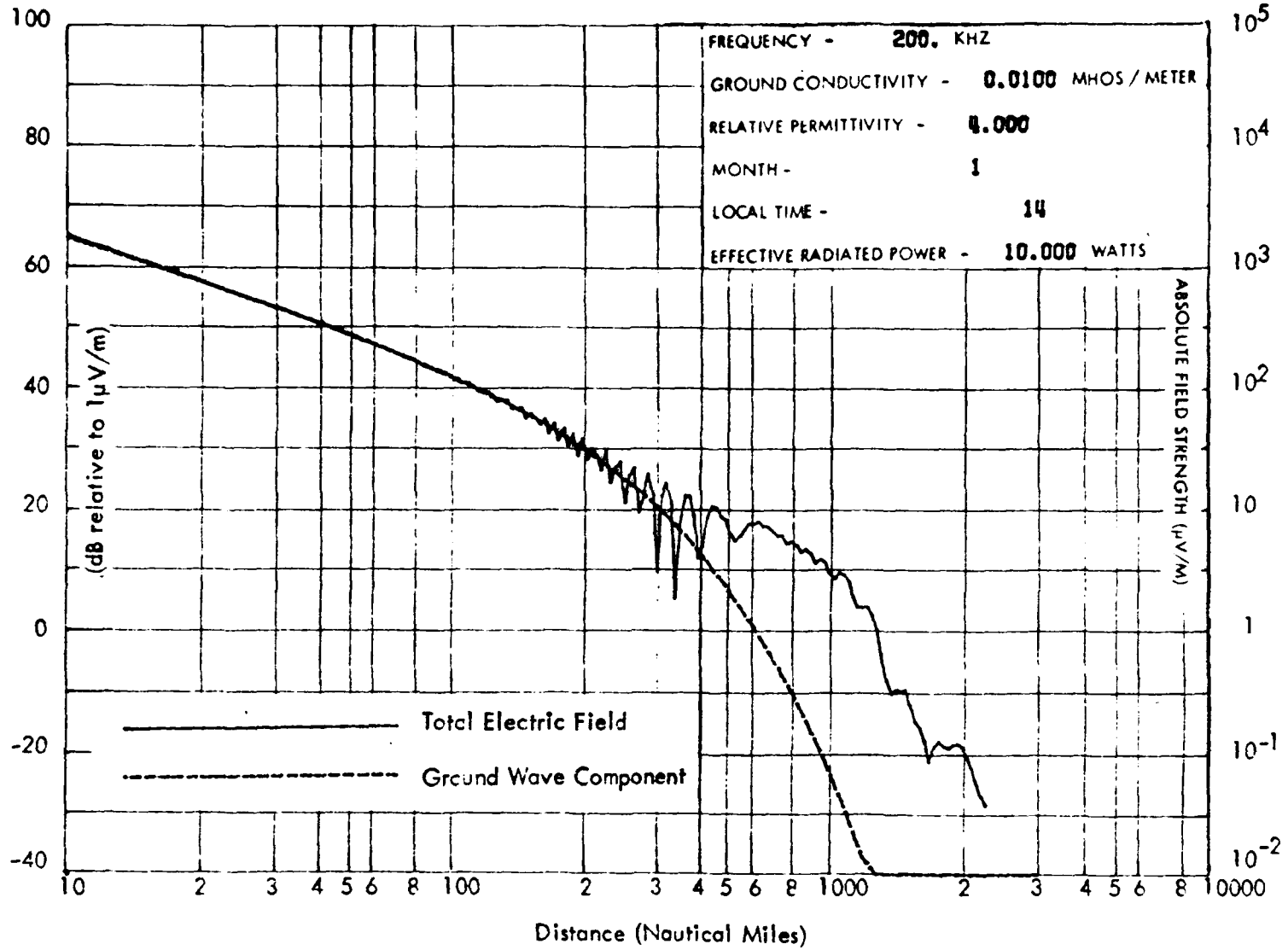

Figure 4-3. Medium Earth Conductivity - Maximum Sun Spot Cycle.

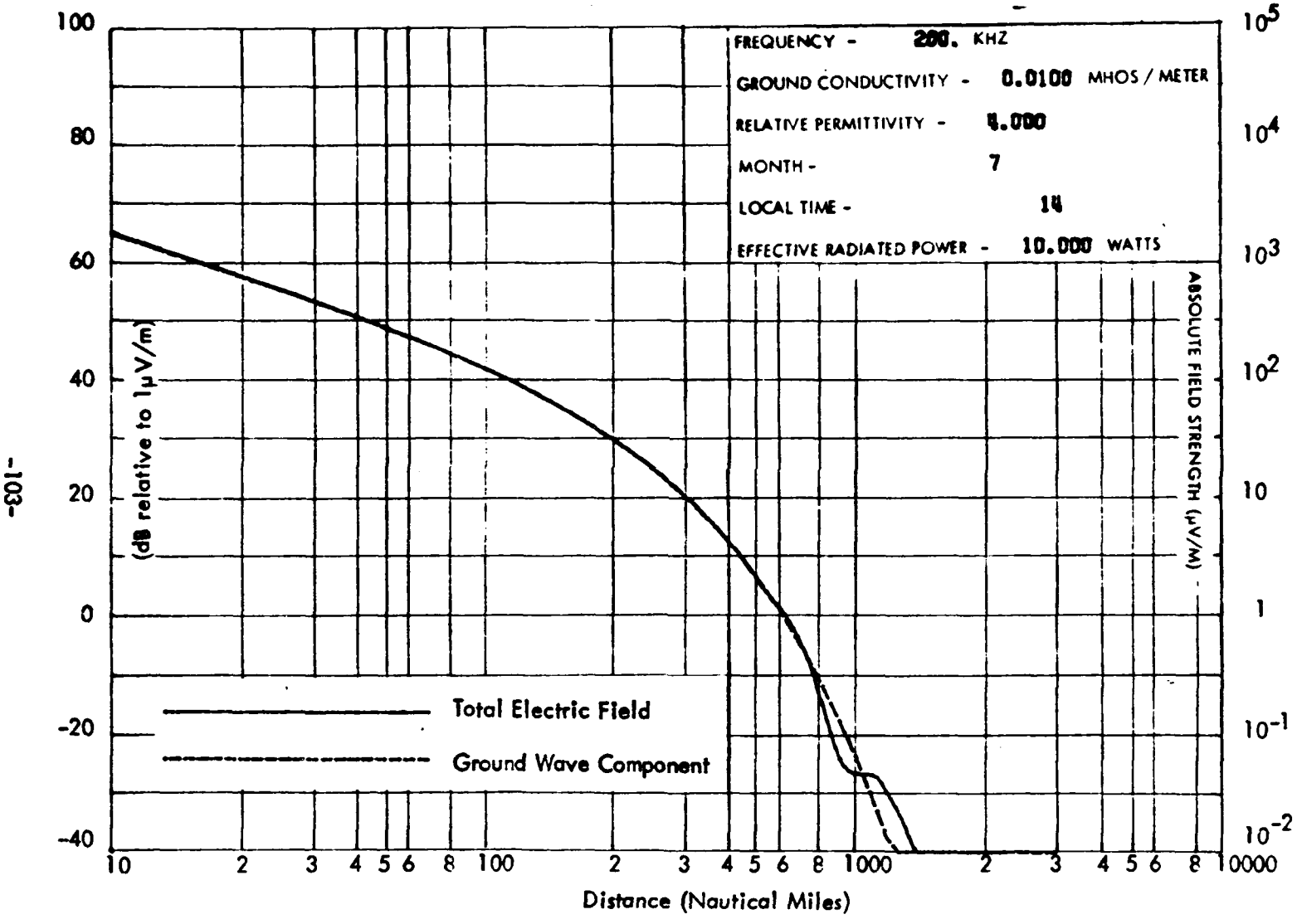

Figure 4-4. Medium Earth Conductivity - Maximum Sun Spot Cycle.

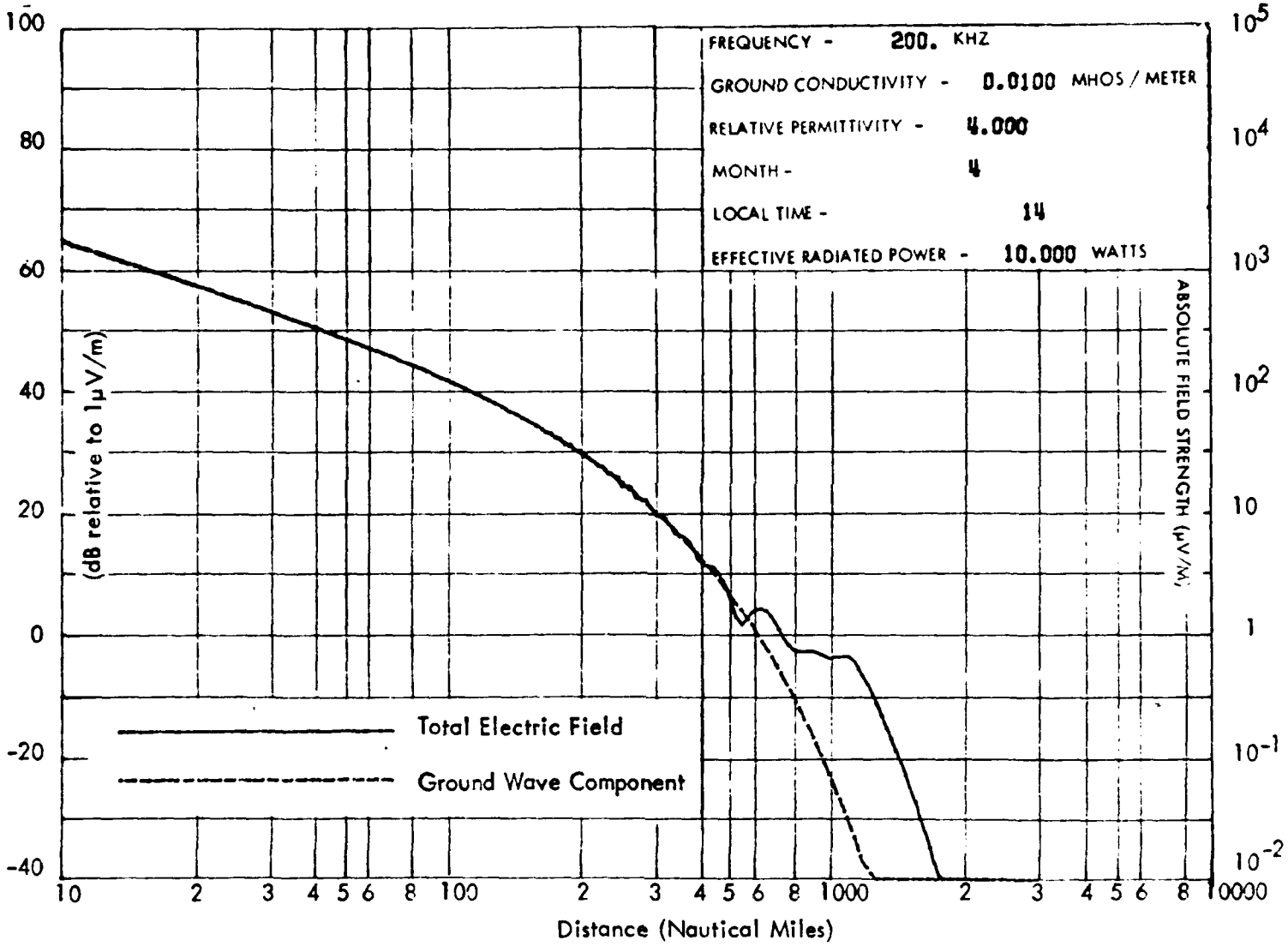

Figure 4-5. Medium Earth Conductivity - Maximum Sun Spot Cycle.

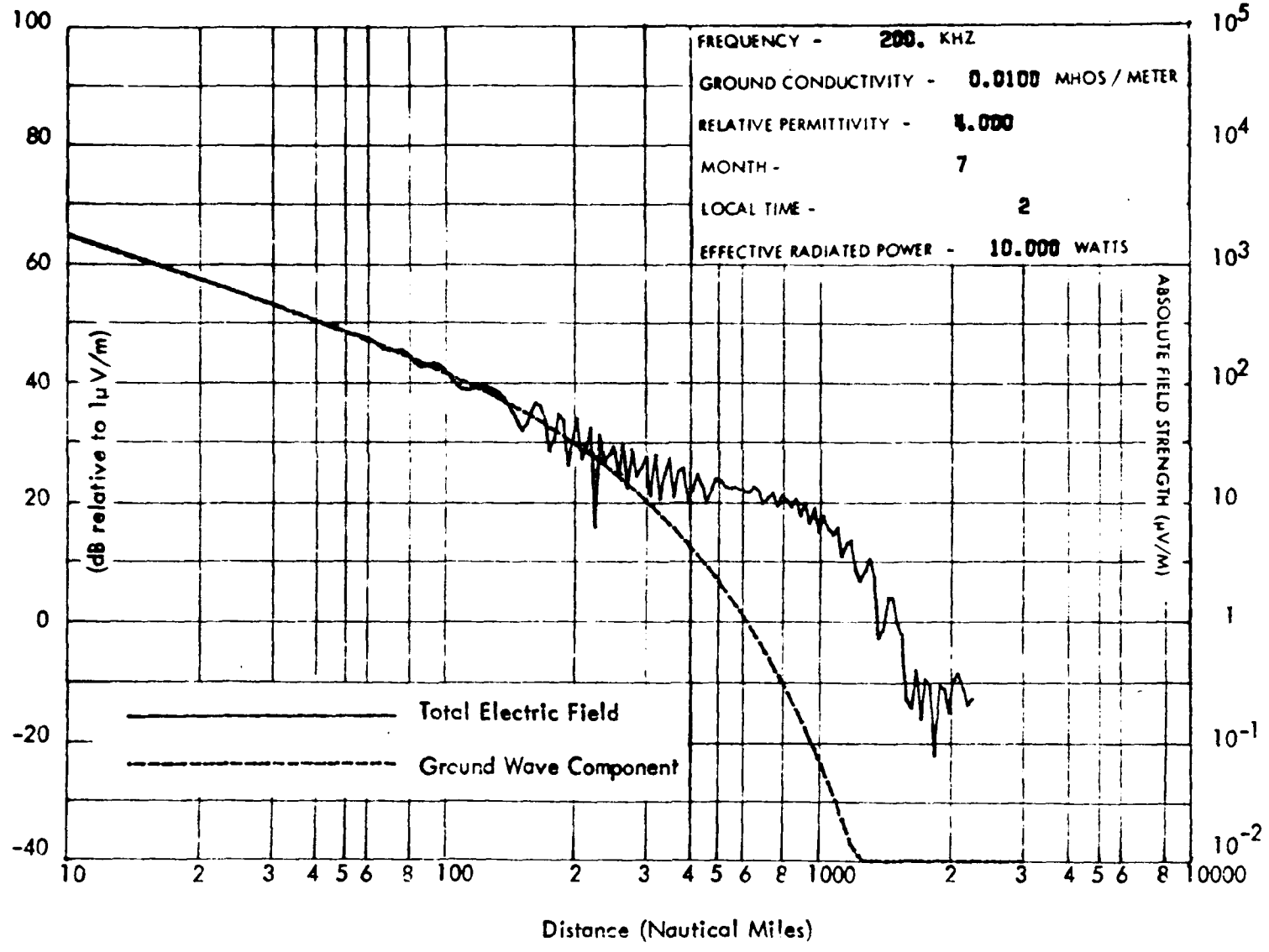

Figure 4-6. Medium Earth Conductivity - Maximum Sun Spot Cycle.

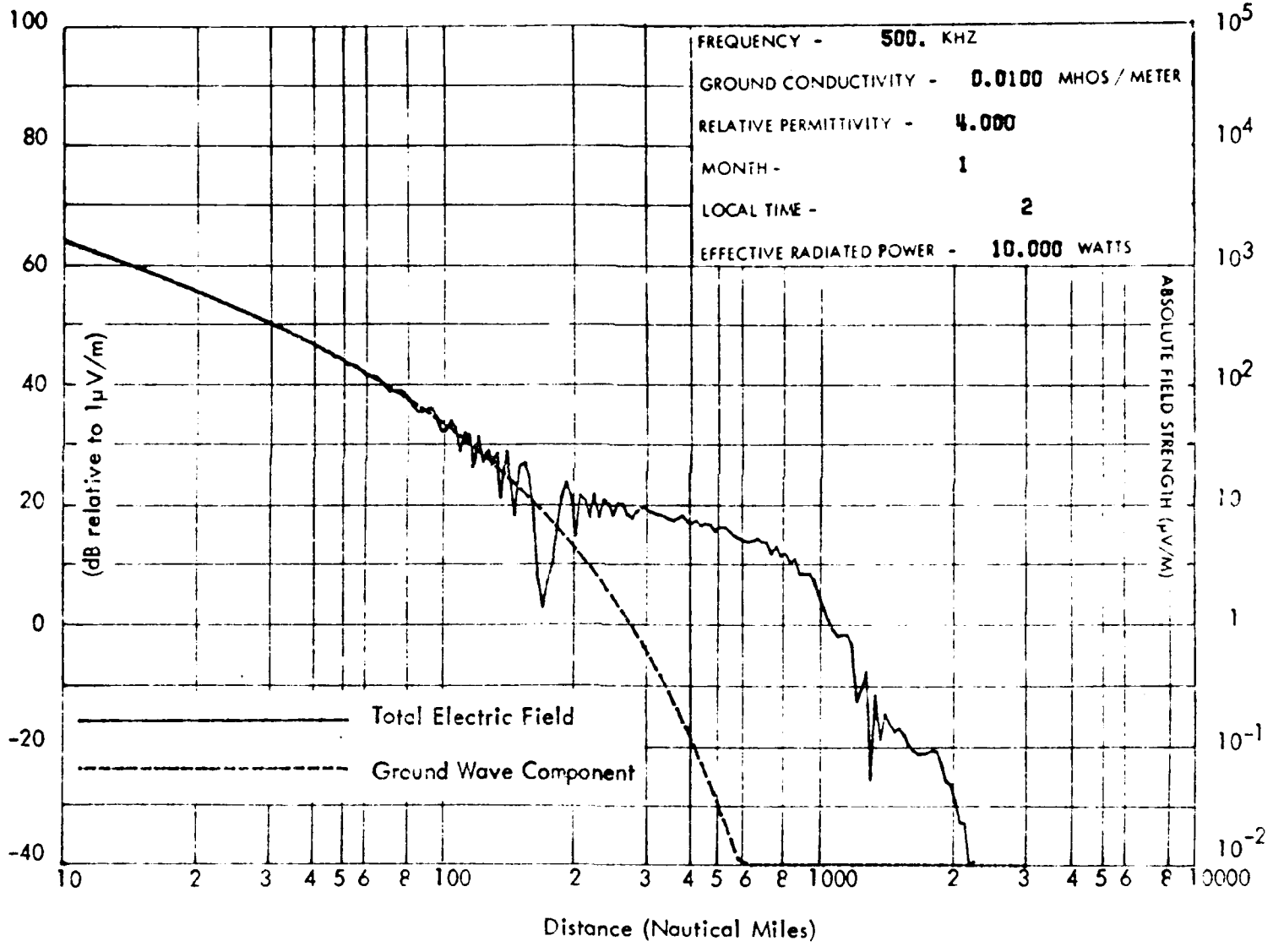

Figure 4-7. Medium Earth Conductivity - Maximum Sun Spot Cycle.

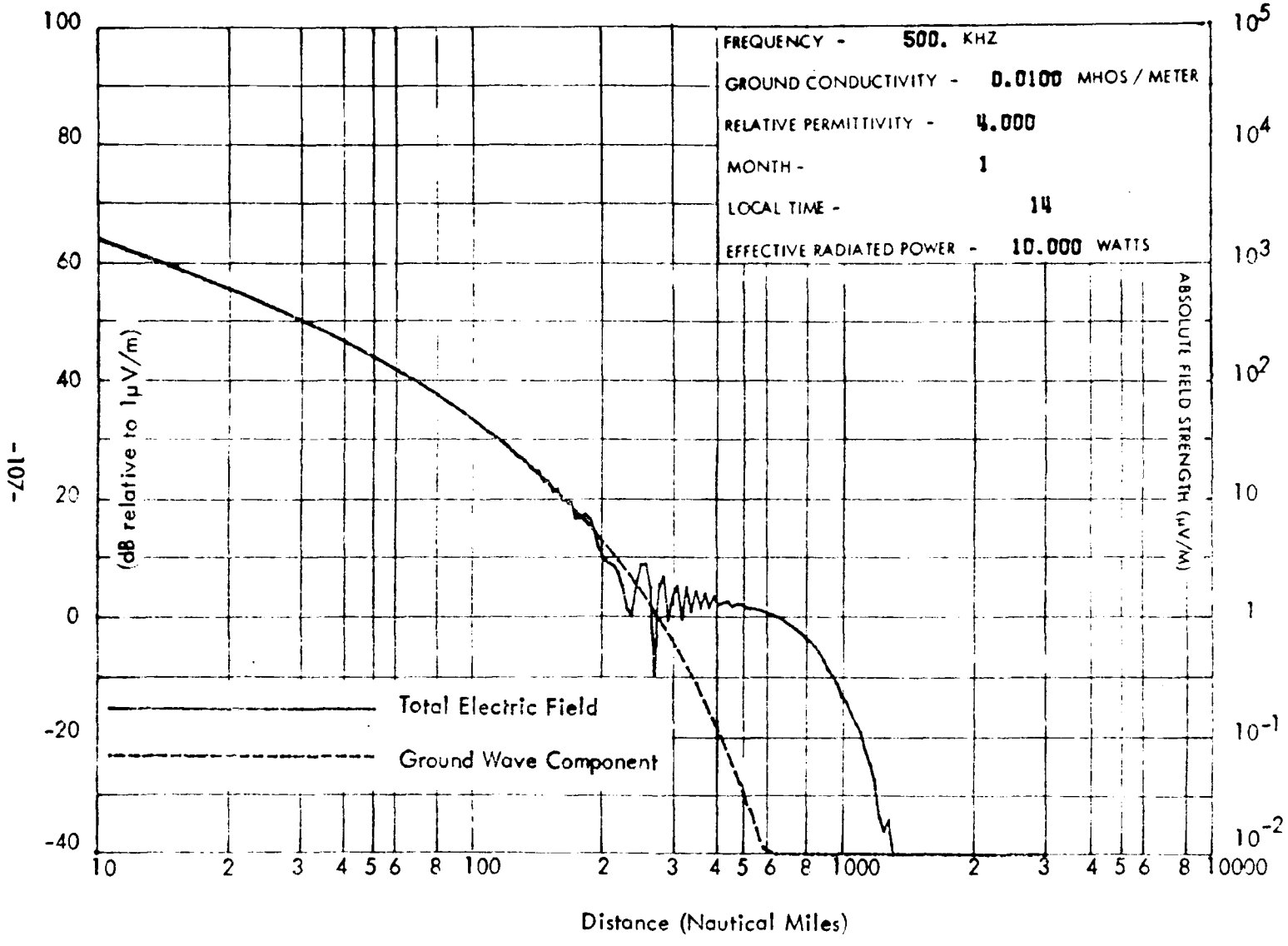

Figure 4-8. Medium Earth Conductivity - Maximum Sun Spot Cycle.

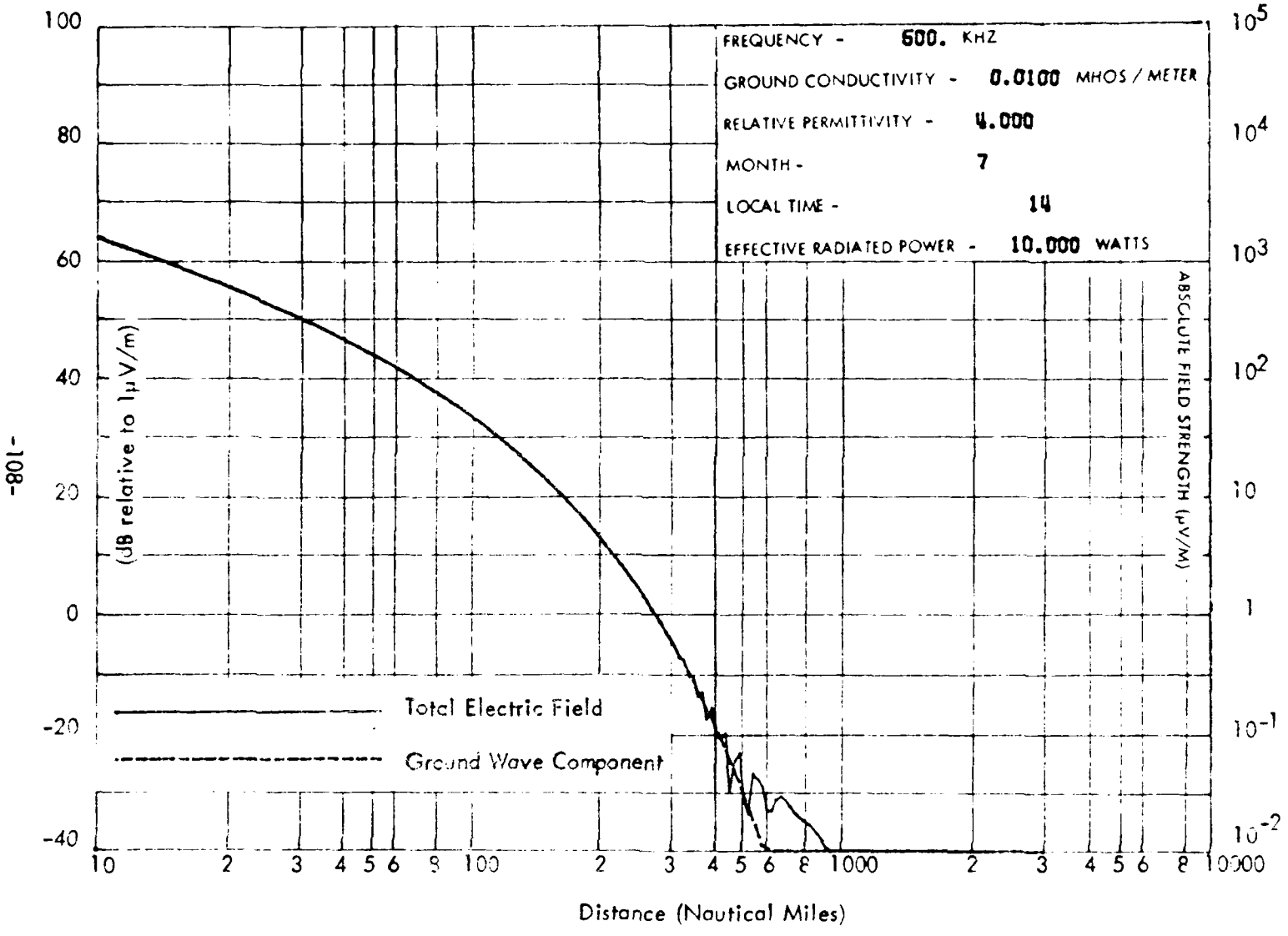

Figure 4-9. Medium Earth Conductivity - Maximum Sun Spot Cycle.

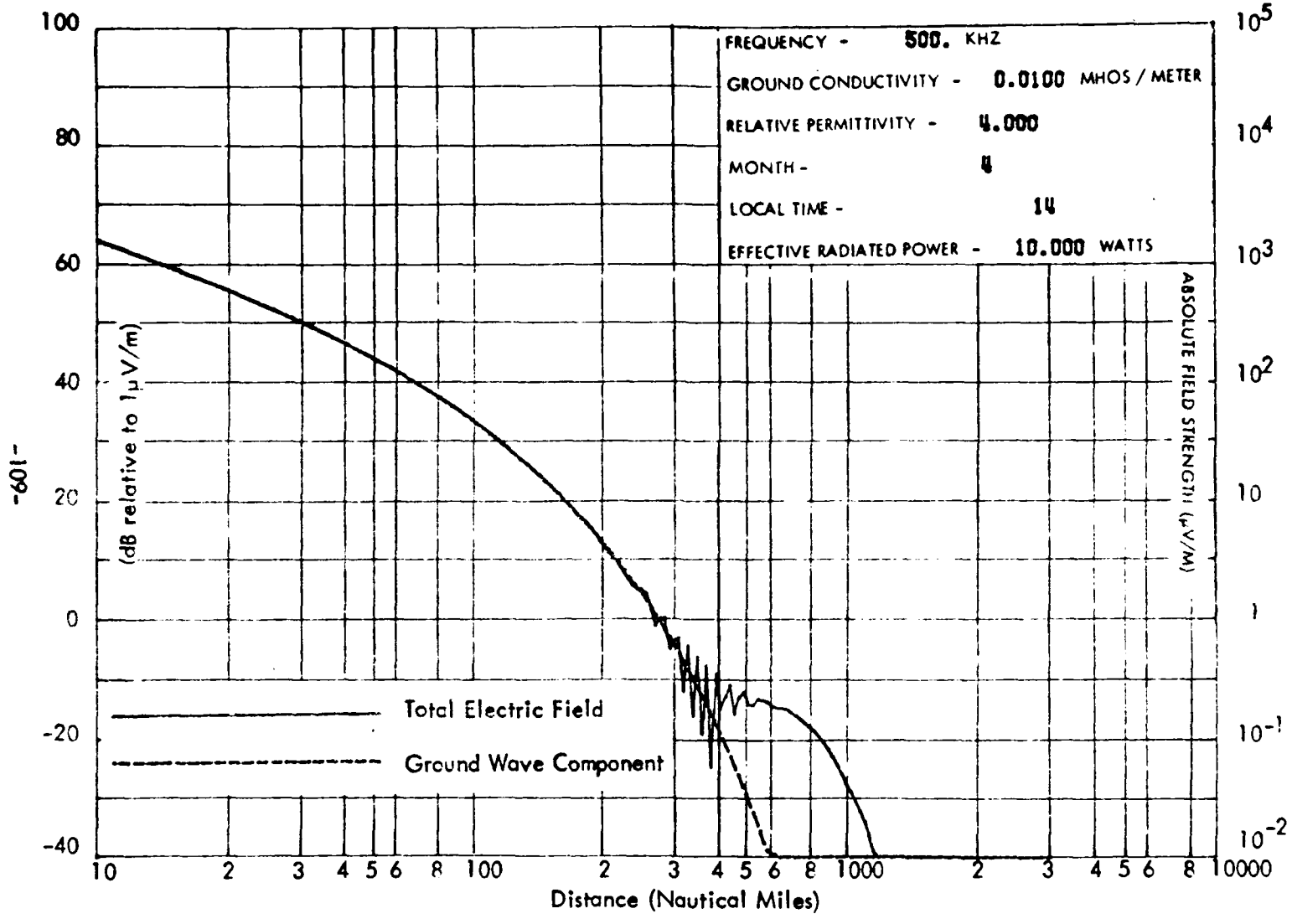

Figure 4-10. Medium Earth Conductivity - Maximum Sun Spot Cycle.

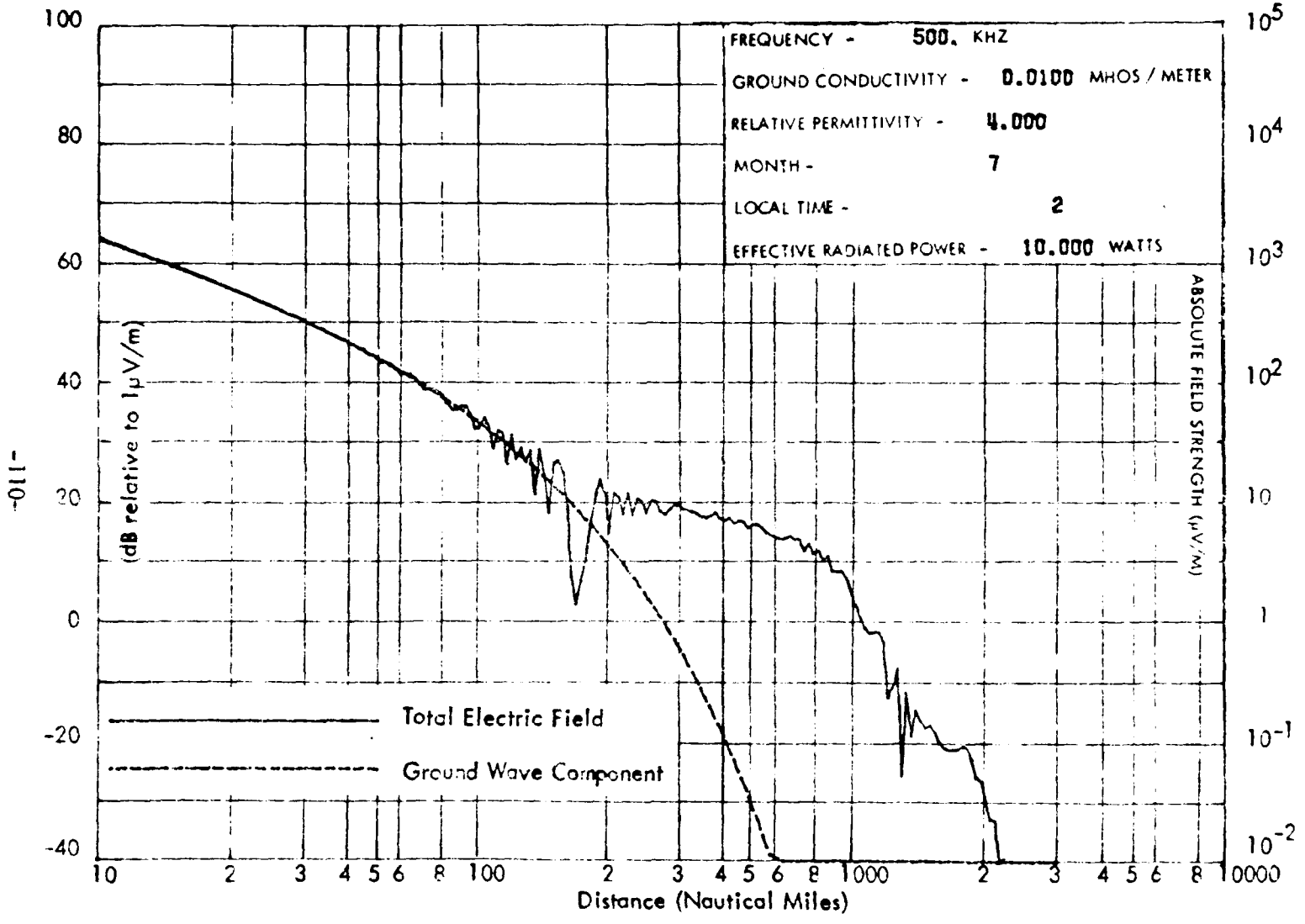

Figure 4-11. Medium Earth Conductivity - Maximum Sun Spot Cycle.

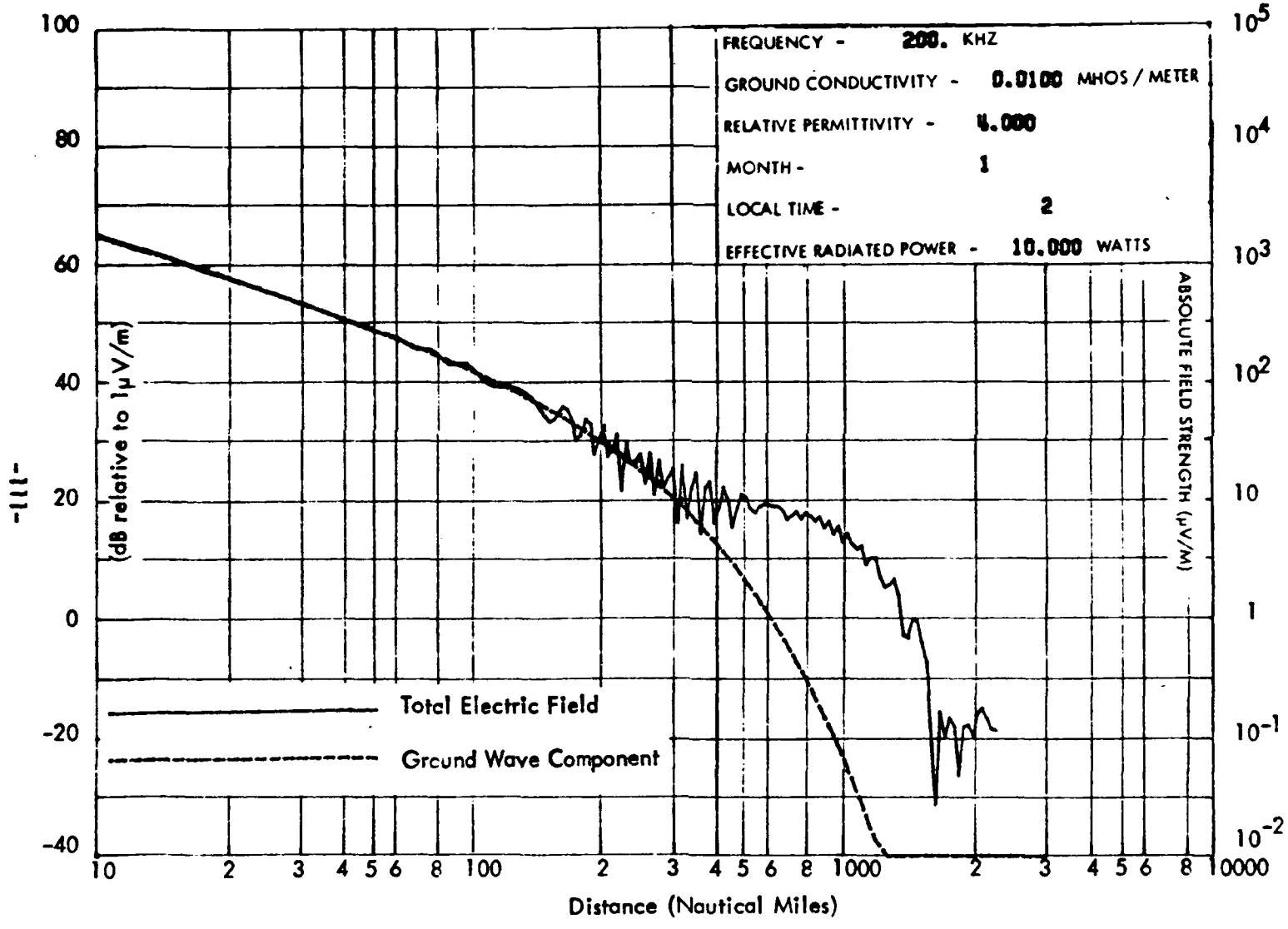

Figure 4-12. Medium Earth Conductivity - Minimum Sun Spot Cycle.

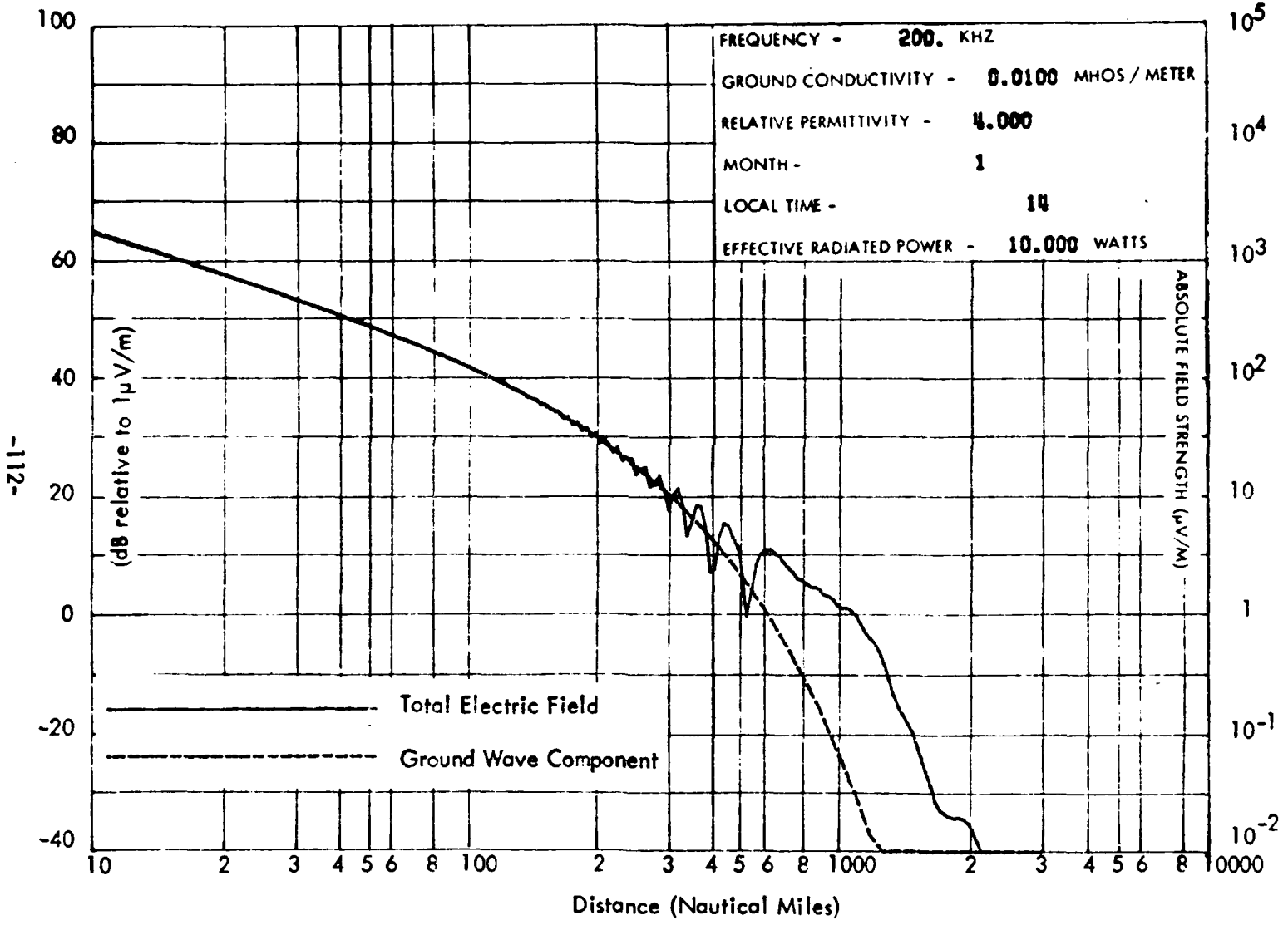

Figure 4-13. Medium Earth Conductivity - Minimum Sun Spot Cycle.

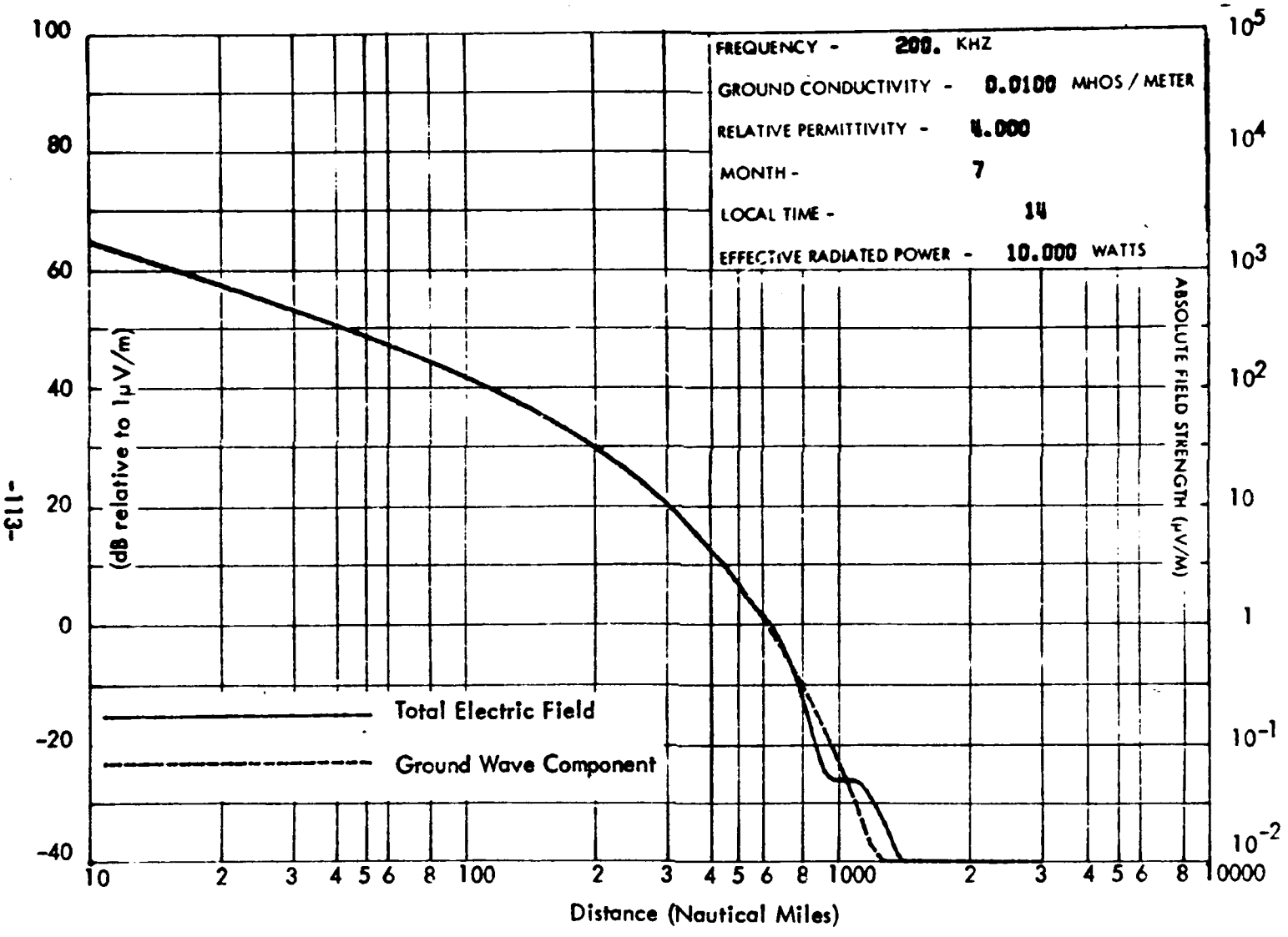

Figure 4-14. Medium Earth Conductivity - Minimum Sun Spot Cycle.

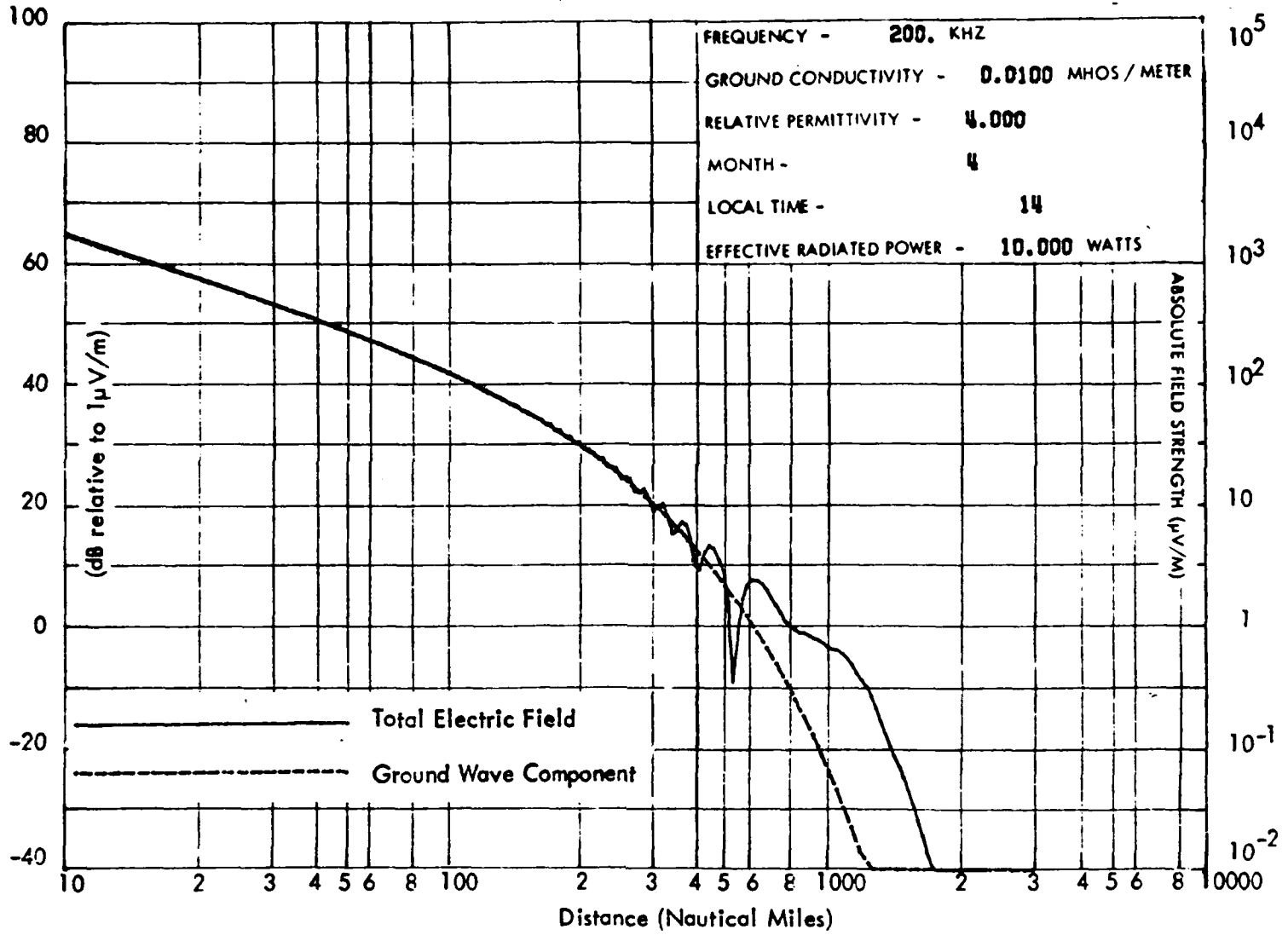

Figure 4-15. Medium Earth Conductivity - Minimum Sun Spot Cycle.

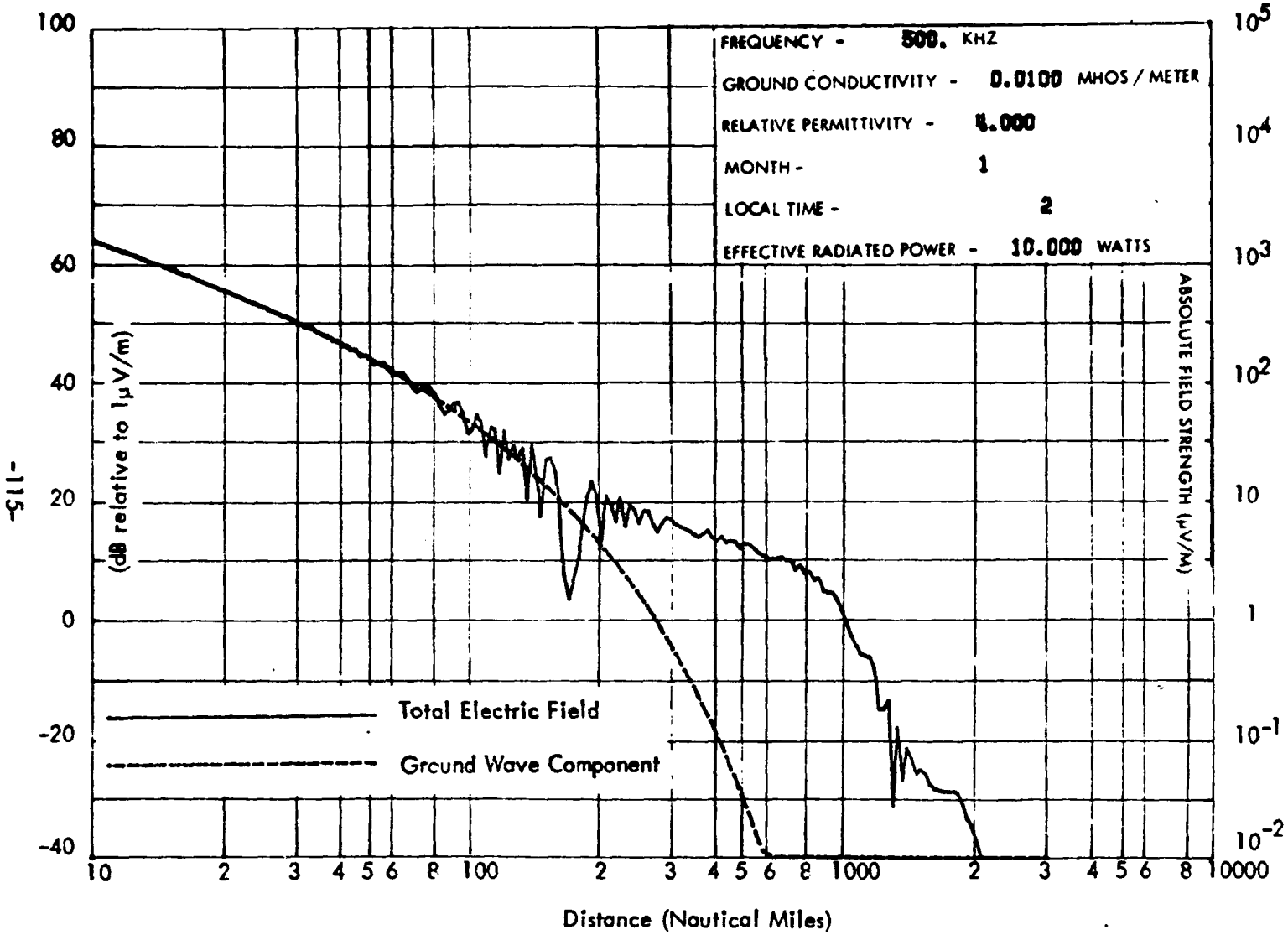

Figure 4-16. Medium Earth Conductivity - Minimum Sun Spot Cycle.

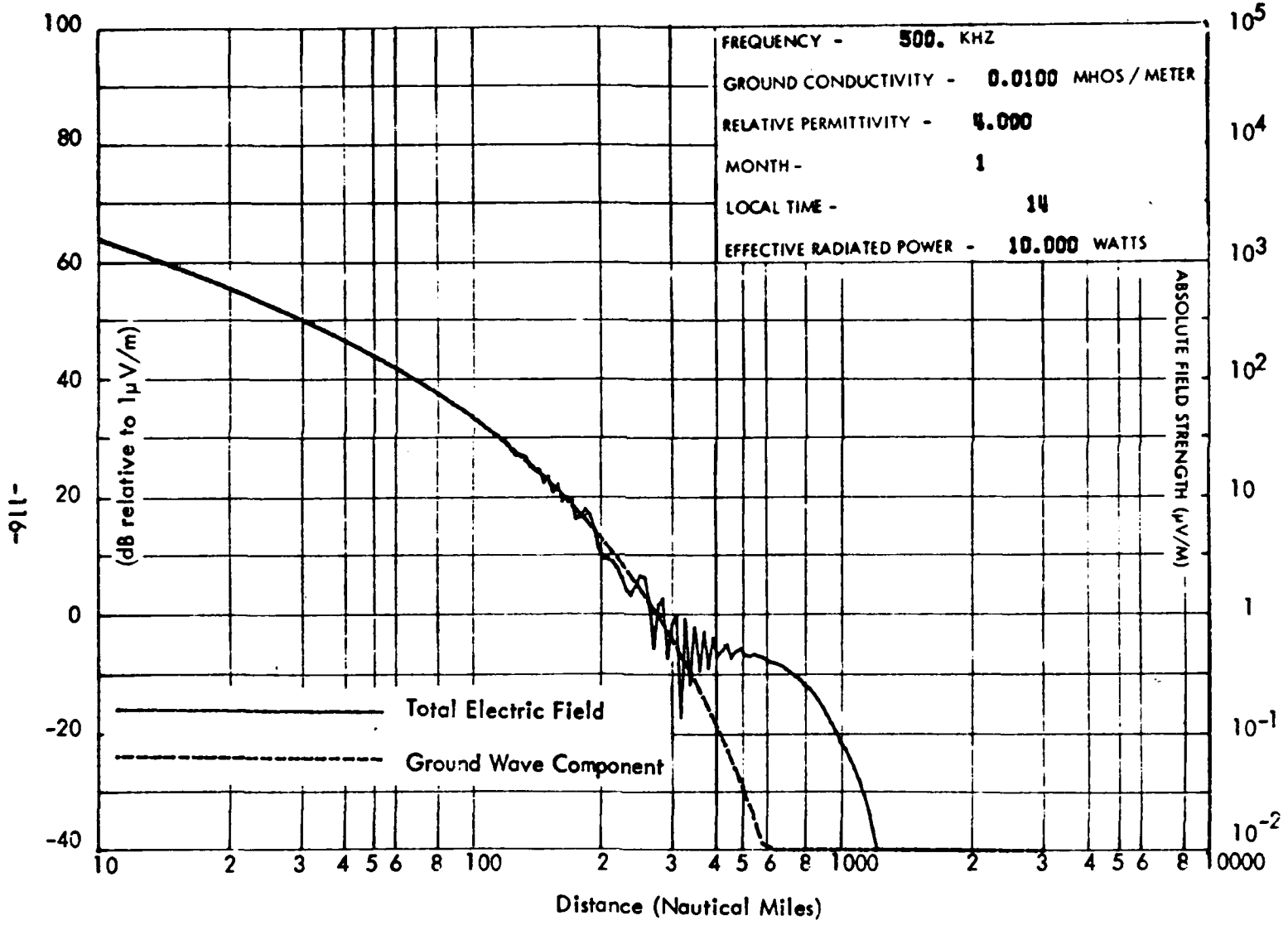

Figure 4-17. Medium Earth Conductivity - Minimum Sun Spot Cycle.

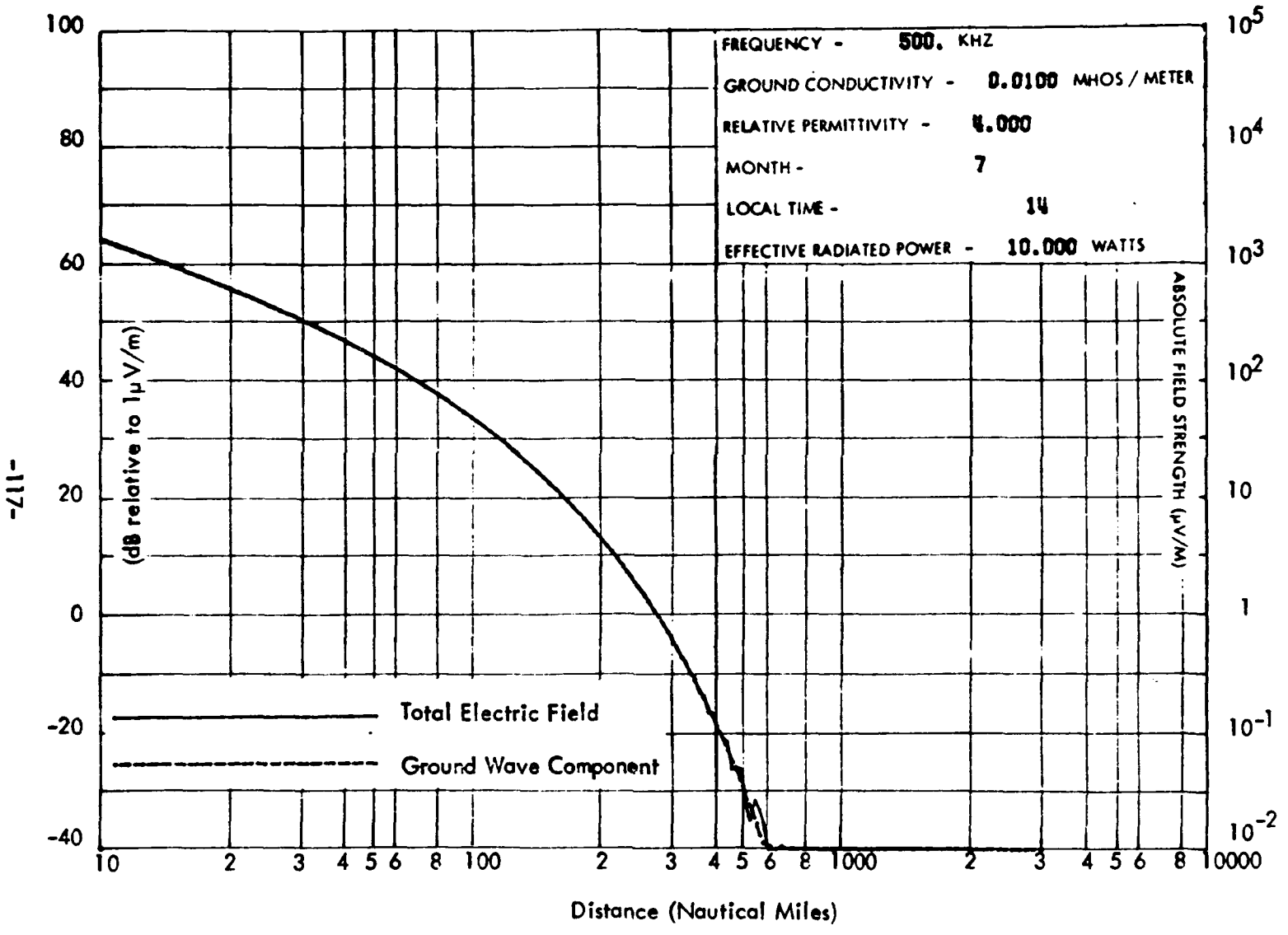

Figure 4-18. Medium Earth Conductivity - Minimum Sun Spot Cycle.

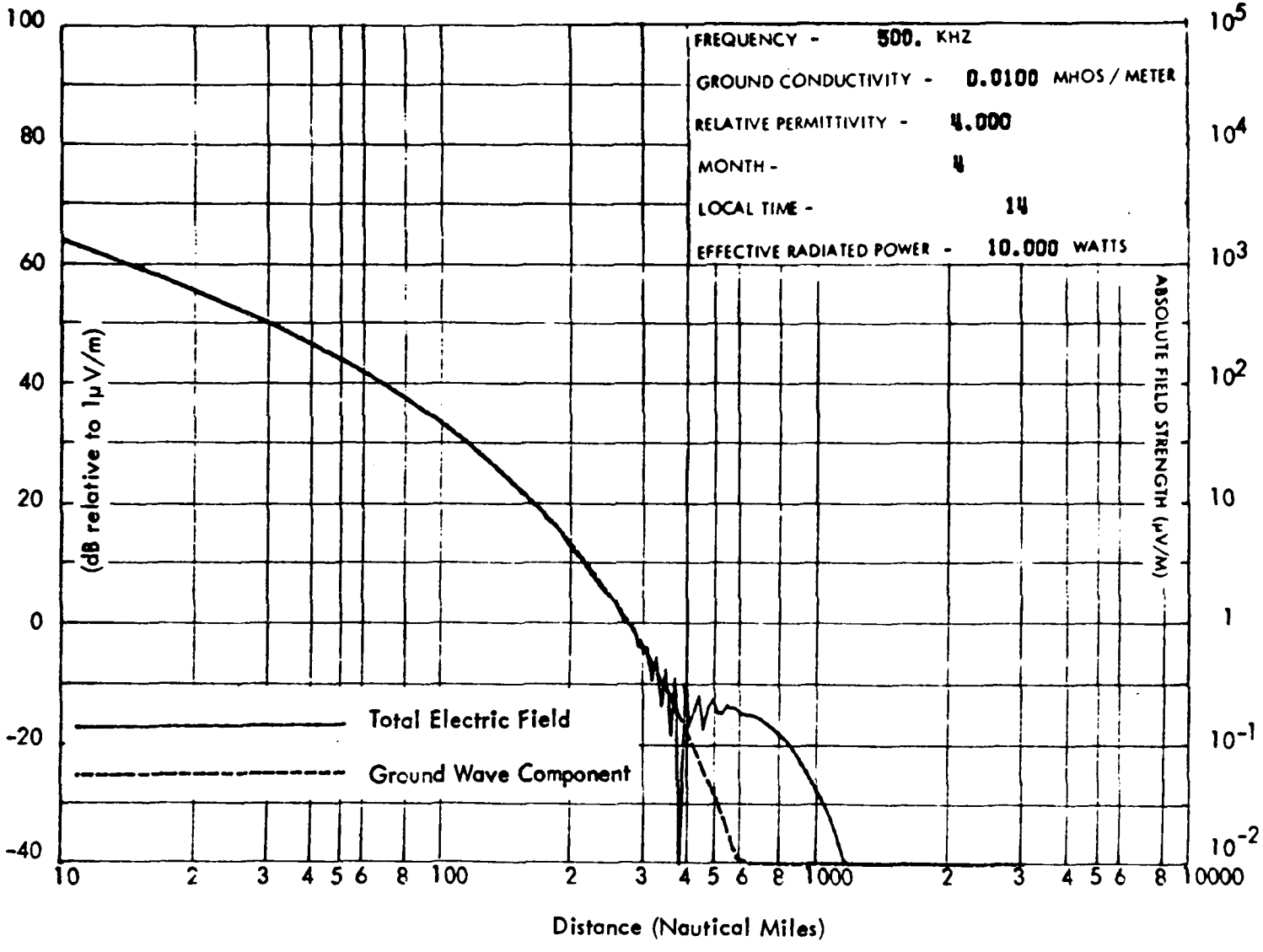

Figure 4-19. Medium Earth Conductivity - Minimum Sun Spot Cycle.

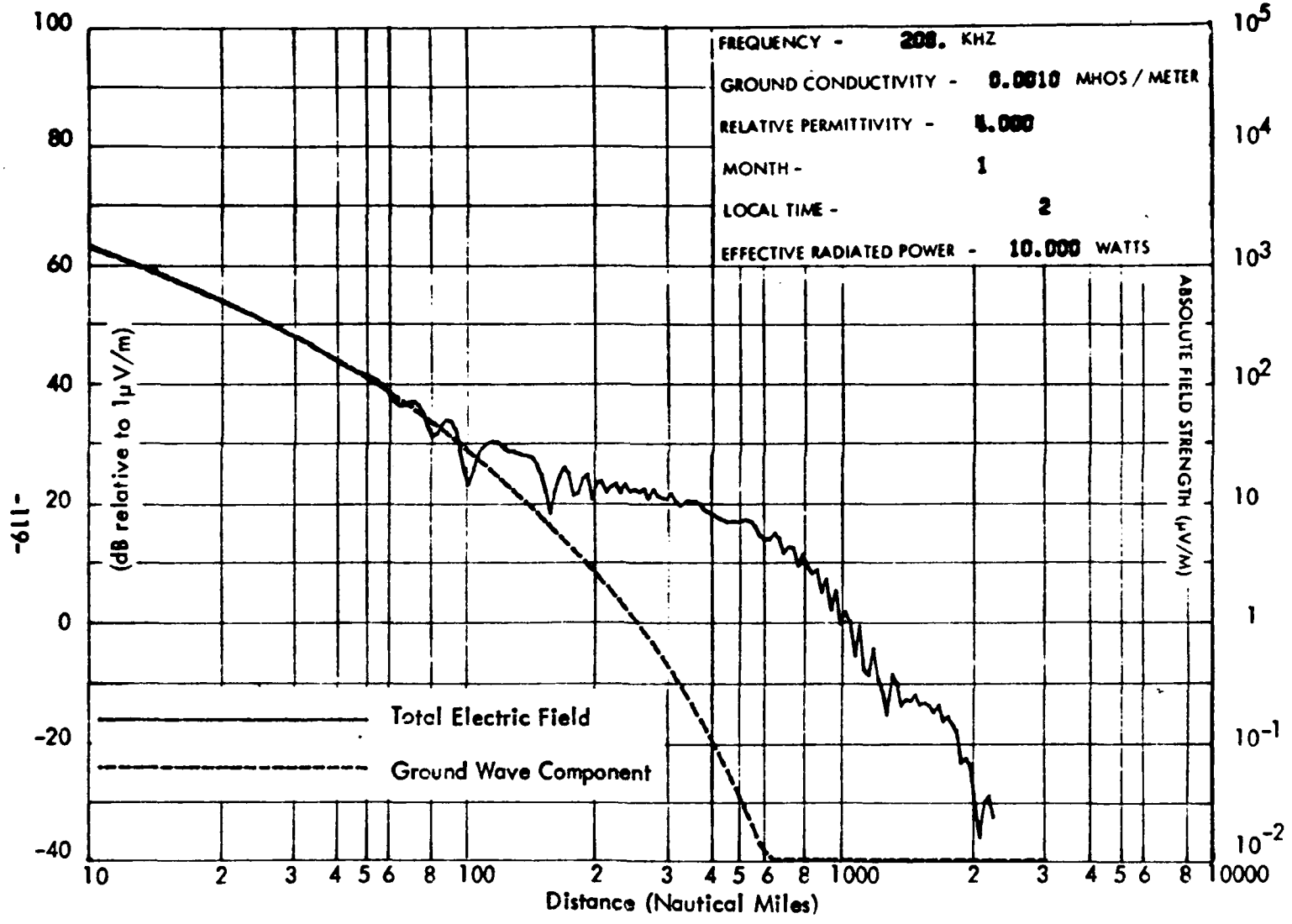

Figure 4-20. Desert Conditions Conductivity - Maximum Sun Spot Cycle.

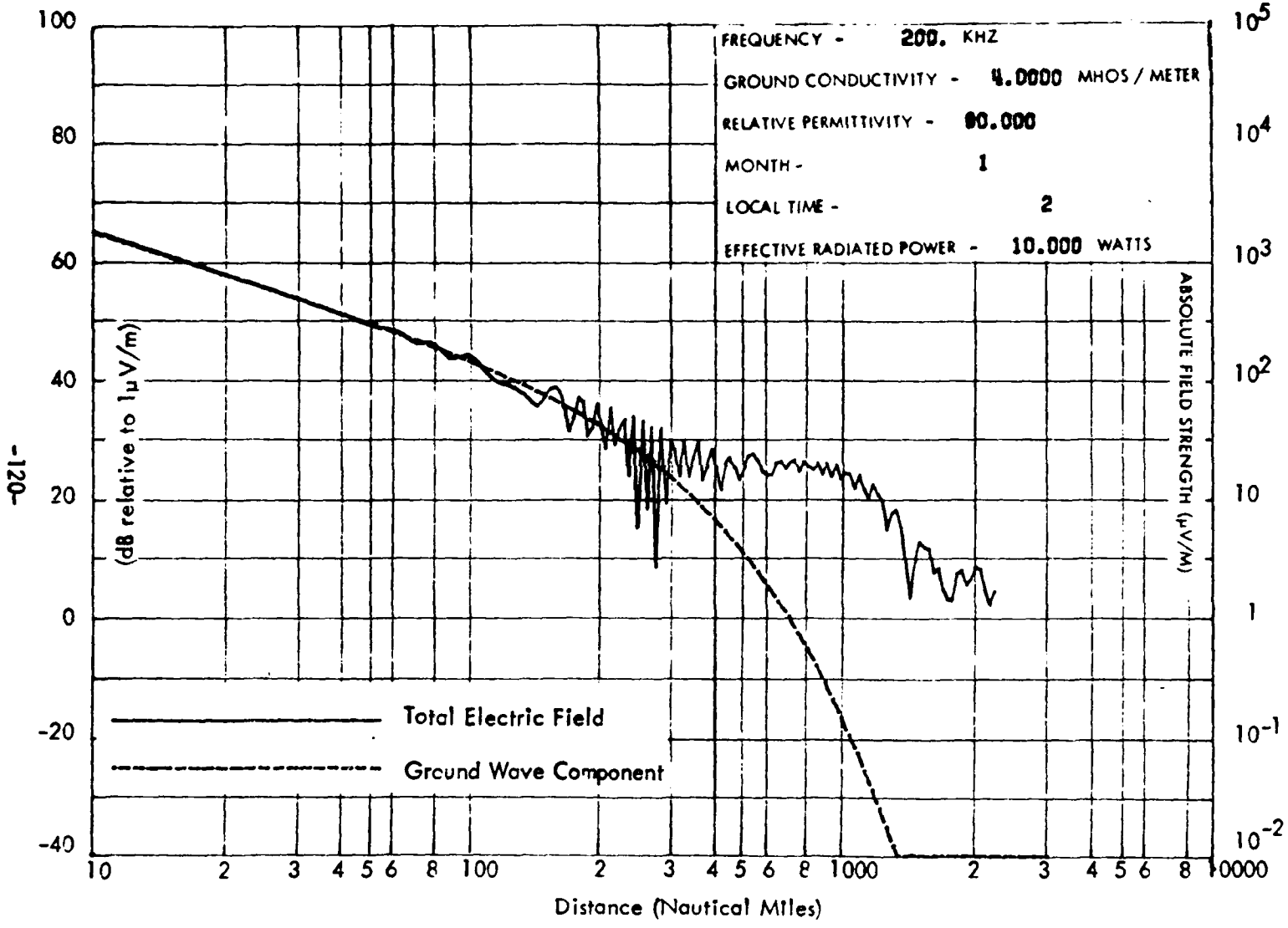

Figure 4-21. Sea Water Conductivity - Maximum Sun Spot Cycle.

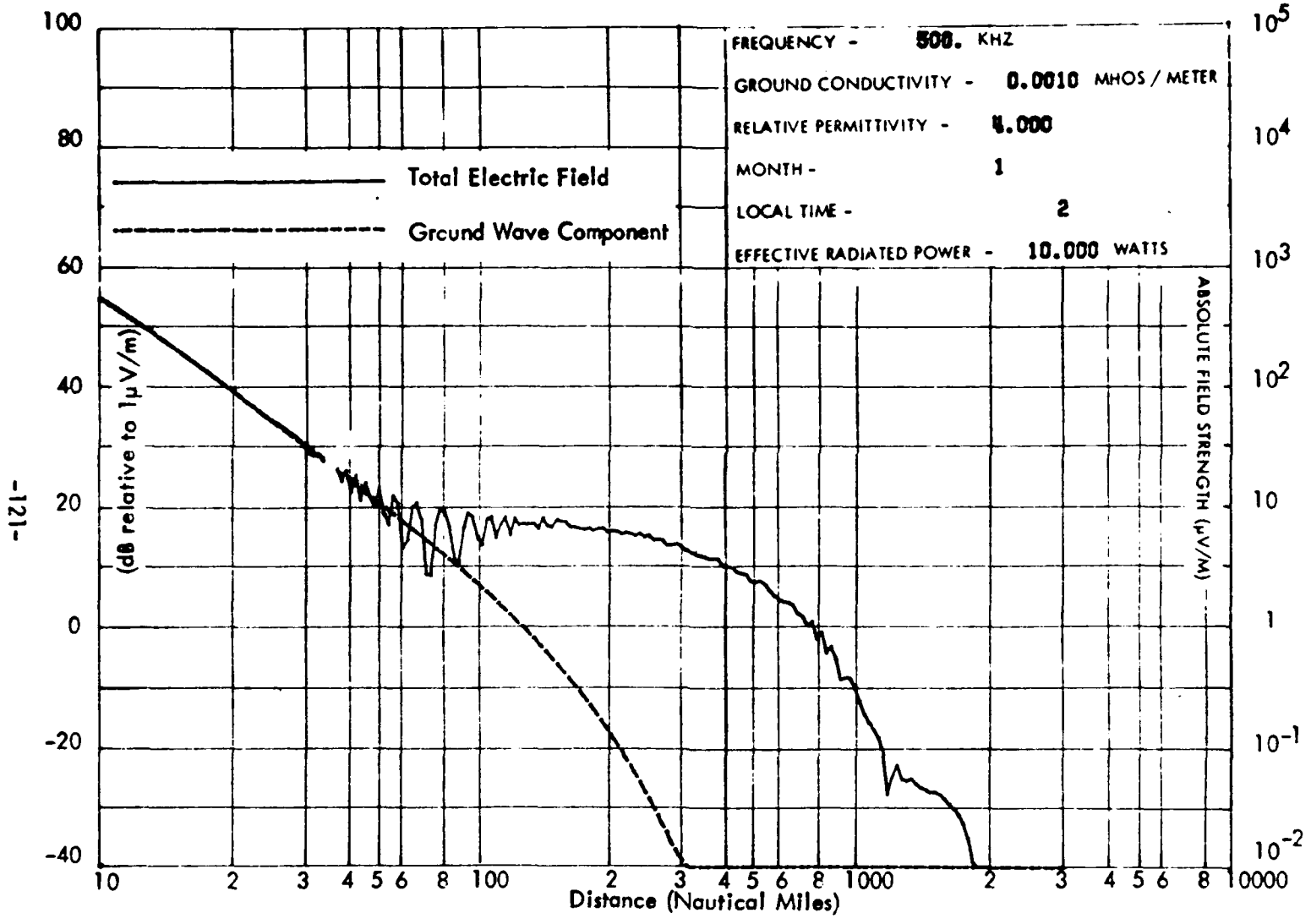

Figure 4-22. Desert Conditions Conductivity - Maximum Sun Spot Cycle.

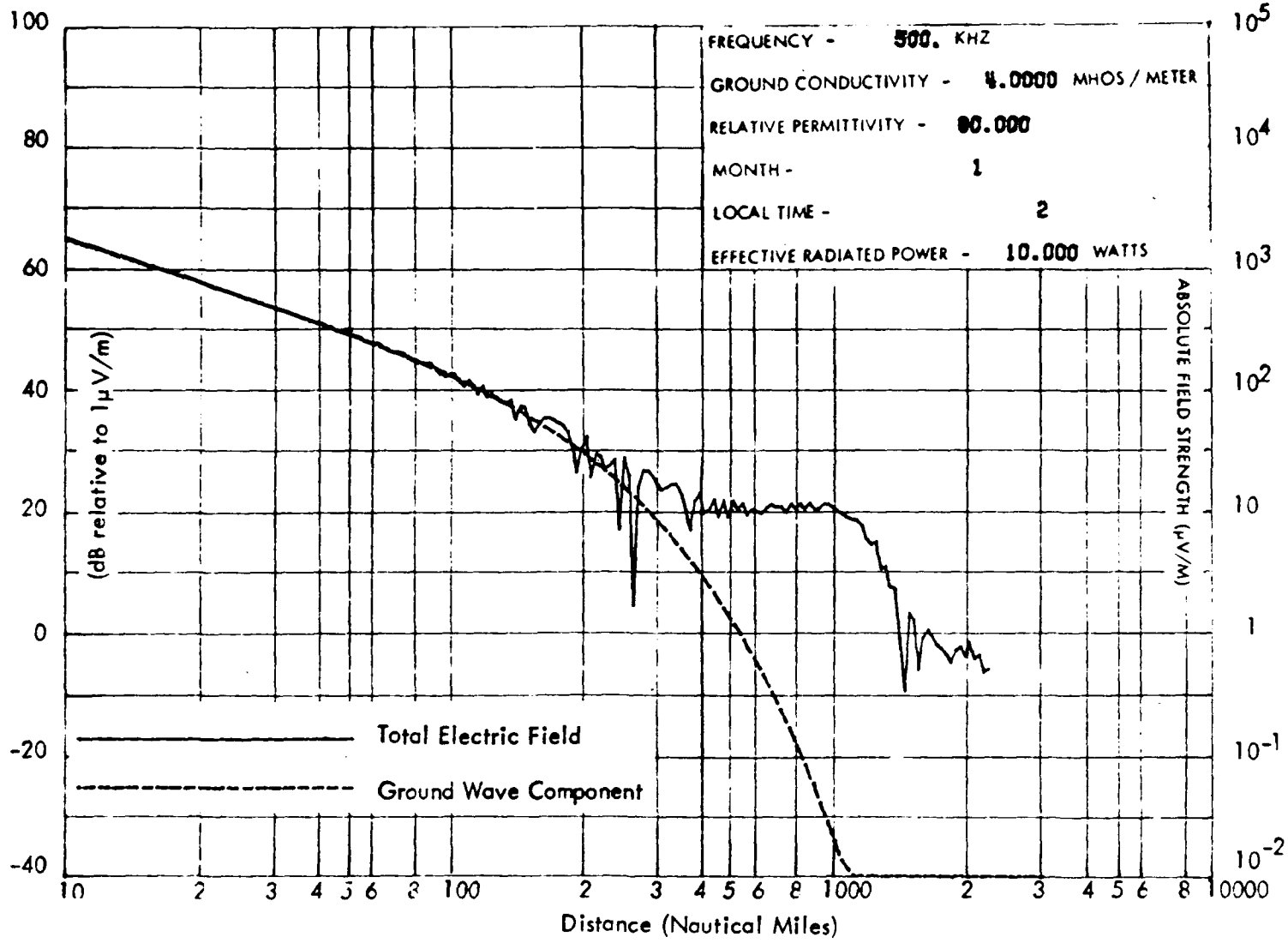

Figure 4-23. Sea Water Conductivity - Maximum Sun Spot Cycle.

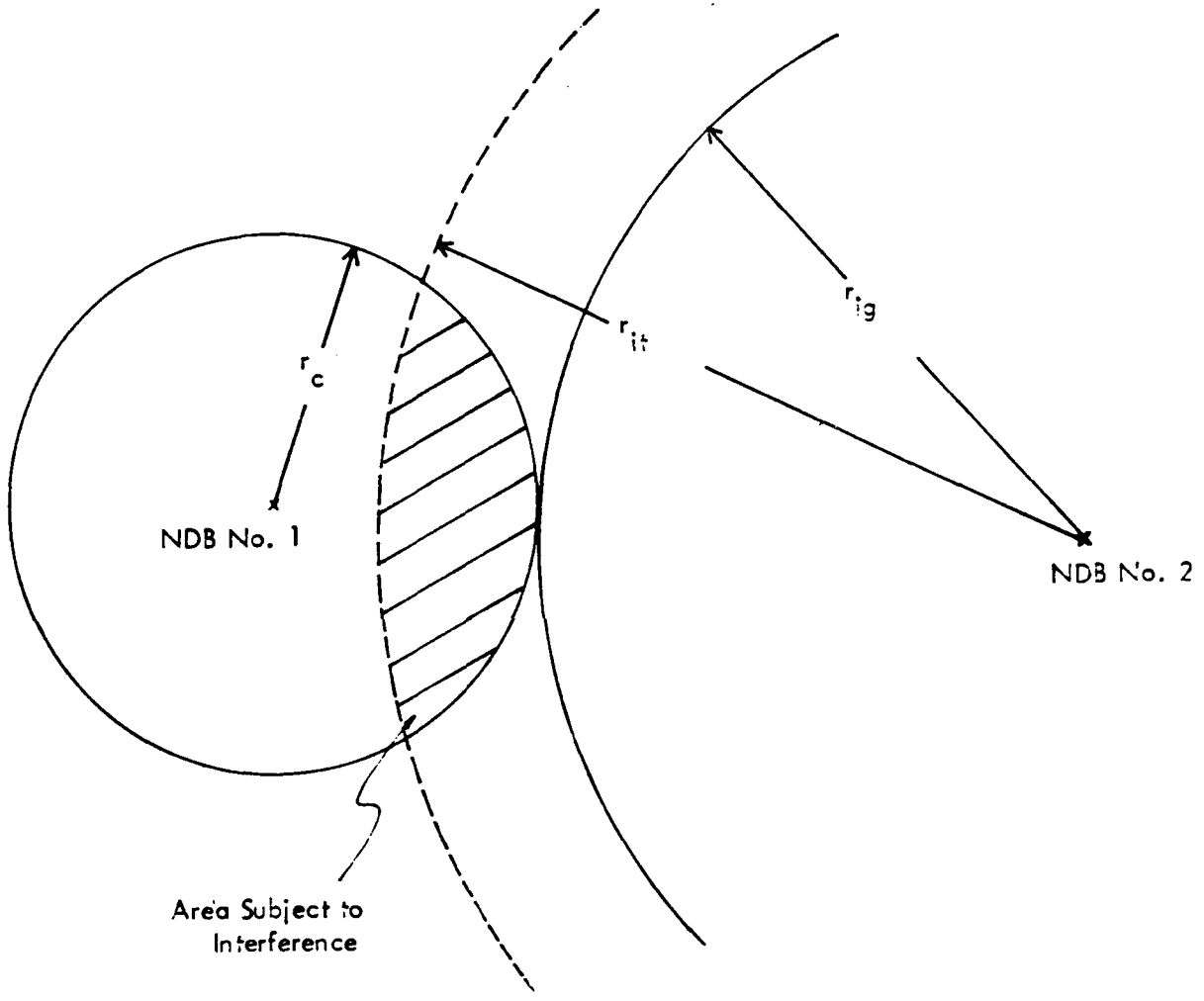

r_c = Coverage Radius

r_{ig} = Interference Radius Determined from Ground Wave Only

r_{it} = Interference Radius when Total Field is Considered (including Sky Wave)

Figure 4-24. Coverage Area Subject to Interference from Sky Wave.

V. AN INVESTIGATION OF THE EFFECTS OF IRREGULAR TERRAIN ON RADIO WAVE PROPAGATION IN THE FREQUENCY RANGE 200-500 KHz

The investigation of radio wave propagation in the preceding sections of this report has assumed that the earth's surface is perfectly spherical with no terrain irregularities whatsoever. In this section this requirement is removed, and the model used here allows an irregular terrain to be described and electric field strength computed for this terrain profile. The investigation presented here utilizes this model to determine predicted field strength for actual terrain profiles from the states of Montana and Ohio. Also, experimental data will be compared with the theoretical values in an attempt to check agreement of the methods.

The theoretical model used, ITSNR (Irregular Terrain Signal-to-Noise Ratio) has been obtained from ITS [1]. It allows any given terrain profile to be defined and the field strength on the earth's surface is computed for this profile. The model also removes the requirement that the propagation path be homogeneous by allowing ground constants to be changed at any given distance from the transmitter. This capability makes the model particularly useful for determining field strength across land-sea boundaries, for instance. Plotted output is presented here for five different terrain profiles. The method used by the model in field strength computation is essentially one of solving numerically an integral equation by determining the contribution from induced currents on intervals of the surface between the source and the receiver. Of course, certain approximations must be made to obtain a usable and economically practical form of the solution. Among these are the assumption that the terrain is uniform in the direction transverse to propagation. This eliminates all side-scatter effects, or contribution from currents induced on sections of the earth not directly along the propagation path. Also, as previously mentioned, only contributions from currents induced on the intervals between the source and receiver are considered in the computation. This obviously neglects backscatter effects or the contribution made by currents on the given terrain profile behind the receiver (as viewed from the source) as well as behind the source (as viewed from the receiver). This certainly will allow computation to be made more economically for if backscatter effects were to be considered, the integration would necessarily extend over the entire terrain profile for computation of field strength at every field point. Similarly, inclusion of sidescatter effects would require integration over an area for each field point, the size of the area being determined by the accuracy required. Clearly, consideration of these effects is limited by computation ability and speed. Another assumption made in the model concerns the terrain profile itself. Program ITSNR requires as input to the program data points which define the terrain in terms of height of the earth's surface as a function of distance from the transmitter. The terrain profile then actually used in the computation of field strength is obtained by performing a quadradic interpolation on these input points to obtain terrain height and slopes which are required in the integration intervals between the points.

These assumptions are a compromise between economical computation and prediction accuracy. However, the model does provide a very useful means of determining attenuation caused by irregular terrain. Errors resulting from the assumptions mentioned above are not severe, especially at the frequency range of interest here. A

slight deviation from the actual terrain, for instance, caused by the assumptions made in determining the terrain profile would be insignificant to computed field strength for these long wavelengths and scattering effects at all frequencies are second-order effects. Further, while the experimental data presented here is limited and not intended to indicate the validity of the model, the agreement obtained between experimental and predicted field strength does suggest that the model can be useful in predicting terrain effects. Complete details of the computer techniques are documented by Ott [28].

As mentioned, theoretical field strength predicted by this model has been computed for five different existing terrain profiles. These profiles have been obtained from geological survey maps and are all directed radially outward from an NDB facility. Four of the profiles illustrate terrain conditions in western Montana, which presents somewhat of a worst case in terms of realistic terrain irregularities. These radials originate at the Kona, Montana NDB located at 47°, 5'N Latitude and 114°, 25'W longtitude, and terminate at points at which measured data has been collected. Experimental data for this facility has been supplied by the FAA and is available at two frequencies--218 KHz and 404 KHz.

The first profile to be considered is shown in Figure 5-1 and describes terrain northwest of the NDB. The terrain itself is shown in Figure 5-1 and results of theoretically predicted field strength and measured field strength for 218 KHz and 404 KHz are shown in Figures 5-2 and 5-3, respectively. Also in these figures, as with all in this section, the field strength expected if terrain were perfectly smooth is indicated with a dashed line. This information has been computed by program GWSNR (see section II). It also should be pointed out that there is a difference in the power levels for the two different frequencies of the Kona, Montana facility. This reflects measurements made at a distance of 2 nm from the NDB which reveal that the ERP of the facility when operating at 404 KHz is 7.06 dB above its ERP at 218 KHz. However, since all propagation models in this report are completely linear in field strength computation, the same effects of the irregular terrain will result regardless of the power level. In general, in Figures 5-2 and 5-3 it can be seen that as the receiver is located on the side of a hill or mountain facing the transmitter, measured field strength is increased. This would be expected, since the receiver is then fully exposed to not only the source, but to the fields due to currents induced on the earth's surface as well. As the receiver moves to sides of terrain irregularities facing away from the beacon, field strength is decreased, again as is to be expected, since it is now shaded from the source. In Figure 5-2, the theoretical field strength considering irregularities in the terrain is seen to vary from the smooth earth model by at most 6 dB, whereas operating at 404 KHz, the variation is nearly 10 dB with the maximum deviation in both cases occurring around 19 nm. The experimental data in both figures at 9.5 and 16 nm agrees well with the predicted value, but the measured data at 21.1 nm falls 8 dB below the calculated value. Although agreement in the two points closer to the facility is good, the validity of the model cannot be established on the basis of this agreement, for the measured data also agrees well with the field strength computed assuming smooth earth conditions.

Figures 5-4 through 5-6 illustrate a profile radially outward to the west of the Kona NDB. As Figure 5-4 shows, this radial exhibits considerably more irregularity. This surface irregularity is also noticeable in the theoretical field strength calculations at both frequencies, as values for both frequencies show more deviation from the field strength computed for a smooth earth. In Figure 5-5, the maximum disagreement with smooth earth for 218 KHz is now 6 dB, and at 404 KHz (Figure 5-6) again differences of 10 dB can be seen. However, although the maximum differences at 404 KHz are the same for the two profiles, Figure 5-2 clearly shows better agreement with the smooth earth model than Figure 5-6. It is quite obvious in both these profiles that the higher frequencies are disturbed more by surface irregularities than the lower frequencies. The experimental data at 13.2 nm is also plotted in Figures 5-5 and 5-6, and is seen now to agree more closely with the field strength computed by ITSNR, especially for 218 KHz.

Figures 5-7 through 5-9 show similar results for a radial east-northeast of the NDB, as do Figures 5-10 through 5-12 for a northeast radial. As the terrain profiles (Figures 5-7 and 5-10) indicate, both are quite irregular. Both terrain profiles have significant effect on wave propagation, even in this frequency range, as shown on the associated figures of plotted field strength versus distance. Again the measured data is considerably closer to the value computed by ITSNR in all cases for these two profiles. The differences between the measured data and the field strength computed by both models are summarized in Table 5-1 for 218 KHz and Table 5-2 for 404 KHz. The results of the data strongly suggest that field strength can be computed more accurately when the terrain is considered, but it must be remembered that this case, though realistic, is an extreme one.

To illustrate a more moderate example, a terrain profile for a radial to the northeast of the Albany, Ohio beacon is shown in Figure 5-13. This radial was chosen because it includes some of the roughest terrain in southeastern Ohio. Figure 5-14 shows computed field strength when this terrain profile is used in program ITSNR. The frequency used is that of the Albany beacon, 250 KHz. Here, the variation from the smooth earth model is not nearly as evident as for any of the Montana terrain profiles, the maximum deviation here being less than 2 dB. Figure 5-5 shows the effect of the same terrain profile on the field strength from a beacon operating at 500 KHz. Effects here are slightly more noticeable, showing a deviation from the values computed by GWSNR of 2 dB, but it appears that the effects of irregular terrain of the type found in southern Ohio on wave propagation are not significant effects.

Terrain	Difference Between Measured Data and ITSNR Prediction (dB relative to 1 μV/m)	Difference Between Measured Data and GWSNR Prediction (Smooth Earth) (dB relative to 1 μV/m)	Distance (nm)
Profile No. 1	1	2	9.5
Profile No. 1	1	3	16
Profile No. 1	5	11	21.2
Profile No. 2	1	5	13.2
Profile No. 3	3	6	13.7
Profile No. 4	4	9	13.5

Table 5-1. Improved Prediction Capabilities at 218 KHz when Irregular Terrain is Considered (Kona, Montana).

Terrain	Difference Between Measured Data and ITSNR Prediction (dB relative to 1 μV/m)	Difference Between Measured Data and GWSNR Prediction (Smooth Earth) (dB relative to 1 μV/m)	Distance (nm)
Profile No. 1	3	3	9.5
Profile No. 1	1	4	16
Profile No. 1	8	9	21.2
Profile No. 2	4	4	13.2
Profile No. 3	4	9	13.7
Profile No. 4	0	6	13.5

Table 5-2. Improved Prediction Capability at 404 KHz when Irregular Terrain is Considered (Kona, Montana).

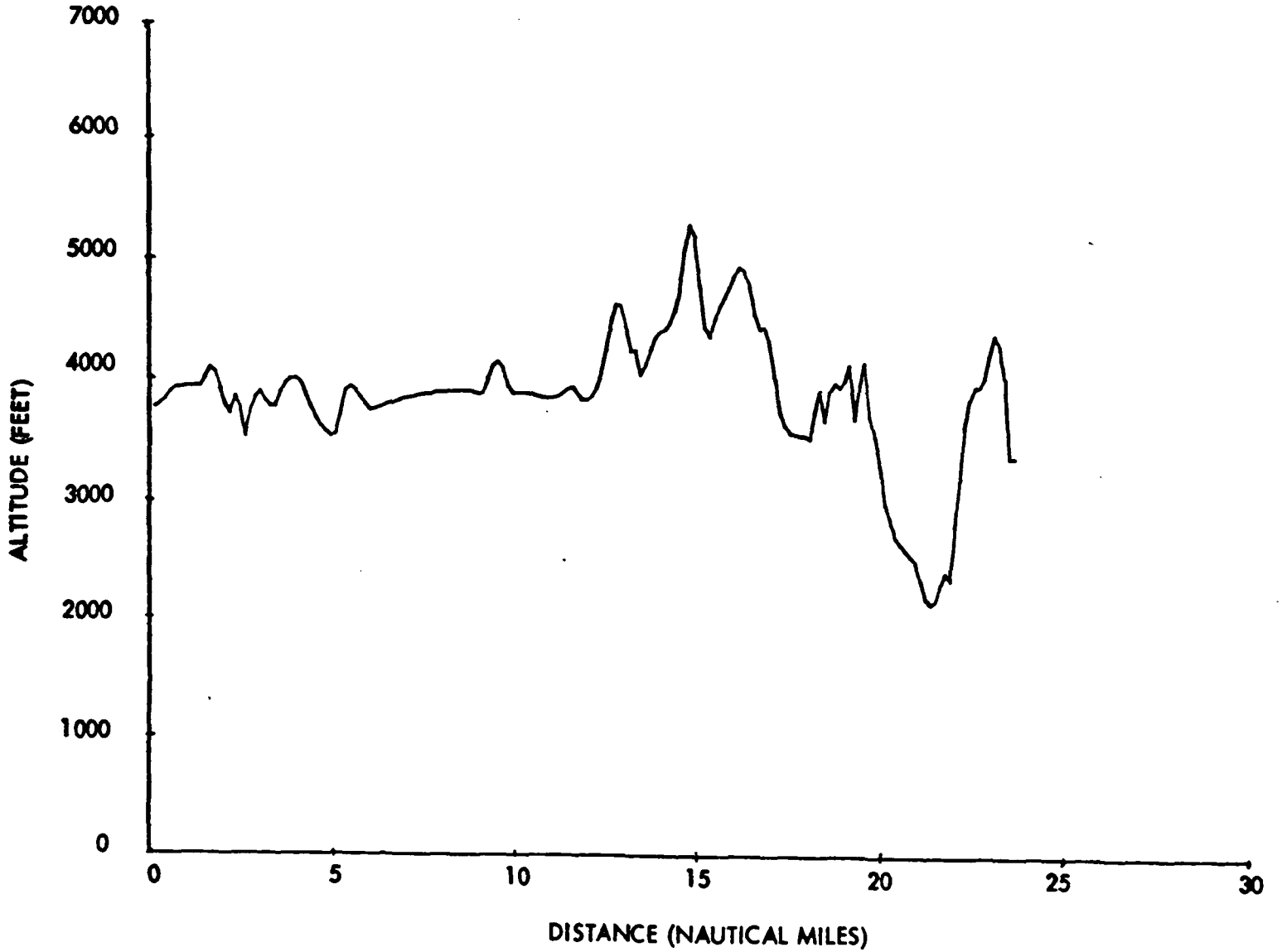

Figure 5-1. Terrain Profile 1 - Montana.

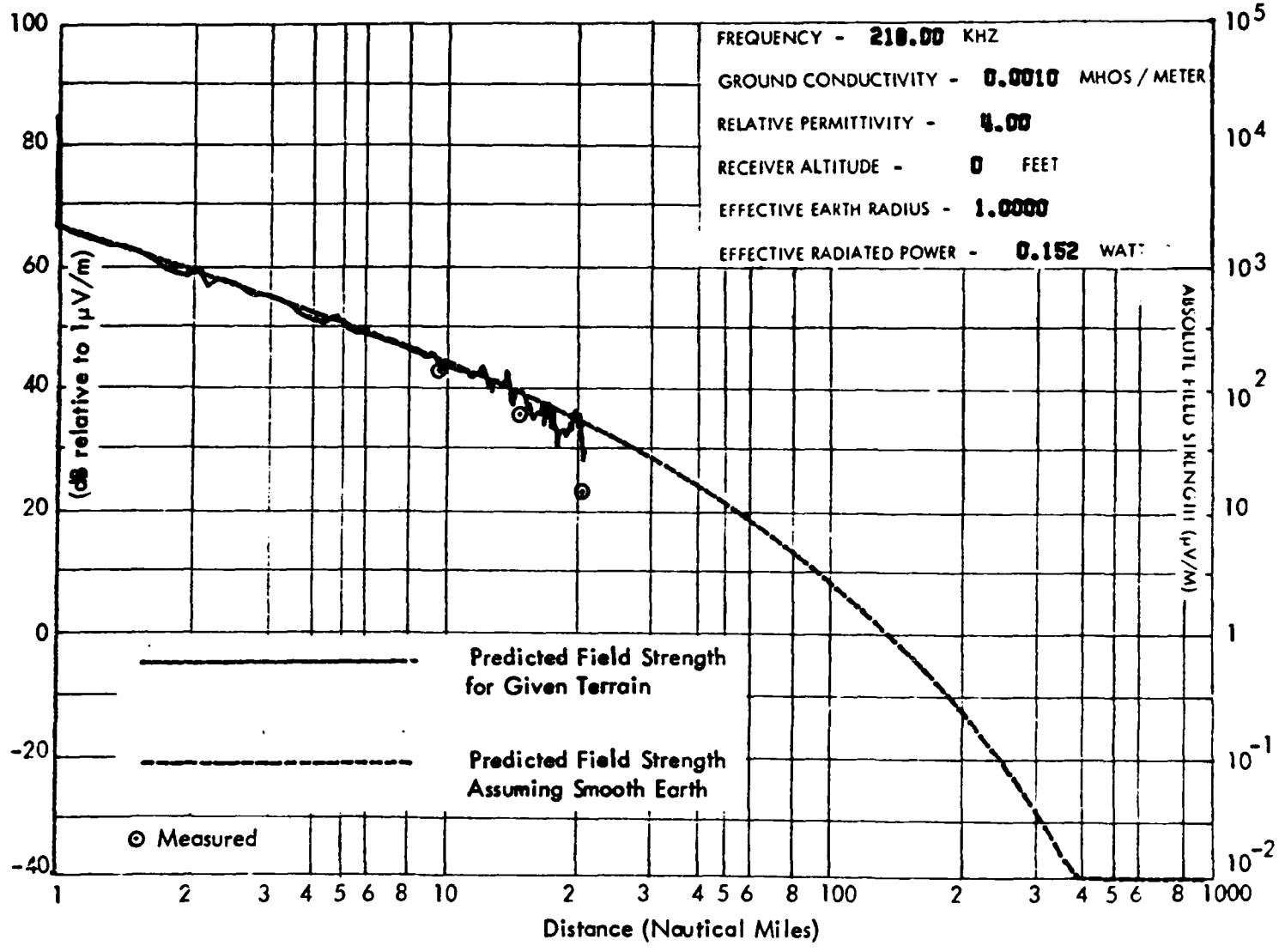

Figure 5-2. Predicted and Measured Field Strength for Profile 1 - Montana.

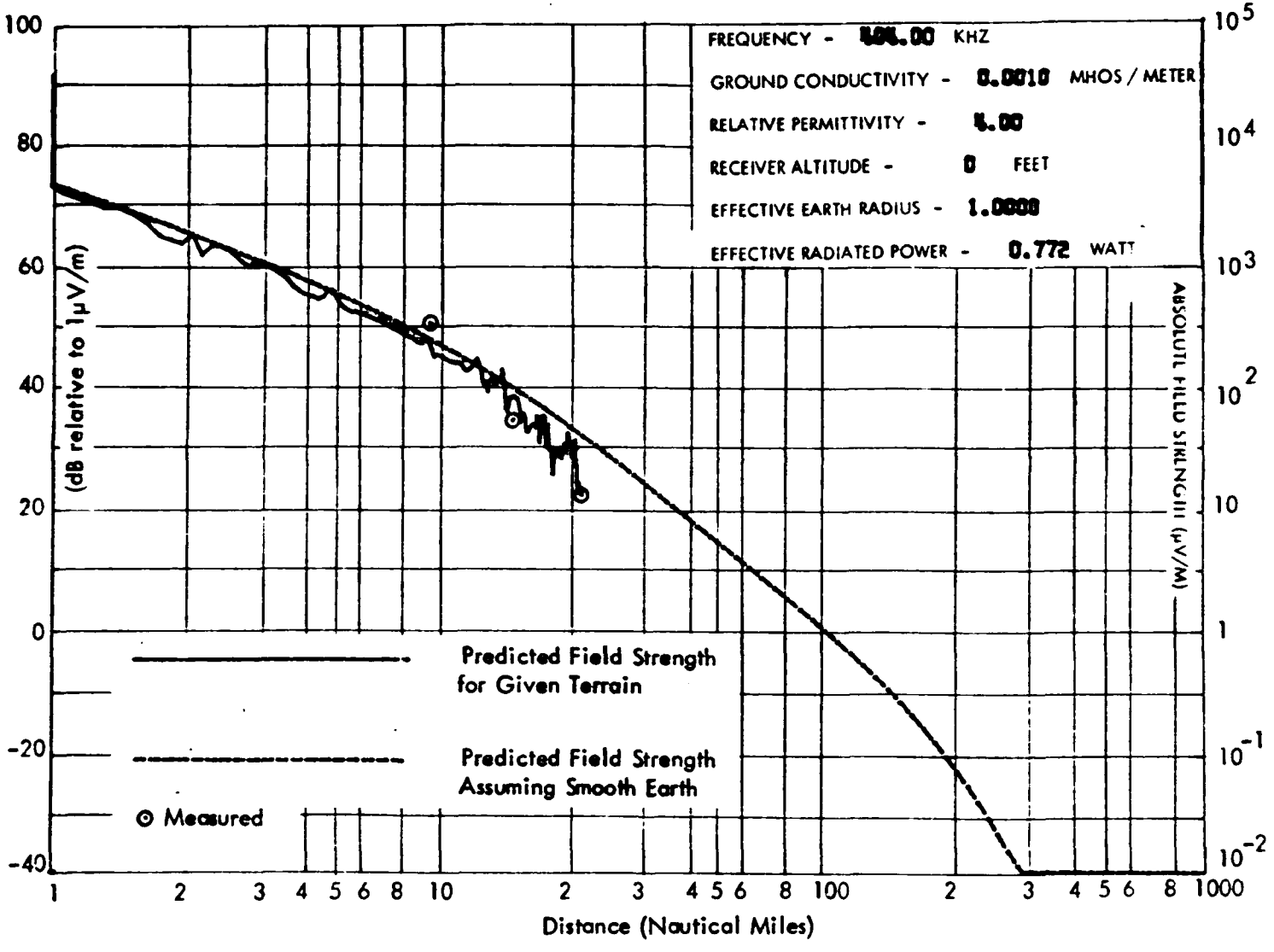

Figure 5-3. Predicted and Measured Field Strength for Profile 1 - Montana.

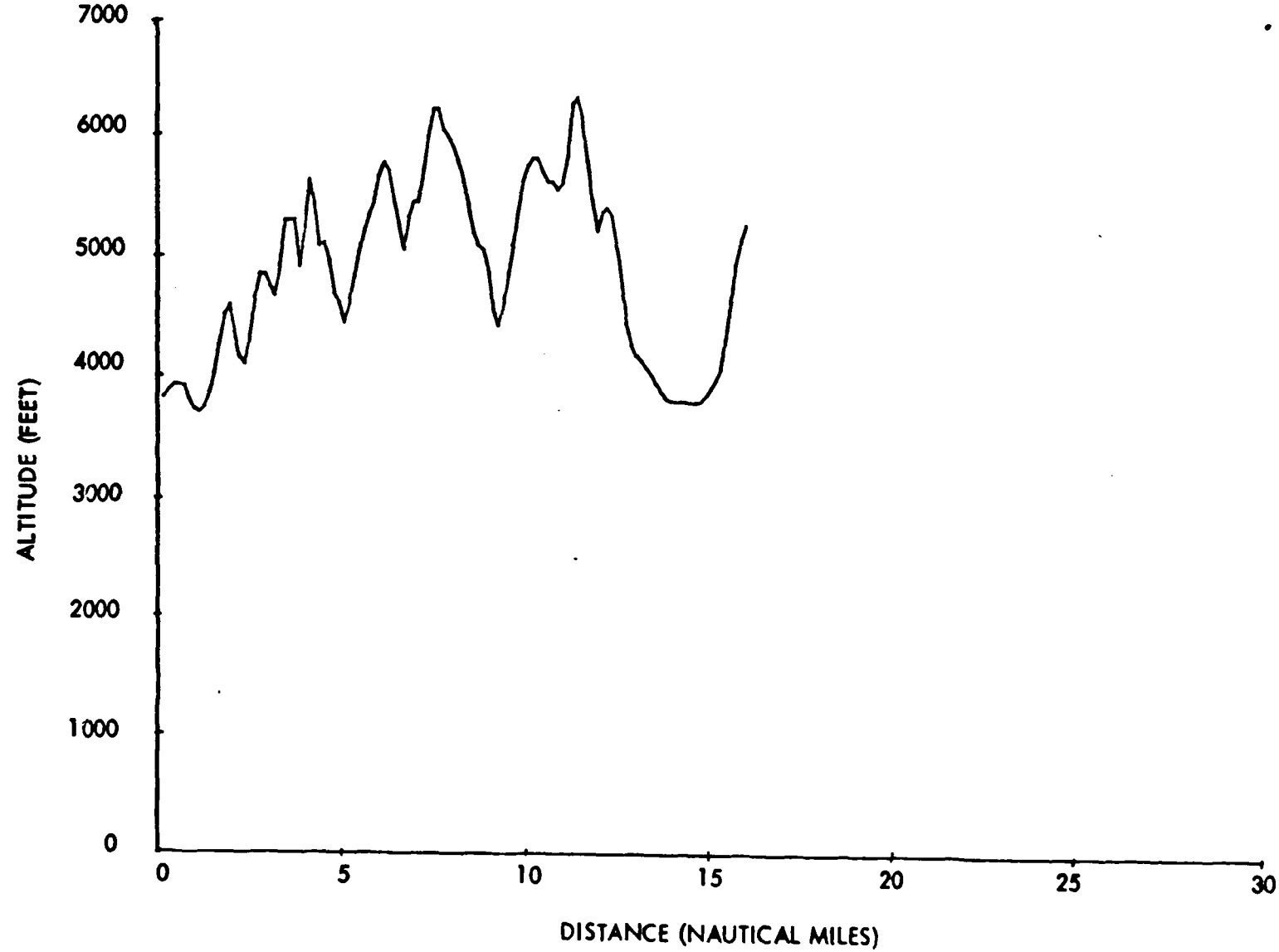

Figure 5-4. Terrain Profile 2 - Montana.

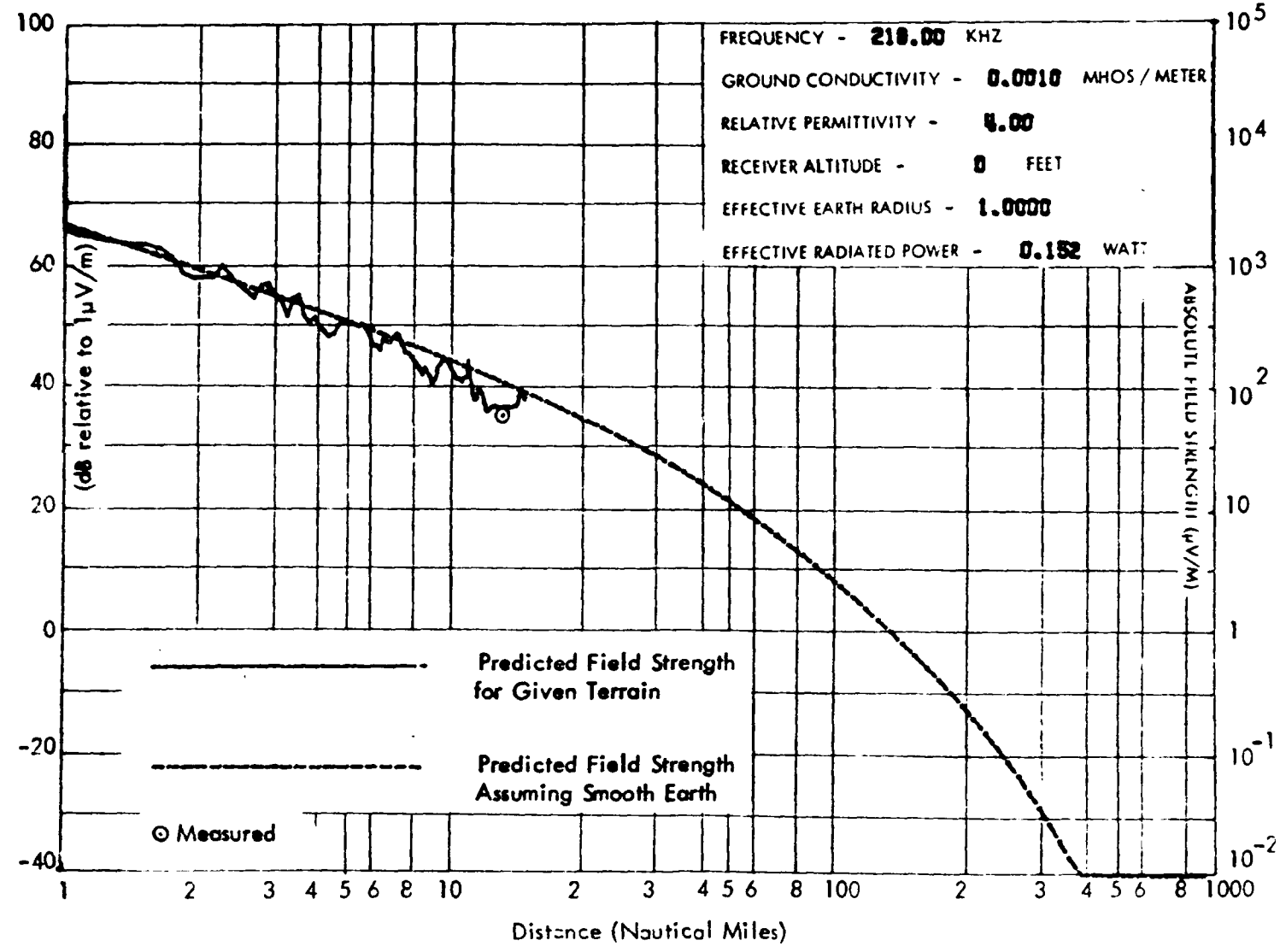

Figure 5-5. Predicted and Measured Field Strength for Terrain Profile 2 - Montana.

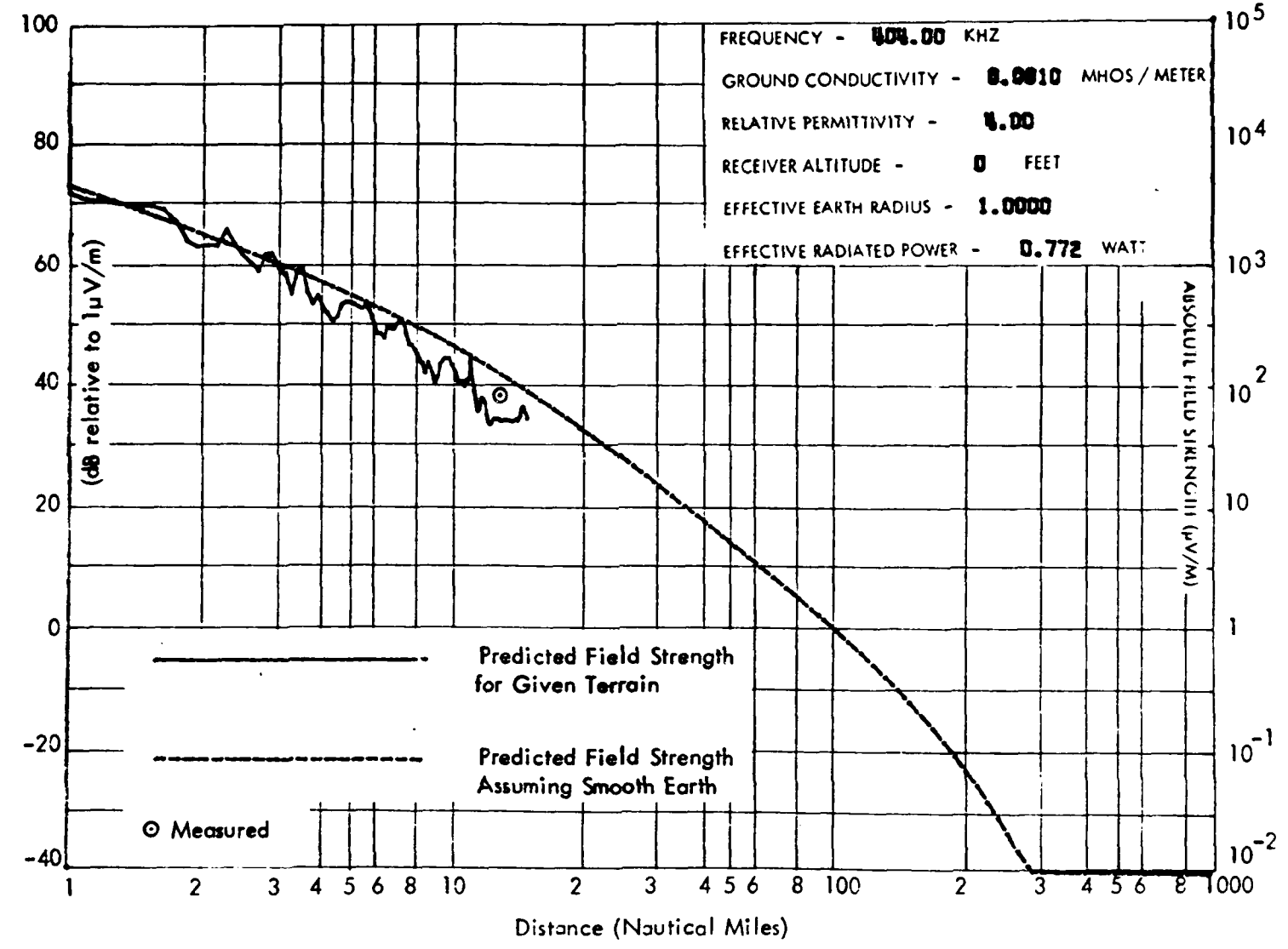

Figure 5-6. Predicted and Measured Field Strength for Profile 2 - Montana.

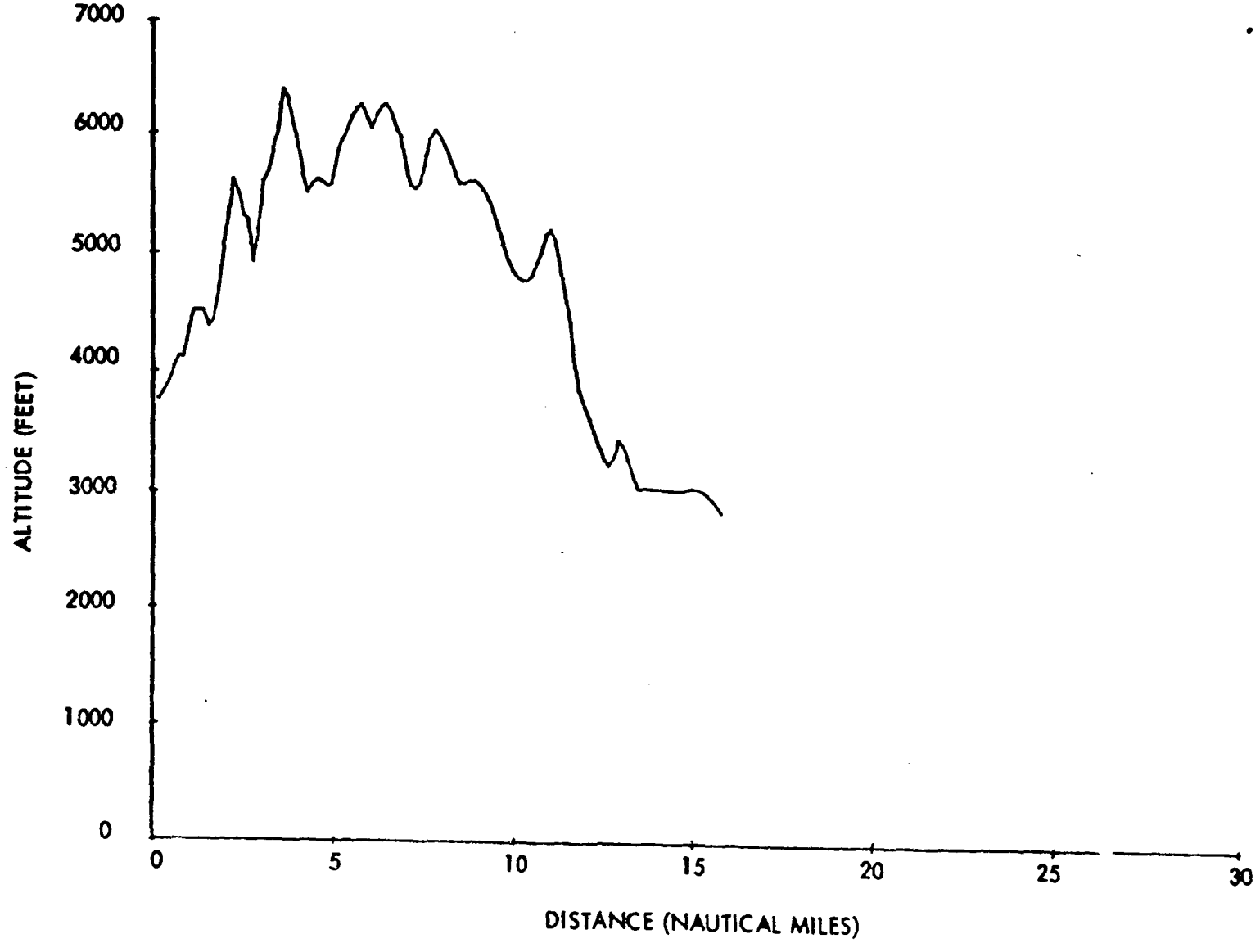

Figure 5-7. Terrain Profile 3 - Montana.

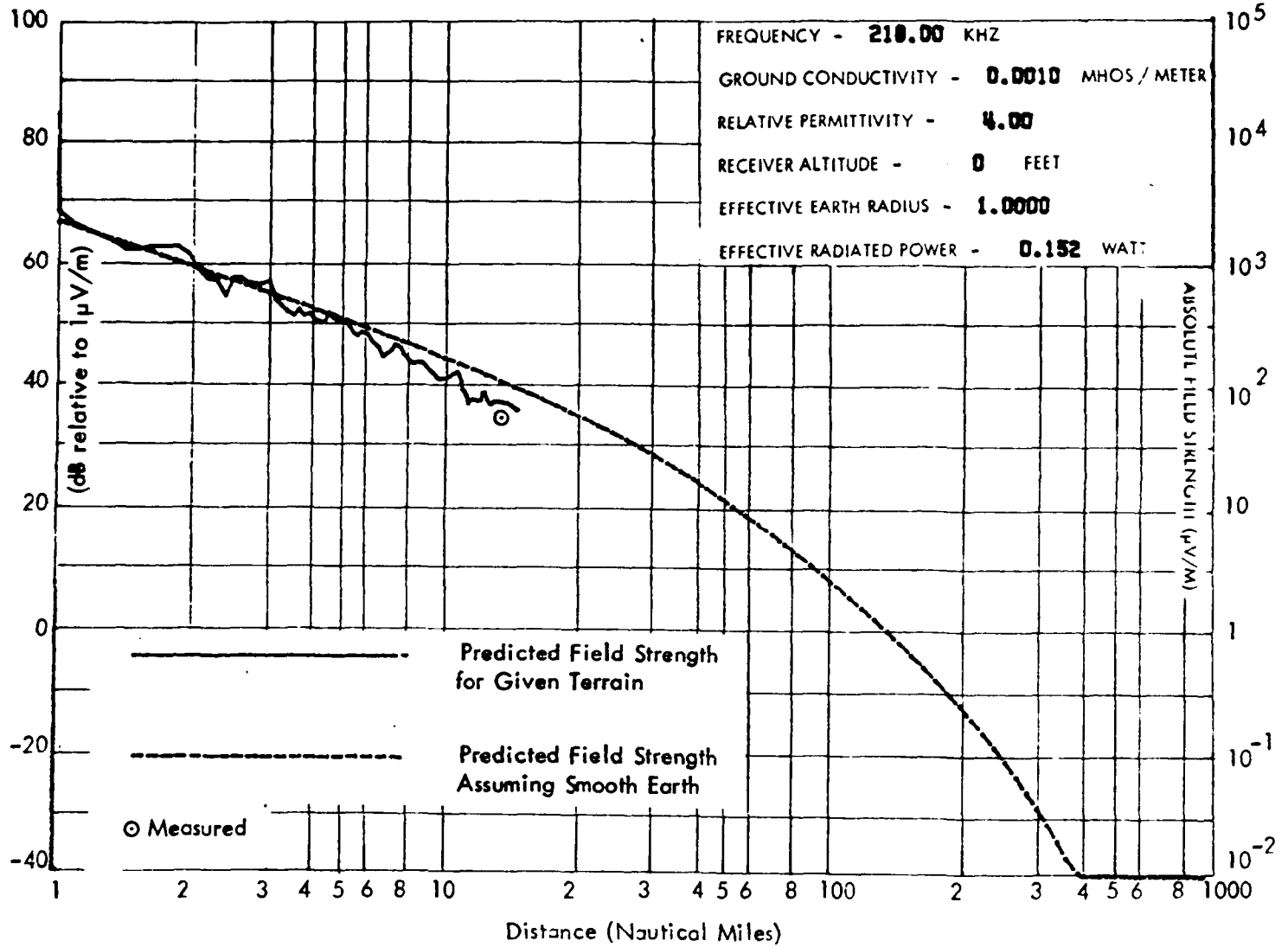

Figure 5-8. Predicted and Measured Field Strength for Profile 3 - Montana.

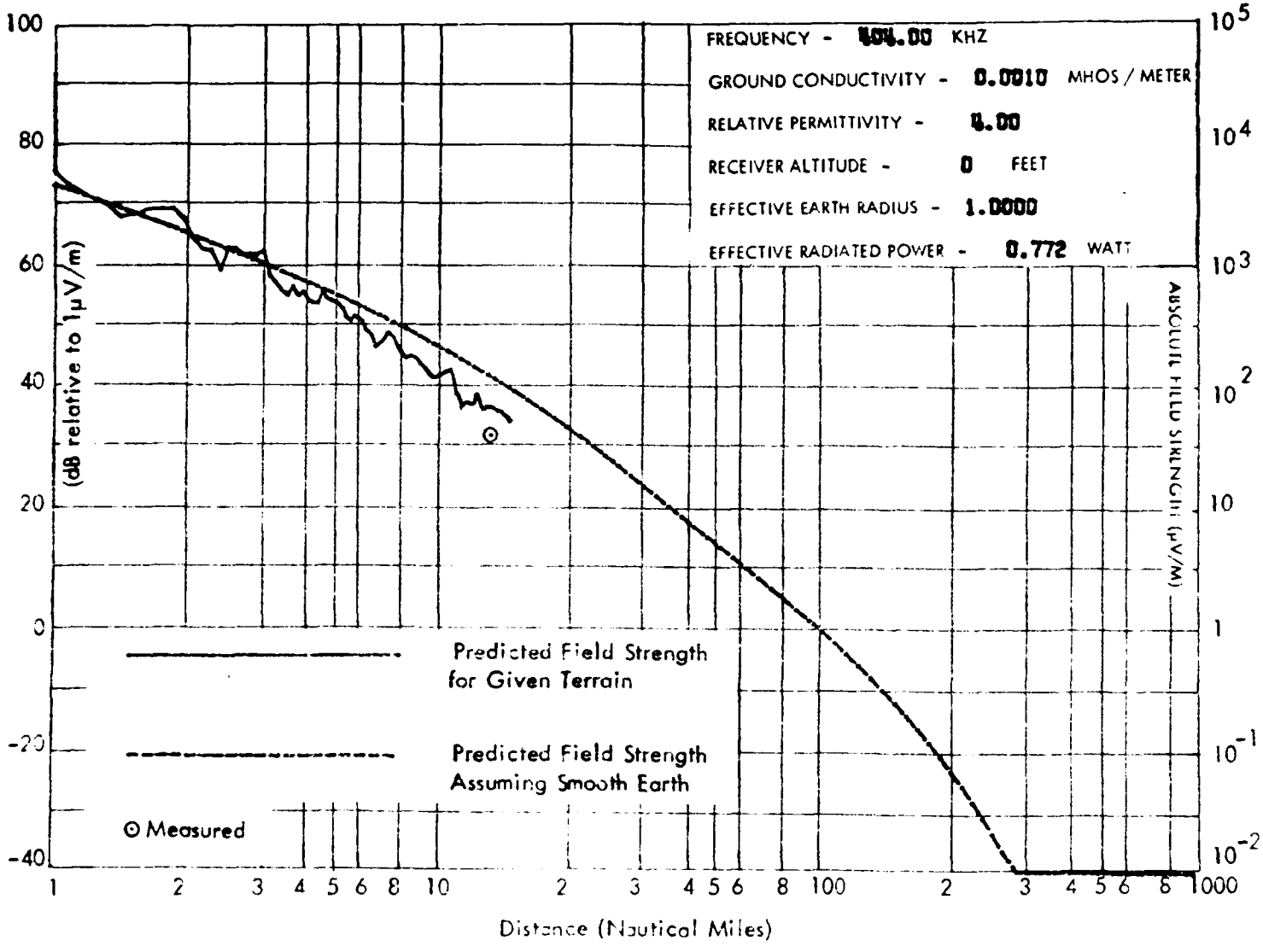

Figure 5-9. Predicted and Measured Field Strength for Profile 3 - Montana.

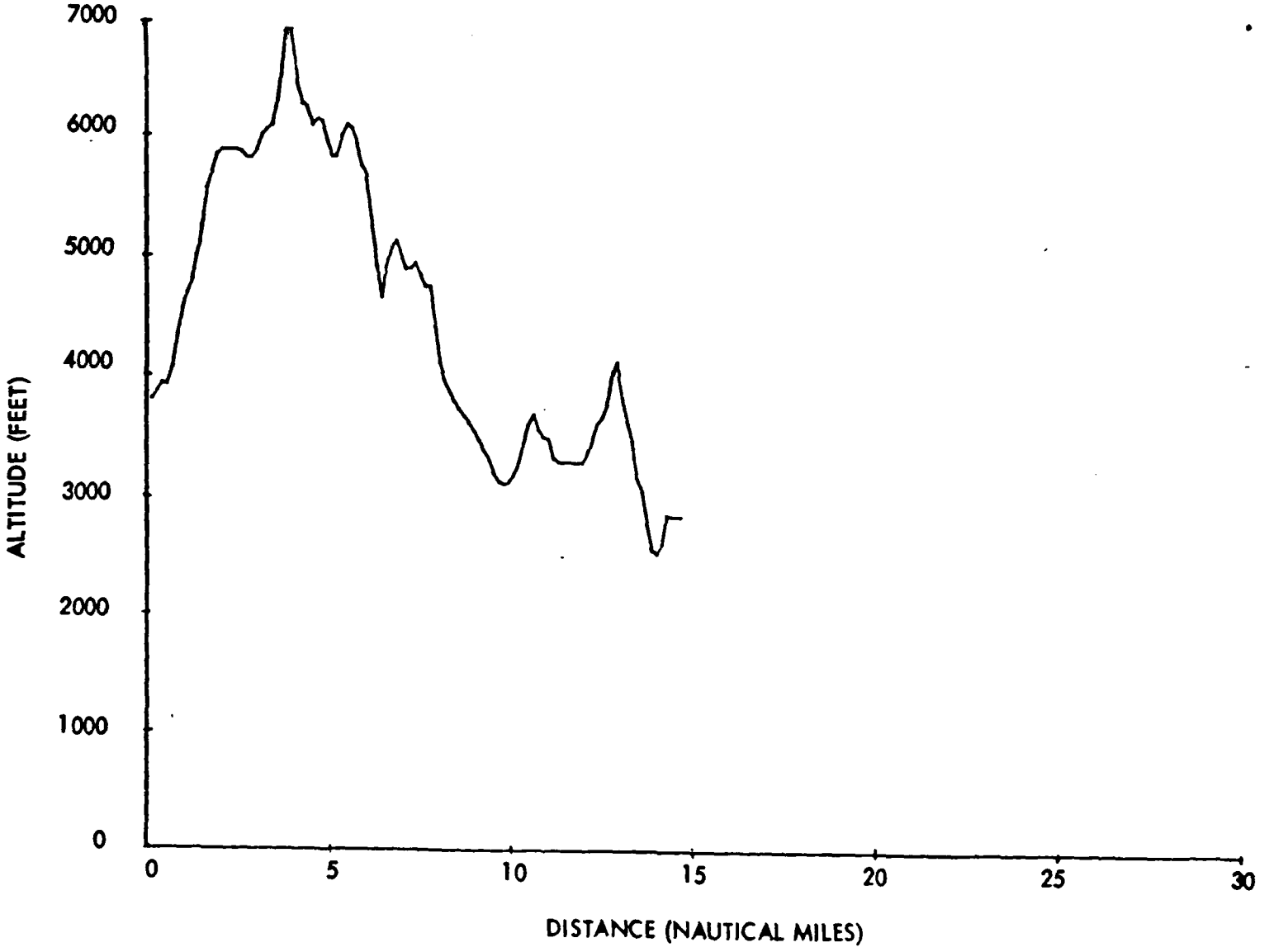

Figure 5-10. Terrain Profile 4 - Montana.

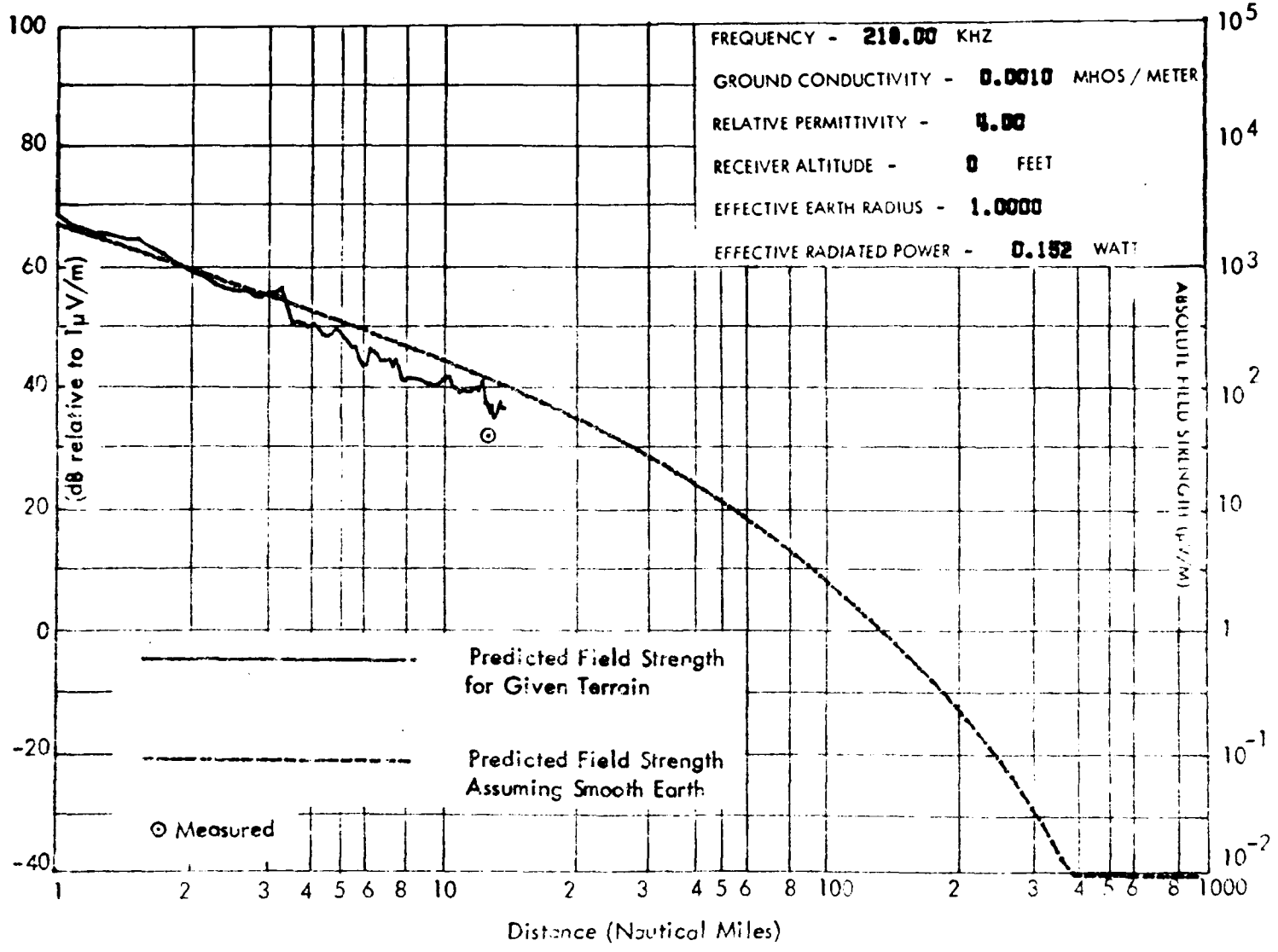

Figure 5-11. Predicted and Measured Field Strength for Profile 4 - Montana.

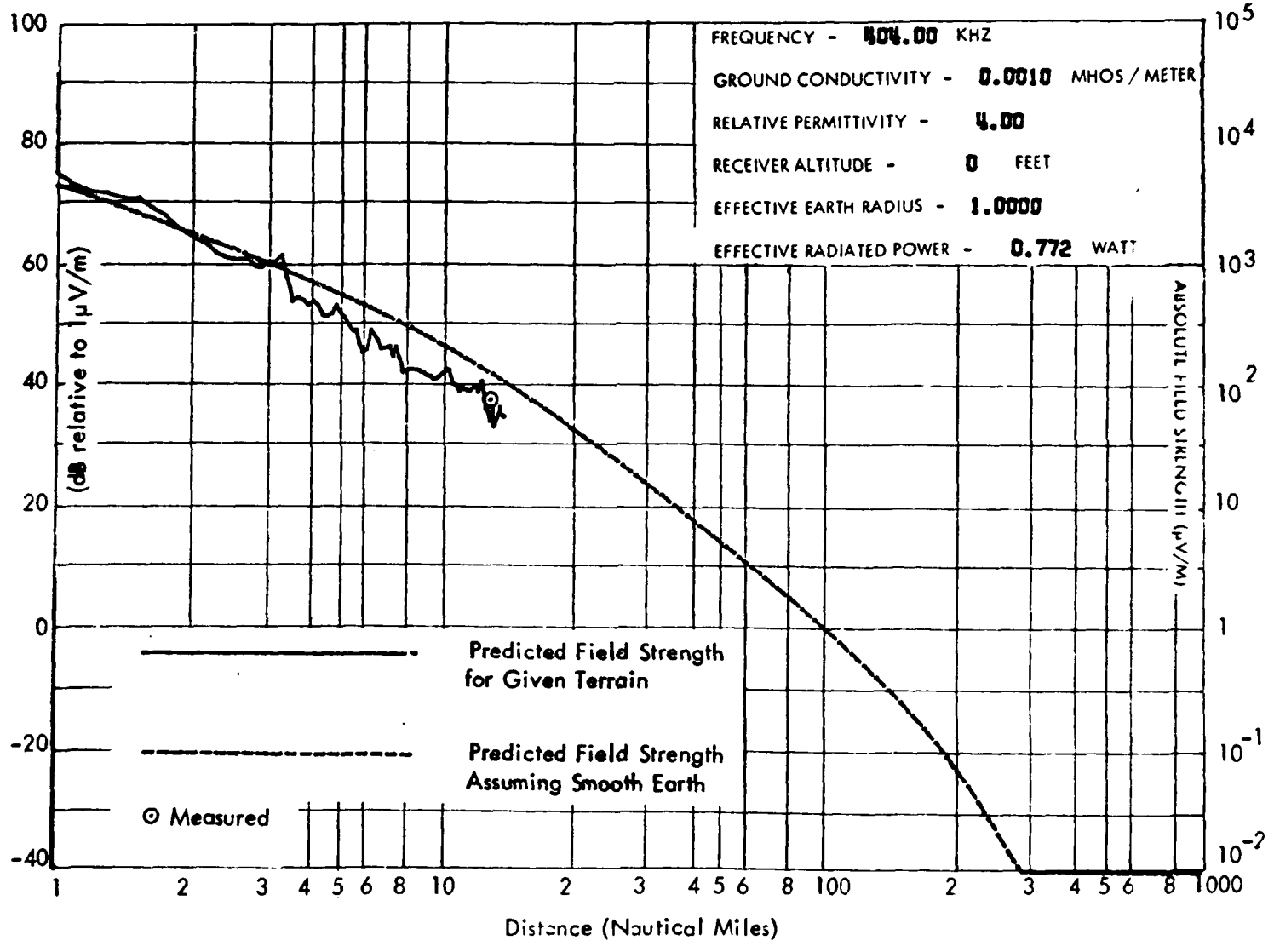

Figure 5-12. Predicted and Measured Field Strength for Profile 4 - Montana.

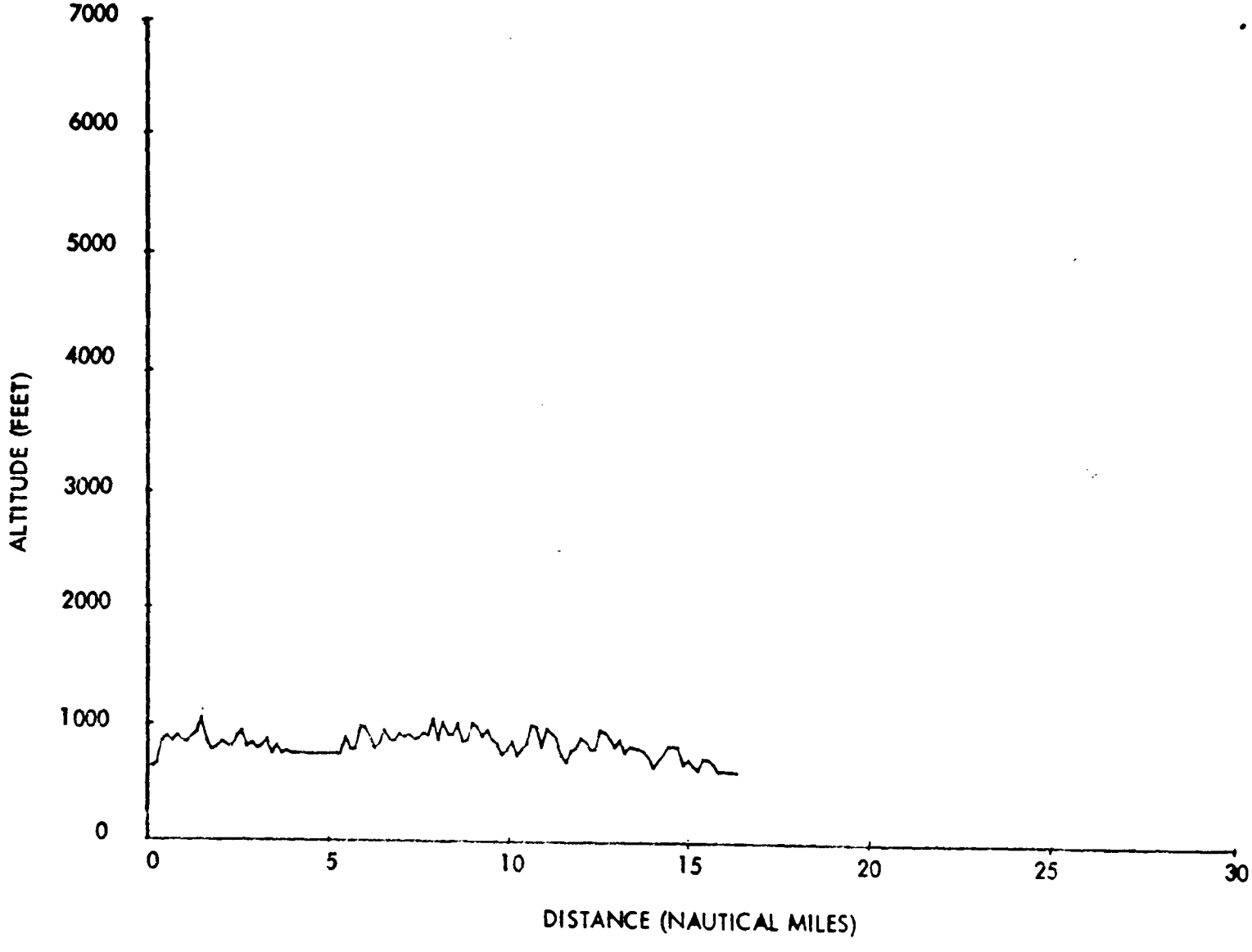

Figure 5-13. Terrain Profile 5 - Ohio.

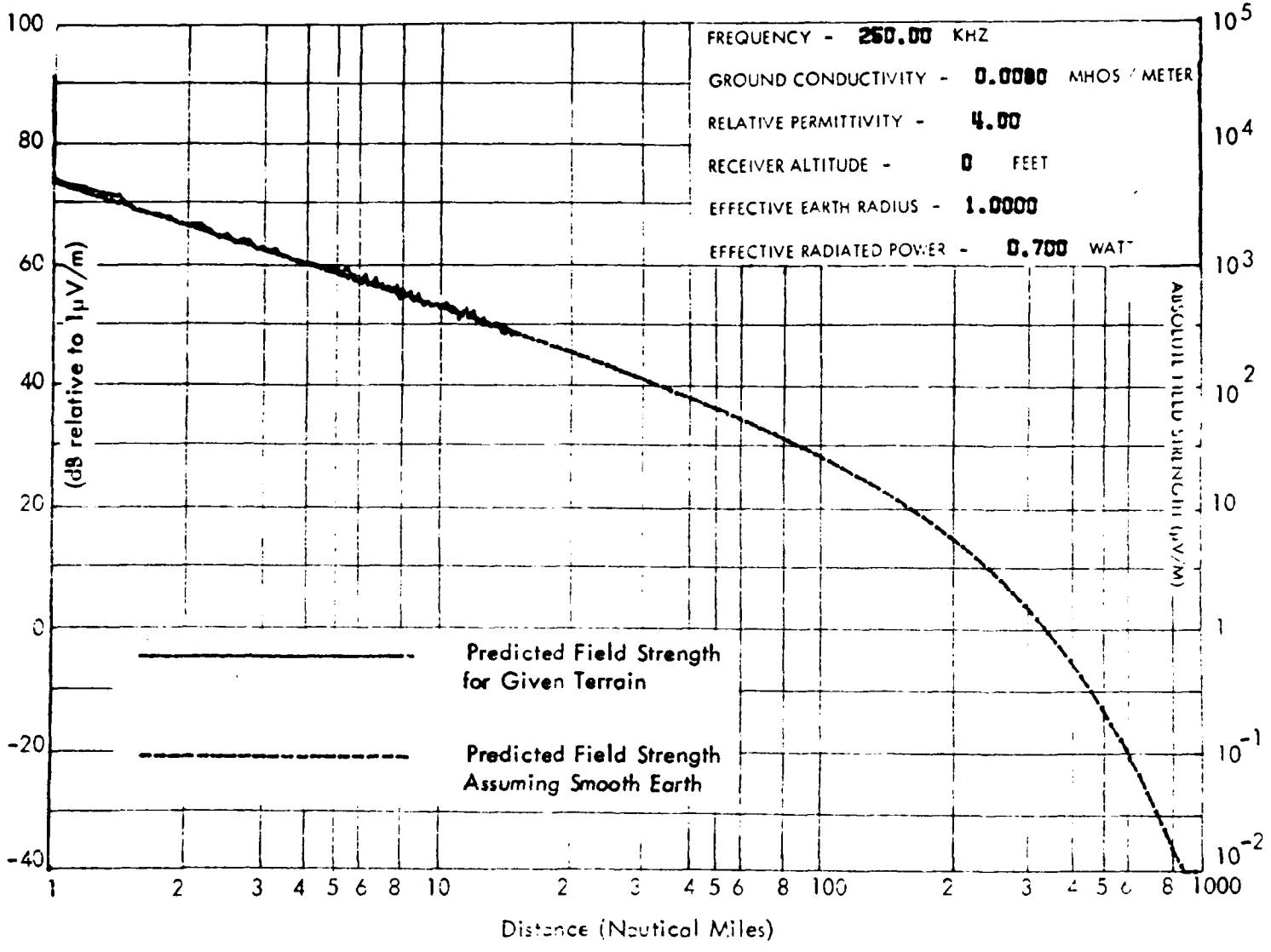

Figure 5-14. Predicted Field Strength for Profile 5 - Ohio.

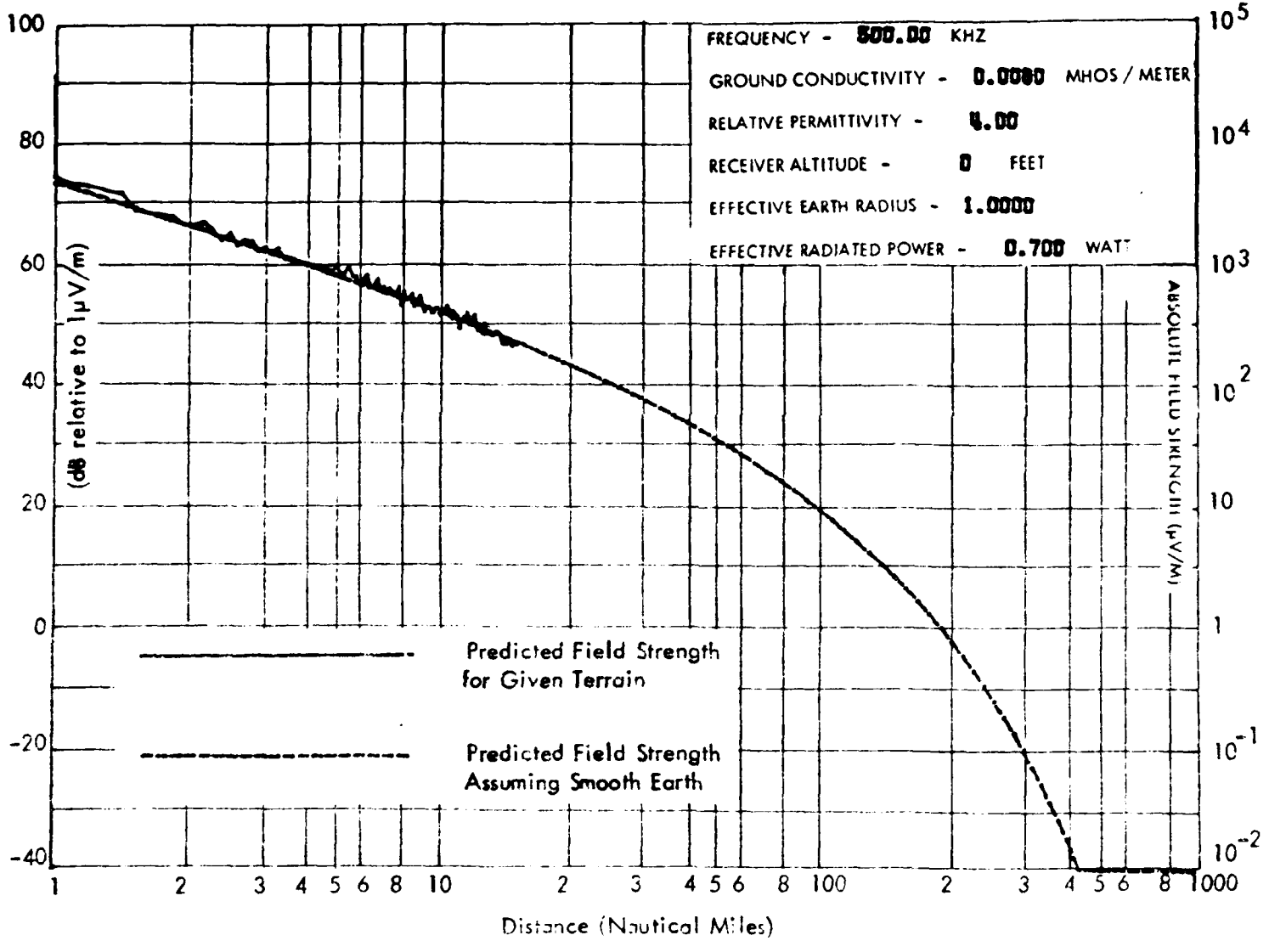

Figure 5-15. Predicted Field Strength for Profile 5 - Ohio.

VI. CONCLUSIONS

Radio wave propagation is a very complex phenomena and, therefore, the modeling and predicting of effects of various parameters is also quite complex. Certain assumptions, the nature of which depend largely upon the radio frequency, are required in all mathematical models of wave propagation. These assumptions concerning the propagation media are also often necessary to reduce the model to a usable form from which effects of parameters can be obtained practically and economically.

Computer models have been utilized in this report to predict field strength under varying conditions. In Sections II and III, the models used assume that the earth possesses a perfectly smooth, spherical surface, completely homogeneous, and that the upper atmosphere is homogeneous as well. The resulting computation is that of field strength due to the ground wave component only. This model has been used in Section II, where its predicted field strength is compared with that measured for navigational non-directional beacons of various frequencies in the range 200-500 KHz located in southern Ohio, Pennsylvania, Connecticut, Massachusetts and New Hampshire. The results of this comparison, when ERP measurements were taken, in general were very good indicating that this model is valid for these frequencies under the terrain conditions encountered in these areas. The agreement also indicates that the measurement techniques used are valid. For those cases where an effective radiated power could not be measured, the trend of the data follows that of the prediction, although the absolute levels may not agree. This can be expected, however, since the cases where ERP was measured resulted in considerable variation from the values obtained from FAA publications [13,14].

The data collected also suggests that some correlation exists between air- and ground-based field strength measurements. Measurements taken at various altitudes are presented in Section II, and trends toward a slight drop in field strength as altitude increases is apparent up to altitudes of 8000 feet, the highest measurement point. This trend is predicted by the model for altitudes up to 20,000 feet, and is due to the fact that the earth's surface is not perfectly conducting. Therefore, the measurements presented in Figures 2-29, 2-30, and 2-31, are expected from the theory and do show a correlation between flight measurements and ground-based data.

Another important fact which is illustrated by the data collected and presented in Section II is that when field strength measurements are repeated, the agreement is very good. This agreement suggests that the field strength from a particular beacon is fairly constant and also shows that the techniques used in the field strength measurements are valid. Another set of measurements showing the validity of the calibration procedure for airborne measurements, which neglects the presence of the aircraft, is presented in Table 2-2. These measurements, made with a DC-3, show that variation with aircraft orientation is not more than 1.4 dB, well within the tolerance of the receiver. Therefore, even the DC-3, the largest aircraft used in measurements for this report, has little effect on the field strength. This can be expected, since the aircraft is still quite small when compared to a wavelength at these frequencies.

The same model (assuming smooth, homogeneous earth and homogeneous ionosphere) is used in Section III to determine effects of various parameters on ground wave propagation in the frequency range 200-500 KHz. The parameters under consideration here are ground conductivity and relative permittivity, receiver altitude, and effective earth radius. The results of this study show that ground conductivity is clearly the most important parameter for these frequencies at the distances of interest for non-directional beacons. Curves were generated for a wide range of ground constants from sea water (σ = 4 mhos/m) to desert (σ = .001 mhos/m). The study of the effect of relative permittivity involved changing this parameter under conditions of sea water, ground of medium conductivity, and poorly conducting earth. The findings here show that the relative permittivity of the earth effects wave propagation in this frequency range only for poorly conducting earth. Even under these conditions, however, this parameter has little effect for all practical values at distances important for NDB use. The next parameter investigated here was receiver altitude. As expected, this parameter had little effect on the measured field strength, since the wavelengths involved are very large. However, the model does correctly predict the slight reduction of field strength as altitude increases, as previously mentioned. The final parameter, effective earth radius, was found to be, like receiver altitude, unimportant for practical values and distances normally encountered with non-directional beacons.

Section IV has utilized a model which, while still assuming a spherical, smooth, homogeneous earth, allows consideration of an inhomogeneous ionosphere. The model, (LFSNR) has generated predicted field strength for various values of radio frequency, ground constants, hour and month, which have been plotted and presented in Section IV. The results of comparisons of these plots shows that radio wave propagation in this frequency range is affected when the sky wave is considered. The predicted effects are most severe at night, regardless of the season, followed by winter day, equinox day, and finally summer day, which shows very little change from the results of model GWSNR, which ignores ionospheric effects entirely. The predicted field strength curves lead to conclusions that the sky wave is always more important for high powered facilities, since these beacons have a larger coverage radius (determined from the ground wave) and, therefore, the sky wave, which becomes significant at larger distances, has more effect. Also, though the sky wave effects are very similar for 200 and 500 KHz, the lower frequency beacons are slightly more subject to interference than are higher frequency facilities, since again the coverage radius is larger. Interference from the sky wave is also more likely at extremes in ground conductivity, for sea water and desert conditions. Sky wave propagation over sea water is enhanced by the good reflecting boundary provided by the water's surface, and therefore the sky wave hops are attenuated less than propagation over earth. Under desert conditions, the ground wave is rapidly attenuated and, therefore, the sky wave component here is relatively large by comparison.

The models used in Section V, ITSNR, again ignores ionospheric effects, but allows consideration of irregular, inhomogeneous terrain. Field strength predicted by this model has been compared with measurements taken in Montana at the same location but at two different frequencies: 218 and 404 KHz. For both these frequencies, on four different terrain profiles, the predicted and measured field strength values have been presented. Comparison of these values show that the model allowing irregular

terrain has indeed predicted the measured values with greater accuracy than the smooth earth model. Field strength predicted for a terrain profile in southern Ohio is also shown in Section V, and at all NDB frequencies the terrain irregularities encountered here have little effect on the predicted field strength.

In summary, the models utilized in this report give one the ability to accurately predict the field strength under a variety of conditions. Although assumptions have been necessary in the models, they nevertheless are very useful in field strength prediction for all conditions. The measurement techniques and calibration procedure used for airborne measurements have also proven to be valid for field strength measurements on non-directional beacons.

VII. INVESTIGATORS

This work was performed by members of the Avionics Engineering Staff at Ohio University. The theoretical work in particular has constituted the essence of a master's thesis written by Mr. Jerry Bash and supervised by Dr. R. J. Luebbers, Assistant Professor, Department of Electrical Engineering at Ohio University. It is a manifestation of the department's policy to encourage the involvement of a degree candidate with a contemporary engineering problem so as to provide a practical solution.

Dr. Luebbers was also responsible for the design for the Field Calibration Unit. Assistance in obtaining the measurement data was provided by Messrs. James Irvine and Tom Mullins. Additionally, Delmar Pullins and Dr. Robert Lilley assisted in making airborne measurement data.

VIII. REFERENCES

[1] Berry, L. A., "User's Guide to Low-Frequency Radio Coverage Programs", Office of Telecommunications, Boulder, Colorado, OT Technical Memorandum 78-247, January 1978.

[2] Norton, K. A., "The Calculation of Ground Wave Field Intensity Over a Finitely Conducting Spherical Earth", Proceedings of the I.R.E., Vol. 29, No. 12, pg. 624, 1941.

[3] Wait, J. R., "Electromagnetic Surface Waves", Advances in Radio Research, Edited by J. A. Saxton, Vol. 1, pp. 157-217, Academic Press, London, 1964.

[4] Harrington, R. F., "Time-Harmonic Electromagnetic Fields", pp. 77-81, McGraw-Hill Book Company, 1961.

[5] Abramowitz, M., and I. A. Stegun, Handbook of Mathematical Functions, National Bureau of Standards, AMS 55, U. S. Government Printing Office, Washington, D. C., 1964.

[6] Sommerfeld, A. N., Partial Differential Equations, Academic Press, New York, N. Y., 1949.

[7] Jordan, E. C., and K. C. Balmain, Electromagnetic Waves and Radiating Systems, pp. 146, 630-633, Prentice Hall, Inc., Englewood Cliffs, New Jersey, 1968.

[8] Woodward, P. M., A. M. Woodward, R. Hensman, H. H. Davies and N. Gamble, "Four-Figure Tables of the Airy Functions in the Complex Plane", Phil. Magazine (7), Volume 37, pp. 236-261, 1946.

[9] Fock, V. A., Electromagnetic Diffraction and Propagation Problems, Pergamon Press, London, 1965.

[10] Bremmer, H., Terrestrial Radio Waves, Elsevier Publishing Company, Amsterdam, Netherlands, 1949.

[11] Jean, A. G., H. E. Taggart and J. R. Wait, "Calibration of Loop Antennas at VLF", Journal of Research of the National Bureau of Standards, Vol. 65, No. 3, July - September 1961.

[12] Arcove, S. A., and A. J. Delaney, "Electrical Ground Impedance Measurements in the United States Between 200 and 415 KHz", U. S. Army Cold Regions Research and Engineering Laboratory, Report No. FAA-RD-78-103, December 1978.

[13] "Frequency Management Engineering Principles", L/MF Frequency Assignment Criteria, FAA Handbook 6050.10, November 23, 1965.

[14] "Master Flight Radio Frequency List", FAA-RIS-6050-12, April 1979.

[15] XII Plenary Assembly, International Radio Consultive Committee (CCIR), New Delhi, 1970.

[16] Hoekstra, Pieter, "Electrical Ground Impedance Measurements in Alaskan Permafrost Regions", Report No. FAA-RD-75-25, USACRREL.

[17] IX Plenary Assembly, International Radio Consultive Committee (CCIR), Los Angeles, 1959.

[18] Wait, J. R., Electromagnetic Waves in a Stratified Media, Second Edition, Pergamon Press, pp. 117-118, 1970.

[19] Op. Cit., Bremmer, H., pp. 146-152.

[20] Op. Cit., Fock, V. A., pp. 116-118.

[21] Op. Cit., Wait, J. R., pp. 403-416.

[22] Berry, L. A., and J. E. Herman, "A Wave Hop Propagation Program for an Anisotropic Ionosphere", OT/ITS, RR 11, Office of Telecommunications, Boulder, Colorado, 1971.

[23] "Sky Wave Propagation at Frequencies Below About 150 KHz with Particular Emphasis on Ionospheric Effects", International Radio Consultive Committee Report 265, Vol. 2, Green Books, International Telecommunications Union, Geneva, 1970.

[24] Op. Cit., Wait, J. R. (1970), pp. 264-287.

[25] Davies, Kenneth, Ionospheric Radio Waves, Blaisdell Publishing Company, pp. 64-72, 1969.

[26] Davies, Kenneth, Ionospheric Radio Propagation, Dover Publications, Inc., New York, pp. 128-129, 1966.

[27] Op. Cit., Davies, Kenneth (1966), pp. 36-44.

[28] Ott, R. H., "A New Method for Predicting HF Ground Wave Attenuation over Inhomogeneous, Irregular Terrain", OT/ITS, RR 7, Office of Telecommunications, Boulder, Colorado, 1971.

IX. GLOSSARY

E	-	Electric Field Strength
H	-	Magnetic Field Strength
I	-	Current
λ	-	Free Space Wavelength
d	-	Distance from Source
ℓ	-	Length of Current Element
k	-	Wave Number
η	-	Intrinsic Impedance of Medium
P_f	-	Complex Radiated Power
P_r	-	Real Part of P_f
H^*	-	Complex Conjugate of Magnetic Field Strength
r	-	Radius
δ	-	Surface Impedance
h_1, h_2	-	Antenna Height from Surface
ϵ_r	-	Relative Permittivity
σ	-	Conductivity
R_G	-	Reflection Coefficient of Ground
erfc	-	Complementary Error Function
f	-	Frequency (Hertz)
ω	-	Angular Frequency
a	-	Radius of Earth
$H_1(h)$, $H_2(h)$	-	Height Gain Functions
$w_n(t)$	-	Airy Functions
∇	-	Del Operator

X. APPENDICES

A. Theoretical Basis for Calibration Technique. As discussed in this report, coverage area of non-directional beacons is determined by their signal strength. However, the capability to accurately measure airborne field strength levels in this frequency range has previously not been available. Present methods measure only the radio frequency voltage at the receiver terminals, neglecting effects of antenna coupling, the transmission line from the antenna to the receiver, and field distortion caused by the aircraft fuselage. This section documents the effort to provide a method of calibrating the entire receiving system (from antenna to receiver system) in absolute volts-per-meter of electric field strength at the antenna described by Luebbers, Irvine, Mullins and Bash [1].

The method chosen involves transmitting a known field strength from a portable oscillator with an attached antenna located near the aircraft receiving antenna and measuring the corresponding receiver AGC voltage. The calibration process can be performed on the ground. One limitation of the approach is that only receiving systems using loop antennas can be directly calibrated using this method. The reason is that the calibration process depends upon a relation between near- and far-zone fields that is valid only for loop antennas. However, once the ADF loop antenna receiving system is calibrated using this near-zone, oscillator method the calibrated loop antenna system can then be used to calibrate other antenna systems (such as the ADF sense antenna system) by placing both antennas in the same far-zone fields. This can easily be accomplished by flying in the vicinity of a transmitting NDB, and the process will be discussed more fully in this Appendix.

One disadvantage of the process is that the effects of the aircraft are not completely included since, in general, they will be different for near- and far-zone fields. However, for the frequencies of interest this should not be a serious source of error since the wavelength is so much greater than the aircraft dimensions.

What is desired is to develop the correspondence of some measurable receiver parameter with the strength of the electric field of the plane wave which exists at the location of the receiving antenna. This is not equivalent to measuring the voltage at the receiver terminals, since the antenna, transmission line, and (for airborne measurements) the presence of the aircraft affect the relationship of electric field to terminal voltage. This relationship is quite difficult to calculate, especially at the relatively low frequencies (200 to 500 KHz) of interest, since the receiving antenna is electrically very small and inefficient. Thus, determining the voltage level at the receiver terminals and relating this to a receiver output, such as the AGC voltage, does not result in the desired information.

One can determine the correspondence of the electric field strength at the antenna to the receiver AGC voltage (or other receiver output) by immersing the antenna in a plane electromagnetic wave of known strength. Unfortunately, this is difficult to do at the frequencies in question. One could fly near a transmitting beacon assumed to be

operating properly and correlate the receiver output with the field strength predicted to be present at the aircraft location. The predictions are, however, based on propagation of the wave over a smooth homogeneous earth of known permittivity and conductivity from an antenna of known radiation pattern radiating a known amount of power. Any actual site will deviate from this ideal causing an error in the calibration. In addition, the receiving system is now calibrated at only one frequency, and for calibration at another frequency either another beacon must be located or the one used must be frequency shifted. However, the advantage of this approach is that the effects of the aircraft are included completely in the calibration.

A similar approach could be used with the aircraft parked on the ground. With this approach, the field strength due to a nearby beacon could be measured near the parked aircraft using a calibrated antenna and receiver such as the Fairchild EMC-25 to determine the electric field strength near the aircraft. The sources of error here are the effects of the ground on the receiving antenna and the field distortion produced by the aircraft itself; and, as before, the system is calibrated at only one frequency.

The calibration method considered here utilizes a portable transmitter and attached transmitting loop antenna. It can be used anywhere, even when the aircraft is parked in a hangar. The entire receiving system from the receiving antenna to the receiver itself is calibrated as a unit. The calibration can be performed at any desired frequency (provided the wavelength is large in comparison to the loop antenna dimensions) and at any desired field strength level. Only loop antennas can be directly calibrated using the method, but the calibrated loop antenna can then in turn be used to calibrate other antenna types (such as the ADF sense antenna) while the aircraft is in flight and in the presence of a signal of desired frequency.

The method is based on work performed at the National Bureau of Standards [2, 3]. It depends upon the determination of the relationship between the signal induced in a receiving loop antenna due to a nearby transmitting loop and that induced in the same antenna due to an incident plane wave such as would be produced by an NDB. The method is illustrated schematically in Figure A-1. The calibration process is shown in Figure A-1a. The portable transmitting loop is located at a distance d from the receiving loop and coaxial with it. The spacing d would be typically 1 meter, and must be a minimum of 4 times the larger of the two loop radii. If the same receiving loop is now placed in a plane wave with electric field strength such that the receiver receives the same signal as in Figure A-1a, then the electric field strength E of the plane wave is given by the equation

$$E = \frac{60 \pi r_1^2 I}{(d^2 + r_1^2 + r_2^2)^{3/2}} \qquad (A.1)$$

where:

E = equivalent free-space field strength in rms volts-per-meter.

r_1 = radius of the transmitting loop in meters.

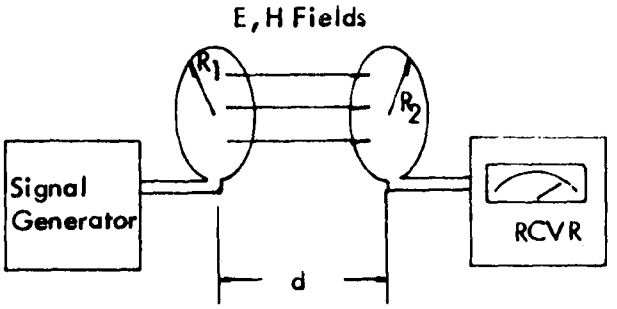

(a) Receiving loop in rear zone of transmitting loop and coaxial with it.

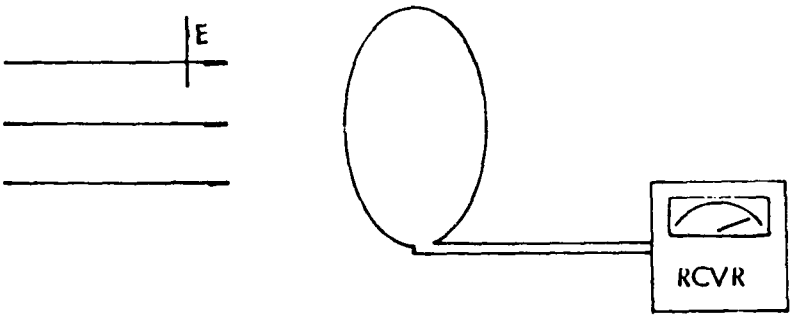

(b) Receiving loop in presence of plane, far-zone field of unknown amplitude.

For same receiver terminal voltage at same frequency,

$$E = \frac{60 \pi r_1^2 I}{(d^2 + r_1^2 + r_2^2)^{3/2}}$$

Figure A-1. Relation Between Near-Zone Loop Calibration Current and Amplitude of Received Far-Zone Electric Field.

r_2 = radius of the receiving loop in meters (if the loops are not circular, use the radius of a circle having the same area).

d = axial spacing in meters between the coaxial loops.

I = transmitting loop current in rms amperes.

For the relation to be accurate, the distance d must be much less than one wavelength, and must be a minimum of 4 times the radii of the larger of r_1 or r_2. Also, the area in the vicinity of the antennas should be free of metal objects for two to three times the distance d from the antennas. This latter requirement is not met due to the presence of the aircraft. However, laboratory experiments involving the placement of large metal plates near the two antennas to simulate the effects of the aircraft fuselage indicate little effect. The main justification for neglecting the near-zone fuselage effect lies in the agreement between field strength measurements based on this calibration technique and calculated field strengths. These results are reported in Section II of this report. Also, it must be assumed that the electric and magnetic fields of the far-zone are related by the characteristic impedance of free space (377 ohms).

To use Equation (A.1) and the approach of Figure A-1 to directly calibrate the receiving system would be somewhat difficult, since the current would have to be measured accurately and the equation itself then evaluated for each desired field strength. This can be avoided, and at the same time the accuracy of the calibration method can be related to the accuracy of a standard, field-strength measuring device, such as the Fairchild EMC-25 selective voltmeter and calibrated loop antenna, by using the technique illustrated in Figure A-2. Rather than measure the current I in the transmitting loop directly, the equivalent transmitted electric field strength E is measured using the calibrated receiving loop and selective voltmeter. If the transmitting loop is now placed near the receiving loop of the receiving system to be calibrated, and the same current I flows in the transmitting loop, the equivalent free space electric field E corresponding to the receiver output can be readily obtained from Equation (A.1) and is:

$$E = E_c \cdot \frac{(d_c^2 + r_1^2 + r_{2c}^2)^{3/2}}{(d^2 + r_1^2 + r_2^2)^{3/2}} \qquad (A.2)$$

where the symbol meanings are as for Equation (A.1) but with a subscript c denoting quantities pertaining to the measurement made using the calibrated loop receiving antenna and selective voltmeter. Since for most practical cases the separation d is much larger than either of the loop radii, if the same spacing d is used for both measurements the equivalent free space electric field E corresponding to a given receiver output is approximately equal to that measured by the calibrated receiving system, E_c, or

$$E \approx E_c \quad \text{if} \quad d_c = d, \quad r_{2c} \ll d, \text{ and } r_2 \ll d . \qquad (A.3)$$

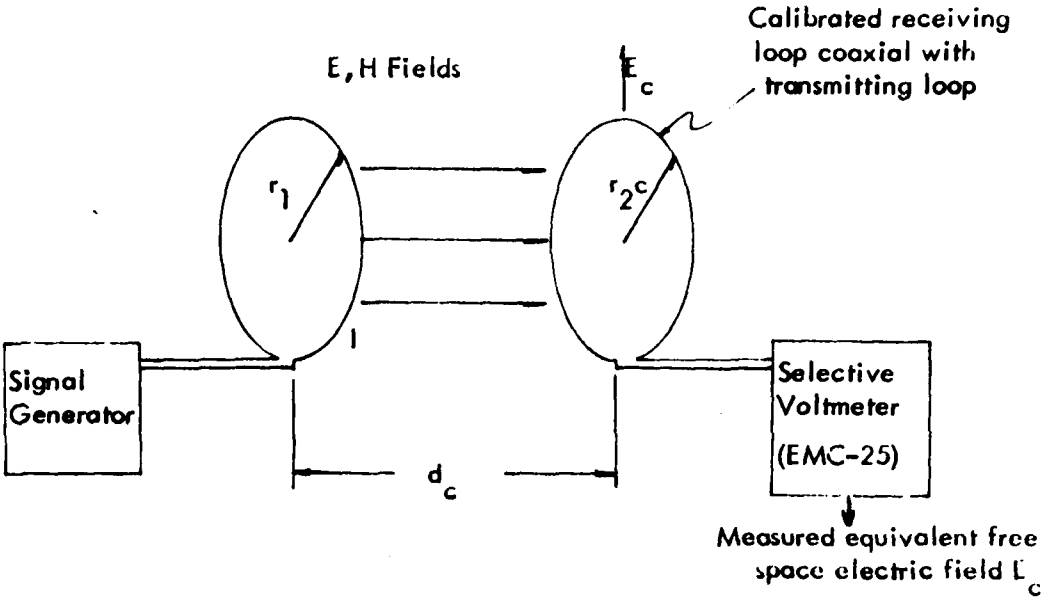

(a) Calibration of generator and loop.

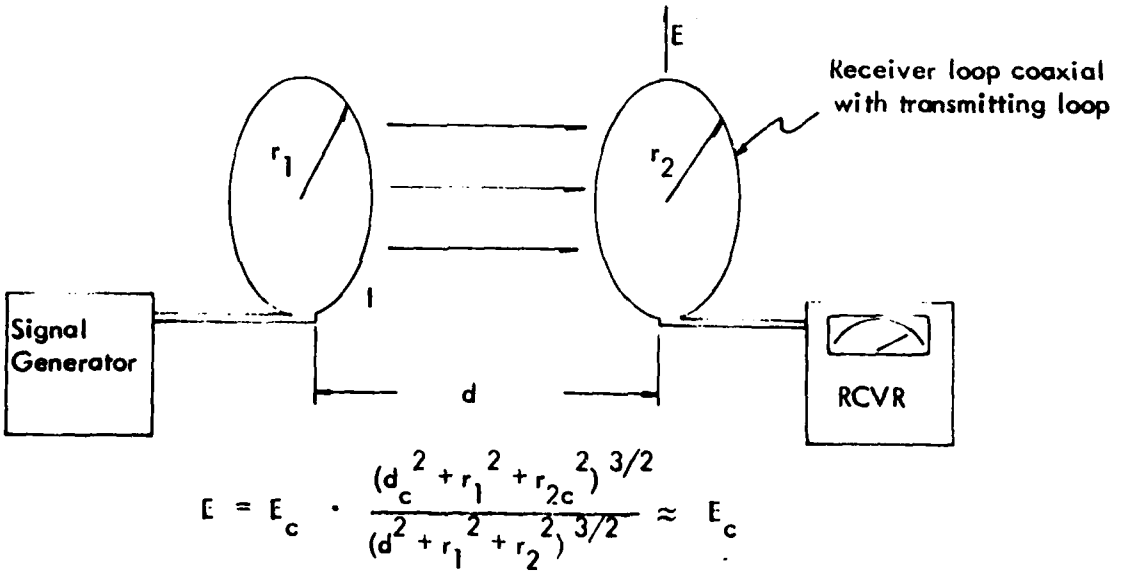

$$E = E_c \cdot \frac{(d_c^2 + r_1^2 + r_{2c}^2)^{3/2}}{(d^2 + r_1^2 + r_2^2)^{3/2}} \approx E_c$$

(b) Determining equivalent free space electric field.

Figure A-2. Determination of Electric Field Corresponding to Given Receiver Output by Comparison with Response of Selective Voltmeter and Calibrated Antenna to Same Signal. The relationship is determined from application of Equation (A.1), assuming same transmission current in (a) and (b).

A similar approach cannot be used with confidence for other types of antennas, such as monopole or dipole antennas, since the equations relating the near-zone and far-zone electric field equivalence are not as simple as Equation (A.1), as they are dependent upon wire diameters, shapes, and method of feeding the antennas, and also are much more affected by the presence of nearby structures such as the airplane fuselage. One could use the results of the calibration technique of Figure A-2, which applies only to loop antennas, to calibrate indirectly another type of airborne antenna as follows. First, calibrate the loop antenna using the near-zone method described. Then place this calibrated antenna together with the other type antenna for which calibration is desired in a plane wave electric field, as indicated in Figure A-3. The loop antenna is used to determine the absolute electric field strength of the plane wave, and this value is then used to determine the calibration factor for the other antenna. For the second antenna, the effects of the supporting aircraft and any other nearby structures are included; however, as discussed previously, they are not completely included to the loop itself. Also, it is assumed that the electric and magnetic fields are related by the characteristic impedance of free space (377 ohms).

Thus the calibration method used depends upon the knowledge of the near-zone coupling between loop antennas as related to the loop reception of plane waves. It is simple to apply and does not depend upon the use of any existing transmitter, but can be performed with a low-power oscillator and loop antenna located within a few feet of the antenna to be calibrated. The calibration method can easily calibrate the entire receiving system from the antenna itself on through to the receiver, including any transmission line losses. The limiting approximation is that the effects of the aircraft fuselage are partially neglected since, in general, they will be different for near- and far-zone coupling.

B. Practical Aspects of Calibrations.

1. Measurement Equipment. To aid the person interested in implementing a measurement capability, the construction of a portable oscillator-antenna combination called an FCU (Field Calibration Unit) will be described in detail. The calibration of the FCU against the Fairchild EMC-25 selective voltmeter will also be described. This calibration ensures that the field transmitted by the FCU has its amplitude level referenced to the EMC-25.

While an important part of the measurement procedure involves setting up the standard reference field using the FCU, attenuation must also be given to the receiver modifications required to obtain the AGC voltage. Experience has been obtained with two receivers that have been modified to allow this voltage to be externally accessible: a vacuum tube type Bendix DFA-70 and a more modern, solid-state King KR-86. The King receiver modifications were slightly more involved since, while the desired AGC voltage must be proportional to the signal received on the loop antenna, this receiver does not have a loop receiving position. The desired performance was achieved with the addition of one multi-pole switch, and this modification will be described in a subsequent section.

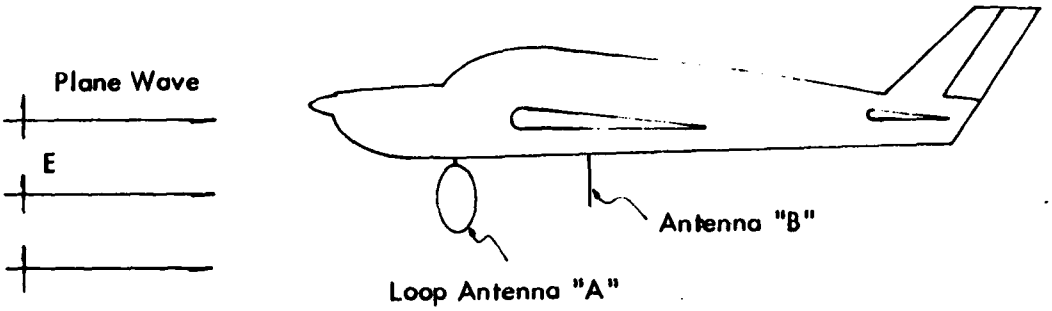

Figure A-3. An Airborne Antenna other than a Loop may be Calibrated Indirectly by First using the Calibrated Loop Antenna "A" to Determine the Electric Field E of an Incoming Plane Wave, then using this Known E Field to Calibrate the Other Antenna Type "B". The antenna "B" calibration will include the effects of the aircraft on that antenna.

2. Design and Construction of a Portable Calibrator. Calibration of the FCU is accomplished fundamentally by causing a current of the desired frequency to flow around a loop of known radius. The loop is located coaxially with and at a given distance from a loop associated with the receiving system to be calibrated.

Depending upon the accuracy required, the desired results might be obtained with the circuit shown in Figure A-1a, utilizing a commercially obtained signal generator connected to the transmitting loop. If the signal generator produced a calibrated output for a given load impedance, such an approach would work quite well. Since the impedance of the loop is very small for the frequency and loop dimensions under consideration (200 to 500 KHz, 0.1 meter radius or less), the load impedance could be properly adjusted by placing, for example, a 50 ohm resistor in series with the loop antenna if the generator were designed to work into a 50 ohm load. With this arrangement it would be a simple calculation to determine the equivalent electric field strength using the equations of the previous section.

However, for more convenient application it was decided to construct a portable calibration oscillator which would be a self-contained unit capable of performing calibration checks without the need for external power or antennas. The unit would provide the required calibration by transmitting a signal with its antenna located a given distance from the receiving loop, giving the resulting name Field Calibration Unit, or FCU. Such a portable calibrator was designed and constructed and will be described in this section. The resulting unit is shown in the photograph of Figure B-1. Visible on the front panel is the frequency control (variable from 200 to 500 KHz), the RF level control (varies the equivalent electric field through 4 steps corresponding to 1000, 500, 100, and 50 microvolts-per-meter for a small loop receiving antenna at an antenna spacing of 1 meter), the modulation on-off switch, and the power on-off switch. The microampere meter monitors the output of the oscillator, thus effectively checking for proper battery voltage as well as component malfunction. Not visible are two female BNC connectors on the rear panel. One is a voltage tap across the loop for checking current level and waveform using an oscilloscope. The other is for connection of an external signal generator with step attenuator when other signal levels in addition to the 4 provided internally are desired for receiver calibration purposes. This external source option is selected by a fifth position (ext.) of the RF level rotary switch. Atop the FCU is the transmitting loop, which has a radius of 0.1 meter. Tied to the base of the loop is a dacron cord 1 meter long, used to space the FCU antenna the proper distance from the receiving loop to be calibrated.

The electrical schematic diagram for the FCU is shown in Figure B-2. The heart of the circuit is the Motorola MC12060 oscillator integrated circuit. This chip is designed to function as a crystal-controlled oscillator, but since the FCU required a variable frequency range, the oscillator frequency is controlled by a lumped LC circuit composed of a 1.3 mH inductor and a variable capacitor. The parameters of the inductor and capacitor were adjusted experimentally to give the desired frequency range while at the same time producing a sinusoidal waveform with little distortion.

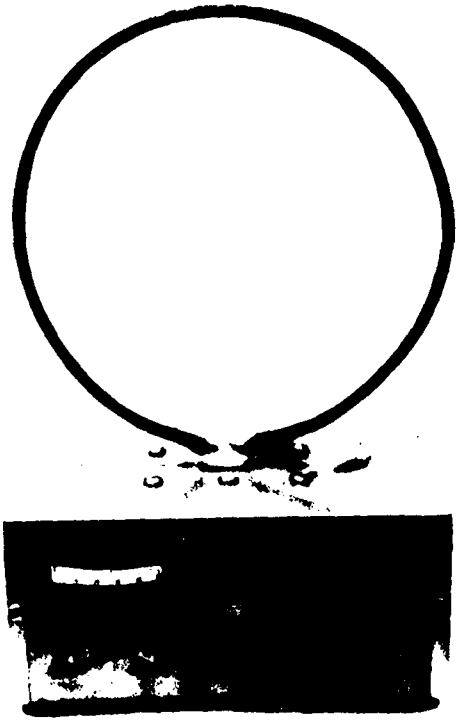

Figure B-1. The Field Calibration Unit Used to Calibrate Loop Antenna Receiving Systems in Absolute Volts-Per-Meter of Electric Field.

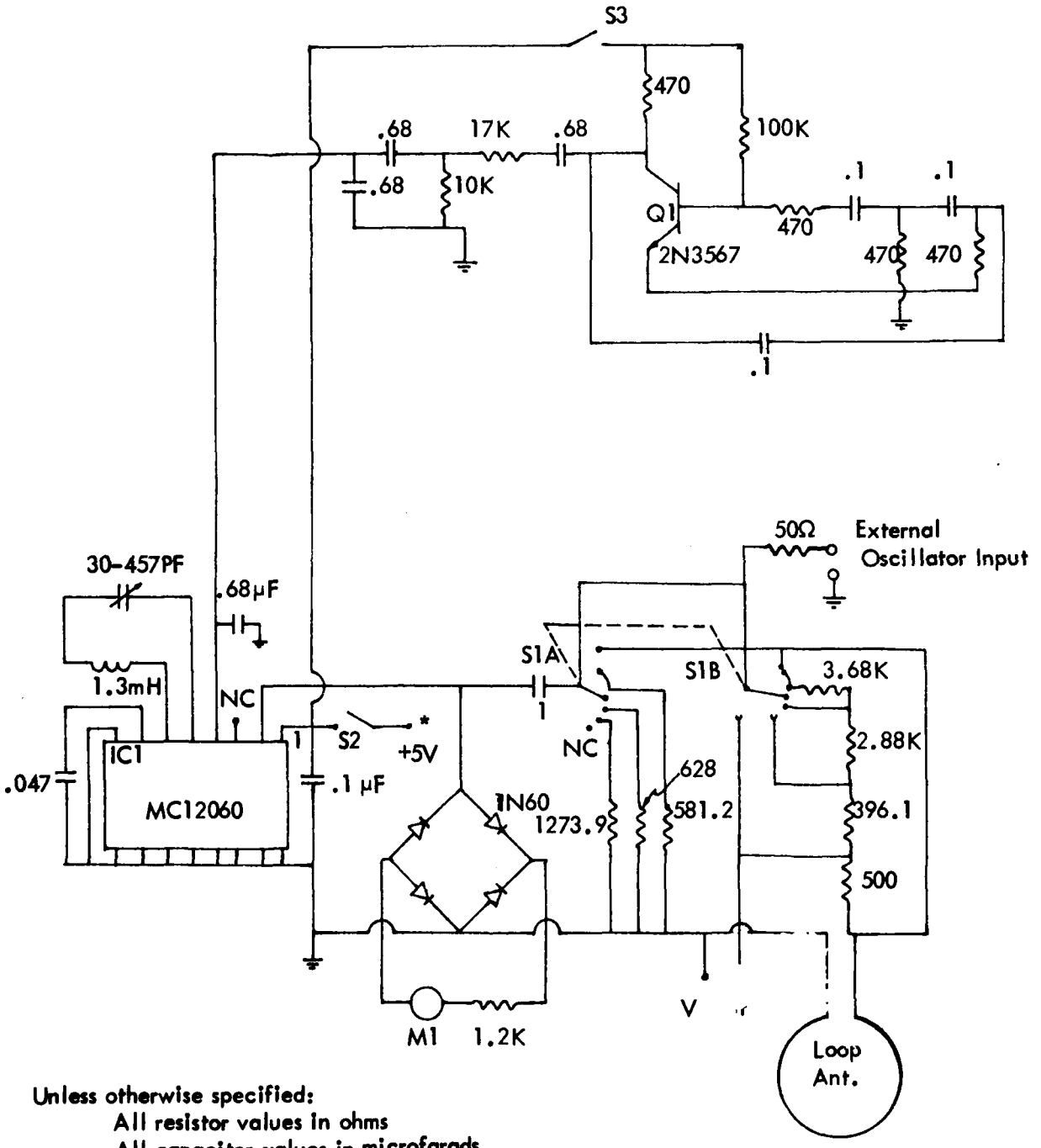

Unless otherwise specified:
All resistor values in ohms
All capacitor values in microfarads
* Supplied by 4 "D" cells

Figure B-2. Schematic Diagram of Field Calibration Unit.

Despite the fact that it is designed for crystal control, the MC12060 is very well suited to this application since it provides a relatively high level output (500 mV pp into 50 ohms) and incorporates an internal amplifier with automatic gain control. The automatic gain control and high output are especially important since it is very desirable that the FCU antenna current stay at the same amplitude as the frequency is changed. This AGC performance is documented in Table B-1, which shows that for the various output levels the output voltage across the loop holds constant to within 0.37 dB as the frequency is varied from 200 to 500 KHz.

In order to identify readily the transmitted signal when tuning in the FCU to the desired frequency, provision is made to modulate the oscillator with a steady tone of approximately 1000 Hz. This modulation is provided by connecting the output of the phase shift oscillator driven by transistor Q1 to the AGC pin of the MC12060. This effectively amplitude modulates the oscillator output. Once the FCU is tuned in by the receiver, the modulation should be removed by opening switch S3, as this modulation method does affect the output level of the oscillator.

The resistor divider network associated with switch S1 is used to obtain the loop currents which correspond to four desired equivalent electric field strengths when the FCU loop is located 1 meter from a small receiving loop. The double-ganged switch and extra set of resistors is included in the design so that the resistance at pin 2 of the IC remains constant as the switch position changes. This was found necessary to avoid frequency shifts for different output levels. The fifth position for switch S1 allows connection of an external signal generator to the transmitting loop. This allows transmission of other equivalent field strengths than the four provided by the resistance divider network for receiver calibration purposes when a signal generator with built-in attenuator is connected.

The entire oscillator circuit, together with a 4 "D" size flashlight batteries, is contained in a chassis box measuring 3 x 6 x 8 inches (1.18 x 2.36 x 3.15 cm) and weighing approximately 3 pounds (1.36 kg), including the attached loop antenna.

3. Calibration of the FCU with the Fairchild EMC-25 Selective Voltmeter. In order to determine the accuracy of the signals transmitted by the FCU described in the previous section, the equivalent field strengths for various frequencies and RF levels transmitted by it were measured using the Fairchild EMC-25 with calibrated loop antenna. The measurement geometry is as indicated in Figure A-2a, with the separation distance d_c equal to one meter. The results of these measurements are given in Figure B-3. The designated field strength equivalents of 1000, 500, 100, and 50 microvolts per meter are indicated in the figure. If one assumes that the EMC-25 is exact, then the FCU signals lie within $\pm$ 3 dB of the design goals with the exception of the peak near 230 KHz, with most points being within $\pm$ 2 dB. Since the published accuracy of the EMC-25 itself is $\pm$ 2 dB neglecting any antenna inaccuracy (as marked on Figure B-3), the FCU is evidently accurate to within 1 dB of the measurement tolerance of the EMC-25. Actually, it may be suspected that the FCU is more accurate, since the variation in output level as measured using an oscilloscope was reported in the previous section to be less than 0.37 dB over the entire frequency range for the

Frequency (KHz)	V_{out} (Volts)			
	RF Level 4	RF Level 3	RF Level 2	RF Level 1
200	.70	.39	.092	.048
230	.70	.39	.092	.048
260	.68	.38	.090	.046
320	.68	.38	.090	.046
380	.68	.38	.090	.046
410	.69	.38	.090	.046
440	.69	.38	.092	.046
470	.68	.38	.090	.046
500	.68	.38	.090	.046

Maximum Deviation - dB

RF Level 4 .25 dB
RF Level 3 .23 dB
RF Level 2 .19 dB
RF Level 1 .37 dB

Table B-1. Output Voltage Variation with Frequency and Attenuator Position.

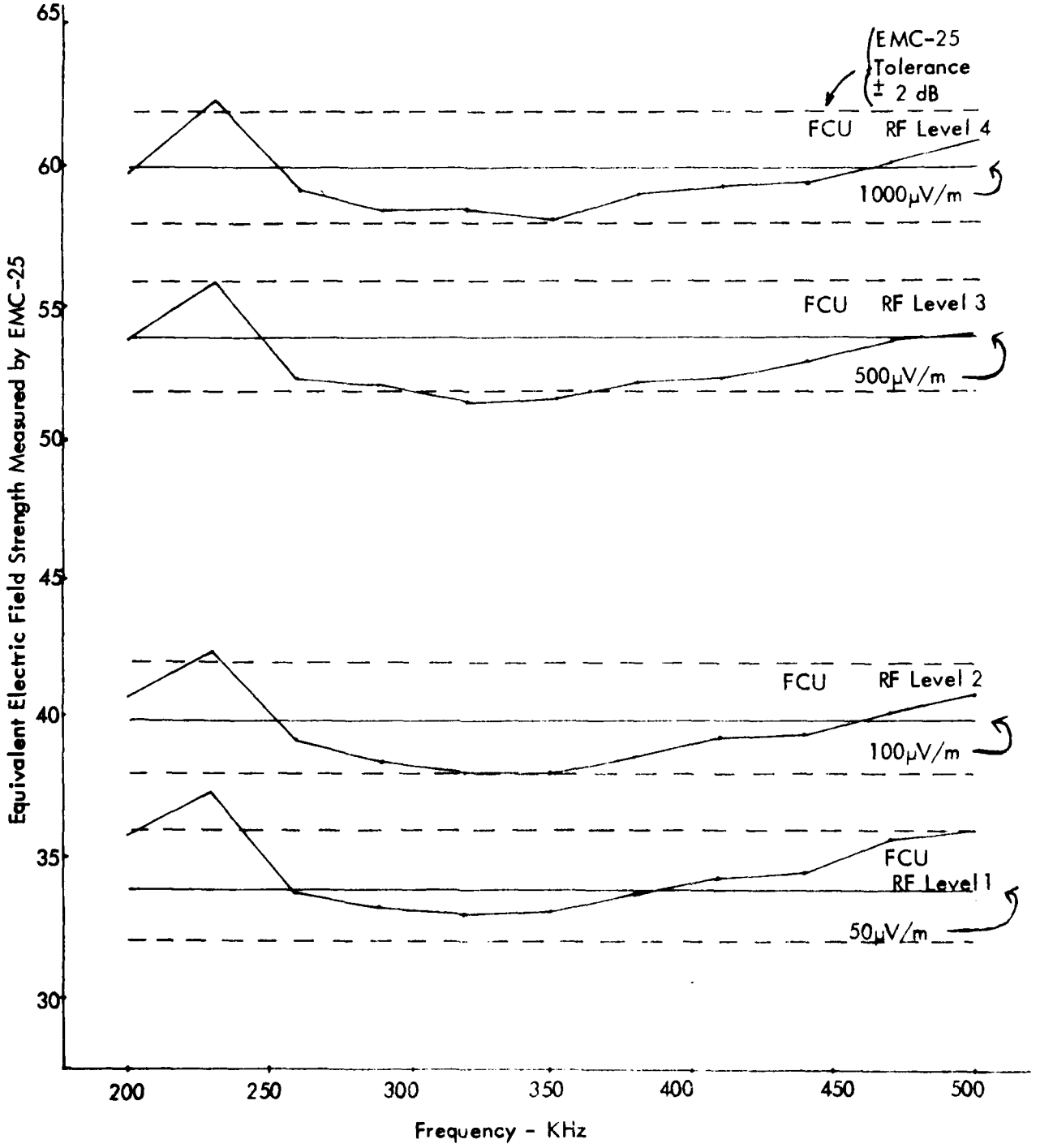

Figure B-3. FCU Calibration with EMC-25 at 1 Meter Separation for the 4 RF Levels.

worst case. Since this output current couples linearly to the EMC-25 receiving loop, it is evident that the variation shown in Figure B-3 is probably due to the inaccuracy of the EMC-25. However, as the EMC-25 is often considered to be an accuracy standard in making electric field strength measurements, the conclusion can be made that since the FCU is always within approximately 1 dB of the accuracy limits of the EMC-25, the FCU itself produces calibration signal of sufficient accuracy for the purpose for which it is intended.

4. Application to Practical ADF Receivers. In order to apply the previously described method for calibration of receiver AGC voltage in terms of absolute electric field strength, several receiver parameters must be available. Depending upon the construction and capabilities of the receiver in question, some simple modifications may be required. The receiver capabilities which must exist, either as a result of modification or inherently in the receiver design, are:

1. Access to the AGC voltage.
2. Capability of receiving on the loop antenna only.
3. Capability of rotating loop or goniometer for maximum signal.
4. Capability of maintaining the loop at this maximum signal position while taking measurements.

After the above capabilities are provided, a calibration curve relating AGC voltage to field strength for the frequencies of interest must be obtained.

In order to illustrate the receiver modification and calibration, and the field strength measurement process, two specific receivers will be discussed: the Bendix DFA-70 Receiver with the CNA-70A Control Panel, and the King KR-86 Receiver. While only the receivers are listed, it should be kept in mind that the calibration process includes the entire receiving system and must be repeated for each specific aircraft installation or if any of the system components is changed.

a. Bendix DFA-70 Receiver with CNA-70A Control Panel. This receiver is well suited to the application of this measurement technique since, of the four previously listed required capabilities, three are available without receiver modification. This is due to the presence of a loop receiving mode which, when selected at the control panel, internally disconnects the sense antenna and provides manual control of the loop position. Thus the only modification required was to obtain external access to the AGC voltage. This was readily accomplished by tapping the voltage which existed across the tuning meter and installing a BNC connector in the control panel, as indicated in Figure B-4 [4]. This did not interfere with the normal operation of the receiver, but did allow ready access to the AGC voltage. As this particular receiver was designed with the AGC operating on one of the audio amplification stages, the AGC voltage is dependent on the volume control setting. For maximum sensitivity, the volume control must be turned to full volume and all measurements were made under this condition. After some experimentation, it was evident that best performance was obtained with the bandwidth selected as sharp and the reception mode as CW. These settings were also used consistently throughout all measurements.

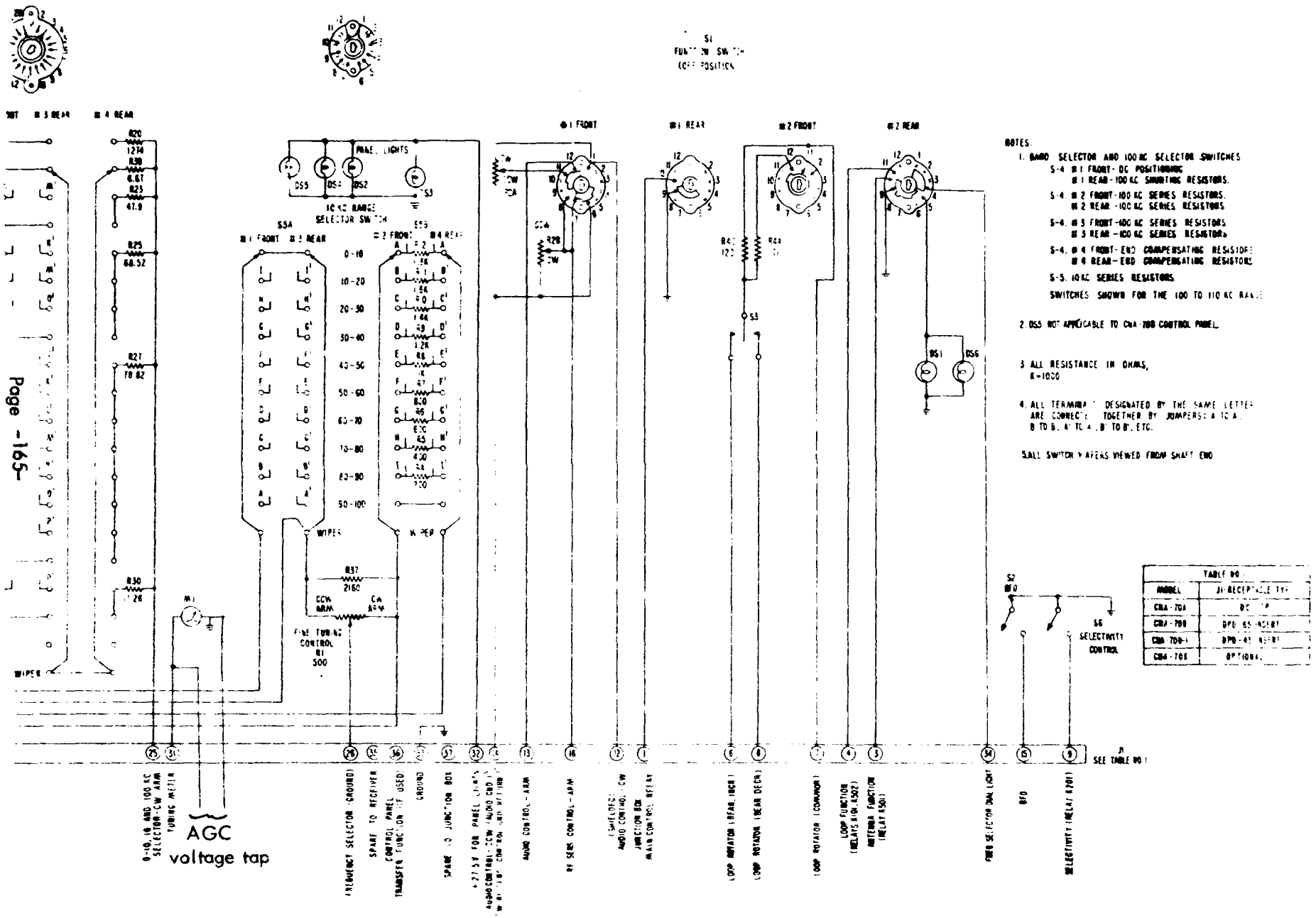

Figure B-4. Type CNA-70(A,B,K) Control Panel, Schematic Diagram, Showing AGC Voltage Connection Added [4].

To calibrate the receiver the FCU was located 1 meter from the center of the loop antenna pod and with the FCU transmitting loop broadside to the pod. (The pod is located on the underside of the fuselage.) After guning to the proper frequency by minimizing the AGC voltage, the receiving loop was rotated manually for maximum received signal (minimum AGC voltage). This should correspond to an ADF pointer position in the direction of the transmitting loop. This may seem incorrect at first consideration, since the ADF pointer direction corresponds to a null in the loop receiving pattern. However, it must be remembered that the pointer indicates the direction of the far-zone reception null, whereas we are in the near zone of the FCU transmitting loop and for this case the near-zone loop null is rotated 90 degrees from the far-zone loop null. Once this configuration is obtained, the receiver AGC may be calibrated in absolute volts-per-meter at the antenna, since for the various FCU transmitting amplitudes the corresponding equivalent electric field strengths for 1 meter separation have been determined by measurement with the EMC-25 (Equation (A.3) is applied) as described in Section B-3 of this Appendix (Figure B-3). While the FCU has only 4 levels of transmission amplitude (nominally 1000, 500, 100, and 50 microvolts-per-meter), other levels can be obtained by connecting a signal generator with calibrated attenuator to the external input jack of the FCU. Using this approach, the calibration curves of Figure B-5 were measured for 5 dB steps of field strength at various frequencies. It must be emphasized that these curves are included only for illustrative purposes and that each receiving system, including antenna, transmission line and receiver, must be calibrated as described if accurate results are to be expected.

Once these calibration curves are obtained, airborne measurements of field strength can be easily obtained as follows:

1. Tune in station frequency on receiver, minimizing AGC voltage, and with controls set as previously described except that the receiver is in the ADF mode.

2. Change to loop reception mode and manually rotate the ADF position indicator 90 degrees (this puts the maximum of the loop reception pattern in the direction of the desired station).

3. Read the AGC voltage.

4. Obtain the corresponding electric field strength from the calibration curve nearest in frequency to the received signal.

b. King KR-86 Receiver. This receiver, while not initially as well-suited for application of the loop antenna measurement technique as the Bendix receiver, can be used quite conveniently after several simple modifications.

Access to the AGC voltage is not difficult for this receiver as this voltage is available at the connector strip located at the rear of the receiver. Thus for a new installation, the AGC and ground pins need only be connected to a cable or meter jack. However, as a rented aircraft was used to obtain many of the measurements required

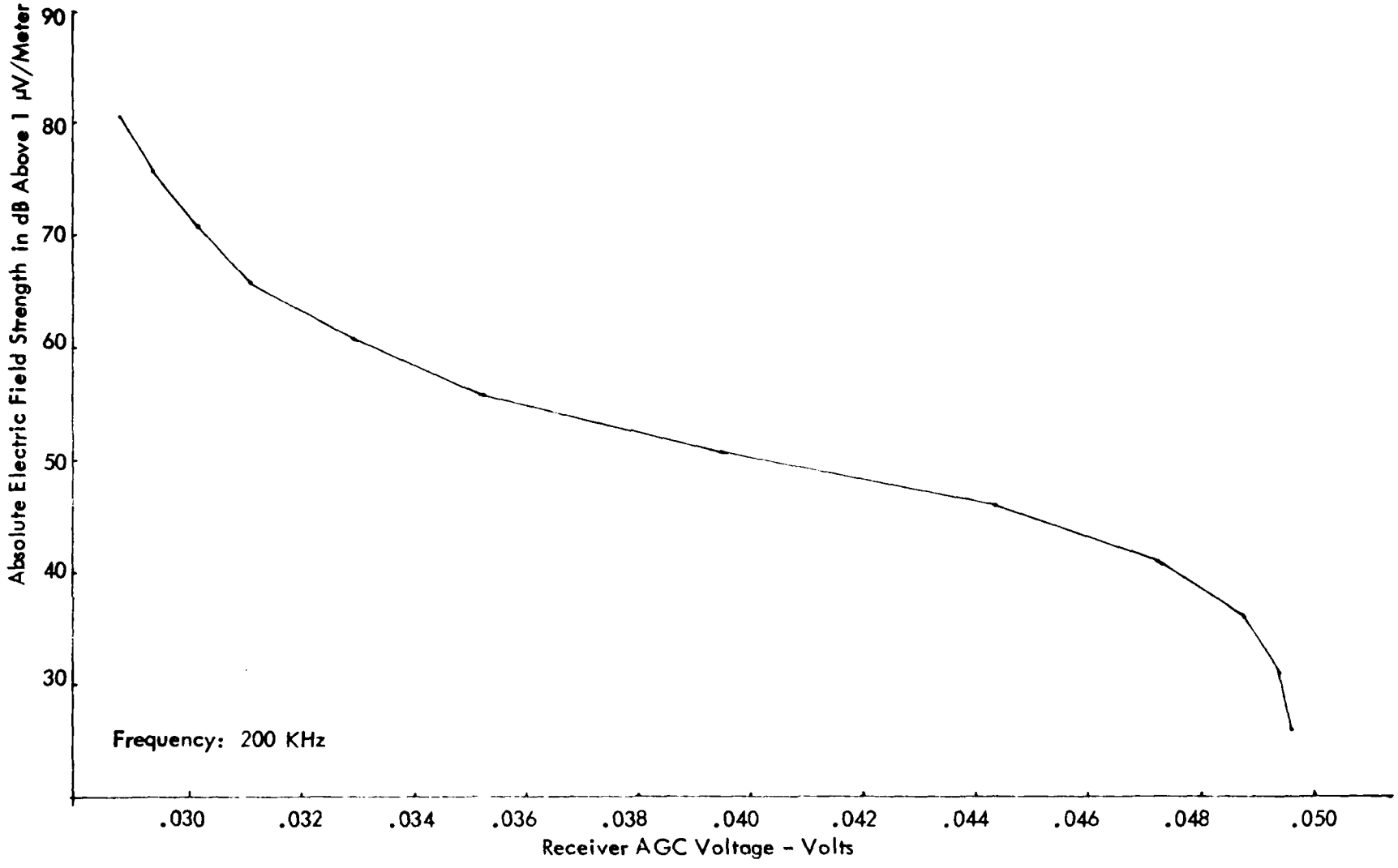

Figure B-5a. Absolute Electric Field Strength Calibration Curve for Bendix DFA-70 Receiver Installed in the Avionics Engineering Center DC-3 Aircraft Operating in Loop Receiving Mode at the Indicated Frequency.

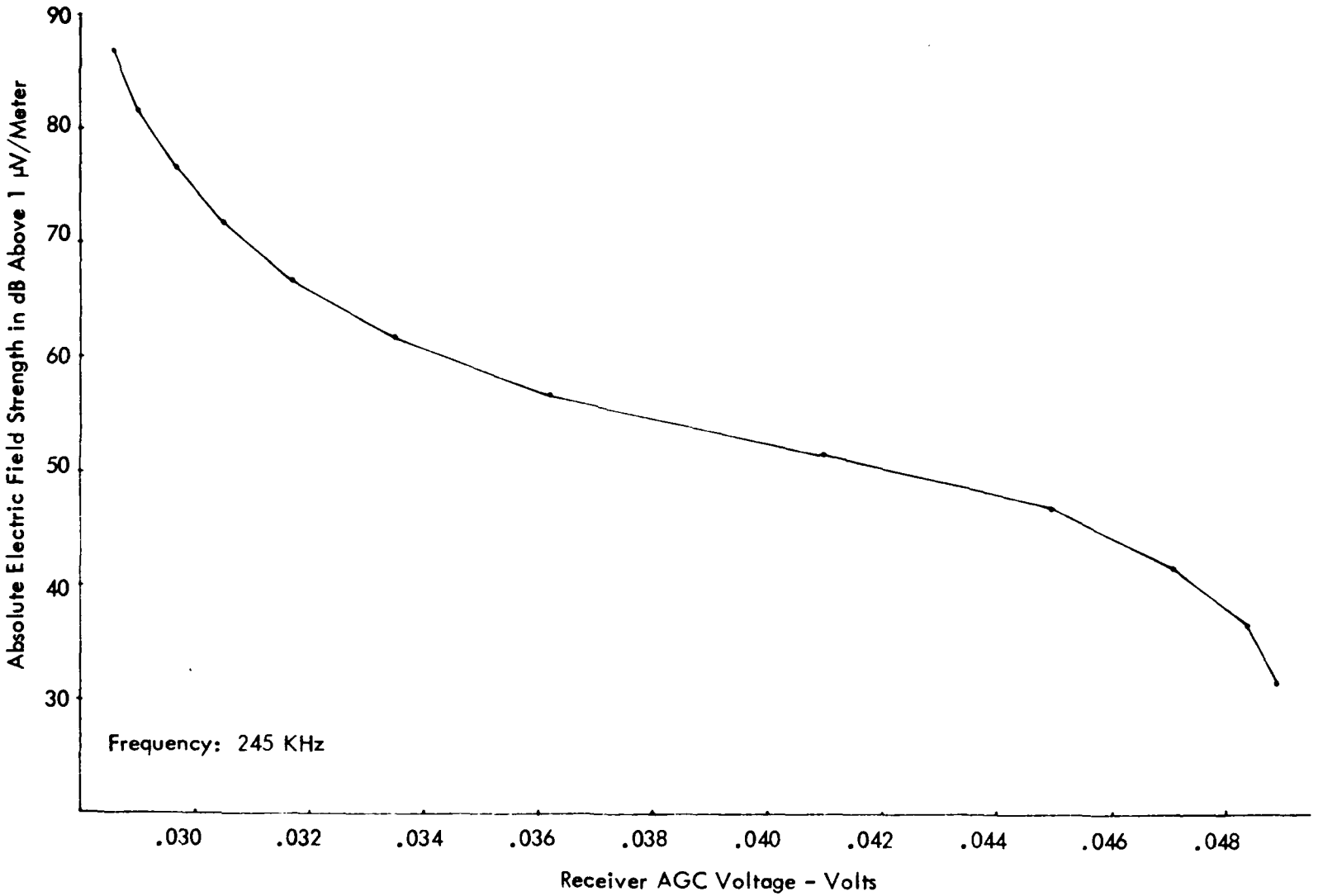

Figure B-5b. Continued.

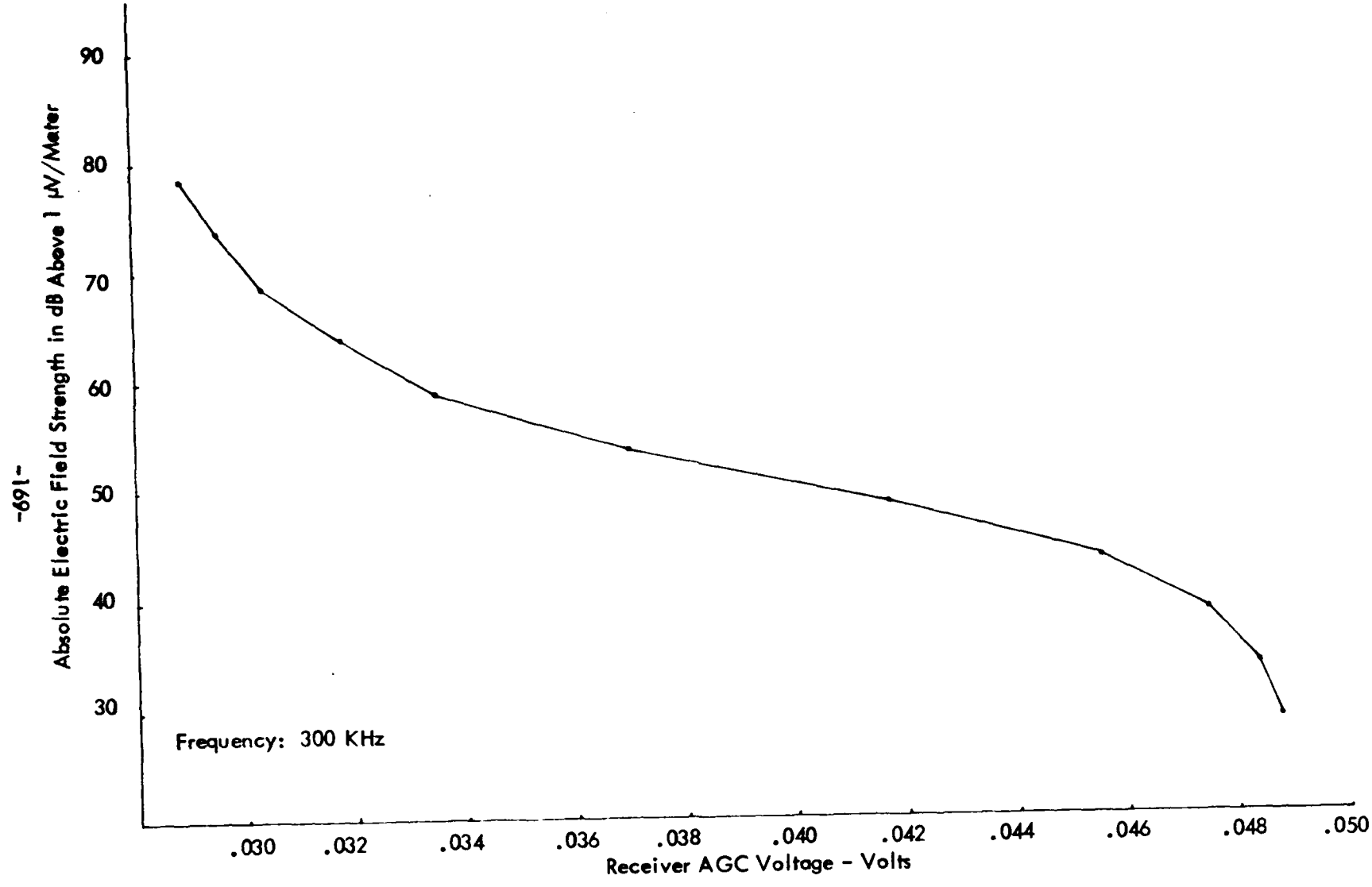

Figure B-5c. Continued.

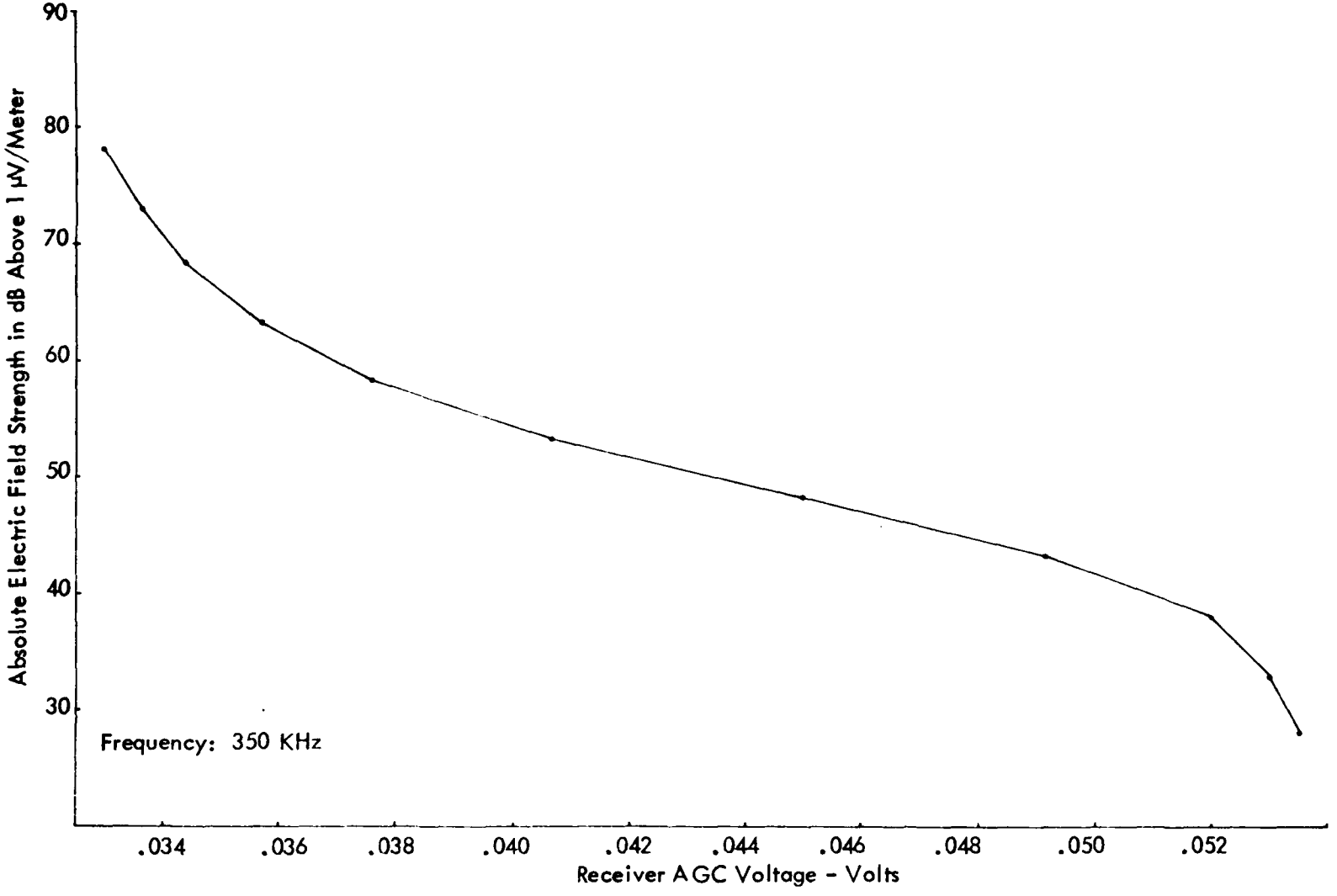

Figure B-5d. Continued.

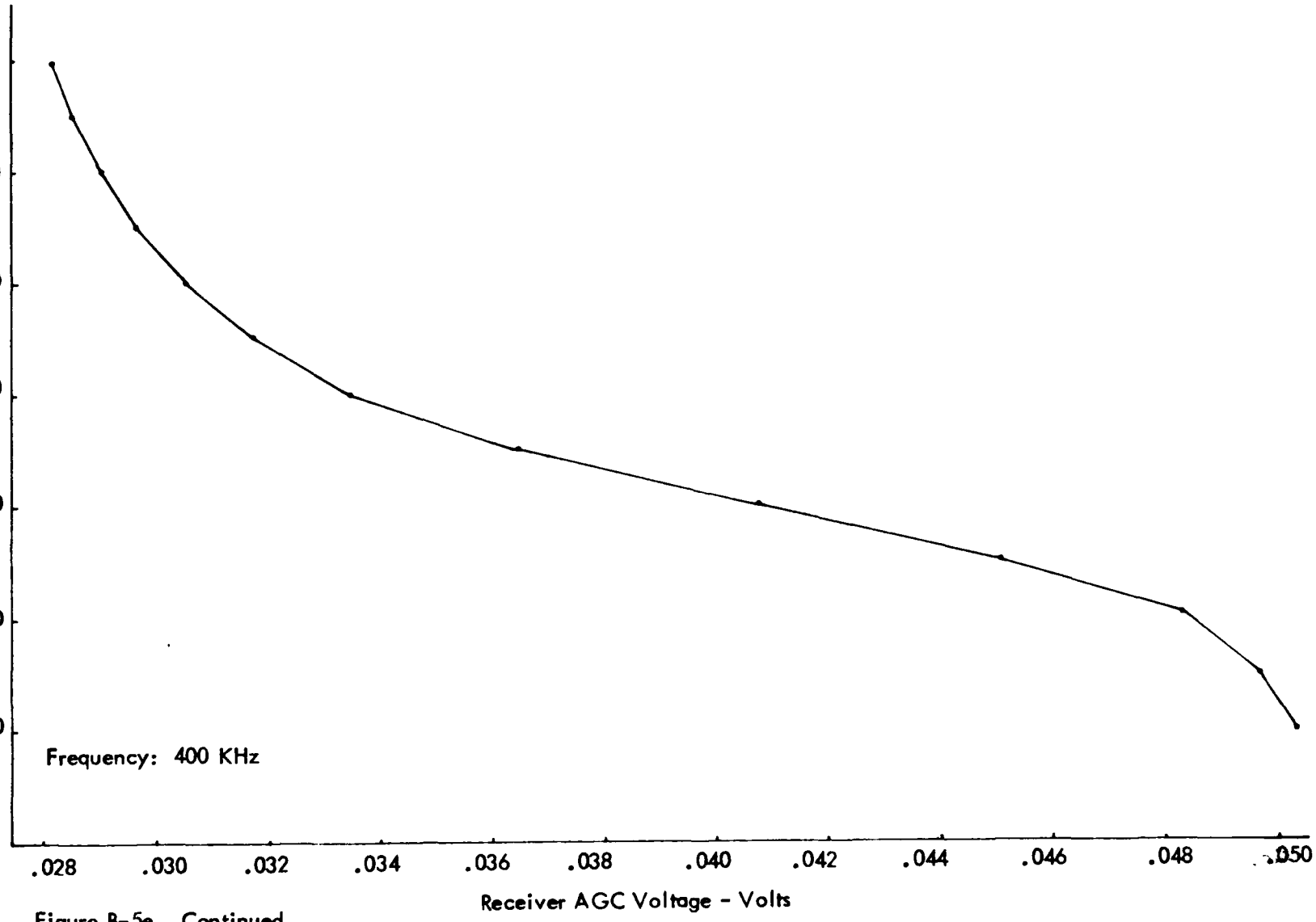

Figure B-5e. Continued.

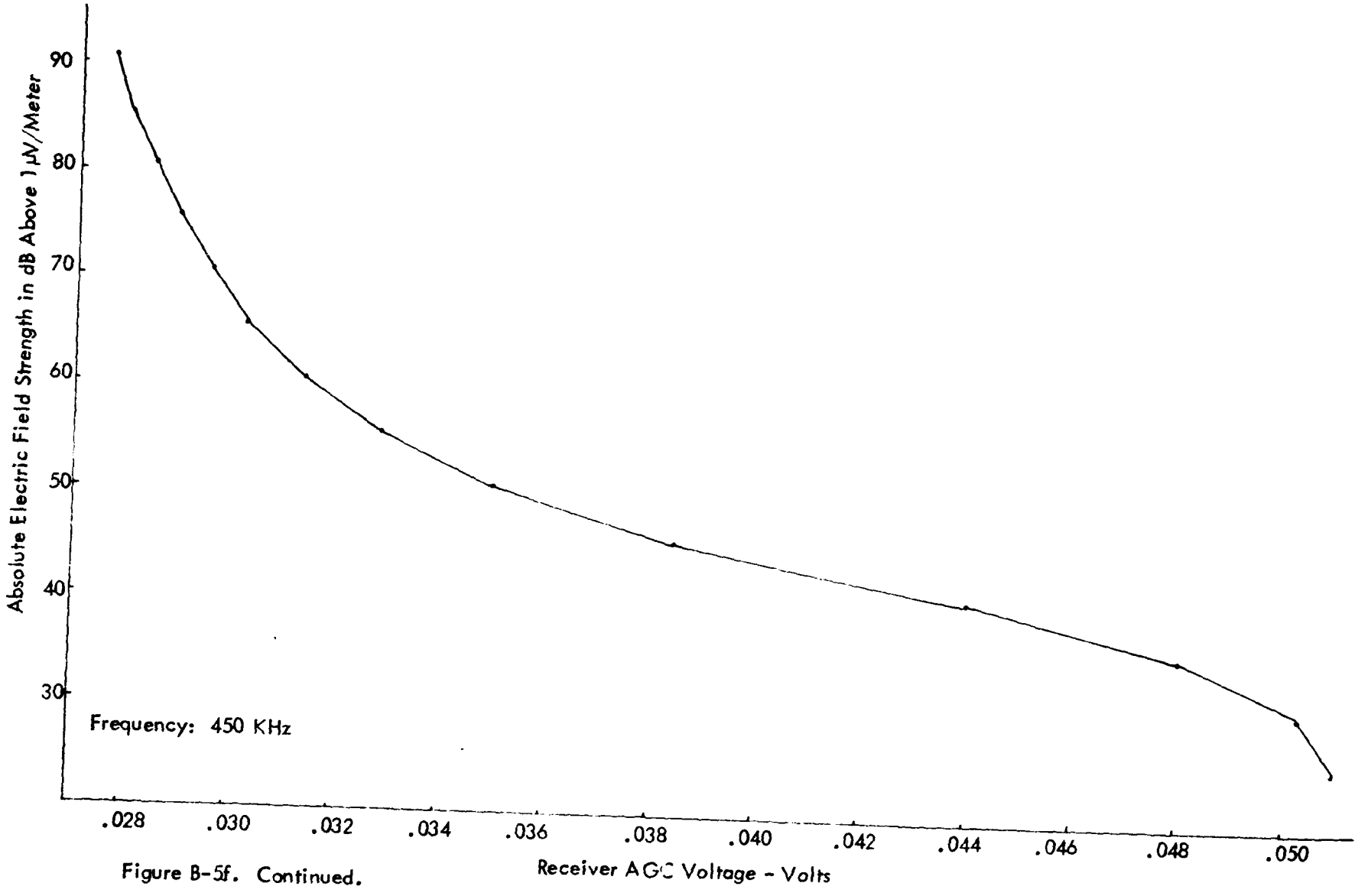

Figure B-5f. Continued.

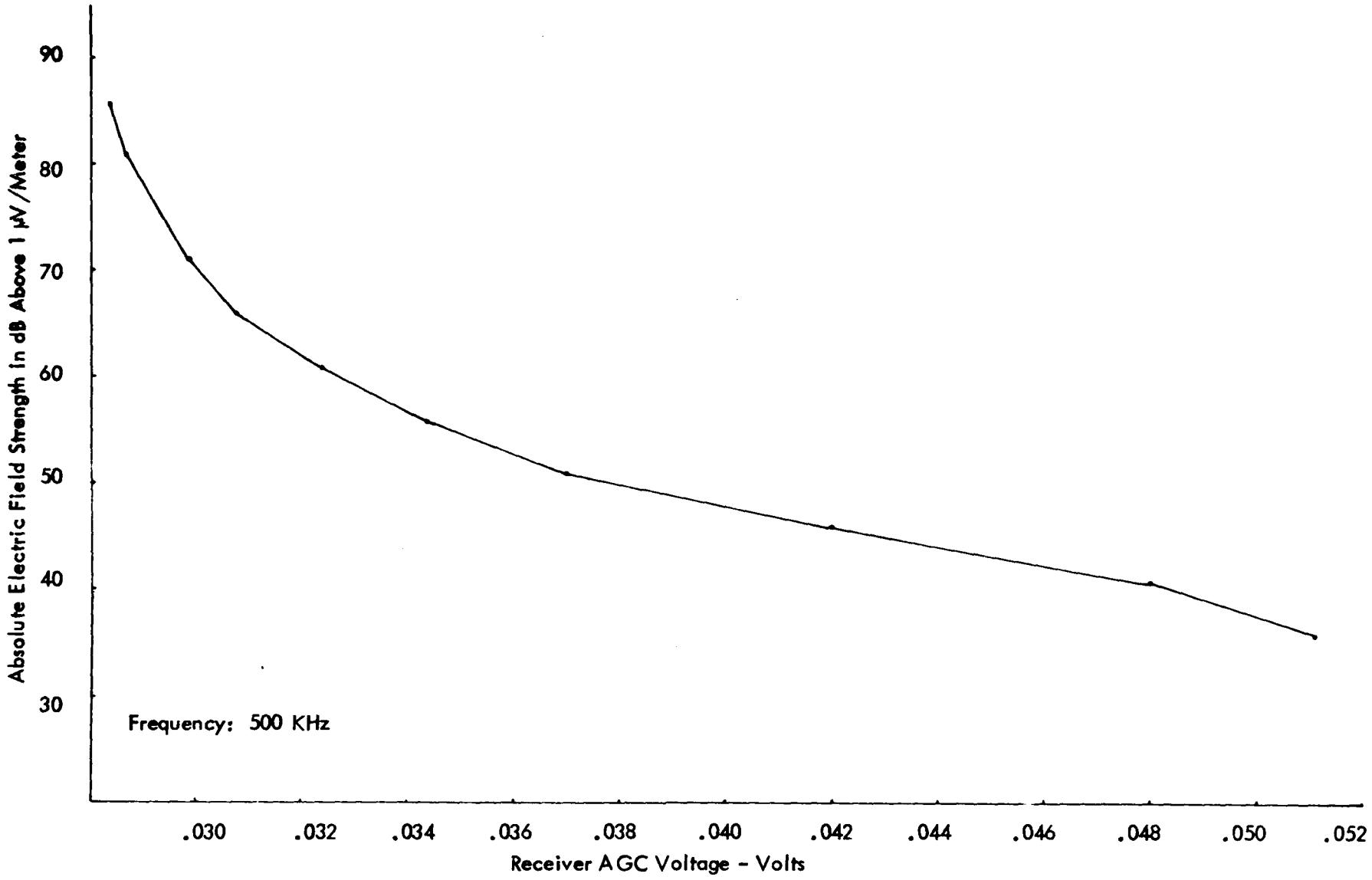

Figure B-5g. Continued.

for this contract, it was not possible to change the installation hardware in the aircraft. For this reason, a hole was drilled in the receiver front panel and a cable connected to the AGC voltage at connector location 12 (see Figure B-6) was passed out through it and terminated in a connector. To measure the AGC voltage a suitable voltmeter was connected to the cable.

As this receiver does not have a loop reception mode, some additional modifications were required. In order to receive on the loop antenna only, one pole of a double pole switch (S2) was connected in series with the sense antenna input as indicated in Figure B-7. Regarding capabilities 3 and 4, while the goniometer could be rotated manually by depressing the test button on the receiver front panel, it would immediately start to seek a null as soon as this button was released. In order to maintain the goniometer in the desired position as a measurement is made, the second pole of same switch used to disconnect the sense antenna input was put in series with the power supply to the goniometer servo motor drive circuitry (S1) as shown in Figure B-8. This switch was then mounted on the front panel of the receiver. In the up position the receiver operates normally. In the down position, the sense antenna is disconnected and the goniometer position is fixed. Since the switch was mounted in the front panel and the AGC voltage was made available at the front panel, the modified receiver could be installed in the rented aircraft by simply interchanging it with the receiver (also a King KR-86) normally used in the aircraft.

To calibrate the receiver as installed in the aircraft, the FCU was positioned 1 meter from the loop antenna mounted on the aircraft (on the underside of the fuselage) with its transmitting loop broadside to it. The receiver was then tuned to the FCU frequency. By using the test button on the receiver front panel to position the goniometer and the added switch to then disconnect the sense antenna and hold the goniometer fixed, the goniometer position corresponding to maximum signal received on the loop is found. This should again correspond with the ADF position indicator pointing toward the direction of the FCU transmitting loop. Once this configuration is obtained, the calibration process proceeds as for the Bendix receiver. The calibration curves obtained for various frequencies with the King KR-86 installed in a Piper Cherokee and using a King Model 42 loop antenna are given in Figure B-9. Again, it must be emphasized that these curves apply only to the particular receiver and installation for which they were measured and are not intended for other use.

Once the calibration curves are made, airborne measurements of field strength are made as follows. With the receiver in ADF mode and the switch S in the up position (normal receiver operation) tune the receiver to the desired station frequency and allow the ADF pointer to seek the station. Push the test button to rotate the direction indicator 90 degrees and keep the indicator in this position by pushing switch S down (i.e., open). This operation directs the loop antenna maximum toward the station and at the same time pushing switch S down disconnects the sense antenna. The AGC voltage can now be read using an appropriate voltmeter, and the corresponding electric field strength read from the calibration curve closest to the station frequency.

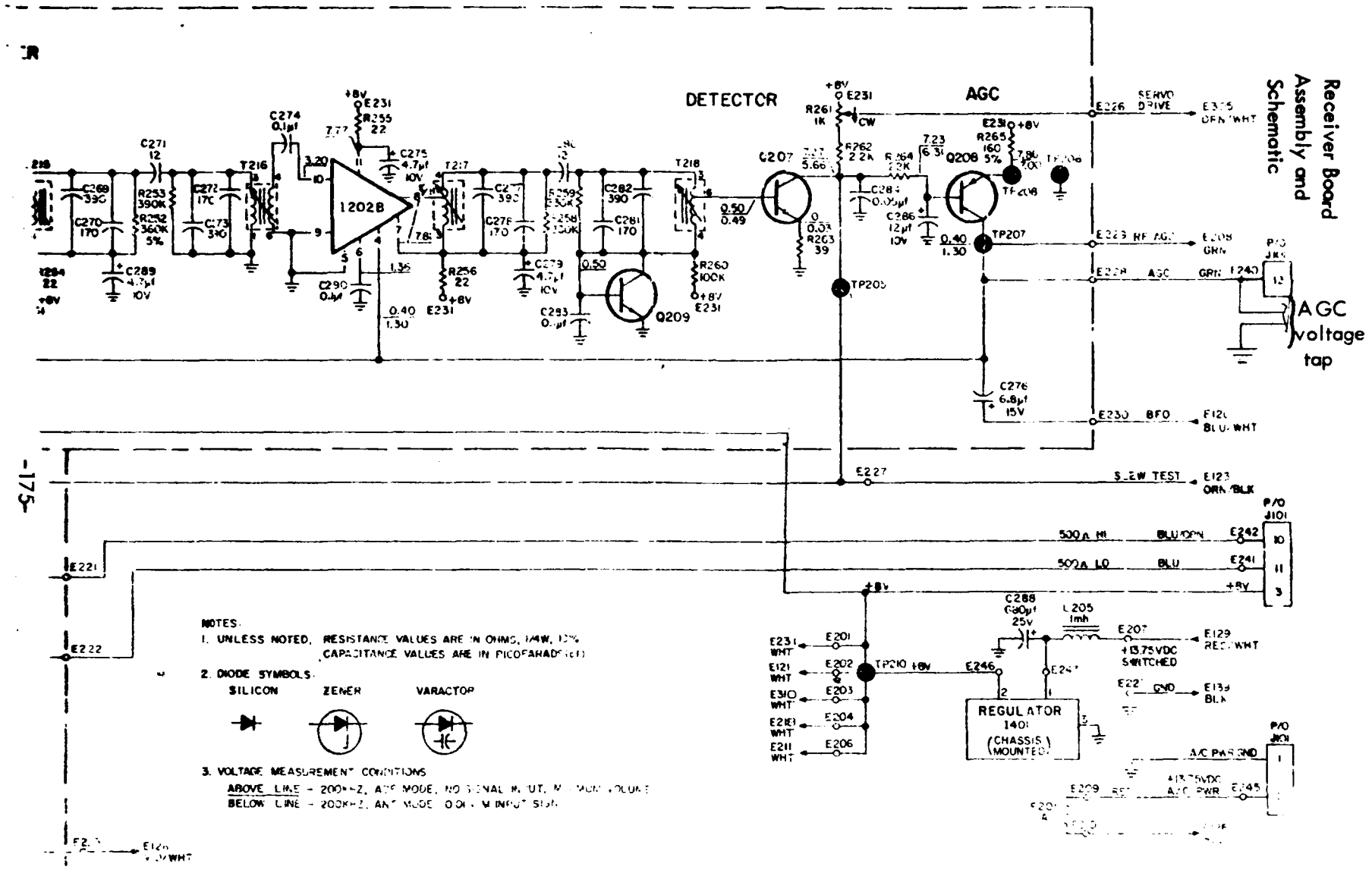

Figure B-6. Portion of Schematic for King KR-86 Receiver Showing AGC Voltage Connection [5].

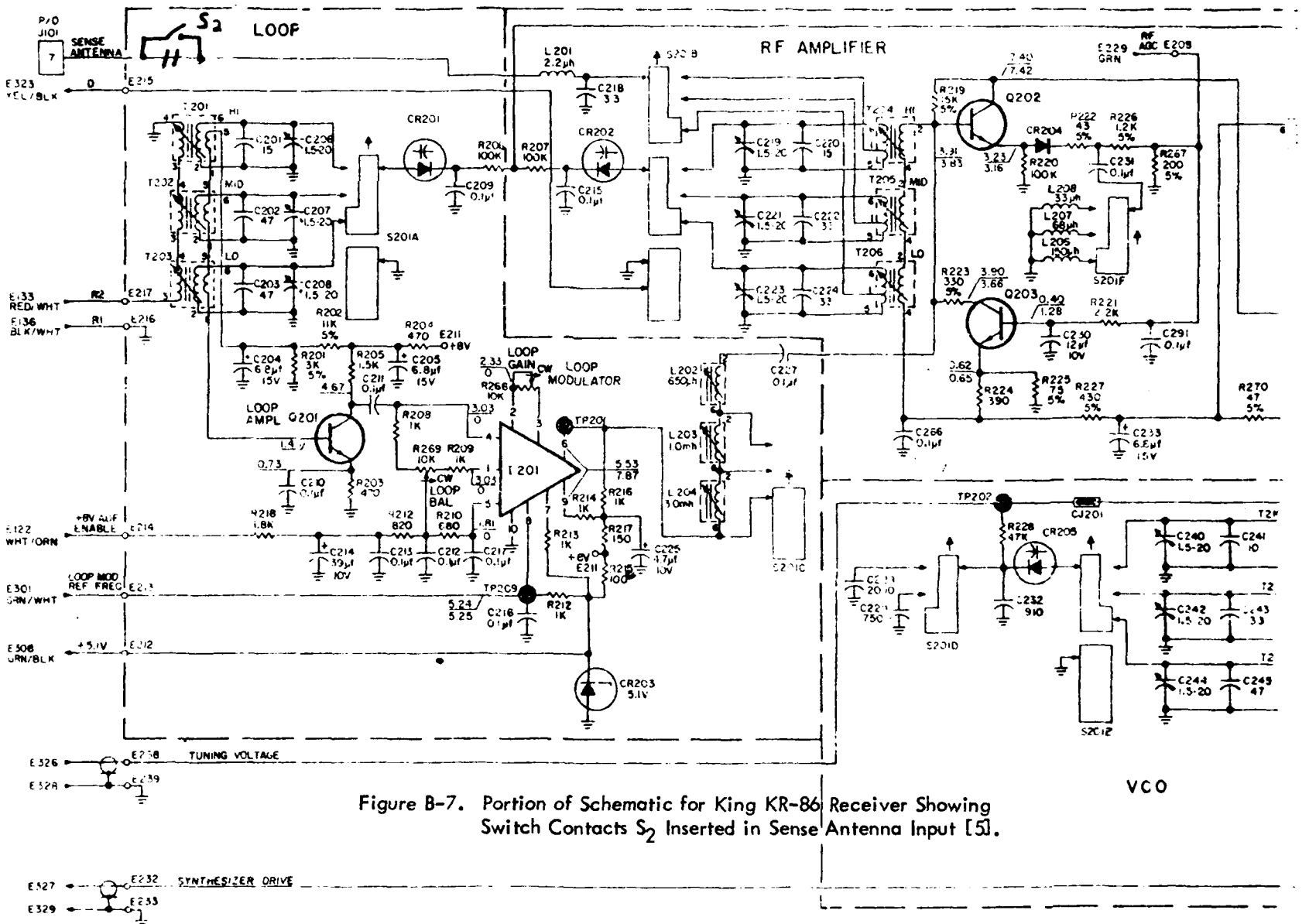

Figure B-7. Portion of Schematic for King KR-86 Receiver Showing Switch Contacts S_2 Inserted in Sense Antenna Input [5].

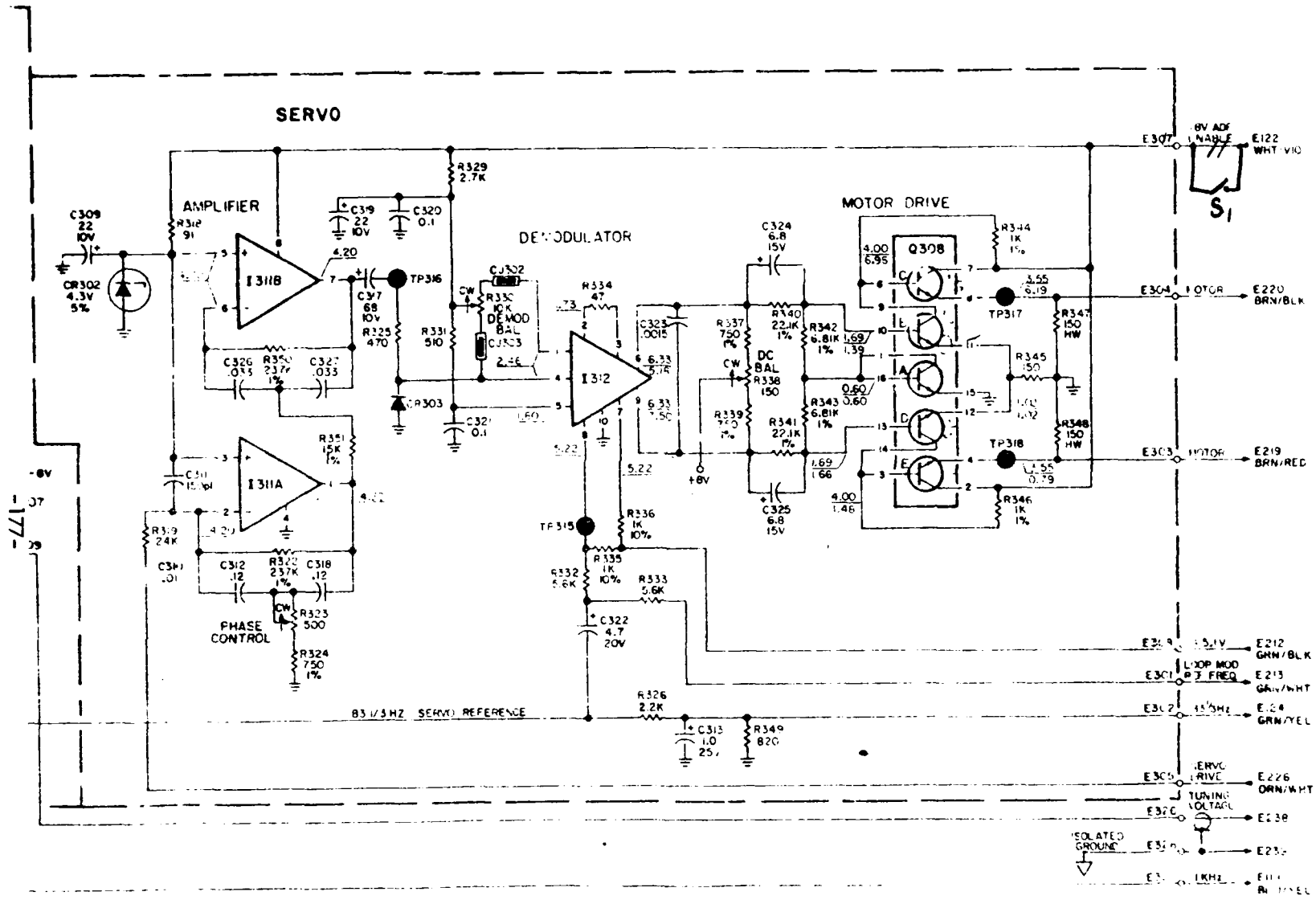

Figure B-8. Portion of Schematic for King KR-86 Receiver Showing Switch Contacts S_1 Inserted in Line Connecting Power Supply to Goniometer Servo Motor Drive [5].

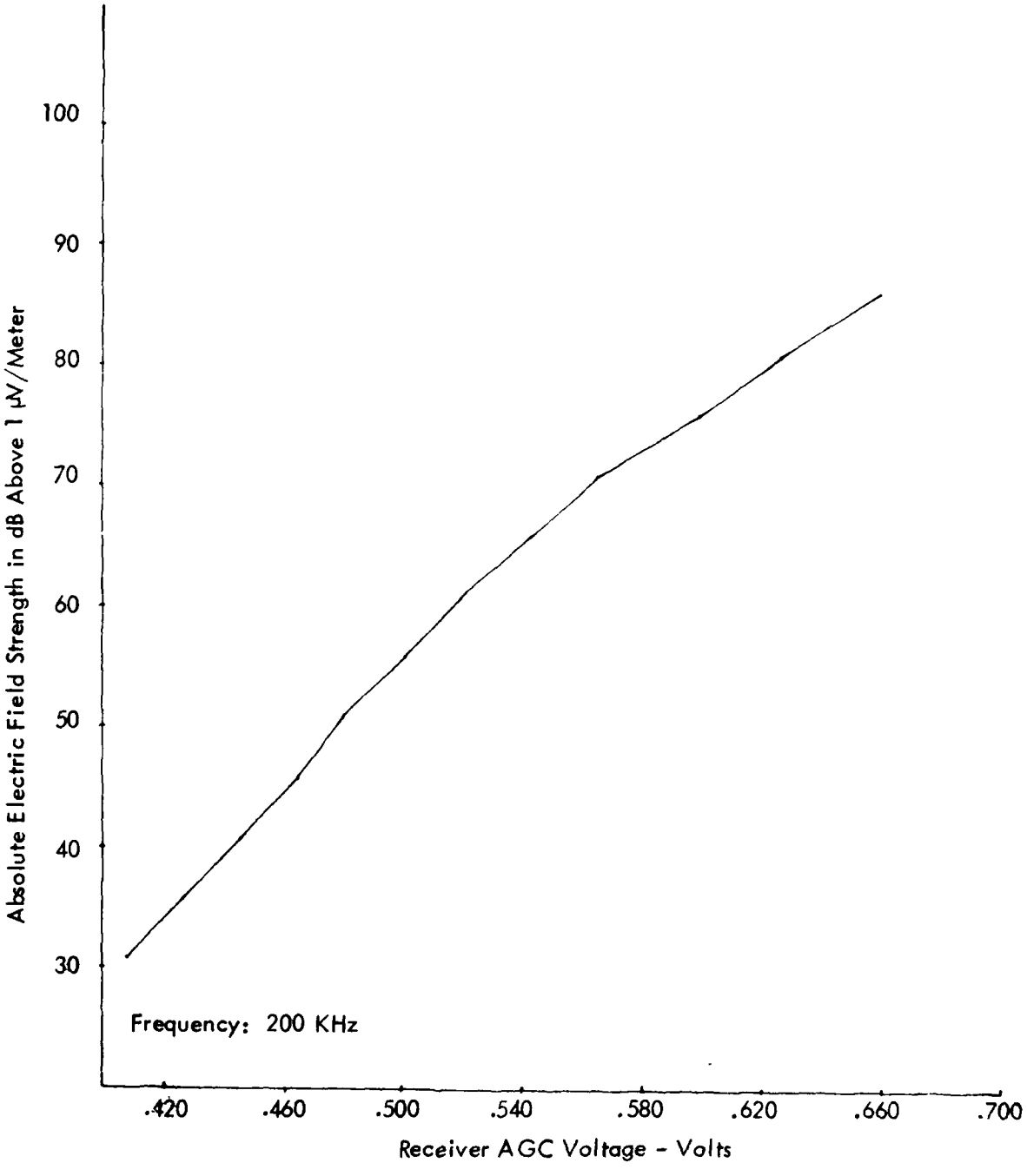

Figure B-9a. Absolute Electric Field Strength Calibration Curve for King KR-86 Receiver Installed in a Piper Cherokee, Modified as Discussed in Text, and Operating at the Indicated Frequency.

AD-A111 187 OHIO UNIV ATHENS DEPT OF ELECTRICAL ENGINEERING F/G 17/7
LOW-FREQUENCY BEACON SIGNAL STRENGTH DETERMINATION.(U)
JAN 80 J L BASH, R J LUEBBERS DOT-FA79WA-4278
UNCLASSIFIED EER-41-2 FAA-R-6050.2 NL

3 OF 3
AD A111 87

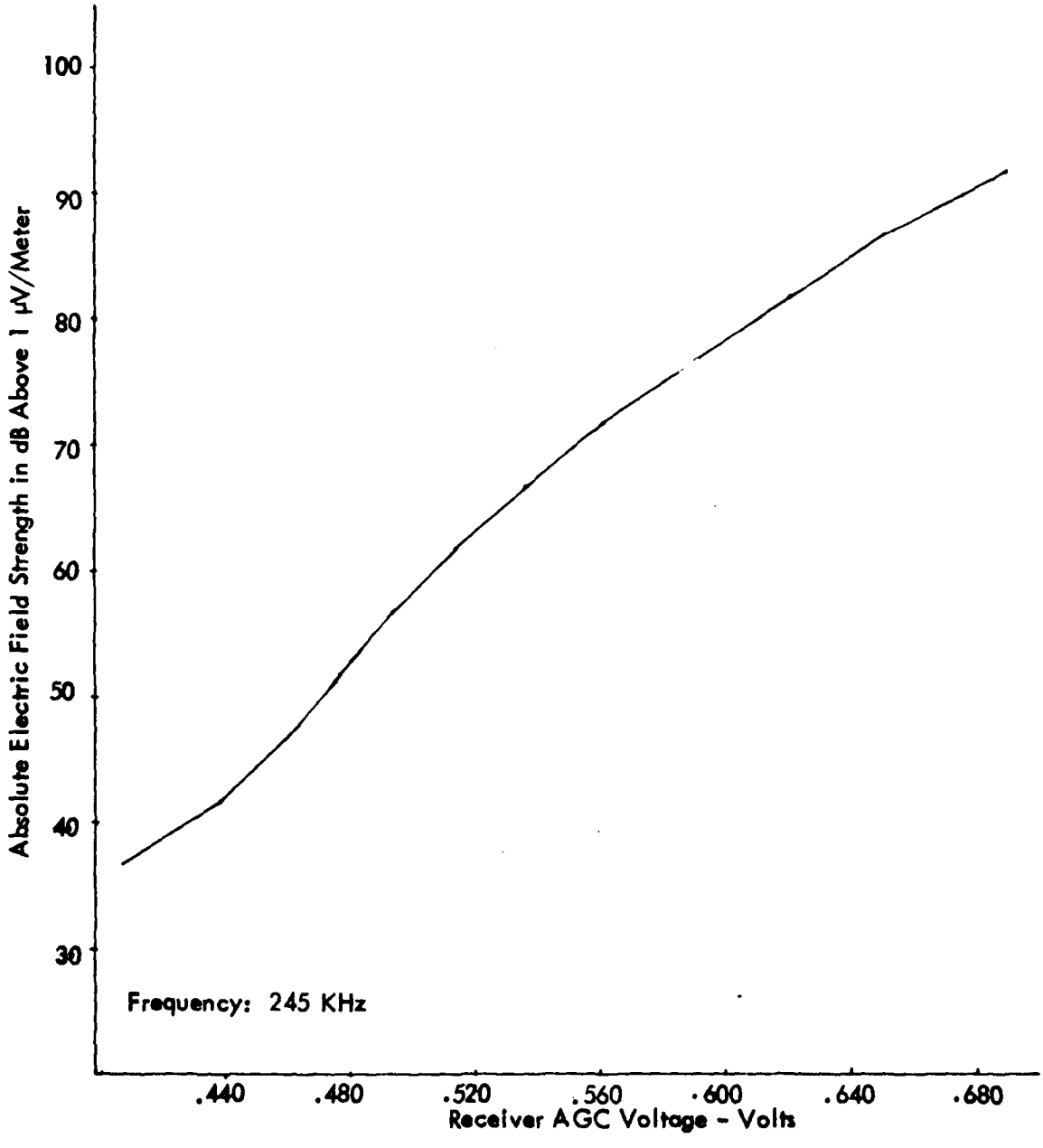

Figure B-9b. Continued.

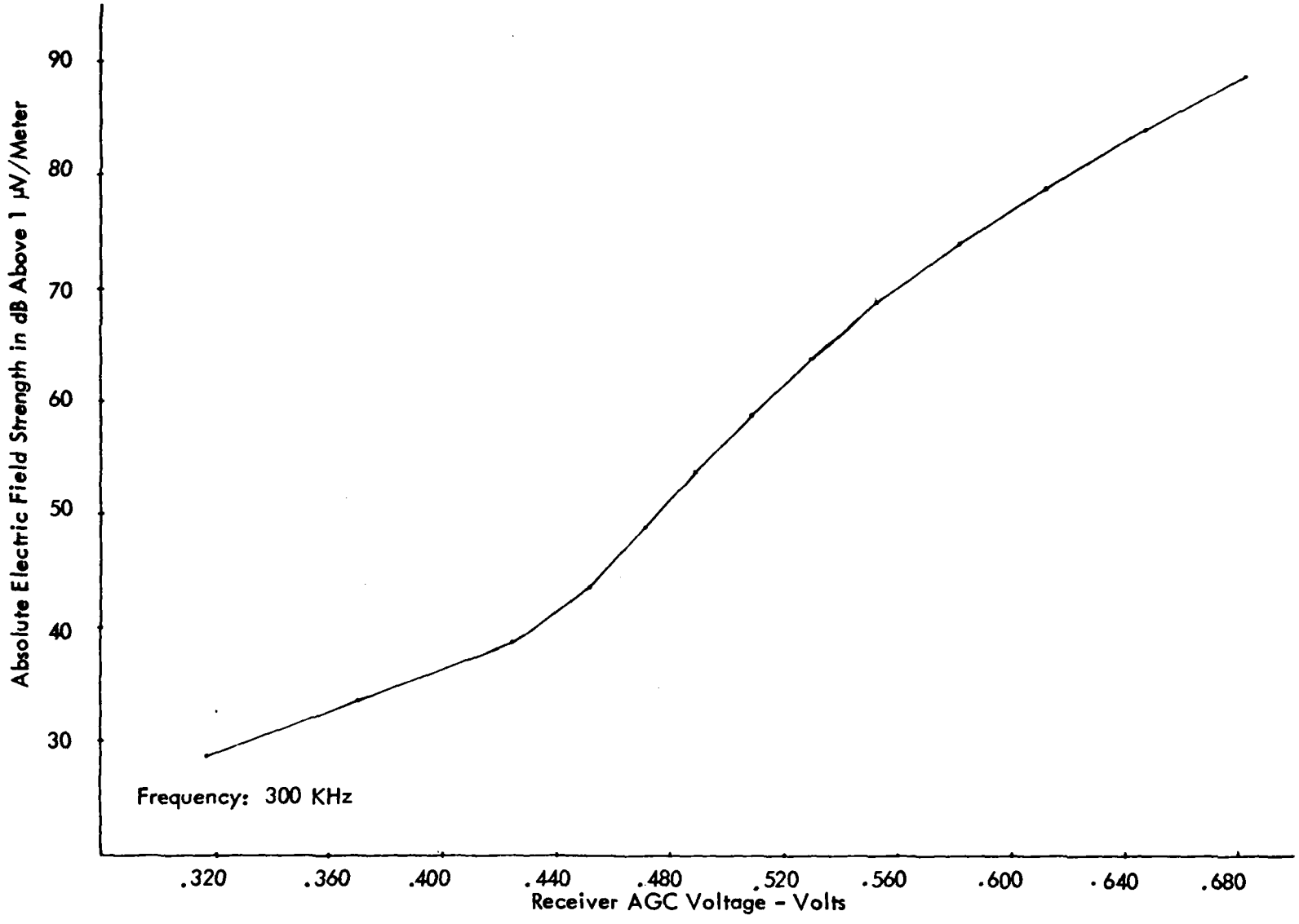

Figure B-9c. Continued.

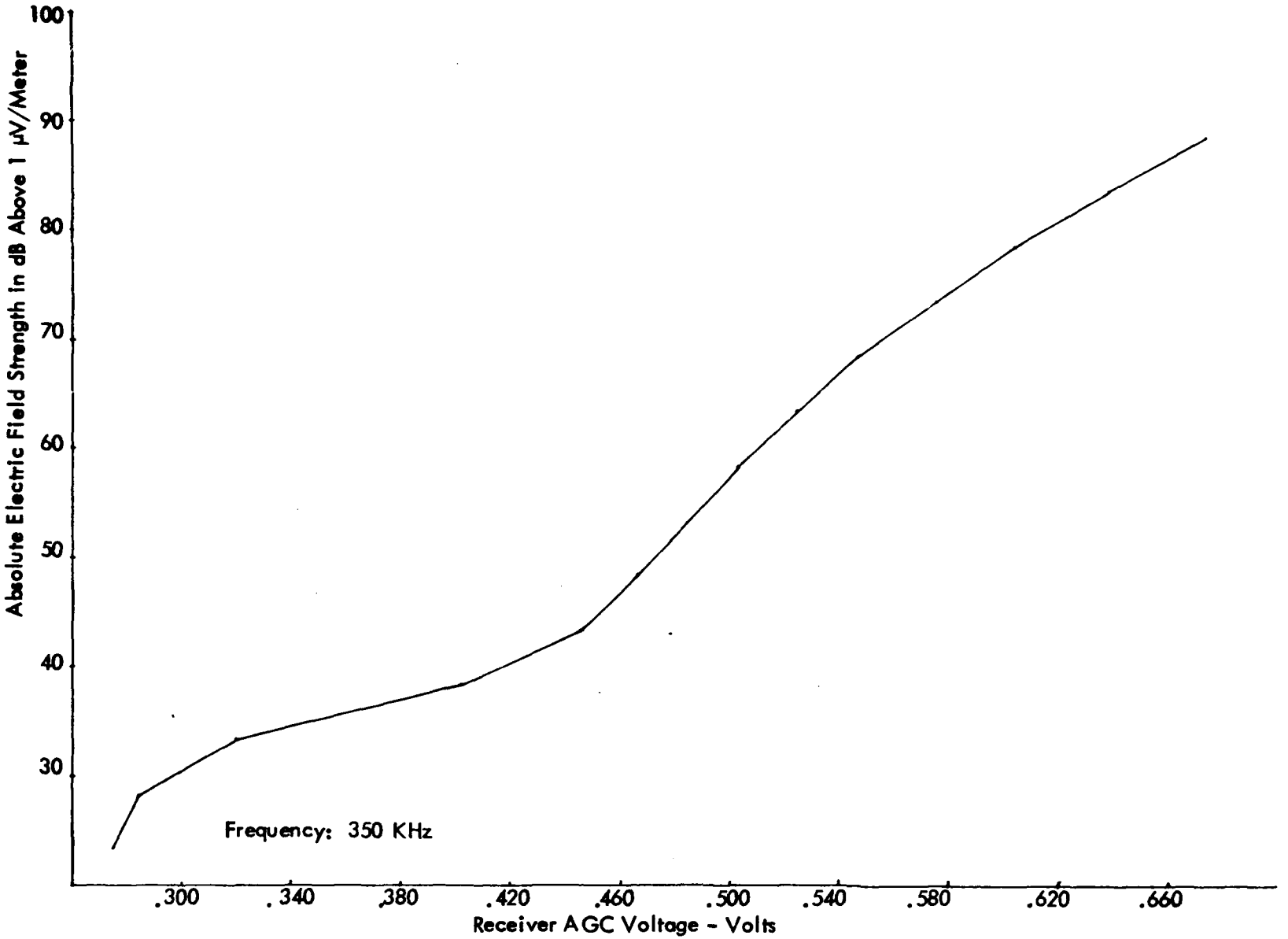

Figure B-9d. Continued.

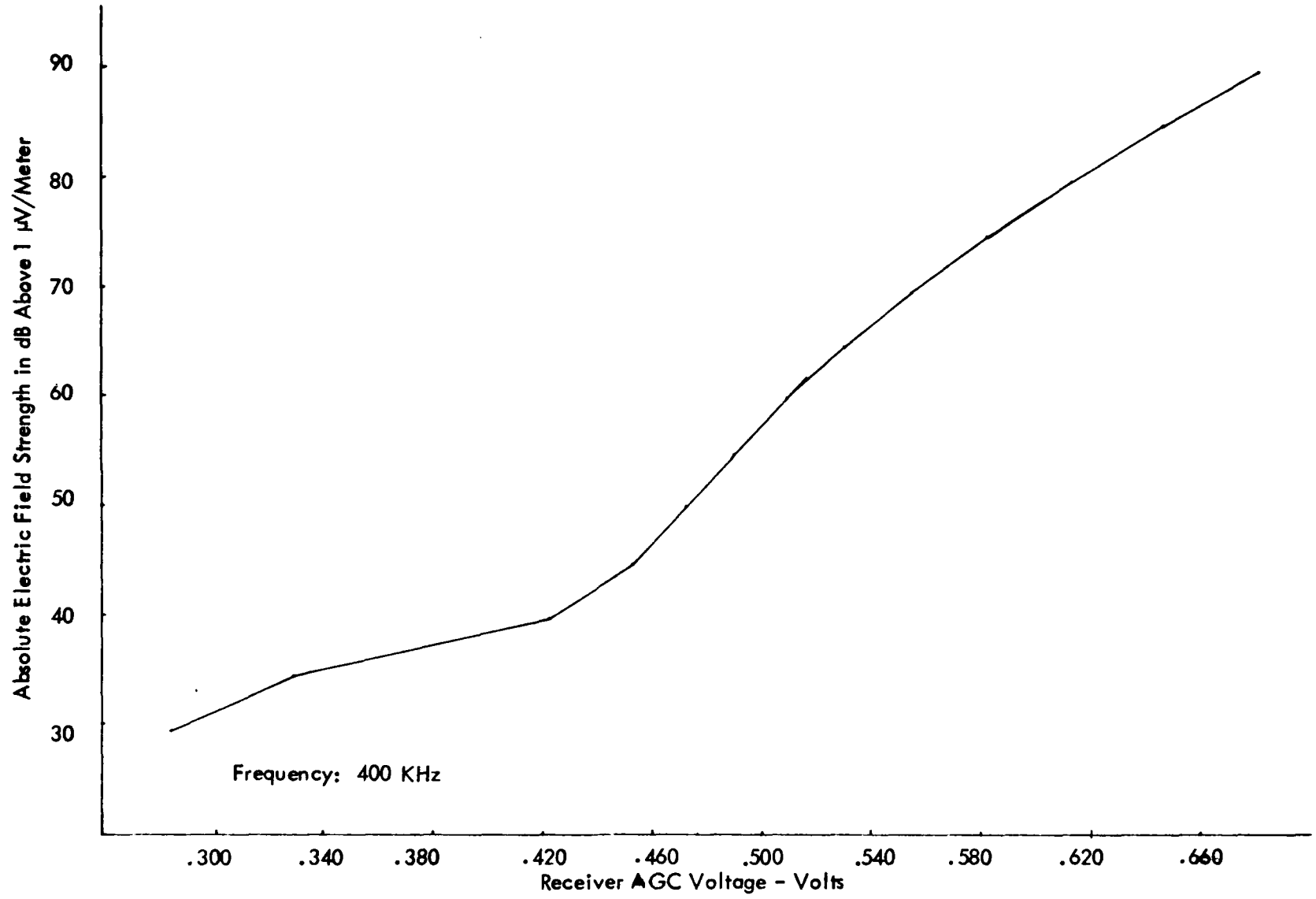

Figure B-9e. Continued.

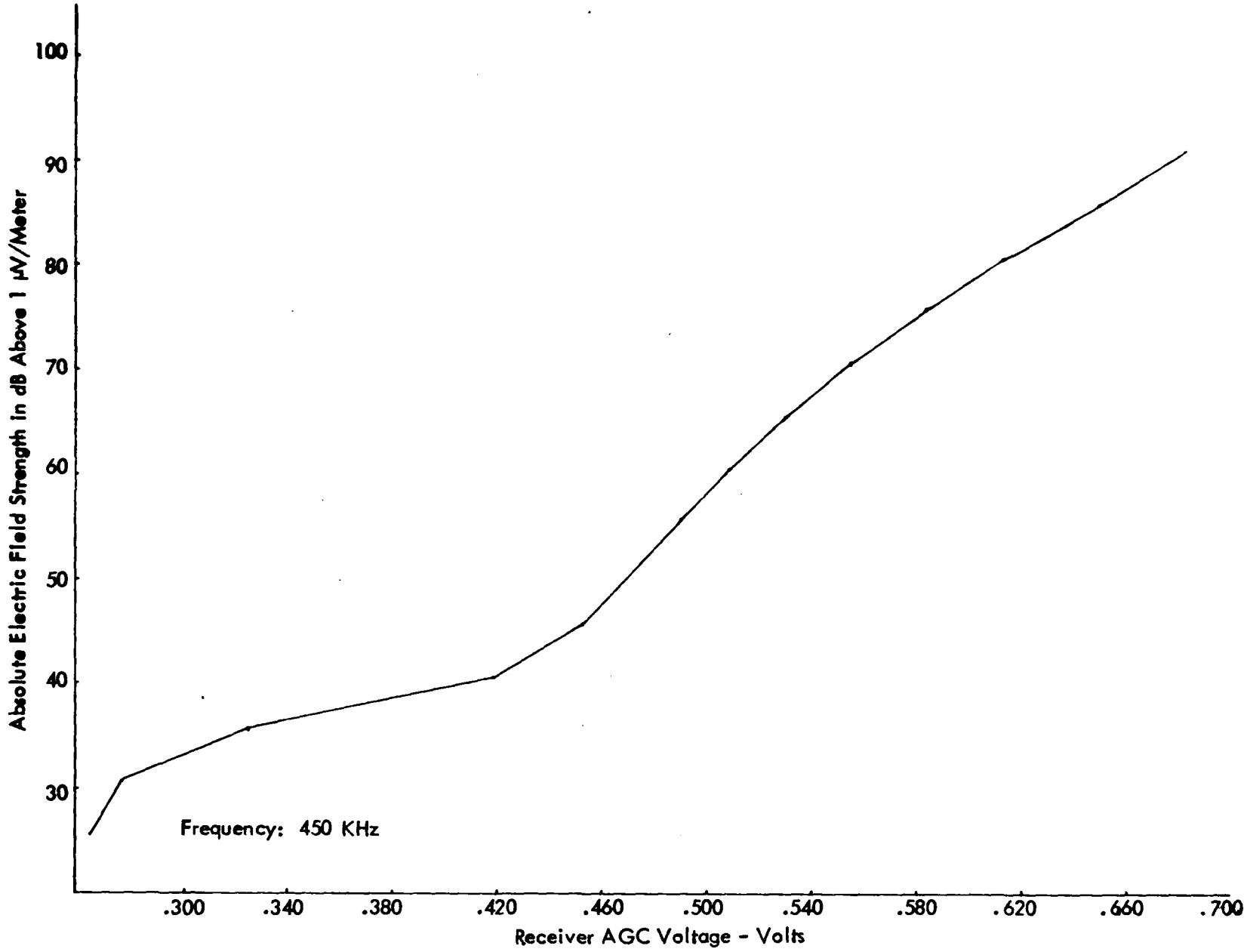

Figure B-9f. Continued.

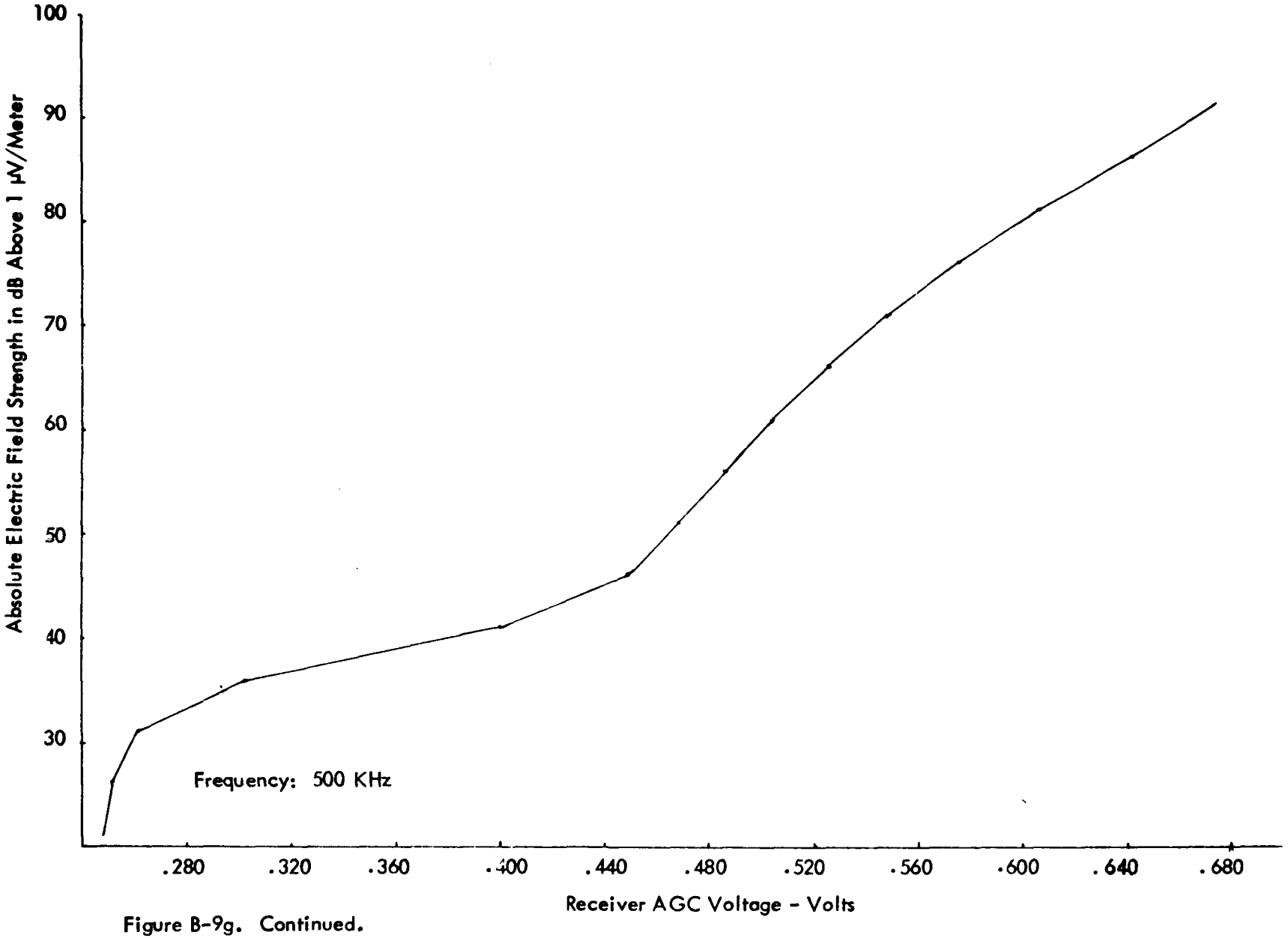

Figure B-9g. Continued.

References for Appendices

[1] Luebbers, Raymond J., James Irvine, Thomas Mullins, and Jerry Bash, "A Method of Calibration of Airborne ADF Receiver AGC in Absolute Volts-Per-Meter", Interim Report, Avionics Engineering Center, Department of Electrical Engineering, Ohio University, Athens, Ohio 45701, October 1979.

[2] Jean, A. G., H. E. Taggart and J. R. Wait, "Calibration of Loop Antennas at VLF", Journal of Research of the National Bureau of Standards, Volume 65, No. 3, July-September 1961.

[3] Taggart, H. E., "Field Strength and RFI Standards at the National Bureau of Standards", 1968 IEEE Symposium on Electromagnetic Compatibility, Seattle, Washington.

[4] Instruction Manual, Type DFA-70 Automatic Direction Finder System, Bendix Avionics Products, Reprinted January 1964.

[5] King Radio KR-86 Automatic Direction Finder Maintenance Manual, April 1973.

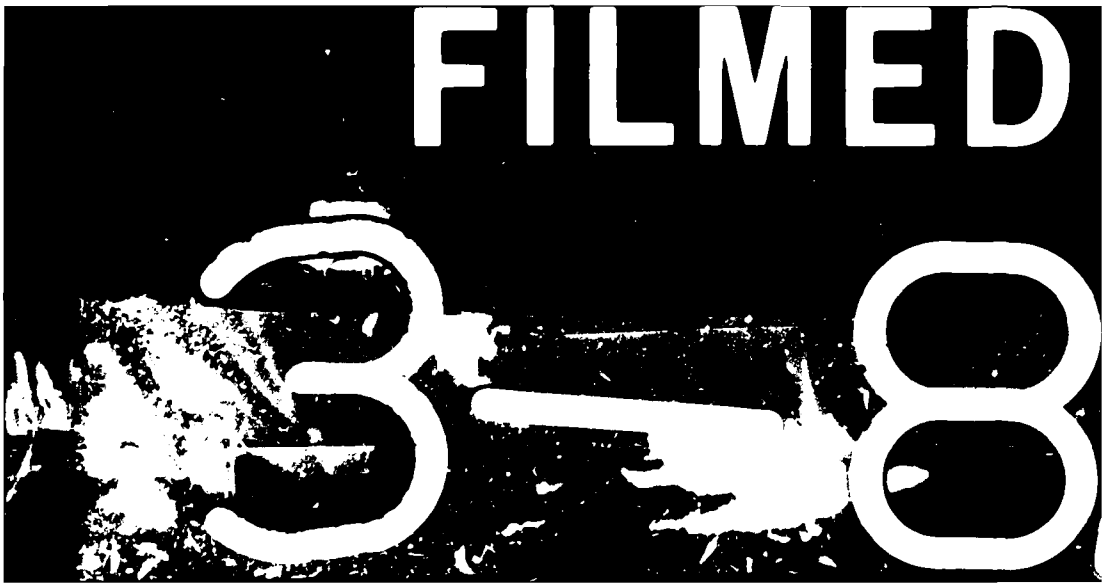
FILMED
3
8